UNIVERZITA PALACKÉHO V OLOMOUCI

PŘÍRODOVĚDECKÁ FAKULTA

Katedra analytické chemie

Využití elektroanalytických metod a jejich kombinace s chromatografií a hmotnostní spektrometrií ke studiu oxidačně-redukčních přeměn xenobiotik

HABILITAČNÍ PRÁCE

RNDr. Jana Skopalová, Ph.D.

Olomouc 2023

Motto:
„Učenec v laboratoři není jen odborník, je to dítě, které hledí na vědu jako na pohádku. Vidí ve vědě krásu.“

Marie Curie-Skłodowská

Poděkování

Na tomto místě chci poděkovat všem, kteří mě podporovali či stále podporují v mém badatelském a pedagogickém snažení. V první řadě děkuji svému učiteli, panu profesoru Milanu Kotoučkovi za to, že ve mně probudil lásku k polarografii a umožnil mi věnovat se elektroanalytickým metodám v mé profesní dráze. Dále děkuji kolegům, kteří vytvářejí příjemné tvůrčí a přátelské prostředí, kteří mi pomáhají lidsky i profesionálně a jsou mi inspirací i vzorem. Jsou to zejména prof. Petr Barták, prof. Juraj Ševčík, prof. Karel Lemr a doc. Petr Bednář. Poděkování patří také mým studentům, kteří se svou pilnou a poctivou prací v naší laboratoři podíleli na dosažených výsledcích, z nichž mnohé se pak staly základem mé habilitační práce. Velký dík náleží mé rodině za nezměrnou trpělivost, toleranci, lásku a pochopení.

Prohlášení

Prohlašuji, že jsem habilitační práci vypracovala samostatně s využitím citovaných literárních zdrojů.

V Olomouci 11. 11. 2023 .....

RNDr. Jana Skopalová, Ph.D.

Obsah

Abstrakt

Habilitační práce s názvem „Využití elektroanalytických metod a jejich kombinace s chromatografií a hmotnostní spektrometrií ke studiu oxidačně-redukčních přeměn xenobiotik“ je koncipována jako komentovaný soubor deseti vybraných publikací, které představují můj vědecký přínos v oblasti elektrochemie a elektroanalýzy biologicky významných organických látek cizorodých lidskému organismu. První část práce přináší souhrn metodických přístupů k výzkumu elektrochemických reakcí organických látek a analýzy reakčních produktů. Vedle přehledu klasických voltametrických metod studia termodynamiky a kinetiky elektrochemických přeměn jsou v práci uvedeny některé novější metody zkoumání produktů elektrochemických reakcí, které využívají off-line nebo on-line spojení elektrochemie s hmotnostní spektrometrií. Představen je nový typ elektrody speciální konstrukce pro hmotnostně spektrometrickou analýzu látek elektrochemicky generovaných a silně adsorbovaných na elektrodovém povrchu. Uvedené přístupy jsou demonstrovány na příkladech významných průmyslových látek ze skupiny bromfenolů a farmakologicky významných látek jak přírodního původu, ze skupin isochinolinových alkaloidů a prenylflavonoidů, tak syntetických léčiv s jednou nebo více oxidovatelnými skupinami. Detekované produkty elektrochemické či chemické oxidace těchto látek jsou porovnávány s produkty jejich oxidačního metabolismu katalyzovaného enzymy cytochromu P450.

Seznam použitých zkratek a symbolů

A	plocha elektrody
APCI	chemická ionizace za atmosférického tlaku
ASAP	sonda pro analýzu pevných látek za atmosférického tlaku (Atmospheric Solids Analysis Probe)
Ber	berberin
BP	bromfenol
BRB	Brittonův-Robinsonův pufr
c	koncentrace látky v roztoku
CE	pomocná elektroda
CFBE	uhlíková štětičková elektroda (Carbon Fiber Brush Electrode)
CYP	enzymy systému cytochromu P450
D	difúzní koeficient
DC voltametrie	stejnosměrná voltametrie
$E_{1/2}$	půlvlnový potenciál
EC/MS	elektrochemie spojená s hmotnostní spektrometrií
E	potenciál
E_p	potenciál píku
ESI	ionizace elektrosprejem
F	Faradayova konstanta (96 485,332 C mol^{-1})
FES	fesoterodin
GCE	elektroda ze skelného uhlíku (Glassy Carbon Electrode)
I	elektrický proud
I_d	difúzní proud
I_L	limitní kinetický proud
I_p	výška proudového píku (vlny)
$I_{p,a}$	výška anodického proudového píku
$I_{p,k}$	výška katodického proudového píku
k	rychlostní konstanta reakce
K_a	rovnovážná disociační konstanta kyseliny
K_{ow}	rozdělovací koeficient v systému oktanol/voda
LC/MS	kapalinová chromatografie spojená s hmotnostní spektrometrií
M	molární hmotnost
MS	hmotnostní spektrometrie
ND-Z	*N*-demethylzopiklon

p	počet protonů přenesených v elektrodové reakci
Pd/H_2	hydrogen-palladiová referenční elektroda
pK	záporný dekadický logaritmus rovnovážné disociační konstanty
Q	elektrický náboj
QqTOF	kvadrupólový analyzátor s analyzátorem doby letu
R	molární (univerzální) plynová konstanta (8,314 J K^{-1} mol^{-1})
RDE	rotující disková elektroda
RE	referenční elektroda
SCE	nasycená kalomelová elektroda
t	čas
t_t	teplota tání (°C)
t_v	teplota varu (°C)
T	termodynamická teplota (K)
TOL	tolterodin
V_m	molární objem látky
WE	pracovní elektroda
x	parametr asociace vztahující se k interakci rozpuštěné látky s rozpouštědlem
z	počet elektronů přenesených v elektrodové reakci
ZE	základní elektrolyt
z_α	počet elektronů zahrnutý v kroku elektrodového procesu určujícím jeho rychlost
α	koeficient přenosu náboje
Γ_0	povrchové pokrytí (množství látky adsorbované na jednotkové ploše elektrody)
γ_{Ox}	aktivitní koeficient oxidované formy elektroaktivní látky
γ_{Red}	aktivitní koeficient redukované formy elektroaktivní látky
δ	distribuční koeficient
ε_r	relativní permitivita
η	dynamická viskozita
ν	rychlost polarizace elektrody
υ	kinematická viskozita
$\Psi(t)$	bezrozměrný elektrický proud
ω	úhlová rychlost

1 Úvod

Tato práce se věnuje problematice elektrochemického výzkumu oxidačně-redukčních reakcí organických látek cizorodých lidskému organismu [**1-10**]. Koncept oxidačně-redukčních dějů se v průběhu věků postupně vyvíjí v souladu s vývojem veškerého lidského poznání. Prvním ze zkoumaných chemických dějů označovaných dnes pojmem oxidačně-redukční (či krátce redoxní) bylo hoření. Oheň byl dlouho považován za jeden ze čtyř základních elementů všeho bytí (řecký filosof Empedoklés z Akragantu, 5. stol. př. n. l.). V 17. století přinesl německý alchymista Johann Joachim Becher novou teorii hoření látek, podle níž existuje element, který je obsažen ve všech hořlavých objektech a který se při spalování uvolňuje. Jeho žák, Georg Ernst Stahl, nazval tento element flogiston a rozvinul teorii, která vysvětlovala nejen hoření, ale i dýchání živočichů a korozi kovů. Koncem 18. století přispěl rozvoj analytické chemie, zejména gravimetrie využívající přesného vážení produktů hoření, ke zpochybnění teorie flogistonu. Definitivně ji vyvrátil francouzský chemik Antoine-Laurent Lavoisier na základě rozsáhlých experimentů inspirovaných mimo jiné objevem kyslíku, který publikoval jeho současník, obhájce teorie flogistonu, Joseph Priestley v r. 1774. Lavoisier pojmenoval nově objevený plyn jako „oxygen“ neboli „kyselinotvorný“ (z řeckého ὀξύς = kyselina, -γενής = tvůrce, ploditel, původce), vycházeje z mylného předpokladu, že kyslík je součástí všech kyselin [11,12]. Lavoisier vysvětlil úlohu kyslíku v procesech hoření, oxidace kovů a dýchání. Jeho teorie odstartovala revoluci, která vedla k přetvoření chemie v moderní vědeckou disciplínu [13].

Podle Lavoisierovy teorie jsou oxidací nazývány reakce, při nichž se spotřebovává kyslík, zatímco reakce, při nichž se kyslík uvolňuje, jsou označovány jako redukce. Rozšíření pohledu na oxidačně-redukční reakce přinesl rozvoj elektrochemie v průběhu 19. století. Zjištění, že např. na anodě v elektrochemickém článku lze generovat ionty železité ze železnatých, podobně jako jejich reakcí s kyslíkem v roztoku, vedlo k závěru, že podstatou oxidačně-redukčních reakcí je výměna elektronů mezi donorem a akceptorem (elektron byl objeven v r. 1897 Josephem Johnem Thomsonem). Na základě studia chemických vazeb ve sloučeninách v první polovině 20. století odhalil Linus Pauling elektronegativitu jako schopnost atomů přitahovat valenční elektrony sdílené s jinými atomy ve sloučenině. Jeho stupnice elektronegativity prvků poskytla pevný základ pro dnešní definici oxidačně-redukčních reakcí jako dějů, při nichž se mění oxidační stav (nebo též oxidační číslo či stupeň) atomů tvořících chemickou vazbu.

Význam redoxních reakcí je dalekosáhlý, a to nejen v chemii, ale i v biologii a geologii. Povrch Země tvoří redoxní rozhraní mezi redukovaným kovovým jádrem planety a oxidující atmosférou. Na povrchu naší planety v kyslíkové atmosféře probíhají spontánně oxidační reakce, a to jak materiálů anorganické povahy (minerálů a hornin), tak i organické hmoty. Redoxní reakce probíhají ve všech živých organismech, většinou za účasti enzymů, které zprostředkovávají a řídí přenos elektronů, atomů vodíku, kyslíku, příp. dalších částic. Prostřednictvím těchto reakcí získávají buňky většinu energie (nezbytné pro syntézu stavebních látek), udržují vnitřní rovnováhu a také odbourávají cizorodé látky – xenobiotika.

V současnost jsou lidé neustále vystavováni působení xenobiotik, tedy látek organismu cizích, jako jsou farmaceutika, pesticidy, potravinářská aditiva a další průmyslové chemikálie, které člověk vyrábí a využívá v různých oblastech svého konání, a které pak následně znečišťují životní prostředí. Vniknou-li tyto cizorodé látky do lidského těla, organismus se je snaží vyloučit s pomocí metabolických procesů. Metabolismus xenobiotik obecně probíhá ve dvou fázích. V první fázi bývá xenobiotikum nejčastěji oxidativně přeměněno na polárnější sloučeninu, která pak ve druhé fázi podléhá konjugaci s glukuronovou kyselinou, glutathionem, nebo bývá sulfatována, případně acetylována či methylována [14]. Výsledkem metabolismu xenobiotik jsou polární látky rozpustné ve vodném prostředí, které mohou být snáze vyloučeny z organismu močí nebo přes žluč stolicí.

Metabolické přeměny xenobiotik v obou fázích jsou katalyzovány enzymy. Hlavní úlohu v 1. fázi metabolismu má systém cytochromu P450 (CYP). Jde o rozsáhlou skupinu enzymů s hemovou prostetickou skupinou, které katalyzují v 1. fázi především oxidační reakce, nejčastěji hydroxylaci, ale mohou katalyzovat také dealkylace, deaminace, dehalogenace, desulfatace, epoxidace a peroxidace [14]. V některých případech mohou tyto reakce vést k aktivaci xenobiotik, kdy vznikají látky reaktivnější, s vyšší biologickou aktivitou oproti látkám původním, a tedy i potenciálně nebezpečnější (toxičtější). Například jedna z metabolických drah paracetamolu, hojně používaného analgetika a antipyretika, vede ke vzniku velmi reaktivního *N*-acetyl-*p*-benzochinonu, který se může vázat na proteiny v játrech a být tak příčinou hepatotoxicity léčiva [15].

Redoxní metabolické reakce xenobiotik lze studovat v různých modelových systémech, od těch nejsložitějších a nejnáročnějších *in vivo* experimentů na živých biologických objektech, přes *in vitro* enzymatické systémy, jako jsou např. jaterní mikrosomální frakce, až po jednodušší neenzymové biomimetické systémy, obsahující např. metaloporfyriny (aktivní centra cytochromu P450) nebo Fentonovy reagenty (směs peroxidu

vodíku a železnaté soli generující vysoce reaktivní hydroxylové radikály) [16]. Jedním z nejjednodušších systémů, v nichž lze velmi účinně napodobovat řadu redoxních reakcí probíhajících v živých organismech, je elektrochemický článek.

V elektrochemickém článku je možné fyzicky oddělit obě redoxní poloreakce, tedy oxidaci a redukci, a sledovat pouze jednu z nich na vhodné pracovní elektrodě. Výsledky elektrochemických experimentů mohou přinést mnoho cenných informací o reaktivitě dané látky, její schopnosti odevzdávat nebo přijímat elektrony (včetně určení jejich počtu), podléhat dalším chemickým reakcím v daném prostředí (protolýza, solvolýza, adsorpce na mezifázích v článku, tvorba komplexů) i o meziproduktech a produktech jejich oxidace nebo redukce, a jejich reaktivitě. Odhalení centra redoxní aktivity xenobiotika stejně jako další informace o jeho reaktivnosti mohou být využity např. pro navržení možných metabolických redoxních přeměn a výsledných meziproduktů či produktů, pro elektrochemickou syntézu určitých metabolitů v dostatečném množství pro jejich izolaci a následnou charakterizaci, případně i pro toxikologická či jiná (např. farmakologická) studia. Znalost redoxního chování xenobiotik lze využít v neposlední řadě při vývoji citlivých analytických metod detekce a stanovení elektrochemickými technikami.

Tato práce je věnována studiu redoxního chování a identifikaci produktů elektrochemických přeměn vybraných xenobiotik, která obsahují elektrochemicky oxidovatelné skupiny, zejména fenolovou, benzodioxolovou a terciární aminoskupinu. Jmenované skupiny bývají velmi často přítomny v léčivech či potenciálních léčivech, ale také drogách, ať už přírodních či syntetických (vč. tzv. „designer drugs“) a úzce souvisejí s jejich biologickou aktivitou. Práce vychází ze souboru deseti publikací [**1-10**] uvedených v příloze, které vznikly v průběhu posledních jedenácti let v laboratoři elektroanalytických metod v úzké spolupráci s laboratoří chromatografických metod a hmotnostní spektrometrie na Katedře analytické chemie Přírodovědecké fakulty Univerzity Palackého v Olomouci. Jejím cílem je poukázat na některé poznatky, které byly v průběhu výzkumné práce dosaženy a které by mohly přispět jak k obohacení přístupů ke studiu redoxních přeměn biologicky významných molekul, tak i k dalšímu vývoji elektrochemické instrumentace a spojených analytických technik. Metodická část práce může sloužit studentům jako doplňující a rozšiřující studijní literatura k přednáškám z elektroanalytických metod.

2 Přínos elektrochemie ke studiu redoxních reakcí biologicky významných látek

2.1 Elektrochemické a biologické redoxní reakce

Elektrochemické metody umožňují studovat reakce přenosu náboje u biologicky významných látek a získat řadu důležitých informací o studovaném systému. Do jaké míry jsou informace získané o reakcích přenosu náboje pomocí těchto technik schopny vypovídat o redoxních reakcích probíhajících v živých organismech? Existuje řada podobností, které poukazují na relevantnost elektrochemického studia biologicky významných molekul [17]:

1. Jak elektrochemický, tak biologický přenos náboje při oxidačně-redukčních reakcích probíhá jako heterogenní proces. V elektrochemickém systému se odehrává v mezifází elektroda/roztok, v biologickém systému zpravidla v mezifází enzym/roztok.
2. Elektrochemické reakce i biologické reakce v živých organismech mohou probíhat za podobných podmínek (pH, iontová síla roztoku, teplota).
3. Biologické i elektrochemické reakce přenosu náboje mohou probíhat v nevodném prostředí lipidových struktur v biosystémech i v nevodných rozpouštědlech v elektrochemii.
4. Pro reakci přenosu náboje se musí molekula substrátu orientovat určitým směrem jak vůči aktivnímu místu enzymu, tak vůči povrchu elektrody.

I přes uvedené podobnosti není možné v elektrochemickém systému simulovat všechny redoxní reakce, které jsou v biologických systémech katalyzovány enzymy. Specificita enzymů vůči některým reakcím substrátů je jedinečná. Např. oxidační reakce katalyzované enzymy systému cytochromu P450 (CYP) iniciované přímým odnětím vodíku z molekuly substrátu, jako jsou hydroxylace alifatického řetězce nebo nesubstituovaného aromatického kruhu, či *O*-dealkylace vyžadují příliš vysoký potenciál (vyšší než je potenciál oxidace rozpouštědla) na to, aby mohly proběhnout za běžných elektrochemických podmínek [18]. Přesto elektrochemické metody mohou být užitečné při zjišťování náchylnosti substrátu k oxidaci a při odhalování jeho redoxně aktivních center.

V následujících odstavcích bude věnována pozornost elektrochemickým technikám a experimentům, které mohou být cenným zdrojem informací nejen o oxidačně-redukčním

chování biologicky aktivních látek. Kombinace elektrochemických experimentů s metodami separačními a hmotnostně spektrometrickými umožňuje identifikovat produkty redoxních přeměn. Přínos uvedených technik bude dokumentován na příkladech výsledků pocházejících z laboratoří Katedry analytické chemie.

2.2 Metody studia elektrochemických dějů

2.2.1 Stejnosměrná (DC) voltametrie

První elektrochemické výzkumy, které předcházely objevu polarografie, se datují k začátku 19. století (M. Faraday). Významný byl přínos práce F. G. Cottrella a H. J. S. Sanda v počátku 20. století, kteří popsali principy difúzního přenosu hmoty v elektrochemických článcích. Ke skutečnému zrození voltametrie došlo až ve 20. letech 20. století [19]. Rozvoj voltametrických metod vychází z rozsáhlého výzkumu elektrolýzy se rtuťovou kapkovou elektrodou akademika Jaroslava Heyrovského, který vedl k objevu polarografie v r. 1922. O 37 let později, v roce 1959, za její objev a rozvoj v jednu z nejdůležitějších analytických metod své doby obdržel J. Heyrovský nejprestižnější vědecké ocenění – Nobelovu cenu.

V současnosti se klasická polarografie s kapající rtuťovou elektrodou v analytické praxi již nepoužívá, avšak její teoretický význam pro studium reakcí přenosu náboje a s ním souvisejících dalších dějů je stále velký. Rtuťová kapková elektroda je téměř ideální elektrodou z hlediska čistoty a homogenity povrchu, jeho snadné obnovitelnosti a polarizovatelnosti do vysokých záporných hodnot potenciálu v důsledku velkého přepětí vůči vývoji vodíku. To umožňuje sledovat redukční reakce analytů v široké katodické oblasti potenciálů. Nevýhodou rtuti je její velmi snadná oxidovatelnost již při nízkých hodnotách potenciálu v anodické oblasti. To značně omezuje využití rtuti při studiu oxidačních reakcí.

Prakticky stejný teoretický význam jako polarografie má stejnosměrná (Direct Current, DC) voltametrie s tuhou rotující diskovou elektrodou (RDE). Tuhé elektrody z inertních kovových nebo uhlíkových materiálů se výborně uplatňují právě při studiu oxidačních reakcí. Teorie k DC voltametrii s RDE je velmi podrobně propracovaná, podobně jako teorie rtuťové kapkové elektrody v polarografii. Metoda je nejčastěji využívána pro studium difúze, kinetiky elektrodových reakcí a kinetiky homogenních reakcí zařazených do posloupnosti elektrodových dějů [20].

Limitní proud voltametrické vlny v DC voltametrii s RDE je základní veličinou, kterou lze použít k rozlišení povahy studované elektrochemické reakce. U elektrodových dějů řízených rychlostí difúze elektroaktivní látky k povrchu elektrody platí pro limitní difúzní proud I_d tekoucí RDE Levičova rovnice:

$$I_d = 0{,}62zFAD^{2/3}\upsilon^{-1/6}\omega^{1/2}c \qquad (1)$$

kde z je počet elektronů přenesených v elektrodové reakci, F – Faradayova konstanta (96 485,332 C mol^{-1}), A – plocha elektrody, D – difúzní koeficient, υ – kinematická viskozita, ω – úhlová rychlost, c – koncentrace elektroaktivní látky v roztoku. Závislosti proudu na druhé odmocnině z rychlosti rotace ω lze využít k diagnostickým účelům pro odhalení mechanismů řídících velikost proudu. Pro konvektivní difúzi je závislost $I = f(\omega^{1/2})$ lineární s nulovým úsekem a směrnicí, z níž lze při známých hodnotách z, A, υ a c velmi přesně určit hodnotu difúzního koeficientu studované elektroaktivní látky v daném prostředí. Je-li proud řízený kinetikou přenosu náboje nebo kinetikou chemické reakce přidružené k reakci přenosu náboje, proud na rychlosti rotace nezávisí (I = konst). Mezi těmito limitními případy existují smíšené kinetiky projevující se rozdílně při různých rychlostech rotace, a tedy různým zakřivením závislosti $I = f(\omega^{1/2})$.

Stejnosměrnou voltametrii s RDE s diskem ze skelného uhlíku jsme využili např. pro studium elektrochemické oxidace anticholinergního léčiva fesoterodinu (FES) **[1]**. Tato látka, chemicky 2-[(1*R*)-3-[bis(propan-2-yl)amino]-1-fenylpropyl]-4-(hydroxymethyl)fenyl 2-methylpropanoát (obr. 1a), podléhá anodické oxidaci v širokém rozmezí pH, jak je patrné z voltamogramů na obr. 1b.

Limitní proud zřetelně narůstal s rostoucím pH roztoku. Jeho závislost na odmocnině z rychlosti rotace měla pro různá prostředí různý průběh (vložený graf v obr. 1b). Pro pH 5,5 se limitní proud měnil s rychlostí rotace pouze nepatrně. Nešlo tedy o proud řízený difúzí, ale rychlostí spřažené (předřazené) chemické reakce (v tomto případě deprotonizace v elektroaktivním centru molekuly). S rostoucím pH rychlost odštěpování protonu rostla a v dostatečně alkalickém prostředí byl proud již řízený pouze difúzí (lineární závislost $I = 0{,}125\ \omega^{1/2}$ se statisticky zanedbatelným úsekem 0,039 μA pro pH 10). Difúzní koeficient vypočítaný pro první stupeň oxidace FES při pH 10 z Levičovy rovnice s použitím hodnot počtu vyměňovaných elektronů z = 2, plochy disku RDE A = 0,033 cm^2, kinematické viskozity υ = 0,01676 cm^2 s^{-1} směsi voda – methanol (1:1, *V*/*V*) při 25 °C [21] a koncentrace fesoterodinu $1 \cdot 10^{-7}$ mol cm^{-3} měl hodnotu $D = 2{,}03 \cdot 10^{-6}$ cm^2 s^{-1}.

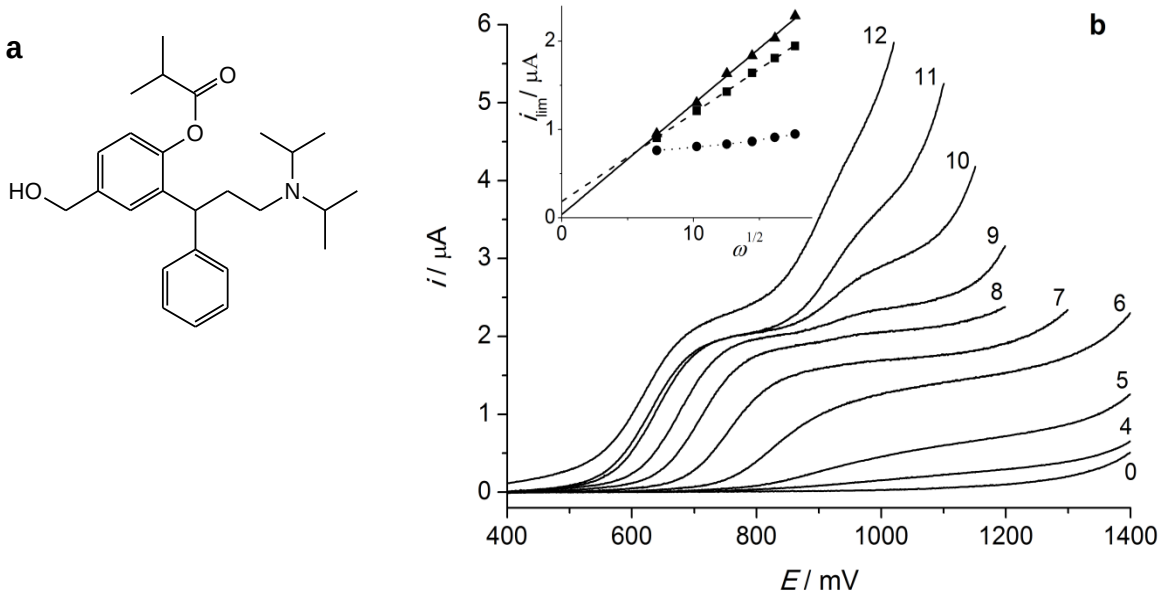

Obr. 1. a) Strukturní vzorec fesoterodinu; b) DC voltamogramy fesoterodinu (c = 0,1 mmol dm^{-3}) zaznamenané na RDE ze skelného uhlíku ve směsi Brittonova-Robinsonova tlumivého roztoku a methanolu (1:1, *V*/*V*) pro různé hodnoty pH (odpovídají číslům u jednotlivých křivek, 0 značí základní elektrolyt, pH 4). Úhlová rychlost 209 rad s^{-1}, rychlost polarizace 5 mV s^{-1}. Vložený graf: Závislost limitního proudu na odmocnině z rychlosti rotace při pH 5,5 (●), pH 7 (▲) a pH 10, první vlna (■). Všechny voltamogrmy byly zaznamenány okamžitě po smíchání roztoku FES se základním elektrolytem.

Podobně byly z Levičovy rovnice vypočítány hodnoty difúzních koeficientů fesoterodinu pro pH 7 a pH 9 (tab. I). Hodnoty *D* narůstají s rostoucím pH a také s rostoucí hodnotou distribučního koeficientu léčiva ve formě volné báze, která je vlastní elektroaktivní formou. Lze předpokládat, že difúze volné báze (jejíž vypočtený molární objem je 394 cm^3) bude rychlejší oproti difúzi iontové formy, ať už v podobě iontového asociátu fesoterodinu fumarátu (molární objem 458 cm^3), nebo solvatovaného kationtu, která převažuje v roztocích s aciditou menší než je hodnota pK_a fesoterodinu (10.31 ± 0.01 při 23.4 °C [22]). Věrohodnost určených difúzních koeficientů byla ověřena porovnáním s hodnotou D = 2,58 · 10^{-6} cm^2 s^{-1} pro volnou bázi fesoterodinu odhadnutou z rovnice Wilkeho a Changa (2) [23].

$$D = \frac{7{,}4 \cdot 10^{-8}(xM)^{1/2}T}{\eta V_m^{0,6}} \qquad (2)$$

kde η a M představují dynamickou viskozitu a molární hmotnost rozpouštědla, V_m je molární objem rozpuštěné látky, T termodynamická teplota a x je parametr asociace vztahující se k interakci rozpuštěné látky s rozpouštědlem. Uvedená hodnota D byla vypočtena pro parametry: η = 1,62 cP [24], x = 2,6 [23], M = 18,01 g mol^{-1}, T = 298,15 K, V_m = 394 cm^3.

Tabulka I. Hodnoty difúzních koeficientů fesoterodinu určených ze závislostí I_d - $\omega^{1/2}$ (z rovnice (1)) a distribučních koeficientů fesoterodinu báze $\delta = K_a/([H_3O^+] + K_a)$ [25] pro $K_a = 10^{-10.31}$.

pH	**Směrnice závislosti $I_d - \omega^{1/2}$ [μC $s^{-1/2}$]**	**Difúzní koeficient *D* [cm^2 s^{-1}]**	**Distribuční koeficient δ [%]**
7	0,0998	$1{,}45 \cdot 10^{-6}$ **[1]**	0,05
9	0,1177	$1{,}85 \cdot 10^{-6}$	4,67
10	0,1253	$2{,}03 \cdot 10^{-6}$	32,88

Z uvedeného příkladu je patrné, že metoda DC voltametrie s RDE může být velmi užitečná pro určování difúzních koeficientů elektroaktivních léčiv a dalších biologicky významných látek, a to v široce nastavitelných experimentálních podmínkách (složení roztoku, pH, iontová síla, teplota apod.). Zejména u farmaceutik je difúze velmi důležitým (a často bohužel opomíjeným) parametrem, neboť vypovídá o pasivním transportu aktivní substance v biologických systémech a tudíž o její biodostupnosti [26].

Vedle informací o řídicím procesu redoxního děje a rychlosti difúze elektroaktivní látky k elektrodovému povrchu, které lze získat z velikosti měřeného limitního proudu v závislosti na rychlosti rotace RDE, mohou poskytnout voltametrické metody další důležité charakteristiky redoxních reakcí biologicky významných látek. Jednou z nich je půlvlnový potenciál $E_{1/2}$, který je měřítkem schopnosti sledované látky v daných podmínkách přijímat nebo odevzdávat elektrony, tedy být redukována či oxidována. Velmi zjednodušeně (při zanedbání vlivu kinetiky přenosu elektronu mezi zkoumanou látkou – depolarizátorem – a elektrodou, chemických reakcí depolarizátoru nebo reakčního meziproduktu při vícenásobném přenosu elektronu a možné adsorpce depolarizátoru na elektrodový povrch) lze říci, že čím vyšší je hodnota $E_{1/2}$, bez ohledu na znaménko, tím větší je energie potřebná pro přenos elektronu mezi elektrodou a látkou, tedy tím odolnější je látka vůči redoxním reakcím.

Hodnota půlvlnového potenciálu může napovědět, zda by zkoumaná látka mohla být substrátem enzymového systému cytochromu P450 (CYP). Z hlediska enzymového oxidativního metabolismu xenobiotik (ale i látek tělu vlastních) enzymy CYP hraje redoxní potenciál substrátu zásadní roli hned po jeho stereospecificitě, která je pro enzymovou

katalýzu charakteristická. Na základě podrobného studia kinetiky oxidativní *N*-demethylace substituovaných *N*,*N*-dimethylanilinů katalyzované CYP, která je zahájena jednoelektronovým přenosem elektronu ze substrátu na aktivní hemové redoxní centrum enzymu označované jako ion FeO^{3+}, byla odhadnuta hodnota zdánlivého redoxního potenciálu CYP $E_{1/2(app)}$ = 1,85 V (vs. SCE). Tato hodnota může být zvýšena vlivem elektrostatických interakcí v proteinu. Ukázalo se, že pro substráty obsahující snadno oxidovatelný heteroatom (např. N, S, P) a nenasycené substráty s redoxními potenciály až do 2 V (vs. SCE), které jsou v dosažitelné vzdálenosti od redoxního centra enzymu, může ion FeO^{3+} v tomto centru působit jako akceptor elektronu, tedy jako „anoda“ [27]. Zde se nabízí elektrochemický článek jako velmi užitečný modelový systém. Při vhodně zvolených experimentálních podmínkách, kdy nedochází na pracovní elektrodě (anodě) z vhodného materiálu (např. skelného uhlíku, borem-dopovaného diamantu) k vedlejším reakcím rozpouštědla a elektrolytu, lze voltametricky sledovat oxidaci látek do potenciálu kolem 2 V (vs. SCE) i vyššího, zejména v nevodných roztocích [28]. Z tohoto pohledu anoda v elektrochemickém článku může napodobit chování přirozeného akceptoru elektronů v hemovém centru CYP.

Pro reverzibilní elektrodové reakce nekomplikované vedlejšími reakcemi se hodnota $E_{1/2}$ získaná DC voltametrií rovná tzv. formálnímu potenciálu E^f redoxního systému. Formální potenciál popisuje potenciál redoxního páru v rovnovážném systému, kde jsou oxidovaná a redukovaná forma přítomny v jednotkových celkových koncentracích (bez ohledu na to, že jak oxidovaná tak redukovaná forma mohou být v rozličných chemických formách) [29]. Formální potenciál zahrnuje vliv vedlejších reakcí a rovnovah, jako jsou tvorba komplexů, dimerů nebo iontových párů, adsorpce na povrch elektrody, vazba na enzymy, DNA nebo účast v acidobazických rovnovahách.

Redoxní reakce organických látek v protických rozpouštědlech, jako je voda, jsou velmi často provázeny přenosem protonů. S rostoucí aciditou roztoku, tedy rostoucí aktivitou hydratovaných protonů, se půlvlnový potenciál posouvá k pozitivnějším hodnotám. Pro reverzibilní redoxní reakci, které se účastní *z* elektronů a *p* protonů, je změna $E_{1/2}$ s rostoucím pH roztoku lineární se směrnicí danou poměrem počtu protonů a elektronů účastnících se elektrochemické reakce:

$$\frac{dE_{1/2}}{d\mathrm{pH}} = -\frac{2{,}303\,pRT}{zF}\,\mathrm{pH} \qquad (3)$$

Pokud známe počet elektronů (metody určení popisuje kapitola 2.2.3), je možné ze směrnice závislosti $E_{1/2}$ na pH určit počet protonů.

U reakcí irreverzibilních, kdy přenos elektronu neprobíhá dostatečně rychle, se mění hodnota $E_{1/2}$ se změnou acidity roztoku rovněž lineárně, avšak kinetika elektronového přenosu má vliv i na směrnici závislosti $E_{1/2}$ na pH:

$$\frac{dE_{1/2}}{d\mathrm{pH}} = -\frac{2{,}303pRT}{\alpha z_\alpha F}\,\mathrm{pH} \qquad (4)$$

kde α je koeficient přenosu náboje a z_α představuje počet elektronů zahrnutý v kroku elektrodového procesu určujícím jeho rychlost [30]. Obvykle je hodnota z_α rovna 1.

Z experimentálně zjištěné závislosti $E_{1/2}$ na pH lze kromě počtu protonů určit také disociační konstanty. Účastní-li se např. dvouelektronové redoxní reakce dva protony:

$$\mathrm{Ox} + 2\mathrm{e}^- + 2\mathrm{H}^+ \rightleftharpoons \mathrm{H_2Red}$$

a redukovaná forma podléhá protolytickým rovnovahám:

$$\mathrm{H_2Red} \overset{K_{a,1}}{\rightleftharpoons} \mathrm{HRed}^- + \mathrm{H}^+$$

$$\mathrm{HRed}^- \overset{K_{a,2}}{\rightleftharpoons} \mathrm{Red}^{2-} + \mathrm{H}^+$$

charakterizovaným rovnovážnými disociačními konstantami $K_{a,1}$ a $K_{a,2}$, pak za předpokladu, že systém je reverzibilní, bez vedlejších reakcí a interakcí, platí pro půlvlnový potenciál rovnice [31]:

$$E_{1/2} = E^f = E° + \frac{RT}{2F}\ln\frac{\gamma_{\mathrm{Ox}}}{\gamma_{\mathrm{Red}^{2-}}} + \frac{RT}{2F}\ln\left(\frac{a_{\mathrm{H}^+}^2}{K_{\mathrm{a},1}K_{\mathrm{a},2}} + \frac{a_{\mathrm{H}^+}}{K_{\mathrm{a},2}} + 1\right) \qquad (5)$$

kde γ_{Ox} a γ_{Red} jsou aktivitní koeficienty oxidované a redukované formy elektroaktivní látky. Je zřejmé, že půlvlnový potenciál závisí na pH a ze závislosti $E_{1/2}$ na pH lze určit hodnoty disociačních konstant K_a za předpokladu, že existují v rozsahu pH stupnice, resp. v experimentálně sledovaném aciditním rozmezí. Hodnoty pK_a oxidované i redukované formy se určí z grafické závislosti $E_{1/2}$ na pH jako průsečíky lineárních částí grafu, které mají odlišné směrnice.

U irreverzibilních reakcí, kdy přenos elektronu je pomalý krok určující celkovou rychlost elektrodové reakce, lze určit disociační konstantu elektroaktivní skupiny

z průsečíku lineárních úseků závislosti $E_{1/2}$ na pH pouze v případě, že protonizace/deprotonizace této skupiny předchází přenosu elektronu (prvního elektronu v případě více-elektronových reakcí) [32]. V případě, že elektroaktivní látka nese elektroneaktivní kyselou nebo bazickou skupinu, která při změně pH roztoku odštěpuje či přijímá proton, pak i když tato protolytická změna není součástí elektrodové reakce, mohou se v grafu závislosti $E_{1/2}$ *vs.* pH objevit lineární úseky s různými směrnicemi. Průsečík těchto úseků však nemusí odpovídat disociační konstantě elektroneaktivní skupiny a může být od termodynamické hodnoty pK_a značně vzdálený, dokonce až o několik jednotek [33].

Příkladem elektroaktivní skupiny, která se ireverzibilně oxiduje na elektrodě ze skelného uhlíku a současně podléhá protolytickým reakcím je bis(isopropyl)aminoskupina fesoterodinu (obr. 1a). Jak bylo uvedeno výše, v neutrálním a alkalickém prostředí poskytuje tato látka difúzí řízenou anodickou stacionární vlnu. Závislost $E_{1/2}$ na pH (obr. 2) vykazuje dva přímkové úseky se směrnicemi -49 mV/pH a -5 mV/pH s průsečíkem při pH 10, který odpovídá disociační konstantě fesoterodinu v daných experimentálních podmínkách. Pro porovnání je v literatuře uváděná hodnota pK_a = 10,31 ± 0,01 při 23,4 °C [22]. Zjištěný průběh pH závislosti půlvlnového potenciálu tedy naznačuje, že oxidaci podléhá terciární aminoskupina fesoterodinu a odštěpení elektronu z atomu dusíku předchází jeho deprotonizace **[1].**

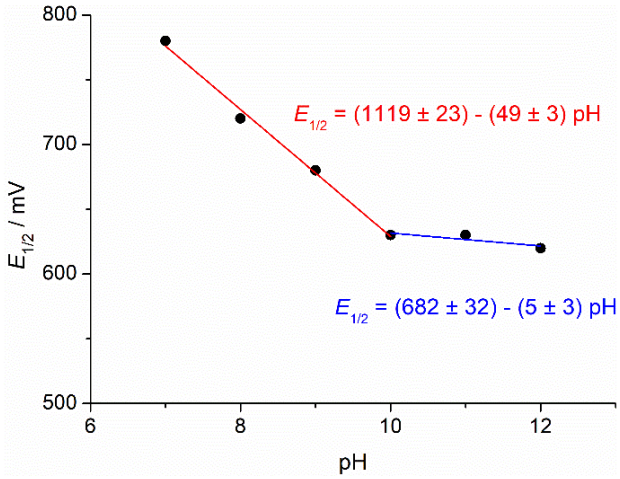

Obr. 2. Závislost půlvlnového potenciálu fesoterodinu (c = 0,1 mmol dm^{-3}) na pH. DC voltametrie s RDE ze skelného uhlíku, základní elektrolyt: směs Brittonova-Robinsonova tlumivého roztoku (pH 7 až 12) a methanolu (1:1, *V*/*V*), úhlová rychlost 209 rad s^{-1}, rychlost polarizace 5 mV s^{-1}.

Hydrodynamická DC voltametrie s RDE může poskytovat důležité informace také o dalších homogenních chemických reakcích spřažených s reakcemi přenosu náboje. Při studiu mechanismu elektrochemických reakcí lze využít závislosti $E_{1/2}$ na rychlosti rotace

RDE. Řada organických látek podléhá postupné dvouelektronové redukci nebo oxidaci, při kterých se látka A přijetím či odštěpením jednoho elektronu přemění na nestabilní meziprodukt B, jenž podléhá homogenní reakci za vzniku elektroaktivní látky C. Ta může být dále redukována či oxidována na látku D nebo může docházet k její homogenní reakci s nestabilním meziproduktem B za vzniku produktu D a výchozí látky A. Celkově lze popsané děje zapsat následujícím schématem [34]:

$$A \pm e^- \overset{E^\circ_{A/B}}{\rightleftharpoons} B \qquad (I)$$

$$B \xrightarrow{k} C \qquad (II)$$

$$C \pm e^- \overset{E^\circ_{C/D}}{\rightleftharpoons} D \qquad (III)$$

$$B + C \rightleftharpoons A + D \qquad (IV)$$

V případě, že reakce (IV) je z kinetického hlediska zanedbatelná a produkt D vzniká dvouelektronovou heterogenní reakcí u povrchu elektrody, označuje se mechanismus jako ECE (E značí přenos elektronu, C chemickou reakci). Když je naopak reakce (III) zanedbatelná a druhý elektron se přenáší při homogenní reakci (IV), jde o disproporcionační mechanismus DISP. Jestliže reakce (II) je reakcí prvního řádu, označuje se celkový mechanismus jako DISP1.

Za předpokladu, že přenos prvního elektronu (v reakci I) je dostatečně rychlý (elektrochemicky reverzibilní), pak změny půlvlnového potenciálu v závislosti na rychlosti rotace elektrody ω mohou být použity pro zjištění rychlostní konstanty k následné homogenní reakce. Pro případ ECE mechanismu platí vztah [34]:

$$E_{1/2} = E^\circ - \frac{2{,}303RT}{F} \log\left[\left(\frac{D}{\nu}\right)^{1/6} \frac{\sqrt{\omega}}{0{,}643\sqrt{k}}\right] \qquad (6)$$

a pro mechanismus DISP1platí:

$$E_{1/2} = E^\circ - \frac{2{,}303RT}{F} \log\left[\left(\frac{D}{\nu}\right)^{1/6} \frac{\sqrt{\omega}}{0{,}643\sqrt{k}}\right] + \log(2) \qquad (7)$$

V případě obou mechanismů, ECE i DISP1, se tedy $E_{1/2}$ mění lineárně s dekadickým logaritmem rychlosti rotace se směrnicí $dE_{1/2}/d\log\omega = 2{,}303RT/2F = 29{,}5$ mV při 25 °C.

Jestliže bude rychlý přenos prvního elektronu (I) následován místo reakce prvního řádu (II) reakcí druhého řádu:

$$B + B \xrightarrow{k_{EC2}} C \qquad (II')$$

nebo:

$$B \rightleftharpoons C \qquad (II'')$$

$$B + C \xrightarrow{k_{DISP}} A + D \qquad (III'')$$

pak se příslušné reakční mechanismy označují jako EC_2 a DISP2. Pro oba tyto mechanismy je charakteristický lineární posun $E_{1/2}$ s log ω se směrnicí 19,7 mV při 25 °C [35].

Závislosti půlvlnového potenciálu na rychlosti rotace RDE ve voltametrických experimentech jsme využili při studiu mechanismu elektrochemické oxidace bromovaných fenolů **[2]**. Hodnoty směrnic lineárního posunu $E_{1/2}$ s hodnotou log ω pro čtyři studované deriváty (2-bromfenol, 3-bromfenol, 4-bromfenol a pentabromfenol) získané DC voltametrií při různých rychlostech polarizace RDE ze skelného uhlíku v prostředí obsahujícím tlumivý roztok o pH 6 a methanol v obsahu 50 nebo 90 objemových procent se pohybovaly v rozmezí 18,1 – 22,1 (tab. II). Hodnoty blízké teoretické hodnotě směrnice 19,7 ukazují na elektrodový proces, v němž je přenos elektronu následován dimerizací meziproduktů v homogenní fázi (mechanismus EC_2).

Dimerizační reakce byly prokázány analýzou produktů elektrolýzy bromovaných fenolů za konstantního potenciálu odpovídajícího limitnímu proudu stacionárních voltametrických křivek. Metodami GC/MS a HPLC/MS byla identifikována řada dimerních produktů, které vznikly rekombinací fenoxylových radikálů jakožto nestabilních meziproduktů jednoelektronové oxidace výchozích monobromfenolů a pentabromfenolu **[2-4]**.

Tabulka II. Posuny půlvlnových potenciálů bromfenolů ($c = 1 \cdot 10^{-4}$ mol dm^{-3}) s dekadickým logaritmem rychlosti rotace (v rozsahu 52 až 314 rad s^{-1}) rotující diskové elektrody ze skelného uhlíku v základním elektrolytu obsahujícím methanol.

	$dE_{1/2}/d\log\omega$ [mV]	Polarizační rychlost [mV s^{-1}]	Obsah methanolu [%]
2-bromfenol	18,1	5	90
	22,1	30	50
3-bromfenol	19,6	100	50
4-bromfenol	20,9	30	50
pentabromfenol	19,6	5	90

Rotující disková elektroda se obvykle nepoužívá v kombinaci s cyklickou voltametrií (viz kap. 2.2.2), neboť produkty vznikající elektrodovou reakcí jsou od povrchu elektrody účinně odstraňovány (odmetány) při její rotaci. V obráceném směru polarizace za podmínek, kdy rychlost skenu je dostatečně pomalá vzhledem k rychlosti rotace elektrody, se zaznamená stejná *I-E* křivka jako při skenu přímém (dopředném) [29]. V některých případech však může obrácený sken odhalit proces, při němž dochází k blokování elektrodového povrchu produkty elektrochemické reakce. Obr. 3 ukazuje voltamogramy tří monobromovaných fenolů a pentabromfenolu zaznamenané na RDE v roztoku základního elektrolytu s obsahem 90 obj. % methanolu. Ani v jednom případě křivka zpětného skenu nekopíruje křivku zaznamenanou v prvním přímém skenu. Nejmenší odchylka (hystereze) byla pozorována u pentabromfenolu. U monobromfenolů ve zpětném skenu poklesl proud zvolna až k nule. Pokud se snížil obsah methanolu v roztoku na 50 %, byl pokles proudu patrný už na limitním proudu v anodickém skenu, kdy byla zaznamenána křivka ve tvaru širokého píku (obr. 3, vložený graf). V dalších opakovaných cyklech byl registrovaný proud téměř shodný s proudem samotného základního elektrolytu. Z uvedeného pozorování je zřejmé, že při oxidaci bromfenolů dochází k tvorbě produktů, které zůstávají silně adsorbovány na elektrodovém povrchu a blokují další výměnu náboje (pasivují elektrodový povrch). Vyšší obsah methanolu, podobně jako vyšší rychlost rotace pasivaci poněkud snížily v důsledku účinnějšího odstraňování produktů elektrochemických reakcí **[2]**. Podobné chování bylo popsáno v literatuře pro oxidaci pentachlorfenolu na grafitové RDE [36]. V případě bromfenolů způsobují pasivaci elektrody dimerní a oligomerní produkty,

které se tvoří následnými elektrochemickými reakcemi reaktivních fenoxylových radikálů. Struktury některých z těchto oligomerních produktů či jejich fragmentů jsme později odhalili hmotnostně spektrometrickou analýzou pevných látek na povrchu elektrody pomocí tzv. ASAP sondy, která bude podrobněji popsána v kap. 2.3.3.

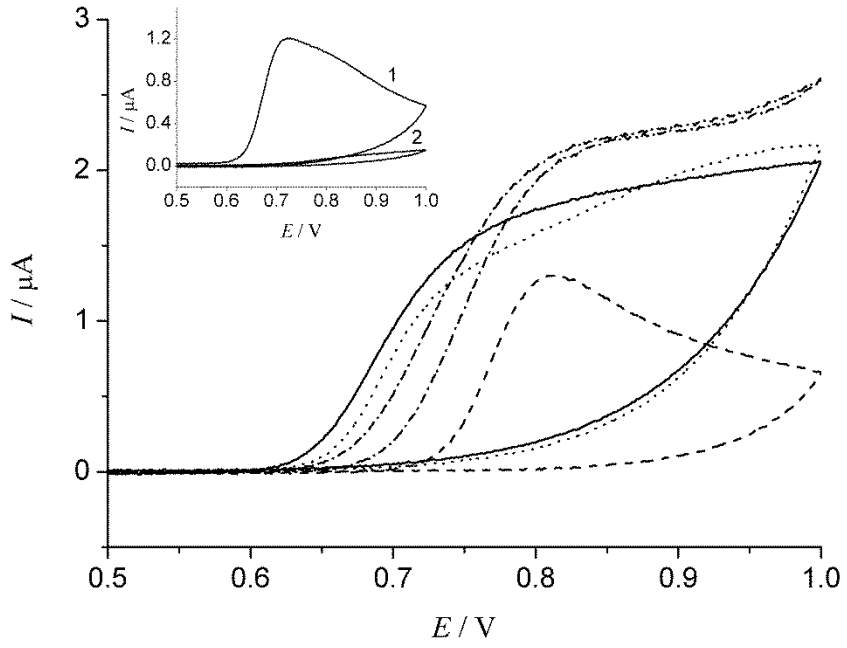

Obr. 3. Cyklické voltamogramy 0,1 mmol dm^{-3} 2-bromfenolu (plná čára), 3-bromfenolu (čárkovaná), 4-bromfenolu (tečkovaná) a pentabromfenolu (čerchovaná) zaznamenané na rotující diskové elektrodě ze skelného uhlíku v prostředí methanol/vodný roztok mravenčanu amonného pH = 6 (9:1, *V*/*V*). Rychlost rotace 314 rad s^{-1}, rychlost polarizace 5 mV s^{-1}. Vložený graf: Cyklický voltammogram (2 cykly, označené 1 a 2) 4-bromfenolu za stejných experimentálních podmínek, pouze ve směsi methanol/vodný roztok mravenčanu amonného pH 6 (1:1, *V*/*V*).

2.2.2 Cyklická voltametrie

Analýza DC voltamogramů umožňuje získat řadu termodynamických i kinetických parametrů popisujících příslušnou elektrodovou reakci. Z tvaru voltametrické vlny lze v případě jednoduchých jednoelektronových reakcí zjistit, zda je daný redoxní systém reverzibilní, kvazireverzibilní nebo irreverzibilní z hlediska rychlosti reakce přenosu elektronu a následně určit v prvém případě termodynamickou veličinu, kterou je formální redox potenciál, u druhých dvou případů kinetické veličiny, jako koeficient přenosu náboje (vyjadřuje symetrii energetické bariéry pro přenos elektronu) a standardní rychlostní konstantu. Pokud však je elektrodový proces komplexnější, zahrnuje přenos většího počtu elektronů v několika následných krocích, je analýza tvaru DC vlny velmi obtížná a může vést k chybným závěrům [29]. Při studiu takovýchto systémů se pak velmi dobře uplatňuje metoda cyklické voltametrie (CV), která dovoluje přímo sledovat reverzibilitu systému a je

schopná poskytnout značné množství experimentálních informací o kinetickém i termodynamickém chování studovaných redoxních systémů [37].

Cyklická voltametrie bývá nezřídka používána pro počáteční studium elektrochemického chování látek. V této metodě je pracovní elektroda stejně jako v DC voltametrii polarizována stejnosměrným napětím rostoucím v čase od počáteční hodnoty po hodnotu tzv. přepínacího potenciálu a zpět. Registrovaná závislost proudu *I* na elektrodovém potenciálu *E* má v přímém směru polarizace v přítomnosti elektroaktivní látky tvar píku (na rozdíl od stacionární sigmoidní vlny v klasické DC voltametrii s RDE nebo s kapající rtuťovou kapkou). V případě reverzibilní reakce se v obráceném směru polarizace registruje pík opačné polarity odpovídající zpětnému transportu elektronů. V případě ireverzibilních reakcí v obráceném směru polarizace pík opačného děje buď zcela chybí, nebo je značně posunutý oproti případu reakce reverzibilní. Rychlost změny potenciálu pracovní elektrody se obvykle pohybuje v rozsahu 10 mV s^{-1} až 1000 V s^{-1} při použití konvenčních stacionárních elektrod s elektroaktivní plochou v řádu desetin až desítek mm^2. Analýzou cyklických voltamogramů zaznamenaných s různými rychlostmi polarizace lze na základě kritérií odvozených Nicholsonem a Shainem [38] určovat parametry popisující rychlost přenosu elektronů i spřažených chemických reakcí.

Pro reversibilní systémy platí lineární vztah mezi velikostí proudu v maximu CV píku (I_p) a odmocninou z rychlosti polarizace $v^{1/2}$ za předpokladu, že je elektrodový proces řízen difúzí (Randles-Ševčíkova rovnice):

$$I_p = \pm 0{,}446\, zFAc\sqrt{\frac{zFvD}{RT}} \tag{8}$$

kde znaménko + platí pro anodický děj, znaménko – pro děj katodický, *z* je celkový počet přenesených elektronů na molekulu elektroaktivní látky difundující k elektrodovému povrchu, *F* je Faradayova konstanta, *A* plocha elektrody, *c* koncentrace látky v roztoku, *v* rychlost polarizace elektrody, *D* difúzní koeficient, *R* molární plynová konstanta (8,314 J K^{-1} mol^{-1}) a *T* termodynamická teplota.

Pro 25 °C a po dosazení hodnot *F* a *R* má rovnice tvar:

$$I_p = \pm 2{,}69 \cdot 10^5 zAc\sqrt{zvD} \tag{9}$$

Potenciál píku E_p v CV má podobný kvalitativní význam jako půlvlnový potenciál $E_{1/2}$ ve stacionární DC voltametrii. Platí mezi nimi vztah (pro katodický děj):

$$E_{\mathrm{p}} = E_{1/2} - 1{,}109\frac{RT}{zF} = E_{1/2} - \frac{28{,}5}{z}\ [\mathrm{mV}]\ \text{při } 25\ °\mathrm{C} \tag{10}$$

U širších píků může být problém určit hodnotu E_p, proto je někdy vhodnější odečítat potenciál v polovině výšky píku, $E_{p/2}$:

$$E_{\mathrm{p}/2} = E_{1/2} + 1{,}09\frac{RT}{zF} = E_{1/2} + \frac{28{,}0}{z}\ [\mathrm{mV}]\ \text{při } 25\ °\mathrm{C} \tag{11}$$

Z rovnic (10) a (11) lze odvodit diagnostický parametr pro reverzibilní děje:

$$\left|E_{\mathrm{p}} - E_{\mathrm{p}/2}\right| = 2{,}20\frac{RT}{zF} = \frac{56{,}5}{z}\ [\mathrm{mV}]\ \text{při } 25\ °\mathrm{C} \tag{12}$$

Z uvedených vztahů (převzatých z literatury [29]) vyplývá, že u reverzibilních systémů potenciál píku nezávisí na rychlosti polarizace elektrody, což je další diagnostické kritérium při určování reverzibility systému. Dalšími diagnostickými kritérii reverzibility redoxního systému jsou shodná velikost katodického a anodického proudového píku, tedy $|I_{p,a}/I_{p,k}| = 1$ a konstantní vzdálenost potenciálů maxim proudových píků $\Delta E = |E_{p,a} - E_{p,k}| = 2{,}218\ RT/zF = 57/z$ [mV] při 25 °C [37].

Pro ireverzibilní systémy platí Randles-Ševčíkova rovnice ve tvaru:

$$I_p = \pm 0{,}496\ zFAc\sqrt{\frac{\alpha z_\alpha F v D}{RT}} \tag{13}$$

kde z_α zastupuje počet elektronů vyměňovaných v kroku určujícím rychlost, z představuje celkový počet přenesených elektronů na molekulu elektroaktivní látky difundující k elektrodovému povrchu, α je koeficient přenosu náboje vyjadřující symetrii energetické bariéry, F je Faradayova konstanta, A je plocha elektrody, c koncentrace látky v roztoku, v rychlost polarizace elektrody, D difúzní koeficient, R molární plynová konstanta a T termodynamická teplota.

Pro 25 °C a po dosazení hodnot F a R má rovnice tvar:

$$I_p = \pm 2{,}99 \cdot 10^5 zAc\sqrt{\alpha z_\alpha v D} \tag{14}$$

Pokud není hlavním řídicím procesem celkového elektrochemického děje difúze, ale elektroaktivní látka je adsorbovaná na povrchu elektrody, registrovaný proud odpovídající oxidaci nebo redukci dané látky je přímo úměrný rychlosti polarizace elektrody podle vztahu [37]:

$$I_{\mathrm{p}} = \pm \frac{z^2 F^2}{4RT} v A \Gamma_0 \tag{15}$$

kde A je povrch elektrody a Γ_0 představuje povrchové pokrytí (množství látky adsorbované na jednotkové ploše elektrody, mol m^{-2}).

Řada elektrodových dějů je předcházena chemickou reakcí, při níž vzniká z elektroinaktivní látky A elektroaktivní látka B podléhající reakci přenosu náboje (CE mechanismus):

$$\mathrm{A} \underset{k_b}{\overset{k_f}{\rightleftharpoons}} \mathrm{B} \tag{V}$$

$$\mathrm{B} \pm z\mathrm{e}^- \rightleftharpoons \mathrm{C} \tag{VI}$$

Tvar a velikost voltametrické *i-E* křivky v takovém případě závisí na velikosti rovnovážné konstanty K chemické reakce ($K = k_f / k_b$), celkové rychlosti reakce ($k = k_f + k_b$) a rychlosti polarizace elektrody v. Pro určité rozsahy hodnot těchto parametrů systém poskytuje voltamogram ve tvaru rovnovážné sigmoidní křivky, rychlost celkové reakce, a tedy i velikost proudu, je určena rychlostí předcházející chemické reakce. Kinetický rovnovážný proud I_L nezávisí na rychlosti polarizace elektrody v [29]:

$$I_{\mathrm{L}} = zFAD^{1/2}cKk^{1/2} \tag{16}$$

Při studiu redoxního systému lze o řídicím mechanismu rozhodnout analýzou logaritmovaných závislostí výšky proudové odezvy (I_p, I_L) na rychlosti polarizace elektrody. Logaritmováním rovnic (8), (9), (13), (14) se získají lineární funkce $\log I_p = a + b \log v$ se směrnicí $b = 0{,}5$ pro případ difúzí řízeného děje. Lineární funkce získaná logaritmováním rovnice (15) má směrnici s hodnotou $b = 1$, která je typická pro případ redoxní reakce částice v adsorbovaném stavu. Podle rovnice (16) je kinetický limitní proud nezávislý na rychlosti polarizace, tedy $I_L = f(v^0)$, odkud logaritmováním získáme konstantní funkci se směrnicí $b = 0$. Řada organických látek poskytuje lineární závislosti $\log I_p = f(\log v)$ s hodnotami směrnic ležícími mezi výše uvedenými teoretickými hodnotami, což poukazuje na smíšený vliv dvou procesů – difúze a adsorpce ($0{,}5 < b < 1$) nebo difúze a kinetiky předřazené homogenní reakce ($0 < b < 0{,}5$). V praxi je před logaritmickou analýzou nutné odečíst od proudu píku (limitního proudu) proud základního elektrolytu [39].

V tabulce III jsou uvedeny hodnoty směrnice závislostí $\log I_p = f(\log v)$ některých látek, jejichž voltametrické chování v anodickém směru polarizace pracovní elektrody ze skelného uhlíku jsme studovali v naší laboratoři. Antimuskarinová léčiva tolterodin,

fesoterodin a jejich společný metabolit 5-hydroxymethyltolterodin vykazovala ve směsném vodně-methanolovém prostředí (H_2O/CH_3OH, 1:1, *V*/*V*) v prvním stupni elektrochemické reakce anodický proud řízený difúzí (směrnice závislosti log I_p – log v jsou rovny nebo velmi blízké teoretické hodnotě 0,5 pro děj řízený difúzí). V čistě vodném pufrovaném prostředí byla zjištěna vyšší směrnice závislosti log I_p – log v (u tolterodinu 0,62), svědčící o částečné adsorpci látky na elektrodový povrch. Řídicí silou adsorpce je hydrofobní interakce lipofilního léčiva (rozdělovací koeficient tolterodinu při pH 7,3 má hodnotu log D = 1,83 [40]) s elektrodovým povrchem. Přítomnost methanolu ve vodném roztoku částečně potlačuje adsorpci organické molekuly v důsledku zvýšení rozpustnosti a konkurenční adsorpce méně polárního rozpouštědla do mezifází elektroda-roztok [41]. Anodický proud odpovídající následné oxidaci (2. pík) je jak v čistě vodném, tak ve směsném vodně-methanolovém prostředí výrazně ovlivněn adsorpcí (směrnice závislosti log I_p – log v jsou 0,74 a 0,75). Lze tedy usuzovat, že meziprodukt vznikající v prvním kroku oxidace se na elektrodový povrch adsorbuje silněji než původní látka a k jeho další oxidaci dochází částečně v adsorbovaném stavu. V prostředí bezvodého methanolu se zdá být anodický proud v obou stupních oxidace tolterodinu ovlivněn kinetikou předřazené homogenní reakce (směrnice závislosti log I_p – log v mají hodnoty 0,34 pro 1. pík a 0,23 pro 2. pík), pravděpodobně deprotonizace provázející přenos elektronu z látky na elektrodu (podrobněji mechanismus elektrochemické oxidace tolterodinu, kap. 3.2.1, obr. 19).

U jiných látek, např. u léčiva zopiklonu nebo přírodního isochinolinového alkaloidu berberinu, byla adsorpce na povrch elektrody ze skelného uhlíku, zjištěná voltametricky ze závislosti log I_p – log v (tab. III), potvrzena jednoduchým experimentem. Elektroda byla po určitou dobu ponořena v roztoku látky a po vyjmutí z roztoku opláchnuta vodou a polarizována v roztoku čistého základního elektrolytu. Na cyklických voltamogramech pak byl pozorován proudový pík látky naadsorbované na povrchu elektrody **[5]**. Popsaný postup adsorpce analytu na elektrodový povrch z roztoku vzorku a přenesení elektrody z adsorbovaným analytem do roztoku základního elektrolytu lze využít pro *ex-situ* adsorpční voltametrické stanovení silně se adsorbujících látek i v poměrně komplexních vzorcích, jako jsou rostlinné extrakty, moč a podobně [10,42,43]. Výhodou metody je velmi jednoduchá příprava vzorku, kdy odpadá nutnost extrakce či jiného způsobu oddělení analytu z matrice vzorku.

Tabulka III. Hodnoty směrnic závislostí log $I_p = a + b \log v$ a $E_p = f(\log v)$ některých studovaných látek pro uvedený rozsah polarizačních rychlostí v daném elektrolytu.

Sloučenina	**Směrnice závislosti log I_p vs. log v**	**Rozsah v [mV s^{-1}]**	**Elektrolyt**	**Odkaz**
Fesoterodin	0,49	5-500	BRB pH 7,4 s 50 % CH_3OH	**[1]**
Tolterodin	0,62 (1. pík); 0,74 (2. pík)	10-500	BRB pH 7,0 (H_2O)	**[6]**
	0,50 (1.pík); 0,75 (2. pík)		BRB pH 7,0 s 50 % CH_3OH	
	0,34 (1. pík); 0,23 (2. pík)		CH_3COOHN_4 v CH_3OH	
5-Hydroxymethyl-tolterodin	0,51 (1. pík)	5-500	BRB pH 7,0 s 50 % CH_3OH	**[7]**
Zopiklon	0,71	10-200	BRB pH 4,8 s 50 % CH_3CN	**[5]**
	0,89	300-900		
Berberin	0,83	100-1000	Na_2SO_4 pH 7,0	**[8]**

BRB – Brittonův-Robinsonův pufr

2.2.3 Určování počtu elektronů

Pro popis mechanismů redoxních reakcí je velmi důležitý počet elektronů vyměňovaných mezi donorem a akceptorem. V elektrochemii existuje celá řada postupů na určování počtu elektronů účastnících se elektrodových reakcí. Nejjednodušší se zdá být metoda coulometrická, v níž se měří náboj Q spotřebovaný na kvantitativní přeměnu studované látky v celém objemu vzorku. Ze známého množství látky n lze podle spojeného Faradayova zákona elektrolýzy určit počet elektronů z:

$$n = \frac{Q}{zF} = \frac{It}{zF} \tag{17}$$

kde F je Faradayova konstanta. Coulometrický experiment se obvykle realizuje za konstantního potenciálu, který se volí z oblasti limitního proudu stacionární polarizační křivky studované látky. Problém může nastat v případech, kdy na pracovní elektrodě probíhají spolu s hlavní elektrodovou reakcí ještě další děje (např. následné reakce

(mezi)produktů, reakce elektrolytu nebo rozpouštědla). Ty lze snadno odhalit z nelineárního průběhu závislosti logaritmu proudu registrovaného v průběhu elektrolýzy na čase.

Mechanismus elektrodové reakce v podmínkách coulometrické elektrolýzy, trvající řádově desítky minut, se nemusí vždy shodovat s reakcí pozorovanou při voltametrickém experimentu, který probíhá v časovém měřítku desetin až desítek sekund. Pro tyto případy je vhodnější zjišťovat počet vyměňovaných elektronů analýzou voltamogramů, ať už logaritmickou analýzou stacionárních DC voltametrických vln, porovnáním výšky vlny se standardem (u něhož je počet vyměňovaných elektronů známý, má podobný difúzní koeficient jako studovaná látka a měření je provedeno za stejných experimentálních podmínek) nebo hodnocením šířky diferenčně pulzních voltametrických píků či vzdálenosti maxim reverzibilních katodických a anodických píků v cyklické voltametrii, případně použitím počítačových programů na simulaci cyklických voltamogramů. K přesnému určení počtu elektronů lze využít také porovnání proudů změřených dvojicí ze čtyř metod – chronoamperometrie, cyklické voltametrie, stacionární voltametrie s RDE a stacionární voltametrie na mikroelektrodách [44].

Další možnost určení počtu elektronů poskytuje matematické zpracování voltamogramu pomocí semiintegrace (konvoluce) [45]. Tento proces transformuje voltametrickou *i*-*E* křívku získanou za nestacionárních podmínek DC voltametrií na křivku podobnou stacionární křivce, která je výhodnější pro další vyhodnocení. Výhodou semiintegrační metody zpracování dat je její univerzální použitelnost na reverzibilní i irreverzibilní reakce přenosu náboje, bez ohledu na výskyt následných chemických reakcí. Pomocí tvaru semiintegrovaného voltamogramu lze také diagnostikovat vliv adsorpce na elektrodovou reakci. Semiintegrované voltamogramy (SIV) ve tvaru monotónně se zvyšující sigmoidy poskytují systémy, u nichž je transport látky řízen pouze difúzí, kdežto SIV ve tvaru píku ukazují na vliv adsorpce, přičemž může jít o adsorpci samotné elektroaktivní látky, produktů elektrodové reakce, ale i dalších neelektroaktivních látek inhibujících povrch elektrody [46].

Pro zjištění stechiometrického počtu elektronů účastnících se elektrodové reakce konvoluční metodou je potřeba nejprve převést proudové hodnoty $i(t)$ voltamogramu na bezrozměrná data pomocí vztahu [47]:

$$\Psi(t) = \frac{i(t)}{FAc\sqrt{\frac{DFv}{RT}}} \tag{18}$$

kde $\Psi(t)$ představuje bezrozměrný proud, F je Faradayova konstanta, A – plocha elektrody (cm^2), c – koncentrace látky (mol cm^{-3}), D – difúzní koeficient ($cm^2\ s^{-1}$), v – rychlost polarizace elektrody ($V\ s^{-1}$), R – molární plynová konstanta ($J\ K^{-1}\ mol^{-1}$) a T – termodynamická teplota (K). Následně lze bezrozměrná data semiintegrovat numericky, např. s využitím rovnice [29]:

$$I(t) = I(k\Delta t) = \frac{1}{\sqrt{\pi}} \sum_{j=1}^{j=k} \frac{\Psi(j\Delta t - \frac{1}{2}\Delta t)\sqrt{\Delta t}}{\sqrt{k - j + \frac{1}{2}}} \tag{19}$$

kde $\Psi(k)$ je soubor k bezrozměrných proudových hodnot zaznamenaných v intervalech Δt a j je celé číslo od 1 do k. $\Psi(j\Delta t - \frac{1}{2}\Delta t)$ odpovídá bezrozměrné hodnotě proudu odečtené v polovině intervalu Δt mezi j a j–1. Výška výsledného sigmoidního SIV je rovna počtu vyměňovaných elektronů z. Je zřejmé, že pro správný výpočet hodnoty z je nutné znát plochu elektrody, koncentraci studované látky a její difúzní koeficient. Celý postup zpracování dat (převedení proudu na bezrozměrná data a jejich numerickou semiintegraci) lze provést např. pomocí volně dostupného programu eL-Chem Viewer [47].

Popsaná semiintegrační metoda byla úspěšně použita pro stanovení počtu elektronů při oxidaci fesoterodinu **[1]**. Voltamogram fesoterodinu byl zpracován v programu eL-Chem Viewer (obr. 4). Počet elektronů určený ze semiintegrovaného voltamogramu jako výška vlny je z = 2,01. Velmi dobré shody ve výsledcích bylo dosaženo při coulometrickém stanovení, kdy byl zjištěn počet elektronů z = 1,89.

Semiintegrační metoda byla použita pro stanovení počtu elektronů také při anodické oxidaci pesticidu azoxystrobinu [48] a protizánětlivého léčiva meloxikamu [49] na bórem dopované diamantové elektrodě. U obou látek odpovídaly jejich voltametrické vlny dvou-elektronovým reakcím. V případě azoxystrobinu nebylo možné určit počet elektronů potenciostatickou coulometrií, neboť průběh *I-t* křivky nebyl exponenciální v důsledku vedlejších reakcí probíhajících na pracovní uhlíkové velkoplošné elektrodě. U meloxicamu byl nalezený počet elektronů potvrzen analýzou stacionárních křivek získaných s rotační diskovou elektrodou při různých rychlostech rotace.

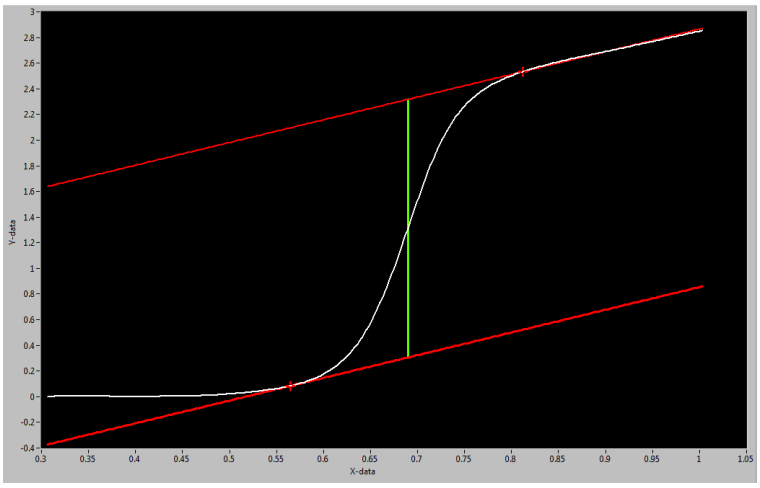

Obr. 4. Semiintegrovaný voltamogram fesoterodinu ($c = 5 \cdot 10^{-5}$ mol dm^{-3}) v Brittonově-Robinsonově tlumivém roztoku o pH 7 s methanolem (1:1, *V*/*V*). Experimentální parametry použité pro převod proudu na bezrozměrné hodnoty: plocha pracovní elektrody ze skleného uhlíku A = 0,077 cm^2, rychlost polarizace pracovní elektrody v = 0,01 V s^{-1}, difúzní koeficient $D = 1{,}45 \cdot 10^{-6}$ cm^2 s^{-1}. Záznam z programu eL-Chem Viewer.

2.2.4 Modelování elektrochemického chování na jednodušších strukturně analogických látkách

K určení redoxně aktivního centra ve složitějších organických molekulách může napomoct srovnání jejich voltametrického chování se strukturně jednoduššími látkami, které obsahují stejný strukturní motiv, jenž je u studované látky podezřelý z redoxní aktivity. Některé rozměrnější molekuly mohou obsahovat více redoxních center. I v tomto případě lze využít jednoduchých modelových látek k prvotnímu odhadu, která z těchto center by mohla reagovat na polarizované elektrodě, případně v jakém pořadí.

Modelování elektrochemického chování pomocí strukturně jednodušších látek jsme v naší laboratoři využili kupříkladu při studiu elektrochemické oxidace benzylisochinolinového alkaloidu berberinu (obr. 5), látky obsažené např. v kořeni a kůře dřišťálu (*Berberis*) a mléku vlaštovičníku většího (*Chelidonium majus*) **[8]**. Berberin poskytuje na elektrodě ze skelného uhlíku v neutrálním prostředí dva voltametrické píky s potenciály maxima kolem 1,2 V a 1,4 V (jsou označeny jako A, B v obr. 6a).

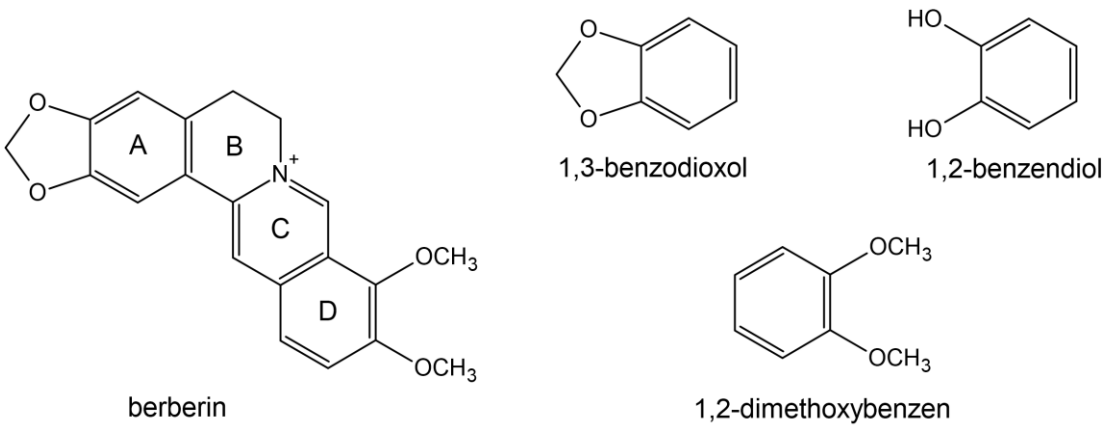

Obr. 5. Strukturní vzorce berberinu a modelových látek 1,3-benzodioxolu a 1,2-dimethoxybenzenu.

Oxidaci berberinu v kyselém a neutrálním prostředí, kde je přítomen ve formě iminiového kationtu (p*K* = 11,7 [50]), lze očekávat na kyslíkových skupinách vázaných na aromatickém jádře, tedy na benzodioxolovém nebo *o*-dimethoxylovém strukturním motivu. DC voltamogramy modelových látek, 1,2-dimethoxybenzenu (veratrolu) a 1,3-benzodioxolu (obr. 5), poskytují anodický proudový signál při potenciálu píku A berberinu za stejných experimentálních podmínek (obr. 6a). V katodickém a následujícím (druhém) anodickém směru polarizace byly u obou modelových látek pozorovány kvazireverzibilní páry píků v méně pozitivní potenciálové oblasti, stejně jako u berberinu píky C – C' a D – D' (obr. 6b). Podobné průběhy voltamogramů naznačují, že elektrochemické oxidaci může u berberinu podléhat jak 1,3-benzodioxolová, tak i 1,2-dimethoxybenzenová část molekuly. Za stejných experimentálních podmínek zaznamenaný voltamogram 1,2-benzendiolu (obr. 6b) ukazuje kvazireverzibilní dvojici píků (oxidace 1,2-benzendiolu na *o*-benzochinon a zpět) ve stejné potenciálové oblasti jako berberin, 1,3-benzodioxol i veratrol. Z toho lze usoudit, že při elektrochemické oxidaci všech tří látek může vzniknout analogické *o*-chinonové uspořádání, redukovatelné v katodickém směru polarizace na příslušný diol, který se reoxiduje v následném anodickém skenu.

Tvorbu benzen-1,2-diolu a *o*-benzochinonu při elektrochemické oxidaci 1,3-benzodioxolového strukturního motivu jsme prokázali metodou EC/MS [51]. LC/MS analýzou roztoku berberinu oxidovaného za konstantního potenciálu 1,4 V jsme zjistili vznik analogického benzen-1,2-diolového derivátu berberinu jako hlavního rozpustného produktu. V menším množství pak byly detekovány *o*-chinonový derivát (vzniklý elektrochemickou oxidací benzodioxolového motivu) a produkt *O*-demethylace 1,2-dimethoxybenzenového kruhu **[8]**. V případě berberinu je tedy hlavním reakčním centrem molekuly 1,3-

benzodioxolový motiv, avšak při vhodné orientaci molekuly berberinu k elektrodovému povrchu dochází k oxidaci i její dimethoxybenzenové části. Pomocí srovnání voltametrického chování berberinu s modelovými látkami se tedy podařilo správně určit obě elektrochemicky aktivní centra v molekule berberinu.

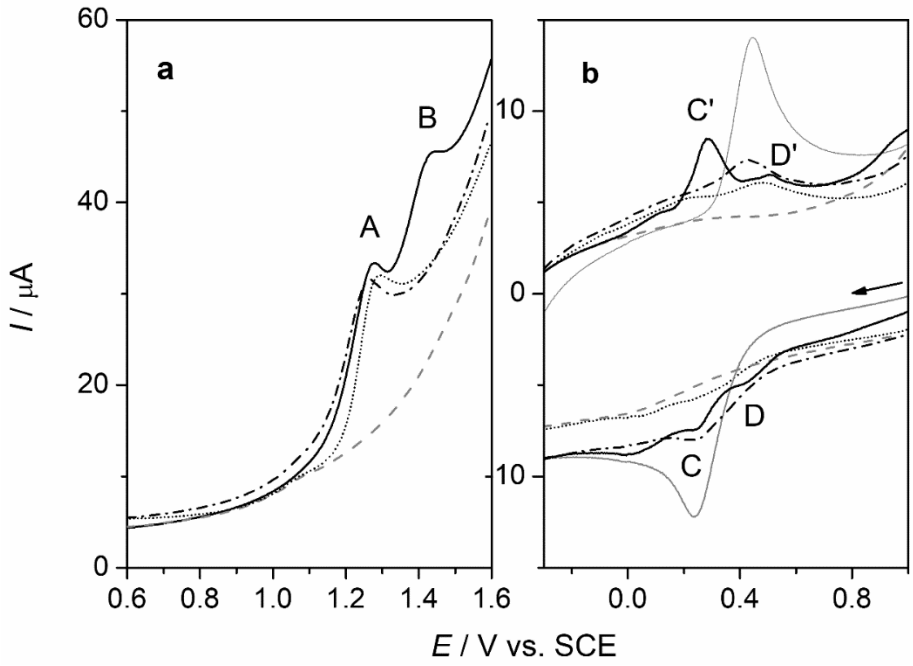

Obr. 6. Porovnání cyklických voltamogramů berberinu (plná čára), 1,3-benzodioxolu (čerchovaná čára) a 1,2-dimethoxybenzenu (tečkovaná čára) v základním elektrolytu 0,02M-Na_2SO_4 (čárkovaná čára). **a** – první anodický sken; **b** – první katodický a druhý anodický sken, přepínací potenciály 1,6 V a -0,4 V; CV 1,2-benzendiolu (šedá plná čára). Koncentrace všech analytů 0,2 mmol dm^{-3}, polarizační rychlost 0,2 V s^{-1}.

Dalším příkladem látky, při jejímž studiu elektrochemické oxidace jsme využili modelových struktur, je xanthohumol (obr. 7). Tato látka ze skupiny prenylovaných flavonoidů je hojně obsažená v chmelu otáčivém (*Humulus lupulus*) **[9]**.

Studie věnované mikrosomální biotransformaci xanthohumolu ukázaly, že oxidačním metabolickým přeměnám podléhá především prenylová skupina. Dalším metabolickým centrem pak je fenolový kruh B [52]. Pro odhalení elektrochemicky aktivních částí molekuly xanthohumolu jsme využili porovnání cyklických voltamogramů této látky s voltamogramy čtyř modelových látek (obr. 8): *p*-kumarové kyseliny (model pro kruh B xanthohumolu s vázanou alkenonovou skupinou), floroglucinolu (pro 2,4-dihydroxy-6-methoxybenzenový kruh A), geraniolu a farnesolu (pro prenylový řetězec vázaný na kruhu A).

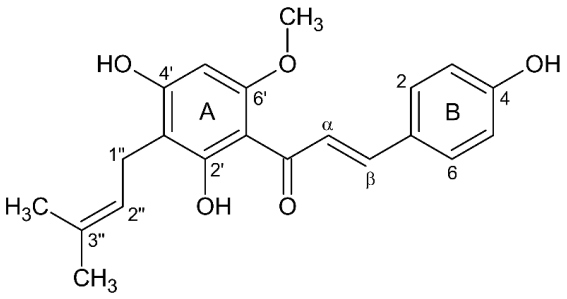

Obr. 7. Strukturní vzorec xanthohumolu.

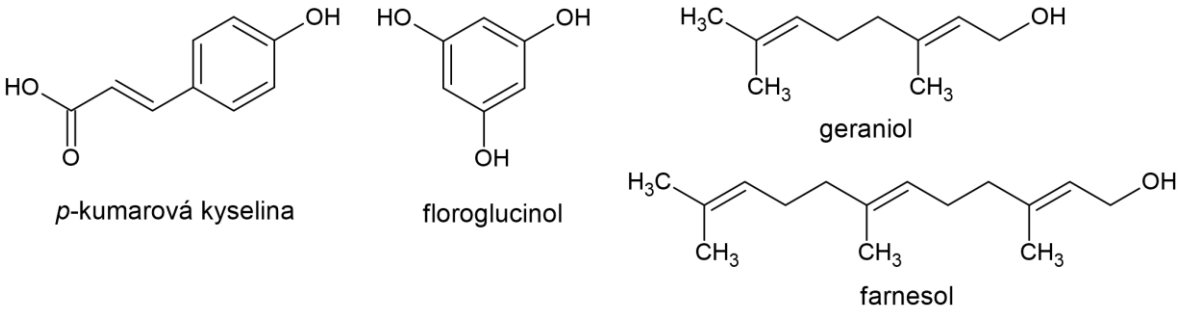

Obr. 8. Strukturní vzorce látek použitých pro modelování elektrochemického chování xanthohumolu.

Cyklický voltamogram xanthohumolu (obr. 9a) ukazuje dva anodické proudové signály při potenciálech 0,7 a 0,85 V, které odpovídají postupné elektrochemické oxidaci. Za stejných experimentálních podmínek poskytují floroglucinol a *p*-kumarová kyselina voltametrický pík při potenciálu velmi blízkém potenciálu první anodické vlny xanthohumolu (obr. 9b,c). Je tedy pravděpodobné, že oba fenolové kruhy xanthohumolu (A i B) by mohly podléhat elektrochemické oxidaci. Naproti tomu geraniol ani farnesol neposkytují ve sledovaném potenciálovém rozmezí 0 V až +1,3 V žádný proudový pík. Z uvedených pozorování lze vyvodit, že prenylová skupina xanthohumolu pravděpodobně je za daných podmínek elektrochemicky inaktivní a oxidovat se mohou fenolové skupiny obou aromatických kruhů.

Platnost závěrů voltametrických srovnávacích experimentů byla potvrzena LC/MS analýzou roztoků xanthohumolu elektrolyzovaných na velkoplošné platinové síťkové elektrodě při potenciálech 0,75 V a 0,90 V. Z monomerních produktů vykazovaly největší intenzitu MS signálu monohydroxylované deriváty xanthohumolu s OH skupinou vázanou na kruhu A a produkty s *o*-chinonovým uspořádáním kruhu A. Vedle monomerních produktů byla detekována řada dimerů xanthohumolu, které vznikly jednoelektronovou oxidací původní molekuly za vzniku fenoxylových radikálů a jejich následnou rekombinací. V identifikovaných produktech byla pozorována dimerace prostřednictvím C-C vazby mezi

kruhy A a B, případně mezi kruhem B a uhlíkem *β* (obr. 7). Intenzity LC/MS píků dimerních produktů byly vyšší v roztocích elektrolyzovaných při nižším potenciálu (odpovídajícím prvnímu anodickému píku), zatímco monomerní produkty měly větší intenzitu odezvy v roztocích oxidovaných při vyšších potenciálech. To je v souladu s výsledky voltametrického studia závislosti potenciálu prvního oxidačního píku xanthohumolu na logaritmu polarizační rychlosti. Hodnota směrnice této závislosti 20 mV při změně rychlosti o 10 mV s^{-1} je typická pro jednoelektronový děj, při kterém je (reverzibilní) přenos elektronu následován dimerizační reakcí [37]. Jednoelektronová reakce přenosu náboje v prvním oxidačním kroku xanthohumolu byla potvrzena logaritmickou analýzou DC-voltametrické křivky **[9]**.

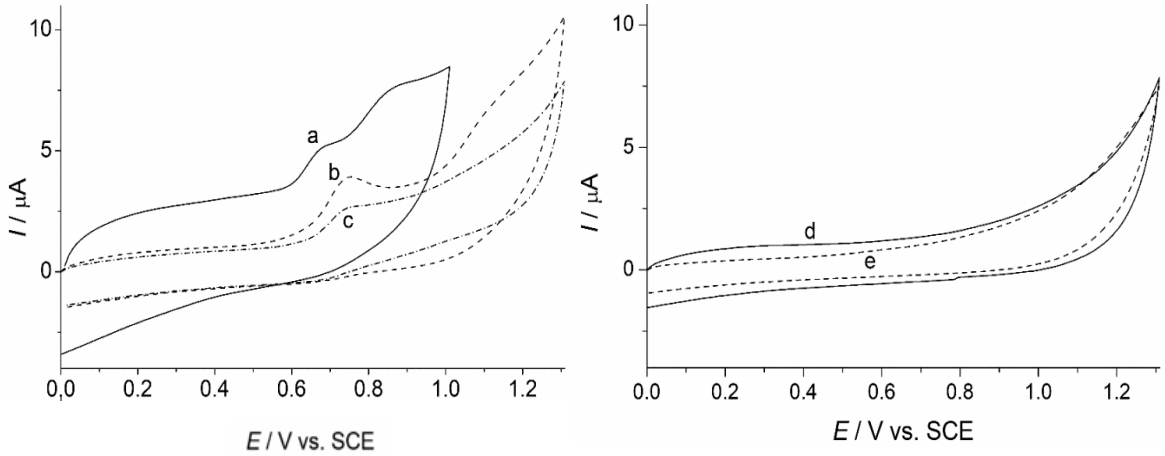

Obr. 9. Cyklické voltamogramy (a) xanthohumolu, (b) floroglucinolu, (c) *p*-kumarové kyseliny, (d) geraniolu a (e) farnesolu v základním elektrolytu (směs 50 mmol dm^{-3} vodného roztoku CH_3COOH/CH_3COONH_4, pH 3,5, a ethanolu 1:1, *V*/*V*), rychlost polarizace elektrody ze skelného uhlíku 0,1 V s^{-1}. Koncentrace depolarizátorů 0,1 mmol dm^{-3}.

Studium elektrochemického chování xanhohumolu s využitím látek modelujících strukturu částí zkoumané molekuly ukázalo, že na rozdíl od metabolických oxidačních reakcí katalyzovaných enzymy cytochromu P450 zůstává prenylová skupina intaktní při elektrochemické oxidaci xanthohumolu v potenciálovém rozsahu do 1,3 V proti nasycené kalomelové elektrodě. Naopak substituovaný floroglucinový kruh A, který se neúčastní metabolických přeměn [52], se velmi ochotně oxiduje elektrochemicky.

2.3 Metody analýzy produktů elektrochemických reakcí

Jak bylo zmíněno v předchozí kapitole, srovnávací voltametrické studium látek s podobnými strukturními motivy dovoluje určit elektrochemicky aktivní centra ve zkoumaných molekulách a v mnoha případech navrhnout strukturu reakčních meziproduktů

či produktů. Potvrzení a identifikaci navržených struktur lze provést analýzou elektrolyzovaných roztoků zkoumaných látek pomocí metod strukturní analýzy, jako jsou infračervená nebo hmotnostní spektrometrie, případně nukleární magnetická resonance. V mnoha případech vzniká při elektrolýze směs meziproduktů a produktů hlavních i vedlejších reakcí (např. následných reakcí se složkami roztoku). V takových případech lze využít výhod spojení separačních metod, zejména chromatografických, s hmotnostní spektrometrií. V následujících kapitolách budou podrobněji popsány některé metody analýzy produktů elektrochemických reakcí využívající jak „off-line“ kombinace elektrolýzy s LC/MS nebo GC/MS, tak „on-line“ spojení elektrochemie s hmotnostní spektrometrií.

2.3.1 Off-line kombinace elektrochemie s LC/MS a GC/MS

Při studiu redoxních přeměn biologicky aktivních látek lze využít preparativní elektrolýzu, při níž se za definovaných podmínek oxiduje či redukuje zkoumaná látka na velkoplošné pracovní elektrodě v roztoku vhodného elektrolytu ve vhodném rozpouštědle. Elektrolytický článek bývá konstruován tak, aby studované reakce na pracovní elektrodě byly odděleny od dějů probíhajících na elektrodě pomocné. Elektrolýza se obvykle provádí za konstantního potenciálu, který se experimentálně určí z polarizační křivky zkoumané látky v daném prostředí. V porovnání s elektrolýzou za konstantního proudu je potenciostatická elektrolýza selektivnější a umožňuje řízeně generovat intermediáty a produkty v různých fázích komplikovanějších elektrochemických reakcí (např. u látek s více redoxně aktivními skupinami), které se mohou na voltamogramech projevovat dvěma nebo více proudovými vlnami.

Velká plocha elektrody zajišťuje efektivní přenos elektronů, a tudíž rychlejší přeměnu látky a získání dostatečného množství produktů pro jejich identifikaci. Klasické elektrolyzéry využívají velkoplošné síťkové platinové elektrody či elektrody ze síťovaného skelného uhlíku, s nimiž se pracuje v roztocích o objemech obvykle 50 – 100 cm^3. Při nedostatku zkoumané látky, např. z důvodu její vysoké ceny, je nezbytné miniaturizovat objem elektrolyzéru i elektrod. V naší laboratoři využíváme pro elektrolýzu trojdílnou elektrochemickou celu (obr. 10), vyrobenou úpravou komerční nízkoobjemové voltametrické nádobky firmy Bioanalytical systems (BASi, West Lafayette, IN, USA). V trojdílné cele jsou všechny tři elektrody umístěny v prostorech vzájemně oddělených skleněnou fritou nebo porézním sklem (Vycor). Porézní rozhraní umožňují přenos iontů

a zajišťují tak elektricky vodivé spojení mezi elektrodovými prostory a zároveň zabraňují rozsáhlejšímu mísení roztoků mezi těmito prostory. Malý objem prostoru pracovní elektrody dovoluje elektrolyzovat objemy 1,0 – 1,5 cm^3 roztoku zkoumané látky o koncentracích typicky 0,05 – 0,50 mmol dm^{-3}. Spotřeba látky na jednu elektrolýzu se tak pohybuje obvykle v řádu desítek μg.

Pro účely elektrolýzy v malých objemech roztoku byly upraveny i konstrukce pracovních elektrod z různých materiálů. Platinová síťková elektroda (obr. 10) má tvar válce o průměru 8 mm a výšce 8 mm s elektroaktivní plochou 11 cm^2 **[1]**. Z uhlíkových elektrod se osvědčily dva konstrukční typy. První typ je tvořen tyčinkou ze spektrálního grafitu o elektroaktivní ploše 5,4 cm^2 **[7]**. Druhý typ je tvořen svazkem uhlíkových mikrovláken spojených měděným drátem, který zajišťuje vodivý kontakt (obr. 13). Štětička uhlíkových vláken vyčnívá ze skleněné kapiláry a tvoří elektrodu (carbon fiber brush electrode, CFBE) s malými geometrickými rozměry a velkým elektroaktivním povrchem (jednotky až desítky cm^2). Rozměry elektrody lze jednoduše upravit podle potřeby použitím různého počtu svazků vláken z uhlíkové tkaniny a různou délkou vláken. Tento typ elektrody může být použit jako sonda pro ASAP-MS analýzu elektrolytických produktů adsorbovaných na povrchu vláken **[4]**, jak podrobněji popisuje kapitola 2.3.3.

Nejčastěji používaným rozpouštědlem pro elektrochemické studium bioaktivních látek, a tedy i pro preparativní elektrolýzu je voda, případně její směsi s acetonitrilem, methanolem nebo ethanolem pro méně polární látky obtížně rozpustné ve vodě. Toto prostředí umožňuje analyzovat elektrolyzované roztoky přímo pomocí spojení kapalinové chromatografie s hmotnostní spektrometrií (LC/MS). Separace se provádí nejčastěji v systému reverzních fází, které se volí podle povahy analytů. Poměrně univerzální jsou stacionární fáze na bázi silikagelu modifikovaného kovalentně vázanými oktadecylovými (C18) nebo oktylovými (C8) skupinami. Pro polárnější bazické látky, např. kvartérní amoniové soli isochinolinových alkaloidů jako je berberin a jeho oxidační produkty, se velmi dobře osvědčila silikagelová fáze s kovalentně vázanými kyano-skupinami **[8]**.

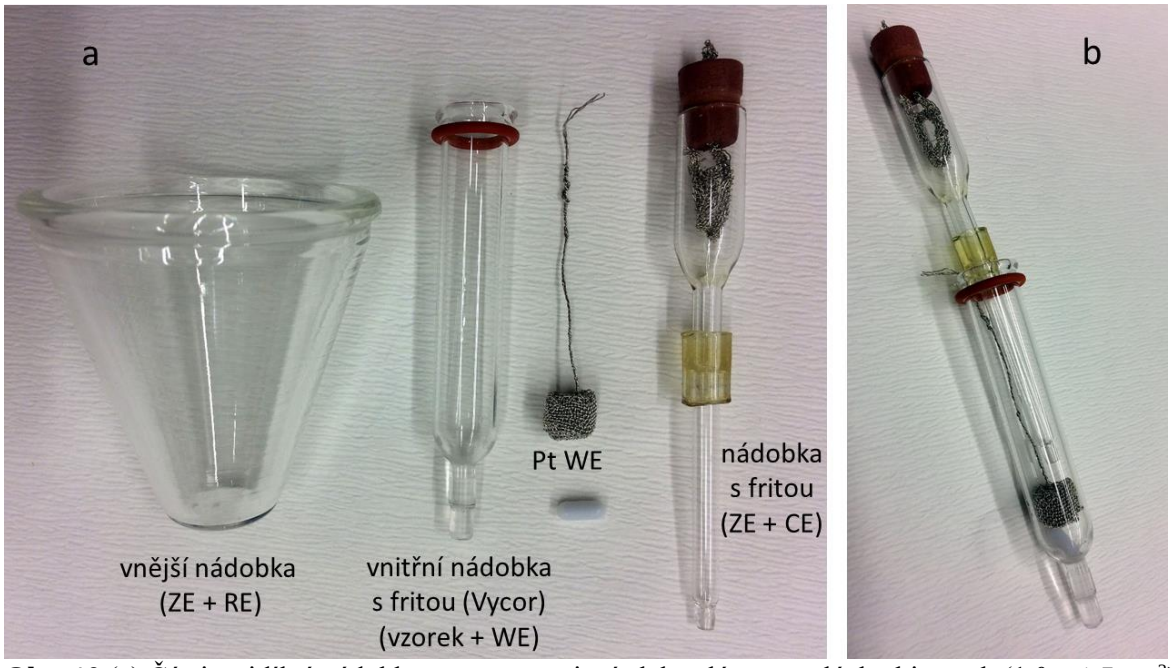

Obr. 10 (a) Části trojdílné nádobky pro preparativní elektrolýzu v malých objemech (1,0 – 1,5 cm^3) s Pt síťkovou elektrodou; (b) Sestava nádobek s pracovní a pomocnou Pt elektrodou. ZE – základní elektrolyt, RE – referenční elektroda (není na obrázku), WE – pracovní elektroda, CE – pomocná elektroda.

Nejběžnějšími ionizačními technikami ve spojení LC/MS jsou ionizace elektrosprejem (ESI) a chemická ionizace za atmosférického tlaku (APCI). Obě tyto ionizační techniky jsou citlivé na vyšší obsah iontových aditiv, jako jsou anorganické soli, kyseliny, báze a pufry používané při elektrolýzách jako podpůrné elektrolyty pro zajištění dostatečné vodivosti roztoku vzorku. Je proto žádoucí elektrolýzy provádět v prostředí těkavých elektrolytů, jako jsou mravenčan či octan amonný, a aciditu podle potřeby upravovat příslušnou těkavou kyselinou (mravenčí nebo octovou) nebo zásadou (amoniakem). Koncentrace elektrolytů by měla být co nejnižší (do 5 – 10 mmol dm^{-3}), neboť vyšší koncentrace iontů významně snižují účinnost ionizace analytů a tedy intenzitu jejich odezvy v hmotnostním spektrometru. Z hlediska identifikace produktů elektrochemických reakcí je velmi výhodné použití hmotnostního analyzátoru s vysokou rozlišovací schopností pro určení elementárního složení analyzovaných látek a s možností kolizně indukované disociace iontů pro určení jejich struktury. To umožňují hybridní hmotnostní analyzátory kombinující např. kvadrupólové analyzátory s analyzátorem doby letu (QqTOF).

Ne vždy je možné najít experimentální podmínky (elektrolyt a jeho koncentrace, acidita roztoku, rozpouštědlo), které by byly vhodné jak pro optimální průběh elektrochemické reakce studované látky, tak pro následnou přímou analýzu elektrolyzovaných vzorků metodou LC/MS. V takovém případě je nutné vzorek před

analýzou upravit použitím vhodných extrakčních technik, jako je extrakce rozpouštědlem nebo extrakce tuhou fází. Jelikož při oxidaci organických látek ve vodném prostředí lze očekávat vznik produktů polárnějších než výchozí méně polární látka (např. hydroxy- a oxo-derivátů, *N*-dealkylovaných aminů), je vhodné použít pro jejich extrakci organická rozpouštědla s vyšší hodnotou relativní permitivity ε_r, s vodou omezeně mísitelná, jako jsou např. octan ethylnatý (ε_r = 6,0; rozpustnost ve vodě 86 g dm^{-3}) nebo chloroform (ε_r = 4,8; rozpustnost ve vodě 10 g dm^{-3}). Extrakt je pak možné odpařit za mírných podmínek, aby nedošlo k odtěkání nebo tepelnému rozkladu analytů a analyzovat po rozpuštění v mobilní fázi metodou LC/MS. Alternativně je možné extrakty analyzovat přímo bez odpaření nebo po odpaření a rozpuštění v jiném rozpouštědle pomocí plynové chromatografie s hmotnostně spektrometrickou detekcí (GC/MS). Do přípravy vzorku pro GC/MS analýzu lze s výhodou zařadit derivatizaci, při níž se analyzované látky chemicky modifikují pro snížení polarity, zvýšení těkavosti a tepelné stability a také pro zlepšení selektivity a citlivosti detekce. Derivatizace může pomoci i při identifikaci produktů elektrolytických reakcí a určení jejich struktury. Značnou výhodou GC/MS metody je možnost využít k identifikaci látek elektronické knihovny hmotnostních spekter. Pro analýzu těkavých látek je velmi užitečná mikroextrace na vlákně v plynné fázi (head-space SPME) kombinovaná s tepelnou desorpcí a GC/MS analýzou. Touto metodou lze detekovat nejen těkavé produkty elektrochemických přeměn xenobiotik, ale i produkty přeměn dalších složek elektrolyzovaných roztoků, např. alkoholů použitých jako rozpouštědla **[3]**.

Preparativní elektrolýza spolu s analýzou reakčních produktů se vedle studia redoxních přeměn xenobiotik a simulace metabolických procesů může uplatnit také v syntéze metabolitů těchto látek [53,54]. Metody syntézy založené na *in vitro* metabolismu zprostředkovaném enzymy cytochromu P450 neumožňují jednoduše získat takové množství metabolitů, které je vyžadováno pro testování toxicity a strukturní charakterizaci např. nukleární magnetickou rezonancí (obvykle v řádu jednotek až desítek mg). Metabolity připravené touto cestou jsou ve složitých směsích a musejí být extenzivně purifikovány. Navíc je problematické izolovat reaktivní produkty I. metabolické fáze, které rychle konjugují (s glutathionem, glukuronovou kyselinou apod.) za vzniku metabolitů II. fáze. Obvykle se proto metabolity připravují organickou syntézou. Preparativní elektrolytické metody nabízejí alternativu pro syntézu metabolitů léčiv. V porovnání s metodami organické syntézy má elektrochemická syntéza některé výhody, např. menší počet reakčních kroků, mírné reakční podmínky, omezené použití organických rozpouštědel a použití poměrně

jednoduchého zařízení. Elektrochemii lze přímo spojit s hmotnostní spektrometrií (EC/MS) pro okamžité monitorování produktů, což usnadňuje optimalizovat reakční podmínky a zároveň umožňuje studovat redoxní přeměny léčiv.

2.3.2 On-line EC/ESI-MS

Na rozdíl od kombinace preparativní elektrolýzy s LC/MS nebo GC/MS analýzou, která využívá elektrolytickou celu jako reaktor ve vsádkovém uspořádání, přímé on-line spojení elektrochemie s hmotnostní spektrometrií (EC/MS) vyžaduje průtokové uspořádání elektrochemického článku. Výhodou průtočného článku je omezení vedlejších a následných elektrodových reakcí, které mohou probíhat v důsledku dlouhodobého kontaktu látky s povrchem pracovní elektrody a které jsou běžné u vsádkových elektrolyzérů. Např. při studiu elektrochemické oxidace fesoterodinu byl v roztocích elektrolyzovaných ve vsádkovém uspořádání identifikován metodou LC/MS produkt s $[M+H^+]$ 426 *m*/*z*, který nebyl pozorován v EC/MS experimentech. Tento produkt vznikal pravděpodobně hydroxylací primárního oxidačního produktu, 5-formylfesoterodinu, při dlouhodobé elektrolýze **[1]**.

Velkou výhodou přímého spojení EC/MS je možnost prakticky okamžitě sledovat v hmotnostním spektru produkty vznikající na pracovní elektrodě, včetně produktů nestabilních, které není možné zachytit při off-line experimentech. Elektrolýza v průtokové cele probíhá obvykle za kontrolovaného potenciálu na pracovní elektrodě – porézní v coulometrické cele nebo planární diskové v tenkovrstvé ampérometrické cele. Potenciál se mění spojitě nebo stupňovitě (obvykle v krocích 20 – 100 mV) v požadovaném rozsahu. Délka potenciálového kroku se volí podle času, za který dojde látka z elektrochemické cely do hmotnostního spektrometru při nastavené průtokové rychlosti (obvykle 2 – 10 µl/min). Hmotnostní spektra se registrují v závislosti na potenciálu pracovní elektrody, který se postupně zvyšuje od hodnot, při nichž nedochází k elektrochemické přeměně studované látky, po hodnoty, kdy se látka elektrochemicky přeměňuje, což se projeví snížením intenzity až ztrátou její odezvy v hmotnostním spektru. Hmotnostní spektra zaznamenaná pro různé hodnoty elektrodového potenciálu lze graficky znázornit tzv. hmotnostními voltamogramy. Pro příklad je na obr. 11 uveden hmotnostní voltamogram zopiklonu. Z něho je patrný postupný pokles intensity signálu protonované molekuly zopiklonu ($[M+H]^+$ *m*/*z* 389) při potenciálu pracovní elektrody nad 0,4 V. Současně se s rostoucím potenciálem objevují

odezvy iontů $[M+H]^+$ oxidačních produktů při *m*/*z* 375 (*N*-demethylovaný zopiklon), 403, 405 a 419.

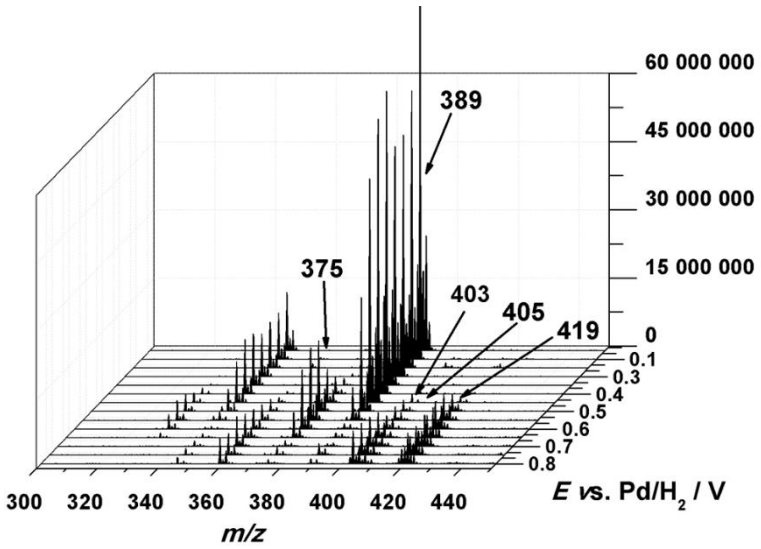

Obr. 11. Hmotnostní voltamogram zopiklonu (c = 0,5 mmol dm^{-3}), získaný v on-line spojení EC/ESI-MS. Základní elektrolyt: vodný roztok octanu amonného (pH 6,8) / acetonitril (1:1, *V*/*V*), porézní uhlíková pracovní elektroda, rychlost průtoku 8 µl min^{-1}. Kladný mód ESI.

Použití elektrospreje jako ambientního iontového zdroje je velmi vhodné pro spojení s elektrochemií, podobně jako pro spojení s LC nebo kapilární elektroforézou. Při použití ESI v on-line EC/ESI-MS je však nutné si uvědomit, že v tomto zdroji může docházet k elektrochemickým reakcím analytu, tedy k oxidaci nebo redukci. ESI se chová jako průtokový elektrochemický článek za konstantního proudu [55-57]. V kladném ionizačním módu (ESI+) dochází k oxidaci na hrotu sprejovací kapiláry, která představuje v galvanostatickém článku pracovní elektrodu (anodu) a k redukci na vstupu do MS, který představuje protielektrodu (katodu). V záporném módu (ESI-) je naopak katodou hrot sprejovací kapiláry a hmotnostní spektrometr je anodou. Na rozdíl od tradičního elektrochemického článku neprobíhá v ESI zdroji přenos náboje v roztoku, ale v proudu nabitých kapiček pohybujících se za atmosférického tlaku mezi sprejovací jehlou a protielektrodou. Proud dosahuje maximálních hodnot kolem 1 µA a frekvence asi 300 kHz v důsledku rychlosti tvorby nabitých kapiček [58]. Redoxní reakce analytů v elektrochemickém článku iontového zdroje mohou v některých případech komplikovat detekci a identifikaci produktů vznikajících v elektrochemické cele. [59,60].

Podobně jako pro off-line kombinaci elektrolýzy s LC/MS, i pro on-line spojení EC/ESI-MS jsou vhodnými rozpouštědly voda, methanol, ethanol a acetonitril a vhodnými podpůrnými elektrolyty těkavé kyseliny, zásady nebo jejich soli (např. octová a mravenčí

kyselina, amoniak, octan amonný) v dostatečně nízkých koncentracích, aby nedocházelo k potlačení ionizace molekul analytu v ESI. Přítomnost elektrolytů, stejně jako rozpouštědla a případných nečistot komplikuje ESI-MS spektra, která často obsahují aduktové ionty (např. $[M+NH_4]^+$, $[M+Na]^+$, $[M+K]^+$, $[M+CH_3COO]^-$), ionty klastrů s rozpouštědlem (např. $[M+H_2O+H]^+$, $[M+CH_3CN+H]^+$) a dimerní ionty (např. $[2M+H]^+$, $[2M+Na]^+$). Ačkoliv signály těchto iontů ESI-MS spektra komplikují, mohou být na druhou stranu využity k jednoznačnému určení molekulové hmotnosti analytu [56]. Menší citlivost na přítomnost stop iontů alkalických kovů vykazuje iontový zdroj APCI (chemická ionizace za atmosférického tlaku). APCI-MS spektra bývají jednodušší, bez signálů iontů aduktů s alkalickými kovy a dimerních iontů [61].

Elektrolyty mohou v on-line spojení EC/ESI-MS rovněž poskytovat vedlejší reakce s meziprodukty elektrochemických reakcí. Například při elektrochemické oxidaci pentabromfenolu na platinové amperometrické elektrodě v prostředí mravenčanu amonného (pH 6) při potenciálu +1,0 V (proti Pd/H_2) byla pozorována tvorba tetrabromnitrofenolu ($[M-H]^-$ m/z = 449,6720) **[2]**. Tento produkt byl v mnohem menším množství detekován pomocí LC/MS i při off-line experimentech po dvouhodinové elektrolýze ve stejném prostředí na platinové síťkové elektrodě při 1 V. Po delší elektrolýze za vyššího potenciálu (20 h při 1,4 V) signál tohoto produktu vymizel pravděpodobně v důsledku nízké stability produktu. Reakce s amoniakem jako složkou elektrolytu byla pozorována také při oxidaci zopiklonu v EC/MS systému **[5]**. V alkalickém roztoku octanu amonného a amoniaku o pH 9,5 s 50 % acetonitrilu byl od potenciálu 0,6 V (proti Pd/H_2) výše pozorován vznik produktu s $[M+H]^+$ m/z 420, obsahujícího kovalentně vázaný dusík z amoniaku, pravděpodobně ve formě nitroso- nebo nitroskupiny.

V průtokovém uspořádání elektrochemického článku v EC/MS je pracovní elektroda neustále omývána roztokem elektrolytu, který obsahuje kromě vody vždy určité množství organického rozpouštědla (acetonitrilu, methanolu). Tyto podmínky částečně zabraňují pasivaci povrchu elektrody. Přesto látky, které tvoří elektrochemickou reakcí oligomerní až polymerní produkty, mohou pasivovat elektrodový povrch v průběhu EC/MS experimentu, což se projeví postupným snižováním signálu elektrochemicky generovaných produktů v MS. Například při EC/MS studiu elektrochemické oxidace 2-bromfenolu byl při testování vlivu průtokové rychlosti na intenzitu odezvy iontu dimerního oxidačního produktu s m/z 342,8 pozorován pokles odezvy o jeden a půl řádu při snížení rychlosti z 9 µl min^{-1} na

3 µl min^{-1}. Při opětovném zvyšování průtokové rychlosti signál klesl o další dva řády (obr. 12) **[2]**.

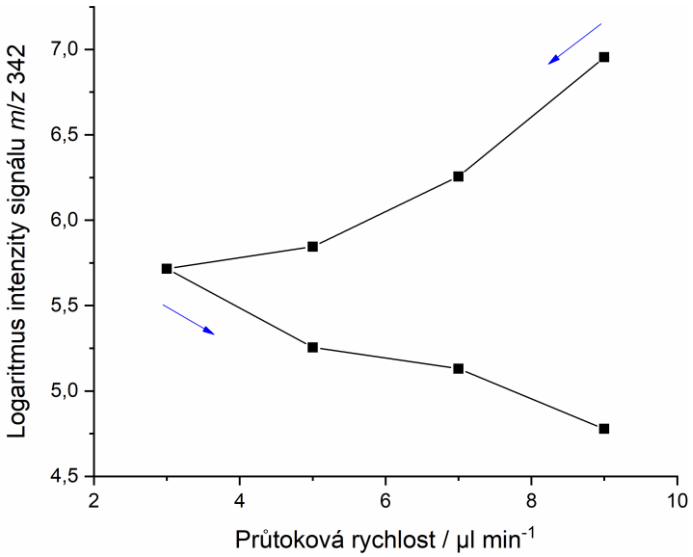

Obr. 12. Závislost logaritmu intenzity iontu dimerního produktu oxidace 2-bromfenolu (*m*/*z* 342,8) na průtokové rychlosti v EC/MS. Roztok obsahoval 0,2 mmol dm^{-3} 2-bromfenolu ve směsi methanol/mravenčan amonný o pH 6 (9:1), potenciál pracovní Pt elektrody v ampérometrické průtokové cele byl nastaven na 1 V (vs. Pd/H_2). Šipky znázorňují směr změny průtokové rychlosti. **[2]**

2.3.3 Uhlíková štětičková elektroda jako substrát pro ASAP-MS

Studium mechanismů elektrochemických přeměn biologicky aktivních látek bývá často komplikováno adsorpcí reakčních (mezi)produktů na povrchu elektrody. Produkty, které jsou špatně rozpustné a silně adsorbované na elektrodě, bývá obtížné až nemožné detekovat v elektrolyzovaných roztocích. K takovým produktům se řadí například látky oligomerního či polymerního charakteru, které vznikají rekombinací elektrochemicky generovaných radikálů. Přímá analýza elektrochemicky generovaných látek adsorbovaných na elektrodových površích není v současnosti příliš rozšířena. Proto byla na našem pracovišti pro tyto účely vyvinuta elektroda speciální konstrukce inspirovaná sondou pro analýzu pevných látek za atmosférického tlaku (Atmosperic Solids Analysis Probe, ASAP). Klasická ASAP-MS sonda je tvořena skleněnou tyčinkou, na kterou se nanese pevný či kapalný vzorek a pomocí speciálního držáku se zavede do iontového zdroje, kde se vzorek desorbuje horkým desolvatačním plynem (dusíkem), ionizuje korónovým výbojem a analyzuje v hmotnostním spektrometru. Elektroda zkonstruovaná pro účely elektrochemického generování produktů, jež zůstávají silně adsorbovány na jejím povrchu (uhlíková štětičková elektroda, carbon fiber brush electrode, CFBE), je tvořená svazkem uhlíkových vláken spojených elektrickým kontaktem (měděným drátem) a částečně vsunutým do skleněné

kapiláry jako elektricky nevodivého pouzdra (obr. 13) **[4]**. Tloušťka svazku uhlíkových vláken (tloušťka jednoho vlákna je cca 5–7 μm, počet vláken ve výsledné štětičce se pohybuje v řádu desítek tisíc) je volena tak, aby upevnila štětičku ve skleněné kapiláře a zabránila jejímu pohybu ven či dovnitř. K upevnění nebylo použito lepidlo, aby se předešlo nežádoucím interferencím při ASAP-MS analýze.

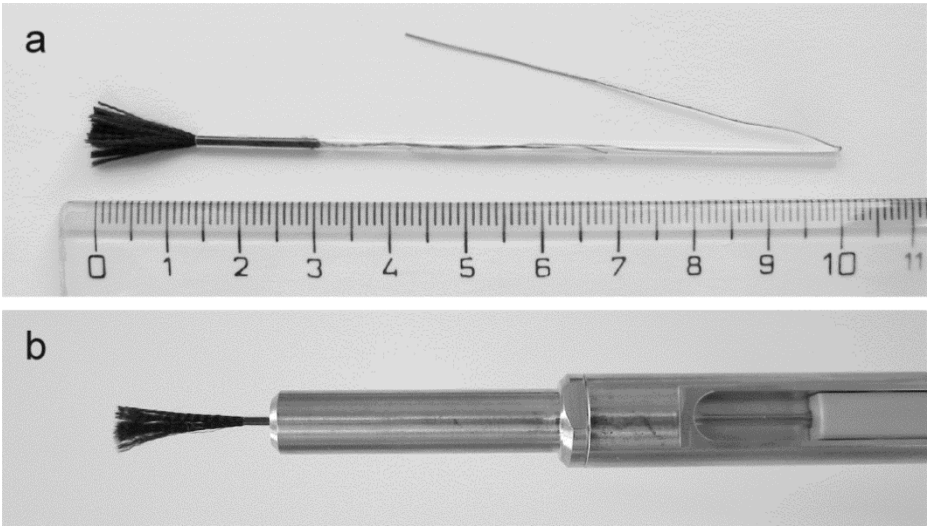

Obr. 13. a) Uhlíková štětičková elektroda (CFBE); b) CFBE v držáku ASAP sondy.

Velmi důležitým krokem je elektrochemická úprava povrchu CFBE před použitím k elektrolytickému generování a nahromadění cílových analytů (tj. produktů elektrochemické reakce zkoumané látky). Úprava spočívá ve střídavé polarizaci elektrody ponořené do roztoku zředěné kyseliny sírové (0,1 mol dm^{-3}) v rozsahu od -1,0 V do +1,5 V proti SCE (50 cyklů při 0,5 V s^{-1}) a následném důkladném vymáchání uhlíkové štětičky v redestilované vodě. Proces cyklické polarizace, při níž se na povrchu vláken střídavě vylučují plynný vodík a kyslík, naruší hladkou strukturu vlákna a zvětší tak jeho povrch (dva- až pětkrát). AFM snímky odhalily na povrchu elektrochemicky aktivovaných uhlíkových vláken zrnité útvary o průměru několika desítek až stovek nm a výšce do 20 nm. Pomocí cyklické voltametrie v roztoku 5 mM-$K_3Fe(CN)_6$ a 5 mM-$K_4Fe(CN)_6$ v 1 M-KCl (se známými hodnotami difúzních koeficientů D_O = 7,17 · 10^{-6} cm^2 s^{-1}, D_R = 6,56 · 10^{-6} cm^2 s^{-1} při 25 °C [62]) a výpočtem z Randles-Ševčíkovy rovnice (9) bylo zjištěno, že celková elektroaktivní plocha aktivované štětičkové elektrody s délkou volných vláken 1,3 cm se pohybuje kolem 20 cm^2, což je přibližně 40 krát více oproti válcové elektrodě ze skelného uhlíku o stejné délce (1,3 cm) a stejném průměru 1,3 mm (vnitřní průměr skleněného pouzdra CFBE). Veliký povrch CFBE je velmi žádoucí vzhledem k následné MS analýze,

neboť lze očekávat, že se na něm zadrží větší množství elektrolytických produktů a získá se tak vyšší odezva analyzovaných látek.

Podobně jako u jiných metod spojení elektrochemie s hmotnostní spektrometrií, i v případě ASAP-MS s CFBE je žádoucí provádět elektrolýzu v roztocích těkavých elektrolytů, jako jsou octan nebo mravenčan amonný. Důležitým parametrem je teplota odpařování vzorku v iontovém zdroji. Pro analýzu oligomerních produktů oxidace tribromfenolu a pentabromfenolu se z hlediska dosažení maximální intenzity odezvy analytů nejlépe osvědčila teplota 400 °C **[4]**. Pro jiné aplikace lze ale použít i vyšší teplotu (až 600 °C).

3 Vybrané příklady studovaných xenobiotik

Studium redoxních přeměn biologicky významných látek je již řadu let jedním z výzkumných směrů na Katedře analytické chemie. V této kapitole se budu věnovat dvěma skupinám xenobiotik studovaných v posledním desetiletí. První skupinou jsou bromfenoly, látky rozšířené v celé biosféře ať už jako sekundární metabolity mořských organismů nebo jako průmyslové chemikálie používané při výrobě bromovaných zpomalovačů hoření či fungicidů. Druhá skupina studovaných látek zahrnuje léčiva využívaná v terapii hyperaktivního močového měchýře (antimuskarinika), nespavosti (zopiklon), tišení bolesti a anestezii (fentanyly) nebo v tradiční čínské a ajurvédské medicíně (berberin).

3.1 Bromované fenoly

Fenoly obecně jsou látky snadno podléhající oxidaci. Mechanismus elektrochemické oxidace je komplikován řadou následných chemických reakcí v závislosti na experimentálních podmínkách, jako je prostředí (rozpouštědlo, acidita), materiál a potenciál pracovní elektrody, koncentrace fenolu apod. [63] Jednoelektronová anodická oxidace fenolů vede k tvorbě fenoxylových radikálů a následné tvorbě dimerů prostřednictvím vazeb C-O-C nebo C-C, v závislosti na reakčních podmínkách. Proces elektropolymerace fenolů vede velmi často k pasivaci povrchu elektrod polymerními filmy produktů. Za určitých podmínek, zejména v kyselém prostředí, vznikají ztrátou dvou elektronů reaktivní fenoxoniové kationty, které podléhají reakcím s nukleofily za vzniku monomerních chinonů či dienonů.

Přestože elektrochemii fenolů byla věnována značná pozornost, poměrně málo informací lze v literatuře nalézt o elektrochemickém chování a produktech elektrochemických reakcí bromfenolů (BP) [64,65]. Tato rozsáhlá skupina látek zahrnuje jak sloučeniny přírodního původu syntetizované zejména mořskými organismy [66-68], tak substance produkované průmyslově a používané např. při výrobě zpomalovačů hoření a pesticidů. Rozsáhlé používání zejména bromovaných zpomalovačů hoření vede ke značnému znečištění životního prostředí jejich degradačními produkty, zejména jednoduššími BP a produkty jejich oxidace. Studium elektrochemické oxidace a jejích produktů může poodhalit reaktivitu BP a modelovat transformace, k nimž by mohlo za určitých podmínek docházet v ekosystému.

V naší laboratoři byla studována série monobromovaných fenolů (2-BP, 3-BP a 4-BP), 2,4,6-tribromfenolu (2,4,6-TBP) a pentabromfenolu (PBP) [**3**,69]. Počet atomů bromu na benzenovém jádře a jejich pozice mají významný vliv na fyzikální a chemické vlastnosti BP. S rostoucím počtem atomů bromu rostou nejen jejich teploty tání a varu, ale také lipofilita a kyselost fenolového vodíku (Tab. IV). Redox potenciál BP, vyjádřený jako potenciál DC-voltametrického píku E_p (Tab. IV) závisí na aciditě roztoku, což značí, že se elektrochemického děje účastní protony. V řadě monobromfenolů hodnoty E_p korelují s hodnotami disociačních konstant. Kladný mezomerní efekt atomu bromu vázaného v pozicích *ortho*- nebo *para*- k fenolové skupině zvyšuje elektronovou hustotu na aromatickém jádře a usnadňuje oxidaci fenolu, která tak probíhá při nižším potenciálu než oxidace *m*-bromfenolu.

Tabulka IV. Fyzikálně-chemické vlastnosti bromfenolů (relativní molekulová hmotnost, teplota tání (t_t), teplota varu (t_v), disociační konstanta kyseliny (pK_a), rozdělovací koeficient v systému oktanol-voda (log K_{ow}) a potenciál DC-voltametrického píku (c_{BP} = 0,1 mmol dm^{-3}) při pH 7 na GCE proti Ag/AgCl/1M-KCl (v = 0,1 V s^{-1}).

Bromfenol	M_r	t_t [°C]	t_v [°C]	pK_a	log K_{ow}	E_p [V]
2-BP	173,01	5,6[a]	194[b]	8,40[e]	2,35[c]	0,673
3-BP	173,01	33[b]	235-236[c]	8,90[e]	2,63[c]	0,724
4-BP	173,01	64[b]	238[c]	8,25[e]	2,62[d]	0,663
2,4,6-TBP	330,80	94-96[c]	244[b]	6,08[d]	4,24[d]	0,585
PBP	488,59	230[a]	sublimuje[a]	4,40[d]	5,30[d]	0,626

[a] [70]; [b] [71]; [c] [72]; [d] (při 25 °C) [73]; [e] (při 25 °C) [74]

Cyklická voltametrie odhalila při oxidaci BP tvorbu elektrochemicky aktivních (mezi)produktů, které se projevily v následném katodickém a druhém anodickém skenu dvojicemi píků s nižšími potenciály, než měl anodický pík v prvním skenu (obr. 14). Při opakovaných cyklech proudy píků nových látek (II a III) narůstaly, zatímco pík oxidace původního BP (pík I) se snižoval (obr. 14b). Toto chování je typické pro elektropolymeraci. Potenciály píků v oblastech označených III odpovídají přibližně oblasti reverzibilní elektrochemické reakce benzochinonů, jak ukázalo porovnání cyklických voltamogramů BP a tetrabrom-1,4-benzochinonu **[2]**.

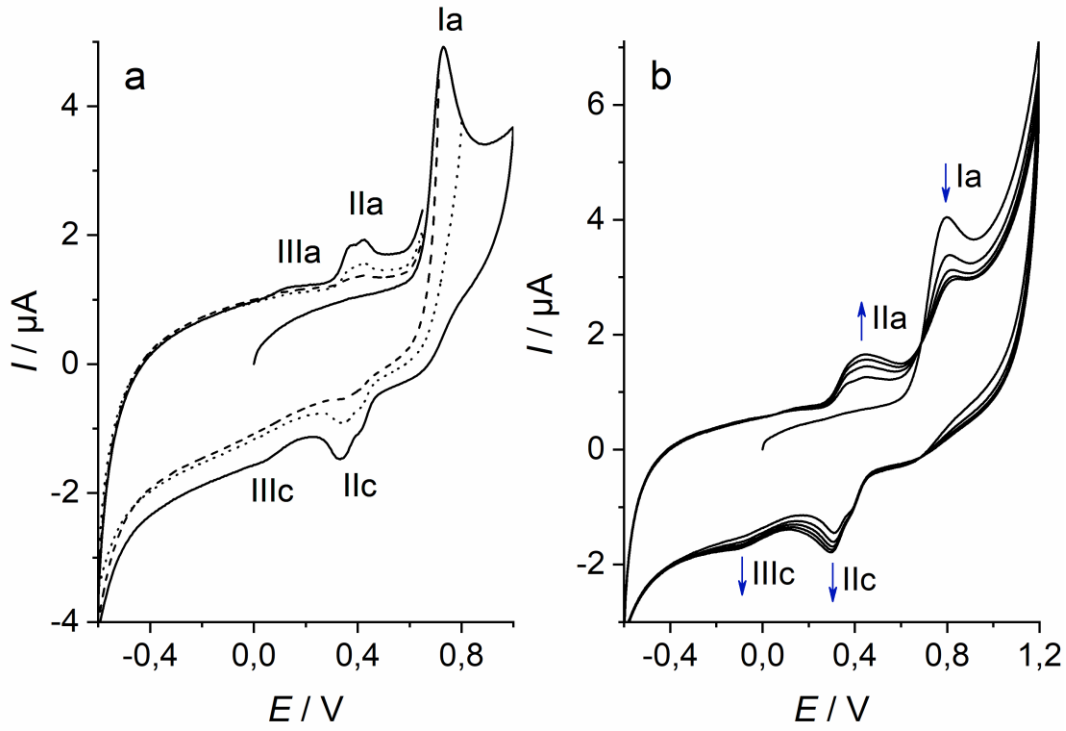

Obr. 14. Cyklické voltamogramy 2-BP (0,1 mmol dm^{-3}) v prostředí methanol/mravenčanový pufr pH 6 (9:1, *V*/*V*) a) při přepínacích potenciálech: 0,7 V (---), 0,8 V (····) a 1,0 V (—); b) při pěti opakovaných cyklech (šipky naznačují změny proudu píků v následných skenech), rychlost polarizace 0,5 V s^{-1} **[2].**

Analýza produktů elektrochemické oxidace BP v roztocích elektrolyzovaných při konstantním potenciálu na platinové síťkové elektrodě ve vodně-alkoholových roztocích (pH 6) byla provedena pomocí LC/MS, GC/MS a přímého spojení EC/MS **[2]**. Pro analýzu produktů adsorbovaných na povrchu elektrody byla použita CFBE a ASAP-MS **[4]**. Metodou LC/MS byly detekovány dva izomerní dimerní a několik trimerních produktů oxidace 2-BP a 4-BP, pět izomerních oxidačních produktů 3-BP a jeden dimerní produkt oxidace PBP. Fenoxylové radikály vznikající jednoelektronovou anodickou oxidací se spojují jak vazbou C-C, tak vazbou C-O-C. Schémta 1 a 2 znázorňují tvorbu dimerů z různých rezonančních struktur fenoxylových radikálů (1) – (3). Při déle trvající elektrolýze za vyššího potenciálu dochází k vedlejším reakcím, které vedou k odštěpení atomu bromu z dimerních oxidačních produktů.

Schéma 1:

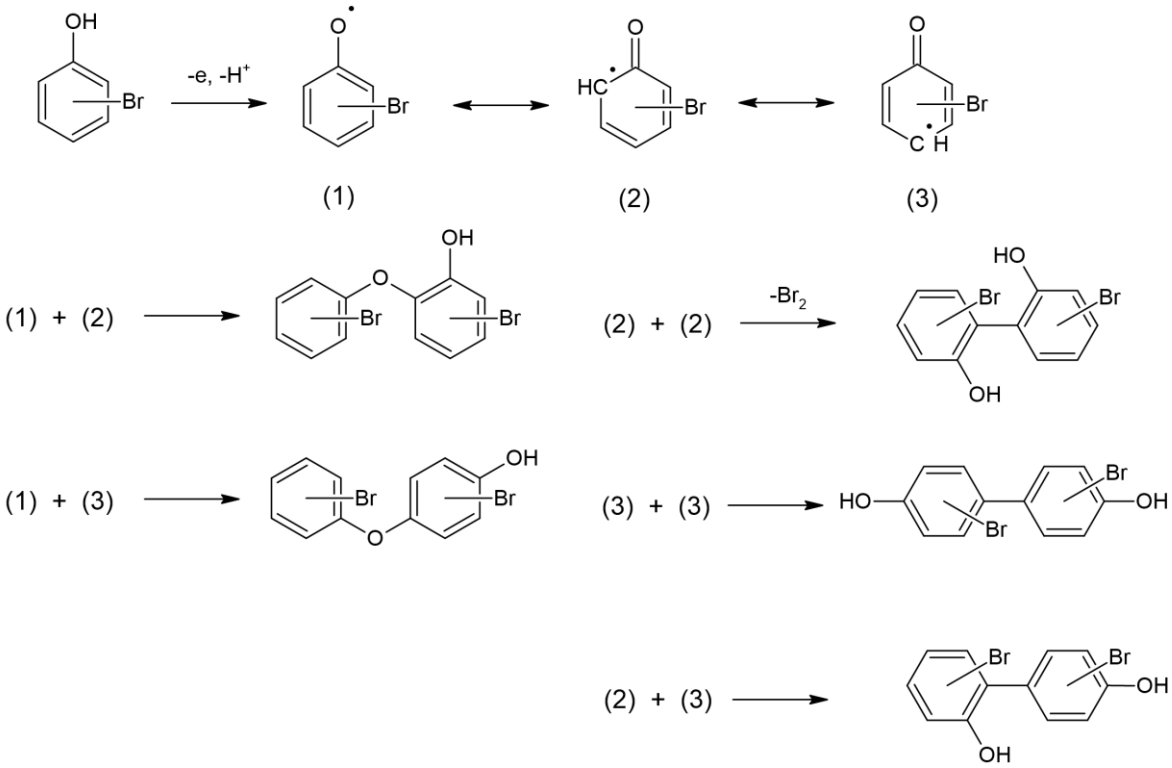

Schéma 2:

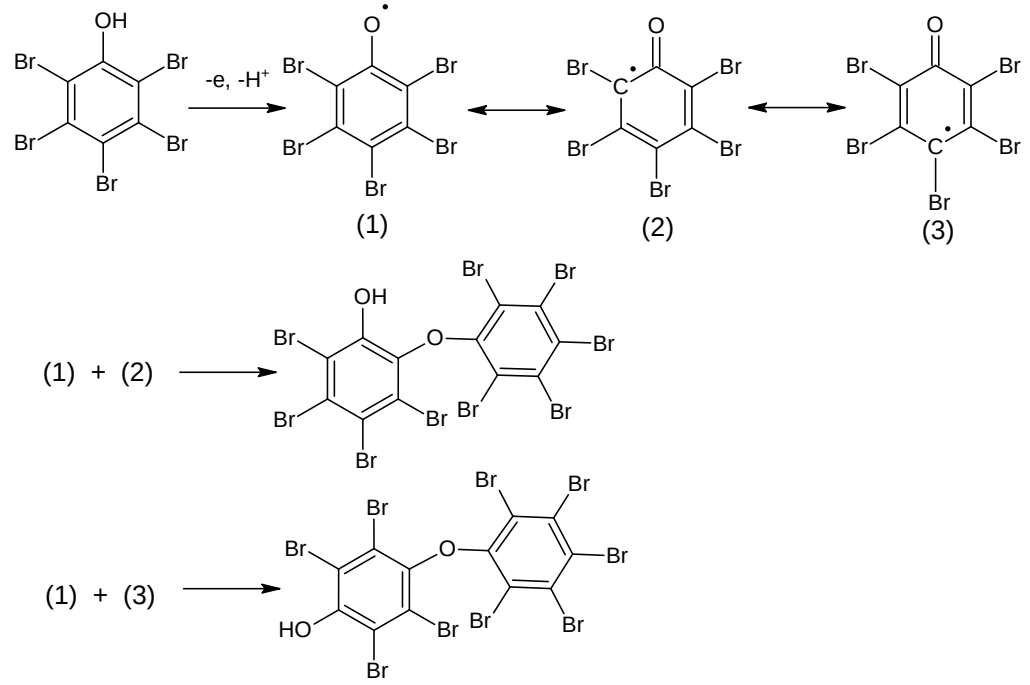

Detekce chinonů pomocí LC/MS může být problematická. Jak ukázal experiment se standardem tetrabrom-1,4-benzochinonu, dochází v prostředí mobilní fáze obsahující mravenčí kyselinu k redoxní reakci, při které přechází benzochinon na redukovanou hydrochinonovou formu **[2]**. To komplikuje analýzu oxidačních produktů BP, mezi nimiž se

chinony obvykle nacházejí. Detekce produktů s chinonovou strukturou byla úspěšná pomocí GC/MS analýzy elektrolyzátů po extrakci octanem ethylnatým. Touto metodou byly mezi produkty elektrochemické oxidace 2,4,6-TBP nalezeny vedle výše zmíněných bromovaných difenylů a difenyletherů také deriváty benzochinonu, a to jak monomerní (obr. 15, struktury ***1*** a ***3***), tak dimerní (***2***). Některé produkty obsahovaly alkoxylové skupiny z alkoholu použitého jako rozpouštědlo (methanol, ethanol, propan-1-ol, butan-1-ol, obr. 15, struktury ***3***, ***4***, ***5*** a **6**) **[3].** Přítomnost uvedených produktů dokazuje adici nukleofilu (vody, resp. příslušného alkoholu) na elekrondeficitní oxidovanou strukturu (fenoxoniový kation). Sloučenina se strukturou ***4*** substituovaná butylem v této studii nebyla detekována.

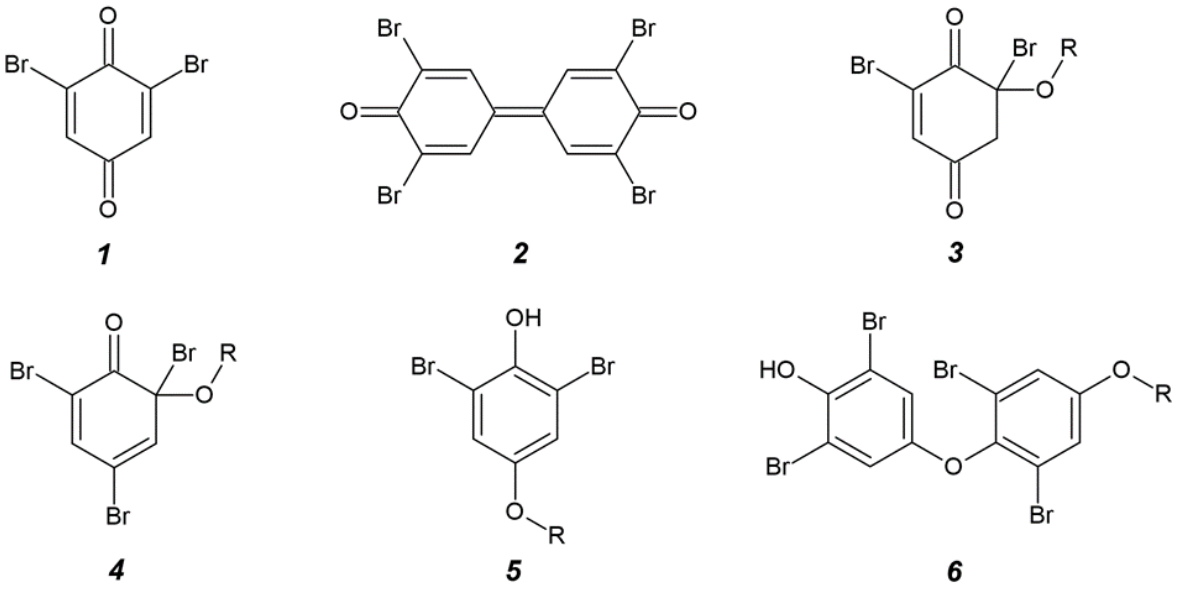

Obr. 15. Struktury produktů elektrochemické oxidace 2,4,6-tribromfenolu v roztocích Brittonova-Robinsonova pufru (pH 6) s 90% obsahem alkoholu (methanol, ethanol, propan-1-ol, butan-1-ol). R = CH_3, C_2H_5, C_3H_7, C_4H_9 **[3].**

Analýzou elektrodového povrchu metodou ASAP-MS byly identifikovány nové dimerní a oligomerní produkty elektrochemické oxídace 2,4,6-TBP a PBP (obr. 16 a 17). Většina z nich, s výjimkou struktury ***9***, nebyla detekována v elektrolyzovaných roztocích těchto dvou BP **[4]**. CFBE jako sonda pro ASAP-MS se tedy ukázala být velmi účinným nástrojem jak pro analýzu látek silně adsorbovaných na elektrodový povrch, které jsou nerozpustné, a tudíž nedetekovatelné v elektrolyzovaných roztocích, tak i látek obtížně analyzovatelných jinými detekčními technikami, k nimž patří deriváty benzochinonů. Technika ASAP-MS s CFBE poskytla výsledky komplementární k výsledkům GC/MS a LC/MS analýz elektrolyzovaných roztoků. Potvrdila u vícebromovaných fenolů elektropolymeraci a spojování oxidovaných molekul jak přes C-O-C vazby, tak i přes C-C

vazby za odštěpení atomu bromu a vzniku bifenochinonů (***7***, ***8***, ***13***, ***15***, ***16***), které nebyly detekovány v roztocích.

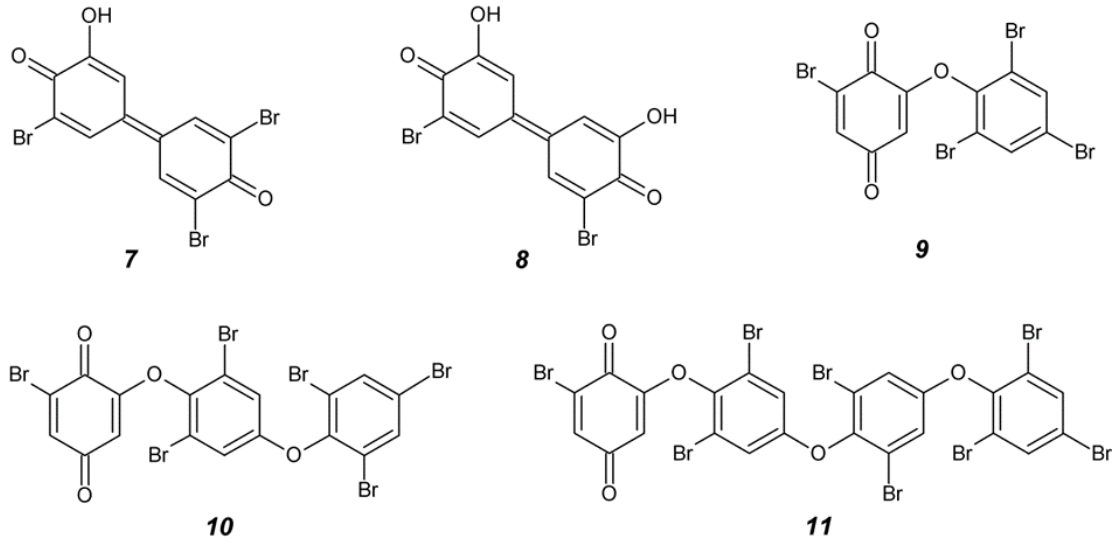

Obr. 16. Navržené struktury produktů elektrochemické oxidace 2,4,6-tribromfenolu adsorbovaných na povrchu pracovní CFBE, nalezených metodou ASAP-MS **[4].**

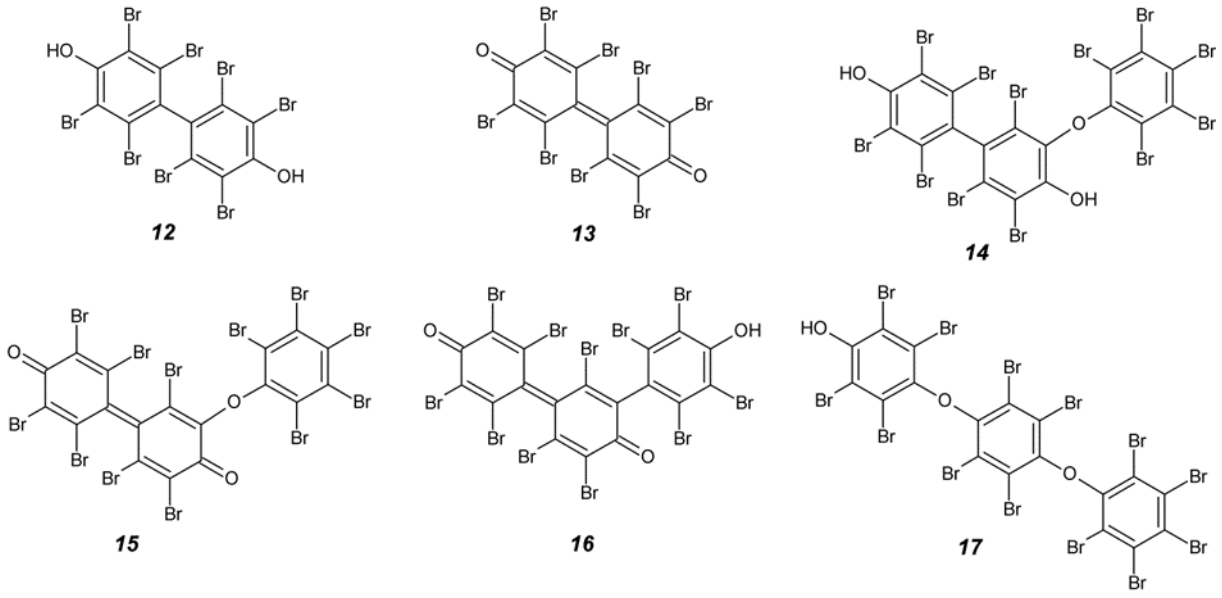

Obr. 17. Navržené struktury produktů elektrochemické oxidace pentabromfenolu adsorbovaných na povrchu pracovní CFBE, nalezených metodou ASAP-MS **[4].**

Hledání produktů oxidace BP není důležité jen z pohledu zkoumání mechanismu analyticky využitelných elektrochemických reakcí, ale také z toxikologického a ekologického hlediska. Produkty oxidační degradace těchto polutantů mohou představovat vážnou hrozbu pro lidské zdraví i zdraví dalších živočichů. Např. bylo prokázáno, že polybromované difenyletherchinony (analogy struktury ***9***) se kovalentně váží na DNA

a mohou tak být příčinou nežádoucích mutací a kancerogeneze [75] Podobně 2,6-dibromhydrochinon (redukovaná forma sloučeniny ***1***), který je produktem oxidativní debromace TBP, reaktivním metabolitem tetrabrombisfenolu A a také pesticidu bromoxynilu, prokazatelně způsobuje v kombinaci s ionty Cu^{2+} oxidativní poškození DNA indikované tvorbou 8-oxodeoxyguanosinu [76].

Elektrochemická oxidace BP vede v řadě případů ke stejným produktům jako oxidace chemická pomocí oxidačních činidel [77,78], fotochemická iniciovaná UV-zářením [79,80], nebo enzymatická při metabolických procesech. Jak bylo rozsáhle studováno u bromovaných difenyletherů [81-85], jaterní enzymy systému cytochromu P450 katalyzují oxidativní hydroxylaci za vzniku hydroxylovaných metabolitů, které jsou reaktivnější a potenciálně toxičtější než mateřské sloučeniny. Bylo prokázáno, že hydroxylované polybromované difenylethery se kompetitivně váží na řadu proteinů, např. na transthyretin, odpovědný za transport thyroxinu [86,87], inhibují enzym aromatázu katalyzující syntézu estrogenů [88], narušují oxidativní fosforylaci a vykazují cytotoxicitu způsobenou přerušením mitochondriálního řetězce přenosu elektronů [89,90]. Experimenty s krysími jaterními mikrosomy prokázaly katalytickou hydroxylaci 4-BP na 4-bromkatechol, který se snadno oxiduje např. superoxidovým aniontem na odpovídající chinon, příp. semichinon, který se kovalentně váže na mikrosomální proteiny [91]. U ryb vystavených působení 2,4,6-TBP a hydroxylovaných difenyletherů bylo pozorováno poškození a malformace embryí [92].

Z uvedených příkladů je zřejmý význam a praktický dopad studia oxidačních přeměn BP. Elektrochemické studie mohou modelovat degradační procesy probíhající jak přirozeně v živých organismech a životním prostředí, tak při využívání tzv. pokročilých oxidačních procesů k čištění odpadních vod a dekontaminaci složek životního prostředí, včetně procesů elektro-oxidačních.

3.2 Léčiva

3.2.1 Antimuskarinika

Zajímavou skupinou látek, jejichž oxidačním přeměnám byla věnována pozornost v naší laboratoři, jsou léčiva z třídy antimuskarinik používaná k léčbě urgentní inkontinence a hyperaktivního močového měchýře (Over Active Bladder, OAB). Tato nemoc projevující se naléhavostí a zvýšenou frekvencí močení a komplikující život zejména osobám, které

nemohou kdykoliv a často opouštět pracoviště, se do seznamu uznávaných nemocí dostala až v roce 2002 a její výskyt ve světě neustále narůstá [93]. Antimuskarinika se váží na acetylcholinové muskarinové receptory a inhibují funkci detrusoru (hladké svaloviny močového měchýře s vypuzovací funkcí) [94]. Chemická struktura tří studovaných látek ze skupiny antimuskarinik, tolterodinu (TOL), fesoterodinu (FES) a jejich společného metabolitu 5-hydroxytolterodinu (5-HMT) je znázorněna na obr. 18.

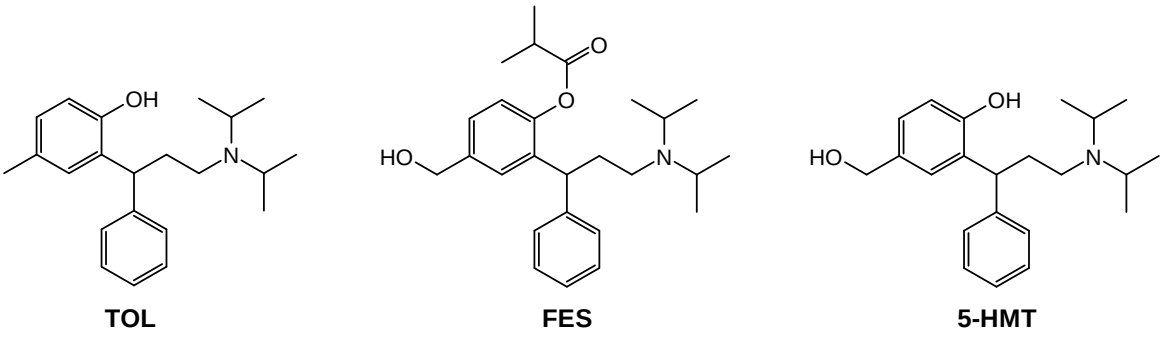

Obr. 18. Strukturní vzorce tolterodinu (TOL), fesoterodinu (FES) a 5-hydroxymethyltolterodinu (5-HMT).

Studiem redoxních vlastností pomocí voltametrických technik a potenciostatické coulometrie v kombinaci s LC/MS analýzou oxidačních produktů se podařilo prokázat dvě vzájemně nezávislá redoxní centra v molekulách těchto látek. Jedním centrem je fenolový kruh nesoucí u TOL methylovou, u FES a 5-HMT hydroxymethylovou skupinu v *para*-pozici k fenolové skupině, která je v případě FES esterifikovaná isomáselnou kyselinou. Druhým je alkylsubstituovaná terciární aminoskupina.

Produkty elektrolýzy lze do jisté míry ovlivnit nastavením hodnoty pH roztoku, elektrodového potenciálu a použitého rozpouštědla. U TOL byl po elektrolýze v kyselém prostředí (pH 3,5) při nižším potenciálu (0,69 V proti SCE) detekován 5-HMT (obr. 19) **[6]**, který je hlavním farmaceuticky aktivním metabolitem enzymové oxidace TOL katalyzované CYP2D6 [95]. Při vyšším potenciálu se hydroxymethylová skupina oxidovala na příslušný aldehyd (obr. 19, P1). Další oxidace až na karboxylovou skupinu, která probíhá při metabolické oxidaci TOL s jaterními mikrosomy myší a psů [96], nebyla za podmínek elektrolýzy pozorována. 5-HMT vznikal také elektrolýzou TOL v acetonitrilu s elektrolytem $LiClO_4$ při potenciálu 0,7 V (vs. Ag/0,1M-$AgNO_3$) **[6]**. Vedle hydroxylace methylové skupiny byla pozorována také hydroxylace fenolového kruhu za vzniku dvou izomerních produktů (obr. 19, P2, P3). Kromě monomerních produktů vznikaly rekombinací elektrochemicky generovaných fenoxylových radikálů dimerní produkty (P4 – P6).

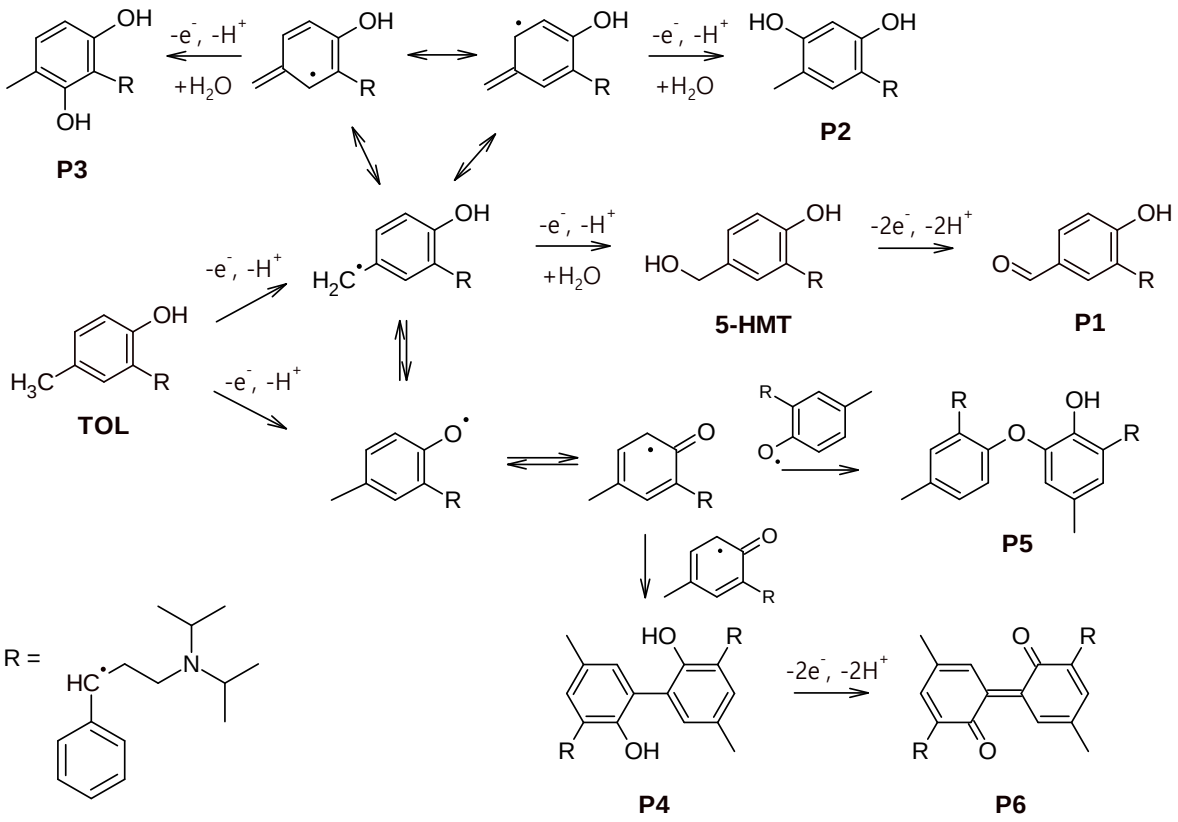

Obr. 19. Navržené schéma elektrochemické oxidace tolterodinu **[6]**.

Stejně jako u TOL byla i při elektrochemické oxidaci 5-HMT (obr. 20) pozorována oxidace fenolové skupiny a vznik aldehydu P1, a to v největším výtěžku v kyselém prostředí (pH 3) při nižším potenciálu (0,65 V proti SCE). Při vyšším potenciálu byl v kyselém a neutrálním prostředí detekován produkt P7 s *p*-benzochinonovou strukturou. Vysoká reaktivita fenoxylového radikálu, vznikajícího jednoelektronovou oxidací 5-HMT, vedla k tvorbě celé řady dalších reakčních produktů, a to jak monomerních, zejména hydroxylovaných na fenolovém kruhu, tak i dimerních, analogických k produktům P2 – P6 u TOL **[7]**. Alkalické prostředí a vyšší oxidační potenciál podpořily reaktivitu terciární aminoskupiny. Dvouelektronová oxidace této skupiny za vzniku iminiového kationtu následovaná jeho hydrolýzou vedla k odštěpení diisopropylaminu P10 a tvorbě aldehydických produktů P8 a P9.

Elektrochemické chování fesoterodinu je poněkud jednodušší v porovnání s TOL a 5-HMT díky absenci reaktivní volné fenolové skupiny, která je ve FES esterifikovaná kyselinou isomáselnou. Hydrolýza esterové vazby FES je hlavní metabolickou reakcí katalyzovanou nespecifickými esterasami v krevní plasmě, kterou vzniká farmaceuticky aktivní 5-HMT [97,98]. Kinetiku alkalické hydrolýzy esterové vazby FES lze velmi dobře sledovat voltametricky **[7]**. Vznik 5-HMT s volnou fenolovou skupinou se na

voltamogramech projevuje voltametrickým píkem při nižším potenciálu, než je potenciál oxidace hydroxymethylové skupiny FES (obr. 21A). Z nárůstu proudu oxidace fenolové skupiny v čase (obr. 21B) lze pak určit rychlostní konstantu hydrolýzy. Pro pH 12 byla zjištěna rychlostní konstanta $k = (1{,}17 \pm 0{,}05) \cdot 10^{-3}$ s^{-1} při (23 ± 1) °C a poločas hydrolýzy FES 10 min.

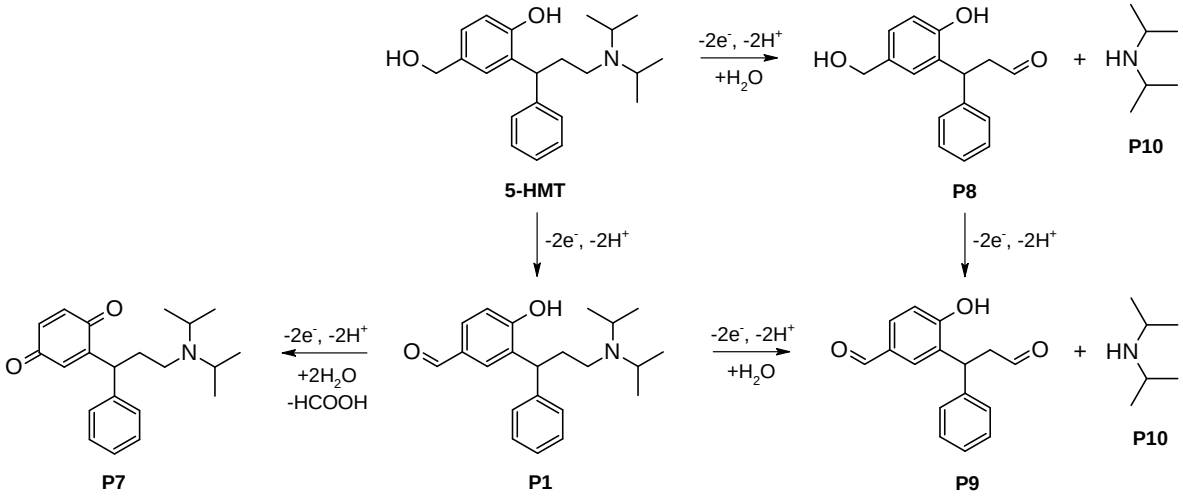

Obr. 20. Navržené základní schéma elektrochemické oxidace 5-hydroxymethyltolterodinu **[7]**.

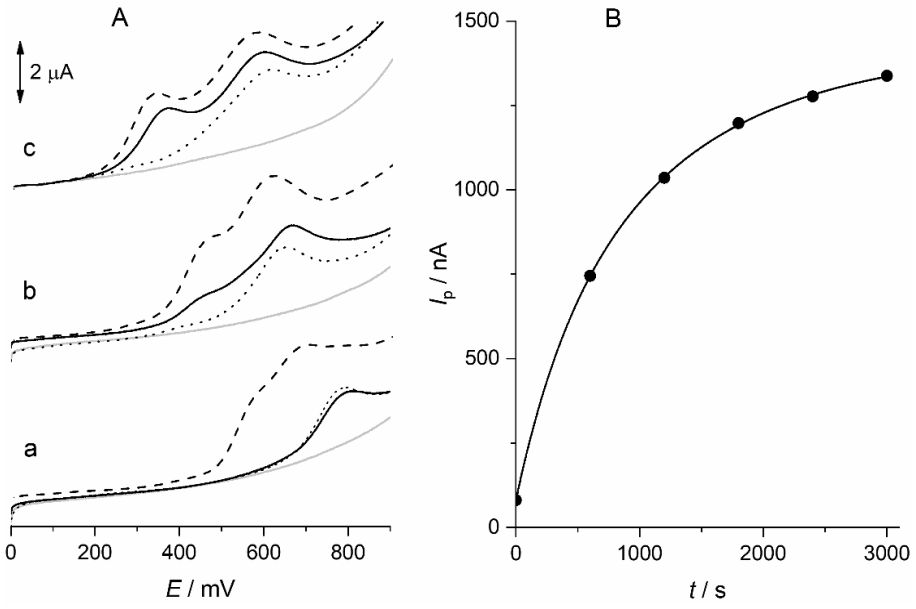

Obr. 21. A: DC voltamogramy 0,1 mmol dm^{-3} FES a 0,2 mmol dm^{-3} 5-HMT (---) v Brittonových-Robinsonových pufrech o pH = 7 (a), pH = 9,5 (b) a pH = 12 (c). Voltamogramy základního elektrolytu (—), voltamogramy FES byly zaznamenány ihned po smíchání zásobního roztoku FES s pufrem v čase 0 min (…) a po 180 min (—), rychlost polarizace 0,1 V s^{-1}. **B**: Časový vývoj voltametrického píku 5-HMT (E_p = 0,367 V) vznikajícího hydrolýzou 0,1 mmol dm^{-3} FES v B-R pufru o pH = 12 **[1]**.

Elekrolýzou FES v kyselém a neutrálním prostředí za nižšího potenciálu vznikaly dva hlavní oxidační produkty: 5-formylfesoterodin P11 a *N*-deisopropylaminoderivát P12 (obr. 22). Při vyšším oxidačním potenciálu byl navíc detekován produkt P13 vznikající hydroxylací 5-formylfesoterodinu P11. Dealkylace terciární aminoskupiny FES probíhala snáze v alkalickém prostředí. Z důvodu alkalické hydrolýzy FES nebyla v tomto prostředí provedena elektrolýza ve vsádkovém uspořádání s off-line LC/MS analýzou produktů, ale byla realizována v on-line EC/MS experimentu, který je proveditelný v krátkém časovém horizontu, při němž nestihne výchozí látka zhydrolyzovat. V EC/MS uspořádání vznikaly pouze produkty P11 a P12, potvrzující vzájemně nezávislou reaktivitu dvou redoxně aktivních center v molekule FES, benzylalkoholové skupiny a terciární aminoskupiny. Produkt souběžné oxidace obou těchto skupin nebyl nalezen, stejně jako nebyly nalezeny produkty oxidativní dimerizace FES **[1]**.

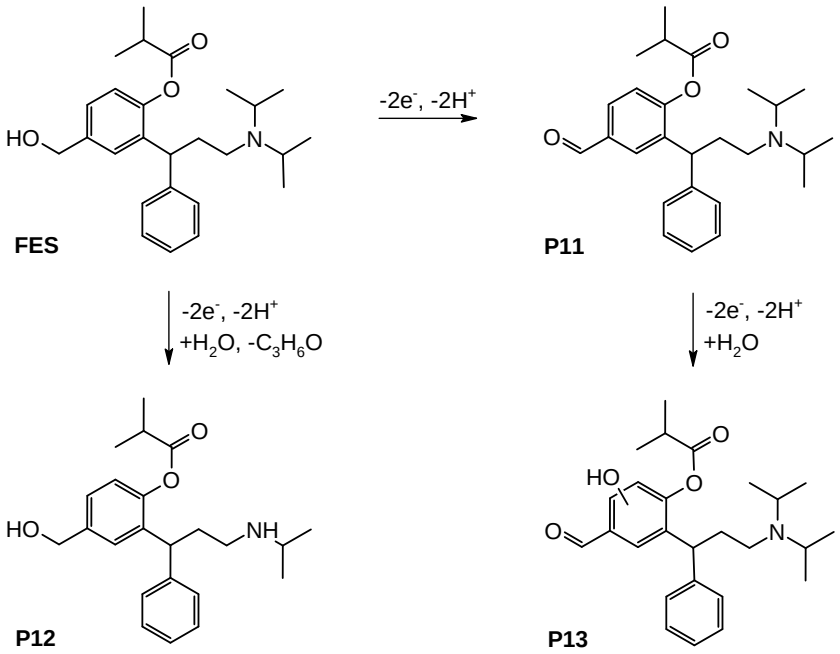

Obr. 22. Navržené schéma elektrochemické oxidace fesoterodinu **[1]**.

Obě reakční centra v molekulách TOL, FES a 5-HMT, jejichž oxidace byla prokázána pomocí elektrochemického studia a analýzy reakčních produktů, podléhají v lidském organismu metabolické oxidaci katalyzované enzymy cytochromu P450 (CYP). Produkty oxidace TOL v jaterních mikrozomech jsou 5-HMT, *N*-dealkylovaný tolterodin a *N*-dealkylovaný 5-HMT [95,99]. Metabolismus FES zahrnuje nejprve hydrolýzu na farmaceuticky aktivní 5-HMT, který je dále metabolizován enzymy jaterních mikrosomů na neaktivní karboxy-, karboxy-*N*-deisopropyl- a *N*-deisopropyl metabolit [97]. Spektrum

produktů vznikajících elektrochemickou oxidací je z důvodu značné reaktivity radikálů a kationtů elektrochemicky generovaných jak z fenolových jader, tak i z terciární aminoskupiny studovaných antimuskarinik mnohem rozsáhlejší a pestřejší, než je spektrum produktů enzymově katalyzovaných metabolických přeměn těchto látek. Na druhou stranu oxidace benzylalkoholové skupiny, která je enzymy CYP metabolizována až na karboxylovou skupinu, proběhla v elektrochemických podmínkách pouze na aldehyd. Přesto studium elektrochemických reakcí poskytlo cenné informace o reaktivních centrech a mechanismech oxidačních reakcí a jeho výsledky mohou být případně využity pro elektrosyntézu vybraných metabolitů vystupujících v procesu biotransformace těchto léčiv.

3.2.2 Berberin

Berberin je isochinolinový alkaloid vyskytující se v řadě bylin rodu dřišťál (*Berberis*), vodilka (*Hydrastis*), *Coptis* a dalších. Je aktivní složkou bylinných léčebných přípravků používaných zejména v tradiční čínské a ajurvédské medicíně k léčbě gastrointestinálního průjmu, diabetu a hypercholesterolémie. Současný klinický výzkum odhalil různé další farmakologické vlastnosti berberinu, které jsou prospěšné při léčbě chronických onemocnění, včetně např. rakoviny, deprese a hypertenze. Tento alkaloid se tedy jeví jako léčivá látka s multispektrálními účinky [100].

Přestože má berberin prokazatelně léčivé účinky, jeho orální biologická dostupnost je podle farmakokinetických studií velmi nízká, neboť koncentrace léčiva v krevní plazmě jsou po podání *per os* extrémně nízké. Příčinou je velmi rychlý metabolismus absorbovaného berberinu katalyzovaný enzymy CYP [101,102]. Lze tedy předpokládat, že redoxní reakce hrají významnou roli v metabolismu berberinu a jeho metabolity přítomné v krevní plazmě mají farmakologické účinky.

Oxidaci berberinu jsme v naší laboratoři studovali jak voltametrickými technikami (kapitola 2.2.4), tak kombinací potenciostatické elektrolýzy s LC/MS analýzou oxidačních produktů v prostředí o různém pH **[8]**. Voltametrické studium ukázalo, že elektrochemická oxidace berberinu je složitý proces provázený tvorbou redoxně aktivního filmu na povrchu uhlíkových elektrod. Cílem dalšího studia proto bylo prozkoumat zejména monomerní oxidační produkty rozpustné ve vodném prostředí.

Elektrolýzou v kyselém a neutrálním prostředí (pH 3,5 a 7,4) při potenciálech odpovídajících druhému anodickému proudovému signálu (1,4 V při pH 3,5 a 1,3 V při

pH 7,4) na cyklických voltamogramech (obr. 23) vznikal v nejvyšším výtěžku produkt Ber-P1 (obr. 24) s katecholovou strukturou kruhu A. Produkt Ber-P1 byl v literatuře popsán jako hlavní metabolit berberinu, jehož tvorbu katalyzují enzymy CYP z lidských jaterních mikrosomů, především CYP2D6 a v menší míře také CYP1A2, 3E4, 2E1 a 2C19 [103]. V roztocích oxidovaných v kyselém prostředí (pH 3,5) byl identifikován v menším výtěžku produkt Ber-P2 s chinonovou strukturou kruhu A a jednou demethylovanou methoxyskupinou na kruhu D. Tento produkt potvrdil jak očekávanou redoxní reaktivitu katecholové struktury vzniklé oxidací benzodioxolové části molekuly berberinu, tak i reaktivitu jeho *o*-dimethoxybenzenového uspořádání na kruhu D. Redoxní aktivita *o*-benzochinonové struktury tohoto produktu se na cyklických voltamogramech berberinu (obr. 23, křivky 1 a 2) projevila proudovými píky v potenciálové oblasti označené písmeny C a C'. Další detekovaný oxidační produkt, Ber-P3, se zachovaným methylendioxolovým cyklem a s jednou demethylovanou skupinou na kruhu D ukázal na vzájemnou nezávislost obou oxidovatelných center v molekule berberinu. Analogicky je demethylace jedné z methoxylových skupin na kruhu D jednou z hlavních metabolických přeměn berberinu katalyzovanou enzymy CYP2D6 a 1A2 [103,104]. Vedle uvedených produktů byly v malých výtěžcích detekovány mono-, di- a trihydroxylované deriváty berberinu. Polohu hydroxylových skupin nebylo možné určit z hmotnostních spekter příslušných produktů. Avšak za předpokladu EC mechanismu elektrochemické oxidace a na základě parciálních nábojů na uhlících v molekule berberinu [105] lze odhadnout, že odštěpení elektronu provázené ztrátou protonu a nukleofilní hydroxylací bude pravděpodobné na uhlících s negativním parciálním nábojem, tj. C5 (-0,22), C12 (-0,16) a C11(-0,12).

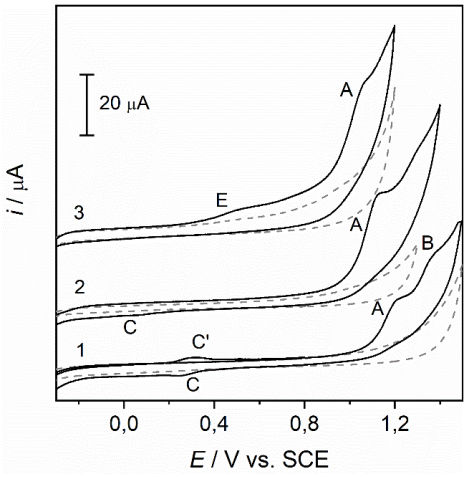

Obr. 23. Cyklické voltamogramy berberinu (0,2 mmol dm^{-3}) ve fosfátovém pufru o pH 3,5 (1), pH 7,4 (2) a pH 11,0 (3) registrované na elektrodě ze skelného uhlíku rychlostí změny potenciálu 0,2 V s^{-1}. Voltamogram základního elektrolytu je vyznačen šedou čárkovanou čarou. Na voltamogramu 1 je záznam anodické větve druhého cyklu v potenciálovém rozsahu od –0,3 V do +0,8 V **[8]**.

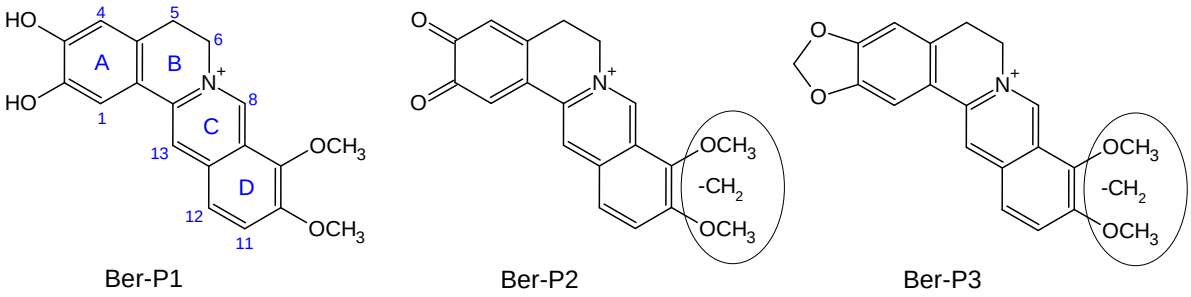

Obr. 24. Navržené strukturní vzorce oxidačních produktů berberinu **[8]**. Pozice methoxylové skupiny substituované při elektrochemické oxidaci hydroxylovou skupinou nebyla MS analýzou určena, proto je změna struktury sumárně naznačena ztrátou CH_2.

V alkalických roztocích je elektrochemické chování berberinu ovlivněno protolytickou rovnováhou mezi iminiovou kationtovou formou berberinu a jeho pseudobází (obr. 25). Cyklický voltamogram (obr. 23) pořízený v prostředí o pH 11 ukazuje oxidační signál (E) s potenciálem kolem 0,5 V, tedy přibližně o 0,4 V pozitivnějším oproti signálu oxidace benzodioxolového cyklu, resp. methoxylových skupin (pík A). Z nárůstu proudového signálu E s rostoucím pH lze vyvodit, že přísluší oxidaci hydroxylové skupiny pseudobáze. V roztocích berberinu elektrolyzovaných v prostředí o pH 11 při potenciálu 0,7 V, tedy v oblasti limitního proudu vlny E, byl po extrakci do ethylacetátu detekován LC/MS analýzou jako oxidační produkt 8-oxoberberin (Ber-P4). Jeho identita byla prokázána porovnáním retenčního času a hmotnostního spektra se syntetizovaným standardem 8-oxoberberinu. Dalším oxidačním produktem v tomto prostředí byl 5,13-dihydroxy-8-oxoberberin (Ber-P5).

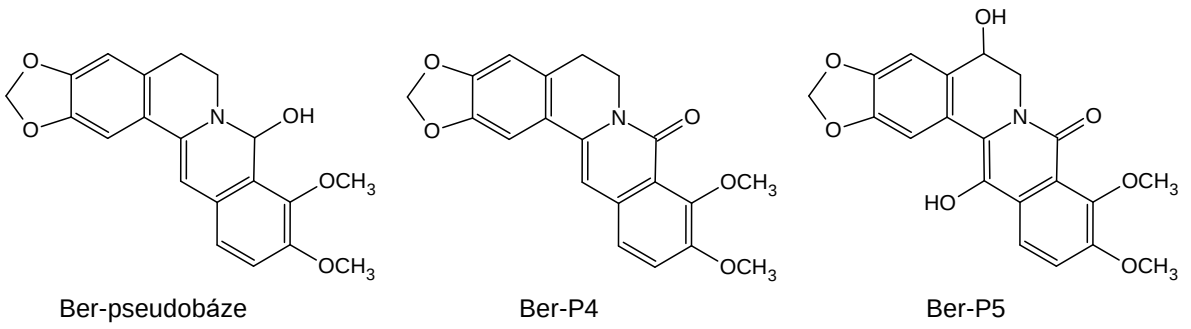

Obr. 25. Strukturní vzorce berberinu pseudobáze a jeho oxidačních produktů 8-oxoberberinu (Ber-P4) a 5,13-dihydroxy-8-oxoberberinu (Ber-P5) **[8]**.

Z uvedených výsledků elektrochemického studia berberinu je patrné, že oxidace tohoto alkaloidu v elektrochemickém článku probíhá na stejných částech molekuly jako metabolická oxidace katalyzovaná enzymy cytochromu P450. Hlavní produkty elektrochemické oxidace, Ber-P1 a Ber-P3, zejména v konjugované formě, patří také mezi

hlavní metabolity berberinu u potkanů a lidí [102,104,106-110]. Elektrochemické metody by tedy mohly být užitečné pro studium oxidačních mechanismů a elektrosyntézy vybraných metabolitů zapojených do oxidativní biotransformace berberinu a dalších strukturně podobných sloučenin.

3.2.3 Zopiklon

Dalším léčivem, u něhož byla v naší laboratoři studována elektrochemická aktivita, je zopiklon, 6-(5-chlorpyridin-2-yl)-7-oxo-6,7-dihydro-5*H*-pyrrolo[3,4b]pyrazin-5-yl-4-methyl-piperazin-1-karboxylát (obr. 26). Jedná se o zástupce tzv. léků Z, hypnotik používaných při léčbě nespavosti. Léky Z, k nimž se dále řadí zolpidem a zaleplon, byly vyvinuty jako alternativa k celosvětově hojně používaným benzodiazepinům, které jsou kontroverzní kvůli obavám z nepříznivých psychických a fyzických účinků, snižující se účinnosti a fyzické závislosti při jejich dlouhodobém užívání. Zopiklon působí krátkodobě (biologický poločas je 4-5 hodin [111]) a má svalově relaxační a protikřečové účinky. V lidském organismu je metabolizován v játrech na dva hlavní metabolity: zopiklon *N*-oxid, který si zachovává nízkou farmakologickou aktivitu a *N*-demethylzopiklon (ND-Z, obr. 26), který je farmakologicky neaktivní. Největší metabolickou aktivitu při *in-vitro* studiu metabolismu zopiklonu vykazovaly enzymy CYP3A4 a CYP2C8 [112].

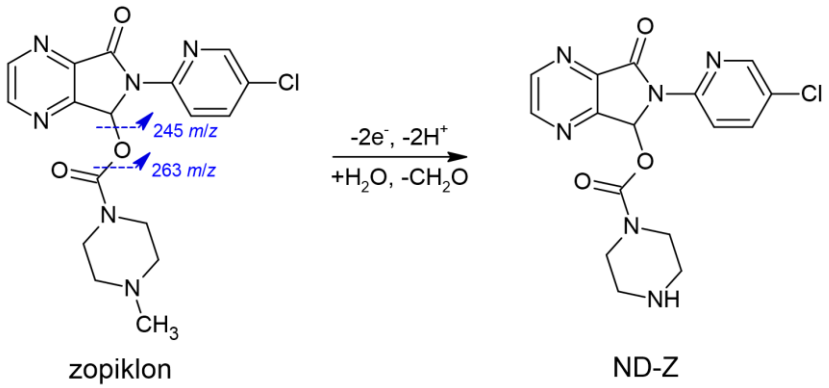

Obr. 26. Strukturní vzorce zopiklonu a jeho hlavního oxidačního produktu *N*-demethylzopiklonu (ND-Z).

Elektrochemická oxidace zopiklonu je poměrně komplikovaný proces. Jak ukazuje diferenčně pulsní voltamogram léčiva zaznamenaný na elektrodě ze skelného uhlíku v prostředí o pH 6,5 (obr. 27), proudový signál je v oblasti limitního proudu zvlněn v důsledku dalších elektrodových dějů následujících po první reakci přenosu elektronu. Ze závislostí výšky proudového píku na změně potenciálu elektrody při stejnosměrné

voltametrii byl prokázán vliv adsorpce. Závislost limitního proudu na odmocnině z rychlosti rotace RDE odhalila vliv kinetiky přenosu elektronu zejména v kyselém prostředí **[5]**.

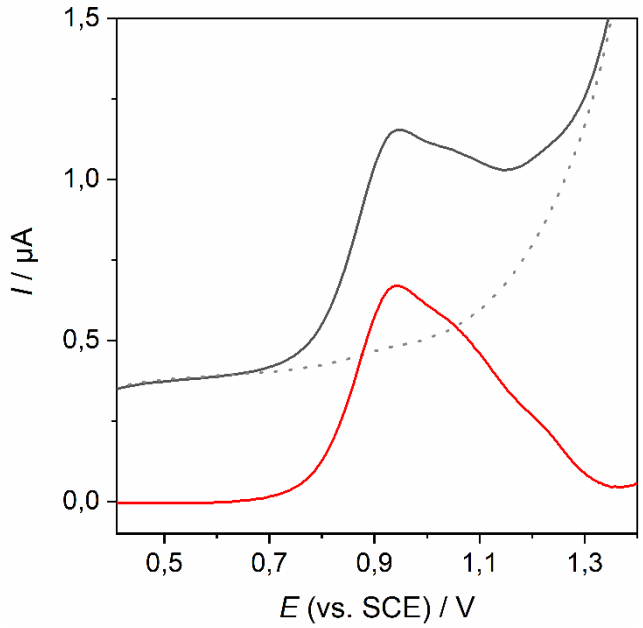

Obr. 27. Diferenčně pulsní voltamogramy zopiklonu (0,5 mmol dm^{-3}) na elektrodě ze skelného uhlíku v Brittonově-Robinsonově pufru o pH 6,5 a acetonitrilu (1:1, *V*/*V*). Rychlost změny potenciálu elektrody 20 mV s^{-1}, modulační amplituda 25 mV, šířka pulsu 50 ms. Červená křivka značí anodický signál zopiklonu po odečtení proudu základního elektrolytu.

Studium elektrochemické oxidace zopiklonu v on-line systému EC/MS odhalilo několik oxidačních produktů. Obr. 28 znázorňuje závislost intenzity MS odezvy protonovaných molekul těchto produktů na potenciálu pracovní elektrody z porézního uhlíku. Nejvyšší intenzitu vykazoval produkt s $[M + H]^+$ při *m*/*z* 375, tedy o 14 *m*/*z* menší oproti protonované molekule zopiklonu ($[M + H]^+$ 389 *m*/*z*). Analýza kolizních spekter iontu *m*/*z* 375 potvrdila, že jde o *N*-demethylovaný zopiklon (ND-Z, obr. 26), který je současně hlavním produktem metabolismu zopiklonu v sytému cytochromu P450. Tento produkt vznikal v kyselém, neutrálním i alkalickém prostředí. Intenzita odezvy ND-Z v závislosti na potenciálu pracovní elektrody procházela maximem (v prostředí o pH 6,8 při hodnotě 0,55 V proti Pd/H_2) a při vyšších potenciálech klesala. Naproti tomu při vyšších potenciálech vznikaly ve větších výtěžcích oxidační produkty s hodnotami *m*/*z* 403, 405 a 419, které se od výchozí molekuly zopiklonu lišily hodnotou *m*/*z* vyšší o 14, 16 a 30 jednotek. Kolizní hmotnostní spektra všech oxidačních produktů obsahovala stejné pásy iontů s *m*/*z* 245 a 263 jako zopiklon (obr. 26). Je tedy zřejmé, že oxidace léčiva proběhla na *N*-alkylpiperazinové části molekuly. Předpokládané struktury oxidačních produktů s *m*/*z* 403 a 405 jsou na obr. 29. Produkt s *m*/*z* 419 měl o atom kyslíku více a o dva atomy vodíku méně než produkt

s *m*/*z* 405, a tedy pravděpodobně obsahoval další oxoskupinu na methylenovém uhlíku piperazinového kruhu.

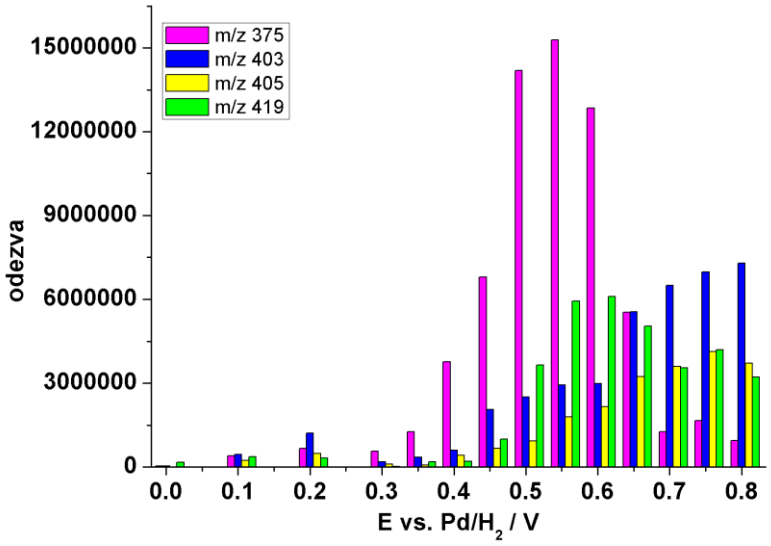

Obr. 28. Intensity MS signálů oxidačních produktů zopiklonu s hodnotami *m*/*z* 375, 403, 405 a 419 zaznamenané při různých potenciálech porézní uhlíkové elektrody v on-line EC/MS systému. Základní elektrolyt: acetonitril/vodný roztok octanu amonného o pH 6,8 (1:1, *V*/*V*), počáteční koncentrace zopiklonu 0,5 mmol dm^{-3}.

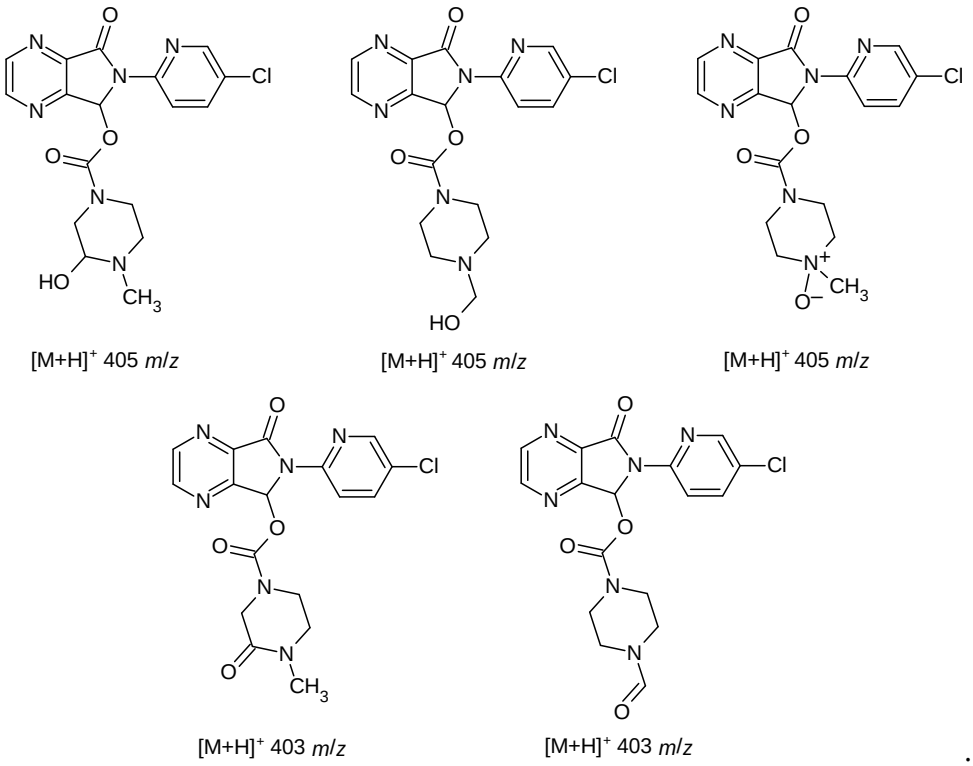

Obr. 29. Navržené strukturní vzorce oxidačních produktů zopiklonu vznikajících elektrochemickou oxidací při vyšších potenciálech.

Přestože nebylo možné z EC/MS experimentů určit přesnou strukturu všech produktů elektrochemické oxidace zopiklonu, získané výsledky jednoznačně dokládají redoxní reaktivitu *N*-methylpiperazinové části molekuly zopiklonu, která podléhá biotransformačním procesům katalyzovaným enzymy cytochromu P450 [111]. I v tomto případě může tedy být elektrochemie přínosná jak pro objasnění oxidačních reakcí léčiva, tak pro syntézu prokázaných i potenciálních metabolitů zopiklonu a jeho strukturních analog.

3.2.4 Fentanyl a jeho analoga

Fentanyl (obr. 30) a velký počet jeho strukturních analog, souhrnně označované jako „fentanyly“, náleží do skupiny nových syntetických opioidů, které se často používají jako léky proti bolesti, anestetika při chirurgických zákrocích a antidepresiva pro symptomatickou léčbu psychiatrických problémů [113]. Během posledních čtyř desetiletí se rozšířilo zneužívání těchto látek zejména drogovými dealery, ale i zdravotníky s přístupem k těmto léčivům a samotnými pacienty. V posledních letech se míra zneužívání a nechtěného předávkování fentanyly zmnohonásobila v souvislosti s jejich nelegální výrobou a distribucí. V USA se dnes hovoří o epidemii zneužívání fentanylů - fentanylové krizi [114]. Počet úmrtí z předávkování fentanyly však roste celosvětově, Českou republiku nevyjímaje [115]. Většina těchto úmrtí je důsledkem požití fentanylů jako náhražky heroinu nebo jiných drog (kokain, metamfetamin), které byly falšovány (řezány) fentanyly. Nebezpečí fentanylů spočívá v jejich vysoké účinnosti (fentanyl je asi 100krát účinnější než morfin, carfentanyl je 30-100krát účinnější než fentanyl) a v malém rozdílu mezi dávkou vyvolávající kýžený účinek a dávkou toxickou.

Vzhledem k vysoké biologické účinnosti a rizikům spojeným s ilegálně vyráběnými a distribuovanými fentanylovými drogami je žádoucí hledat možnosti jejich rychlé a bezpečné likvidace a dekontaminace prostor a míst jimi zasažených. Pro tyto účely se nabízejí různé degradační procesy, z nichž jako nejúčinnější se jeví procesy oxidační. Z testovaných oxidačních činidel vedly k účinnému a rychlému rozkladu fentanylu běžná desinfekční činidla na bázi peroctové kyseliny nebo aktivního chloru [116], směs peroxouhličitanu sodného s *N*,*N*′-(ethan-1,2-diyl)bis(*N*-acetylacetamidem) a trichloriso-kyanurová kyselina [117]. Při degradaci fentanylu docházelo především k oxidativní *N*-dealkylaci, a to jak na piperidinovém dusíku za vzniku norfentanylu (obr. 30), tak na amidovém dusíku za tvorby *N*-fenylpropanamidu. Při použití trichlorisokyanurové kyseliny

a chlornanu vápenatého byla v reakčních směsích identifikována řada chlorovaných degradačních produktů. Směs $NaBrO_3/NaHSO_3/Na_2SO_3$ v kyselém prostředí rozložila fentanyly během 30 min s účinností více než 99 %. Během degradace vznikala řada bromovaných sloučenin, vč. mono-, di- a tribromanilinu, dibromethylbenzenu, 2-brom-*N*-fenylpropanamindu [118]. Testována byla i degradace 0,3% roztokem peroxidu vodíku [119]. Ta se však ukázala jako málo účinná, neboť po 24 hodinách reakce zůstalo nezreagováno 92 % fentanylu. Degradačními produktem byl *N*-oxid fentanylu.

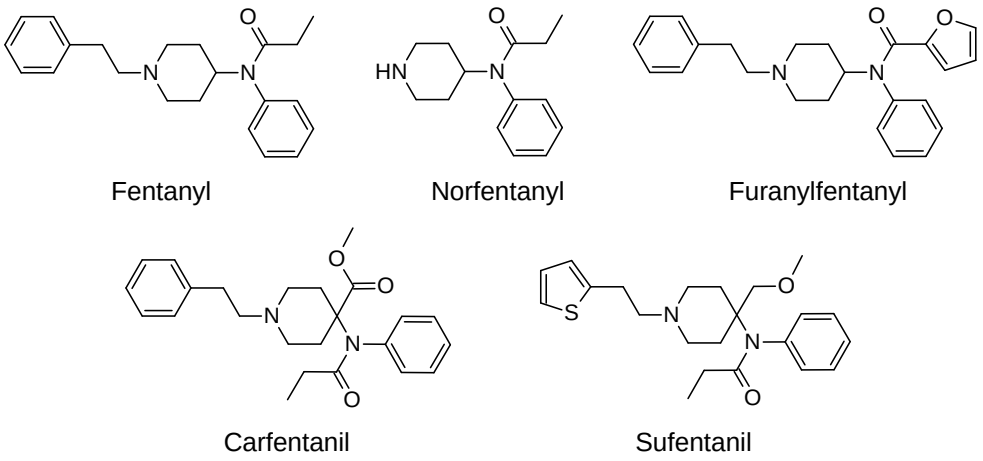

Obr. 30. Strukturní vzorce fentanylu a jeho analog, které byly studovány v práci [**10**].

V našem výzkumu prováděném ve spolupráci s týmem dr. Langmaiera z Ústavu fyzikální chemie J. Heyrovského AV ČR jsme použili k degradaci fentanylů (obr. 30) reaktivní hydroxylové radikály vznikající katalytickým rozkladem peroxidu vodíku železnatou solí (Fentonovo činidlo) **[10]**. Metodou cyklické voltametrie přenosu iontů přes rozhraní membrány mikroporézního filtru napojeného nízkotající iontovou kapalinou (tridodecylmethylamonium tetrakis[3,5-bis(trifluormethyl)-fenyl]borátem) bylo zjištěno, že krokem určujícím rychlost degradace je generování hydroxylových radikálů, která závisí především na koncentraci železnatých iontů v reakční směsi. Při nadbytku těchto iontů se poločas reakce u studovaných fentanylů pohyboval v rozmezí 2-8 min.

Vedle studia kinetiky jsme se zabývali detekcí meziproduktů degradace fentanylu metodou LC/MS. Z reakční směsi obsahující na počátku vodný roztok fentanylu (0,1 mmol dm^{-3}), Mohrovy soli (0,2 mmol dm^{-3}), peroxidu vodíku (44 mmol dm^{-3}) a chloridu lithného (1 mmol dm^{-3}), využívaného jako elektrolyt při voltametrii přenosu iontů, byly v časovém rozmezí 0 – 300 min odebírány vzorky, extrahovány chloroformem a analyzovány pomocí LC/ESI-MS. Po 15 a 30 minutách reakce bylo detekováno značné

množství hydroxyderivátů fentanylu v různých izomerních formách, což potvrdilo předpoklad, že hydroxylové radikály generované reakcí peroxidu vodíku s železnatými ionty jsou hlavním oxidačním agens. Analýza kolizních spekter odhalila, že hydroxylace proběhla v největší míře na fenethylové části molekuly fentanylu a na piperazinovém cyklu. Derivát hydroxylovaný na esterově vázané propionylové skupině byl přítomen v mnohem menším výtěžku. Jako nejodolnější vůči hydroxylaci se jevila anilinová část molekuly fentanylu. Kromě mono-, di- a trihydroxylovaných derivátů byla prokázána tvorba norfentanylu, který je známý také jako hlavní, biologicky neaktivní metabolit enzymatických reakcí fentanylu katalyzovaných cytochromem P450 [113] a rovněž jako hlavní produkt elektrochemické oxidace fentanylu [115,120] i jiných procesů jeho oxidační degradace. Dalšími detekovanými degradačními meziprodukty byly hydroxynorfentanyl a *N*-fenylpropanamid, popsané rovněž jako produkty degradace fentanylu peroctovou kyselinou [117]. Po pěti hodinách reakce už nebyl v reakční směsi detekován fentanyl ani žádný z uvedených degradačních meziproduktů.

Fentonovo činidlo, obsahující levné, netoxické a k životnímu prostředí šetrné složky, se tedy jeví jako velmi účinné pro rychlou degradaci fentanylů. Může být velmi snadno aplikováno ve formě roztoku i ve spreji pro rychlou a účinnou dekontaminaci odpadních vod a povrchů kontaminovaných těmito nebezpečnými látkami.

Problematikou detekce a stanovení fentanylových drog se na našem pracovišti věnujeme i nadále. Naší snahou je vyvinout citlivou a selektivní voltametrickou metodu pro rychlou detekci fentanylu v terénních podmínkách, vhodnou například pro rychlé odhalení pančovaného heroinu [43]. Mimoto se snažíme objasnit mechanismus elektrochemické oxidace fentanylu, která podle výsledků našich dosavadních výzkumů vede k řadě produktů analogických k produktům metabolických přeměn těchto látek [121].

4 Závěr

Výsledky studií uvedené v této habilitační práci ukazují, že elektrochemické metody mají značný potenciál pro výzkum redoxních přeměn biologicky významných látek. Umožňují simulovat v instrumentálně jednoduchém experimentálním uspořádání řadu redoxních procesů, které probíhají v přírodě chemickou nebo biochemickou cestou. I když anodická oxidace nedokáže napodobit všechny enzymově řízené metabolické procesy, může být cenným nástrojem jak pro odhalení redoxních center v molekulách xenobiotik, tak pro syntézu řady oxidačních produktů, které vznikají metabolickou cestou.

K reakcím, které probíhají velmi snadno v elektrochemickém článku podobně jako v eko- a biosystémech, patří oxidace bromfenolů. Anodická oxidace fenolové skupiny za vzniku fenoxylových radikálů a fenoxoniových kationtů vede k tvorbě bromovaných difenyletherů, bifenylů a benzochinonů, které jsou schopny v organismu negativně zasahovat do řady fyziologických procesů (např. inhibice enzymů, narušení oxidativní fosforylace, přerušení mitochondriálního přenosu elektronů, poškození DNA).

U studovaných léčiv se podařilo prokázat elektrochemické oxidační přeměny hydroxybenzylového, benzodioxolového a *N*-methylpiperazinového strukturního motivu a alkylsubstituované terciární aminoskupiny, které jsou analogické přeměnám katalyzovaným enzymy cytochromu P450. Anodické štěpení benzodioxolového motivu, prokázané u alkaloidu berberinu, vede k tvorbě reaktivní katecholové a *o*-benzochinonové struktury. Benzodioxolový motiv je velmi častý také u dalších biologicky významných látek, ať už přírodních (např. piperin, safrol), či syntetických, včetně nelegálních drog (extáze, ethylendioxypyrovaleron, metylon a dalších). Podobně piperazinový kruh, podléhající při anodické oxidaci *N*-dealkylaci, *N*-oxidaci a *C*-oxidaci, analogicky jako u enzymových oxidací, se velmi často vyskytuje u léčiv (např. sildenafil, dasatinib) i nelegálních drog (např. benzylpiperazin, 3-trifluormethylfenylpiperazin, *m*-chlorfenylpiperazin, MT-45). Terciární aminoskupina je rovněž častou strukturní jednotkou mnohých léčiv (např. syntetických anticholinergik).

Poznatky o oxidačních reakcích látek s uvedenými strukturními motivy mohou pomoct při studiu metabolismu nově syntetizovaných látek s podobnou strukturou, mohou být využity pro elektro-syntézu metabolitů a v neposlední řadě pro vývoj nových citlivých elektroanalytických metod detekce a stanovení těchto látek. Elektroanalytické metody jsou také vhodné pro sledování kinetiky reakcí elektrochemicky aktivních látek v homogenní fázi

(redoxních, hydrolytických apod.) a umožňují tedy studovat např. stabilitu léčiv při stresových zkouškách nebo rychlost degradace nebezpečných látek a polutantů životního prostředí.

Přínosem k vývoji analytické instrumentace je miniaturizace elektrolytických článků vhodných pro studium redoxních přeměn mikrogramových množství látek a rovněž konstrukce nového typu elektrody, uhlíkové štětičkové elektrody, pro hmotnostně spektrometrickou analýzu produktů redoxních reakcí, vč. oligomerních a polymerních produktů, které zůstávají silně adsorbovány na elektrodových površích.

5 Literatura

1. Kučerová, P.; Skopalová, J.; Kučera, L.; Hrbáč, J.; Lemr, K. Electrochemical oxidation of fesoterodine and identification of its oxidation products using liquid chromatography and mass spectrometry. *Electrochimica Acta* **2015**, *159*, 131-139, doi:10.1016/j.electacta.2015.01.190.

2. Marková, E.; Kučerová, P.; Bednář, P.; Barták, P.; Skopalová, J. Electrochemical oxidative dimerization of monobrominated phenols and pentabromophenol in methanol-aqueous media. *Monatshefte fur Chemie* **2016**, *147*, 75-87, doi:10.1007/s00706-015-1597-2.

3. Marková, E.; Kučerová, P.; Skopalová, J.; Barták, P. Electrochemical oxidation of 2,4,6-tribromophenol in aqueous-alcoholic media. *Electroanalysis* **2015**, *27*, 156-165, doi:10.1002/elan.201400412.

4. Skopalová, J.; Barták, P.; Bednář, P.; Tomková, H.; Ingr, T.; Lorencová, I.; Kučerová, P.; Papoušek, R.; Borovcová, L.; Lemr, K. Carbon fiber brush electrode as a novel substrate for atmospheric solids analysis probe (ASAP) mass spectrometry: Electrochemical oxidation of brominated phenols. *Analytica Chimica Acta* **2018**, *999*, 60-68, doi:10.1016/j.aca.2017.11.024.

5. Táborský, J.; Švidrnoch, M.; Kurka, O.; Borovcová, L.; Bednář, P.; Barták, P.; Skopalová, J. Electrochemical oxidation of zopiclone. *Monatshefte fur Chemie* **2016**, *147*, 53-60, doi:10.1007/s00706-015-1602-9.

6. Macíková, P.; Skopalová, J.; Cankař, P.; Papoušková, B.; Straková, R.; Jirovský, D.; Maier, V. Electrochemical oxidation of tolterodine. *Electroanalysis* **2013**, *25*, 205-212, doi:10.1002/elan.201200388.

7. Kučerová, P.; Skopalová, J.; Kučera, L.; Táborský, J.; Švecová, H.; Lemr, K.; Cankař, P.; Barták, P. Electrochemical oxidation of 5-hydroxymethyl tolterodine and identification of its oxidation products using liquid chromatography and mass spectrometry. *Electrochimica Acta* **2016**, *215*, 617-625, doi:10.1016/j.electacta.2016.08.137.

8. Skopalová, J.; Vacek, J.; Papoušková, B.; Jirovský, D.; Maier, V.; Ranc, V. Electrochemical oxidation of berberine and mass spectrometric identification of its

oxidation products. *Bioelectrochemistry* **2012**, *87*, 15-20, doi:10.1016/j.bioelechem.2011.09.002.

9. Guido, L.F.; Carvalho, D.O.; Táborský, J.; Skopalová, J.; Saldanha, H.M.E.B.; Bednář, P. Study of electrochemical oxidation of xanthohumol by ultra-performance liquid chromatography coupled to high resolution tandem mass spectrometry and ion mobility mass spectrometry. *Chromatographia* **2015**, *78*, 1233-1243, doi:10.1007/s10337-015-2954-3.

10. Langmaier, J.; Skopalová, J.; Cechová, M.Z.; Kahánková, T.; Jerga, R.; Barták, P.; Samec, Z.; Navrátil, T. Ion transfer voltammetric and LC/MS investigations of the oxidative degradation process of fentanyl and some of its structural analogs. *Electrochimica Acta* **2023**, *441*, doi:10.1016/j.electacta.2023.141848.

11. Crosland, M. Lavoisiers theory of acidity. *Isis* **1973**, *64*, 306-325, doi:10.1086/351125.

12. Legrand, H.E. Lavoisiers oxygen theory of acidity. *Annals of Science* **1972**, *29*, 1-18, doi:10.1080/00033797200200331.

13. Olson, M.V. Encyclopedia britannica: *Oxidation-reduction reaction*. https://www.britannica.com/science/oxidation-reduction-reaction, staženo 22. 10. 2023.

14. Murray, R.K.; Bender, D.; Botham, K.M.; Kennelly, P.J.; Rodwell, V.W.; Weil, P.A. *Harper's illustrated biochemistry*; McGraw-Hill Lange: Columbus, 2012; str. 818.

15. Graham, G.G.; Davies, M.J.; Day, R.O.; Mohamudally, A.; Scott, K.F. The modern pharmacology of paracetamol: Therapeutic actions, mechanism of action, metabolism, toxicity and recent pharmacological findings. *Inflammopharmacology* **2013**, *21*, 201-232, doi:10.1007/s10787-013-0172-x.

16. Lohmann, W.; Karst, U. Biomimetic modeling of oxidative drug metabolism. *Analytical and Bioanalytical Chemistry* **2008**, *391*, 79-96, doi:10.1007/s00216-007-1794-x.

17. Dryhurst, G. *Electrochemistry of biological molecules*; Elsevier Science: 2012; str. 614.

18. Jurva, U.; Wikstrom, H.V.; Weidolf, L.; Bruins, A.P. Comparison between electrochemistry/mass spectrometry and cytochrome P450 catalyzed oxidation

reactions. *Rapid Communications in Mass Spectrometry* **2003**, *17*, 800-810, doi:10.1002/rcm.978.

19. Bard, A.K.; Zoski, C.G. Voltammetry retrospective. *Analytical Chemistry* **2000**, *72*, 346A-352A, doi:10.1021/ac002791t.
20. Opekar, F.; Beran, P. *Rotující disková elektroda*; Academia ČSAV: 1974; str. 84.
21. Gonzalez, B.; Calvar, N.; Gomez, E.; Dominguez, A. Density, dynamic viscosity, and derived properties of binary mixtures of methanol or ethanol with water, ethyl acetate, and methyl acetate at t=(293.15, 298.15, and 303.15) K. *Journal of Chemical Thermodynamics* **2007**, *39*, 1578-1588, doi:10.1016/j.jct.2007.05.004.
22. Pfizer. *Toviaz: Fesoterodine fumarate extended-release tablets 4 mg and 8 mg. Product monograph*; Pfizer Canada, ULC: Kirkland, Quebec, 2021.
23. Wilke, C.R.; Chang, P. Correlation of diffusion coefficients in dilute solutions. *AIChE Journal* **1955**, *1*, 264-270, doi:10.1002/aic.690010222.
24. Snyder, L.R.; Kirkland, J.J.; Dolan, J.W. *Introduction to modern liquid chromatography*, 3rd edition; John Wiley & Sons: Hoboken, 2010, doi:10.1002/9780470508183.
25. Kotouček, M. *Teoretické aspekty analytické chemie*; PřF UPOL: Olomouc, 1989.
26. di Cagno, M.P.; Clarelli, F.; Vabeno, J.; Lesley, C.; Rahman, S.D.; Cauzzo, J.; Franceschinis, E.; Realdon, N.; Stein, P.C. Experimental determination of drug diffusion coefficients in unstirred aqueous environments by temporally resolved concentration measurements. *Molecular Pharmaceutics* **2018**, *15*, 1488-1494, doi:10.1021/acs.molpharmaceut.7b01053.
27. Macdonald, T.L.; Gutheim, W.G.; Martin, R.B.; Guengerich, F.P. Oxidation of substituted *N*,*N*-dimethylanilines by cytochrome P450 - estimation of the effective oxidation reduction potential of cytochrome P450. *Biochemistry* **1989**, *28*, 2071-2077, doi:10.1021/bi00431a016.
28. Barek, J.; Opekar, F.; Štulík, K. *Elektroanalytická chemie*; Karolinum: Praha, 2005.
29. Bard, A.J.; Faulkner, L.R. *Electrochemical methods: Fundamentals and applications*, 2nd edition; John Wiley & Sons: New York, 2002.

30. Janik, B.; Elving, P.J. Electrochemical reduction of 6-substituted purines correlation with structural and energetic characteristics. *Journal of the Electrochemical Society* **1969**, *116*, 1087-1097, doi:10.1149/1.2412221.

31. Scholz, F. (ed.) *Electroanalytical methods: Guide to experiments and applications*, 2nd edition; Springer-Verlag: Berlin Heidelberg, 2010, doi:10.1007/978-3-642-02915-8.

32. Heyrovský, M.; Vavřička, S. On the pH-dependence of polarographic half-wave potentials. 1. Fundamental relations. *Journal of Electroanalytical Chemistry* **1972**, *36*, 203-221, doi:10.1016/S0022-0728(72)80459-5.

33. Heyrovský, M.; Vavřička, S. On the pH-dependence of polarographic half-wave potentials. 2. Protonation of an electro-inactive group. *Journal of Electroanalytical Chemistry* **1972**, *36*, 223-233, doi:10.1016/0368-1874(72)85063-9.

34. Compton, R.G.; Harland, R.G.; Unwin, P.R.; Waller, A.M. Rotating-disk electrodes. ECE and DISP1 processes. *Journal of the Chemical Society-Faraday Transactions I* **1987**, *83*, 1261-1268, doi:10.1039/f19878301261.

35. Compton, R.G.; Mason, D.; Unwin, P.R. Rotating-disk electrode voltammetry. Waveshape analysis for DISP2 and EC_2 processes. *Journal of the Chemical Society-Faraday Transactions I* **1988**, *84*, 473-482, doi:10.1039/f19888400473.

36. Gattrell, M.; MacDougall, B. The anodic electrochemistry of pentachlorophenol. *Journal of the Electrochemical Society* **1999**, *146*, 3335-3348, doi:10.1149/1.1392475.

37. Marken, F.; Neudeck, A.; Bond, A.M. Cyclic voltammetry, v knize: Scholz, F. (ed.) *Electroanalytical Methods: Guide to Experiments and Applications*, 2nd edition; Springer-Verlag: Berlin Heidelberg, 2010, pp. 57-106, doi:10.1007/978-3-642-02915-8.

38. Nicholson, R.S.; Shain, I. Theory of stationary electrode polarography. Single scan and cyclic methods applied to reversible, irreversible, and kinetic systems.. *Analytical Chemistry* **1964**, *36*, 706-723, doi:10.1021/ac60210a007

39. Gosser, D.K.J. *Cyclic voltammetry—simulation and analysis of reaction mechanisms*; VCH: New York, 1993.

40. Pfizer. Detrol la (tolterodine l-tartrate extended release capsules), v knize *Product monograph*; Pfizer Canada Inc.: Quebec, 2011, 2015; pp. 1-15.

41. Skopalová, J.; Lemr, K.; Kotouček, M.; Čáp, L.; Ondra, P. Electrochemical reduction of prometryne and the other 2-methylthio-4,6-dialkylamino-s-triazine herbicides at mercury electrodes. *Electroanalysis* **1998**, *10*, 331-335.

42. Jerga, R.; Müllerová, V.; Štěpánková, J.; Barták, P.; Tomková, H.; Rozsypal, J.; Skopalová, J. Phospholipid-modified carbon fiber brush electrode for the detection of dopamine and 3,4-dihydroxyphenylacetic acid. *Monatshefte fur Chemie* **2019**, *150*, 395-400, doi:10.1007/s00706-019-2371-7.

43. Mádr, J. *Využití voltametrie v analýze vybraných opioidů*. Bakalářská práce, Univerzita Palackého v Olomouci, Olomouc, 2022.

44. Amatore, C.; Azzabi, M.; Calas, P.; Jutand, A.; Lefrou, C.; Rollin, Y. Absolute determination of electron consumption in transient or steady-state electrochemical techniques. *Journal of Electroanalytical Chemistry* **1990**, *288*, 45-63, doi:10.1016/0022-0728(90)80024-Z.

45. Grenness, M.; Oldham, K.B. Semi-integral electroanalysis - theory and verification. *Analytical Chemistry* **1972**, *44*, 1121-1129, doi:10.1021/ac60315a037.

46. Bernard, M.O.; Bureau, C.; Soudan, J.M.; Lecayon, G. Diagnosis of adsorption on solid electrodes using semi-integral voltammetry: A generalization via asymptotic analysis. *Journal of Electroanalytical Chemistry* **1997**, *431*, 153-162, doi:10.1016/S0022-0728(97)00273-8.

47. Hrbáč, J.; Halouzka, V.; Trnková, L.; Vacek, J. El-chem viewer: A freeware package for the analysis of electroanalytical data and their post-acquisition processing. *Sensors* **2014**, *14*, 13943-13954, doi:10.3390/s140813943.

48. Šelešovská, R.; Herynková, M.; Skopalová, J.; Kelíšková-Martinková, P.; Janíková, L.; Cankař, P.; Bednář, P.; Chýlkova, J. Oxidation behavior of insecticide azoxystrobin and its voltammetric determination using boron-doped diamond electrode. *Electroanalysis* **2019**, *31*, 363-373, doi:10.1002/elan.201800647.

49. Šelešovská, R.; Hlobeňová, F.; Skopalová, J.; Cankař, P.; Janíkova, L.; Chýlkova, J. Electrochemical oxidation of anti-inflammatory drug meloxicam and its determination using boron doped diamond electrode. *Journal of Electroanalytical Chemistry* **2020**, *858*, 113758, doi:10.1016/j.jelechem.2019.113758.

50. Armarego, W.L.F.; Chai, C.L.L. Purification of laboratory chemicals sixth edition preface to the sixth edition. *Purification of Laboratory Chemicals, 6th Edition* **2009**, XII-XIII, doi:10.1016/B978-1-85617-567-8.50003-2.

51. Macúchova, J. *Využitie spojenia elektrochémie s hmotnostnou spektrometriou pre štúdium premeny biologicky aktívnych látok.* Diplomová práce, Univerzita Palackého v Olomouci, Olomouc, 2018.

52. Yilmazer, M.; Stevens, J.F.; Deinzer, M.L.; Buhler, D.R. In vitro biotransformation of xanthohumol, a flavonoid from hops (humulus lupulus), by rat liver microsomes. *Drug Metabolism and Disposition* **2001**, *29*, 223-231.

53. Rahman, M.H.; Bal, M.K.; Jones, A.M. Metabolism-inspired electrosynthesis. *ChemElectroChem* **2019**, *6*, 4093-4104, doi:10.1002/celc.201900117.

54. Gul, T.; Bischoff, R.; Permentier, H.P. Electrosynthesis methods and approaches for the preparative production of metabolites from parent drugs. *Trac-Trends in Analytical Chemistry* **2015**, *70*, 58-66, doi:10.1016/j.trac.2015.01.016.

55. Vanberkel, G.J.; Zhou, F.M. Characterization of an electrospray ion-source as a controlled-current electrolytic cell. *Analytical Chemistry* **1995**, *67*, 2916-2923, doi:10.1021/ac00113a028.

56. Pramanik, B.N.; Ganguli, A.K.; Gross, M.L. *Applied electrospray mass spectrometry*; Marcel Dekker, Inc: New York, Basel, 2002.

57. de Hoffmann, E.; Stroobant, V. *Mass spectrometry: Principles and applications*, 3rd edition; Wiley: Chichester, 2007.

58. Charbonnier, F.; Rolando, C.; Saru, F.; Hapiot, P.; Pinson, J. Short time-scale observation of an electrospray current. *Rapid Communications in Mass Spectrometry* **1993**, *7*, 707-710, doi:10.1002/rcm.1290070805.

59. Lemr, K.; Skopalová, J.; Kotouček, M.; Orság, D.; Zimpl, M.; Pěchová, D.; Hušková, R. Contribution of mass spectrometry to evaluation of electrochemical reduction mechanism of some physiologically active compounds. Sborník z konference 18th Informal Meeting on Mass Spectrometry, Praha, 30.4.-4.5.2000, 2000; str. 43.

60. Boys, B.L.; Kuprowski, M.C.; Noël, J.J.; Konermann, L. Protein oxidative modifications during electrospray ionization: Solution phase electrochemistry or

corona discharge-induced radical attack? *Analytical Chemistry* **2009**, *81*, 4027-4034, doi:10.1021/ac900243p.

61. Orság, D. *Příspěvek HPLC/MS a MS k řešení redukčních mechanismů heterocyklických dusíkatých sloučenin.* Diplomová práce, Univerzita Palackého v Olomouci, Olomouc, 2002.

62. Konopka, S.J.; Mcduffie, B. Diffusion coefficients of ferricyanide and ferrocyanide ions in aqueous media, using twin-electrode thin-layer electrochemistry. *Analytical Chemistry* **1970**, *42*, 1741-1746, doi:10.1021/Ac50160a042.

63. Morrow, G.W. *Organic electrochemistry*, v knize: Lund, H., Hammerich, O. (eds.); Marcel Dekker: New York, 2001.

64. Taj, S.; Ahmed, M.F.; Sankarapapavinasam Electrooxidation of p-chlorophenol and p-bromophenol in aqueous-medium. *Journal of Chemical Research-s* **1993**, 232-233.

65. Iguchi, M.; Nishiyama, A.; Etoh, H.; Okamoto, K.; Yamamura, S.; Kato, Y. Anodic-oxidation of some bromophenols - syntheses of highly brominated diphenyl ethers and related-compounds. *Chemical & Pharmaceutical Bulletin* **1986**, *34*, 4910-4915.

66. Howe, P.D.; Dobson, S.; Malcolm, H.M. Concise International Chemical Assessment Document 66: 2,4,6-tribromophenol and other simple brominated phenols. World Health Organization: Geneva, 2005.

67. Whitfield, F.B.; Helidoniotis, F.; Shaw, K.J.; Svoronos, D. Distribution of bromophenols in species of marine algae from eastern australia. *Journal of Agricultural and Food Chemistry* **1999**, *47*, 2367-2373, doi:10.1021/jf981080h.

68. Kicklighter, C.E.; Kubanek, J.; Hay, M.E. Do brominated natural products defend marine worms from consumers? Some do, most don't. *Limnology and Oceanography* **2004**, *49*, 430-441, doi:10.4319/lo.2004.49.2.0430.

69. Marková, E.; Smyslová, P.; Macíková, P.; Skopalová, J.; Barták, P. Study of anodic oxidation of 2,4,6-tribromophenol. *Chemicke Listy* **2012**, *106*, 195-199.

70. Lide, D.R. (ed.) *CRC handbook of chemistry and physics*, 84th edition; CRC Press: London, 2002; Volume 225, str. 2664.

71. *The Merck Index - An encyclopedia of chemicals, drugs, and biologicals*, 13th edition; Merck & Co. Inc.: Whitehouse Station, NJ, 2001.

72. Leo, A.; Hansch, C.; Elkins, D. Partition coefficients and their uses. *Chemical Reviews* **1971**, *71*, 525-616, doi:10.1021/cr60274a001.

73. Kuramochi, H.; Maeda, K.; Kawamoto, K. Water solubility and partitioning behavior of brominated phenols. *Environmental Toxicology and Chemistry* **2004**, *23*, 1386-1393, doi:10.1897/03-279.

74. Kortum, G.; Vogel, W.; Andrussow, K. Disssociation constants of organic acids in aqueous solution. **1960**, *1*, 187-536, doi:10.1351/pac196001020187.

75. Lai, Y.Q.; Lu, M.H.; Gao, X.; Wu, H.Z.; Cai, Z.W. New evidence for toxicity of polybrominated diphenyl ethers: DNA adduct formation from quinone metabolites. *Environmental Science & Technology* **2011**, *45*, 10720-10727, doi:10.1021/es203068f.

76. Shao, B.; Mao, L.; Qu, N.; Wang, Y.F.; Gao, H.Y.; Li, F.; Qin, L.; Shao, J.; Huang, C.H.; Xu, D.; Xie, L.N.; Shen, C.; Zhou, X.; Zhu, B.Z. Mechanism of synergistic DNA damage induced by the hydroquinone metabolite of brominated phenolic environmental pollutants and Cu(II): Formation of DNA-Cu complex and site-specific production of hydroxyl radicals. *Free Radical Biology and Medicine* **2017**, *104*, 54-63, doi:10.1016/j.freeradbiomed.2016.12.050.

77. Jiang, J.; Gao, Y.; Pang, S.Y.; Wang, Q.; Huangfu, X.L.; Liu, Y.Z.; Ma, J. Oxidation of bromophenols and formation of brominated polymeric products of concern during water treatment with potassium permanganate. *Environmental Science & Technology* **2014**, *48*, 10850-10858, doi:10.1021/es5008577.

78. Lin, K.D.; Yan, C.; Gan, J. Production of hydroxylated polybrominated diphenyl ethers (OH-PBDEs) from bromophenols by manganese dioxide. *Environmental Science & Technology* **2014**, *48*, 263-271, doi:10.1021/es403583b.

79. Omura, K.; Matsuura, T. Photoinduced reactions-L: Photolysis of halogenophenols in aqueous alkali and in aqueous cyanide. *Tetrahedron* **1971**, *27*, 3101-3109, doi:10.1016/S0040-4020(01)98103-7.

80. Durand, A.P.; Brown, R.G.; Worrall, D.; Wilkinson, F. Study of the aqueous photochemistry of 4-fluorophenol, 4-bromophenol and 4-iodophenol by steady state and nanosecond laser flash photolysis. *Journal of the Chemical Society-Perkin Transactions 2* **1998**, 365-370, doi:10.1039/a705287a.

81. Feo, M.L.; Gross, M.S.; McGarrigle, B.P.; Eljarrat, E.; Barcelo, D.; Aga, D.S.; Olson, J.R. Biotransformation of BDE-47 to potentially toxic metabolites is predominantly mediated by human CYP2B6. *Environmental Health Perspectives* **2013**, *121*, 440-446, doi:10.1289/ehp.1205446.

82. Krieger, L.K.; Szeitz, A.; Bandiera, S.M. Evaluation of hepatic biotransformation of polybrominated diphenyl ethers in the polar bear (*Ursus maritimus*). *Chemosphere* **2016**, *146*, 555-564, doi:10.1016/j.chemosphere.2015.11.120.

83. Krieger, L.K.; Szeitz, A.; Bandiera, S.M. Hepatic microsomal metabolism of BDE-47 and BDE-99 by lesser snow geese and japanese quail. *Chemosphere* **2017**, *182*, 559-566, doi:10.1016/j.chemosphere.2017.05.027.

84. Erratico, C.A.; Szeitz, A.; Bandiera, S.M. Oxidative metabolism of BDE-99 by human liver microsomes: Predominant role of CYP2B6. *Toxicological Sciences* **2012**, *129*, 280-292, doi:10.1093/toxsci/kfs215.

85. Erratico, C.A.; Szeitz, A.; Bandiera, S.M. Biotransformation of 2,2',4,4'-tetrabromodiphenyl ether (BDE-47) by human liver microsomes: Identification of cytochrome P450 2B6 as the major enzyme involved. *Chemical Research in Toxicology* **2013**, *26*, 721-731, doi:10.1021/tx300522u.

86. Ucan-Marin, F.; Arukwe, A.; Mortensen, A.; Gabrielsen, G.W.; Fox, G.A.; Letcher, R.J. Recombinant transthyretin purification and competitive binding with organohalogen compounds in two gull species (larus argentatus and larus hyperboreus). *Toxicological Sciences* **2009**, *107*, 440-450, doi:10.1093/toxsci/kfn240.

87. Legler, J. New insights into the endocrine disrupting effects of brominated flame retardants. *Chemosphere* **2008**, *73*, 216-222, doi:10.1016/j.chemosphere.2008.04.081.

88. Canton, R.F.; Sanderson, J.T.; Letcher, R.J.; Bergman, A.; van den Berg, M. Inhibition and induction of aromatase (CYP19) activity by brominated flame retardants in H295R human adrenocortical carcinoma cells. *Toxicological Sciences* **2005**, *88*, 447-455, doi:10.1093/toxsci/kfi325.

89. Legradi, J.; Dahlberg, A.K.; Cenijn, P.; Marsh, G.; Asplund, L.; Bergman, A.; Legler, J. Disruption of oxidative phosphorylation (OXPHOS) by hydroxylated polybrominated diphenyl ethers (OH-PBDEs) present in the marine environment.

Environmental Science & Technology **2014**, *48*, 14703-14711, doi:10.1021/es5039744.

90. Van Boxtel, A.L.; Kamstra, J.H.; Cenijn, P.H.; Pieterse, B.; Wagner, M.J.; Antink, M.; Krab, K.; Van Der Burg, B.; Marsh, G.; Brouwer, A.; Legler, J. Microarray analysis reveals a mechanism of phenolic polybrominated diphenylether toxicity in zebrafish. *Environmental Science & Technology* **2008**, *42*, 1773-1779, doi:10.1021/es0720863.

91. Monks, T.J.; Lau, S.S.; Highet, R.J. Formation of nontoxic reactive metabolites of para-bromophenol - identification of a new glutathione conjugate. *Drug Metabolism and Disposition* **1984**, *12*, 432-437.

92. Kammann, U.; Vobach, M.; Wosniok, W. Toxic effects of brominated indoles and phenols on zebrafish embryos. *Archives of Environmental Contamination and Toxicology* **2006**, *51*, 97-102, doi:10.1007/s00244-005-0152-2.

93. Koukal, M. Nová hrozba: Hyperaktivní měchýř. 21. století. http://21stoleti.cz/2009/11/19/nova-hrozba-hyperaktivni-mechyr/, staženo 19.9.2023.

94. Pešl, M.; Zámečník, L.; Hanuš, T.; Soukup, V.; Pavlík, J.; Dvořáček, J. Farmakologická léčba hyperaktivního močového měchýře. *Urologie pro praxi* **2006**, *3*, 102-107.

95. Postlind, H.; Danielson, A.; Lindgren, A.; Andersson, S.H.G. Tolterodine, a new muscarinic receptor antagonist, is metabolized by cytochromes P450 2D6 and 3A in human liver microsomes. *Drug Metabolism and Disposition* **1998**, *26*, 289-293.

96. Andersson, S.H.G.; Lindgren, A.; Postlind, H. Biotransformation of tolterodine, a new muscarinic receptor antagonist, in mice, rats, and dogs. *Drug Metabolism and Disposition* **1998**, *26*, 528-535.

97. Ellsworth, P. Fesoterodine for the treatment of urinary incontinence and overactive bladder. *Therapeutics and Clinical Risk Management* **2009**, *5*, 869-876.

98. Malhotra, B.; Darsey, E.; Crownover, P .; Fang, J.Z.; Glue, P. Comparison of pharmacokinetic variability of fesoterodine vs. tolterodine extended release in cytochrome P450 2D6 extensive and poor metabolizers. *British Journal of Clinical Pharmacology* **2011**, *72*, 226-234, doi:10.1111/j.1365-2125.2011.03948.x.

99. Aberg, A.K.G. Tolterodine metabolites. Patent US20030027856A1 (2003).

100. Vuddanda, P.R.; Chakraborty, S.; Singh, S. Berberine: A potential phytochemical with multispectrum therapeutic activities. *Expert Opinion on Investigational Drugs* **2010**, *19*, 1297-1307, doi:10.1517/13543784.2010.517745.

101. Murakami, T.; Bodor, E.; Bodor, N. Approaching strategy to increase the oral bioavailability of berberine, a quaternary ammonium isoquinoline alkaloid: Part 1. Physicochemical and pharmacokinetic properties. *Expert Opinion on Drug Metabolism & Toxicology* **2023**, *19*, 129-137, doi:10.1080/17425255.2023.2203857.

102. Feng, X.C.; Wang, K.; Cao, S.J.; Ding, L.Q.; Qiu, F. Pharmacokinetics and excretion of berberine and its nine metabolites in rats. *Frontiers in Pharmacology* **2021**, *11*, 594852, doi:10.3389/fphar.2020.594852.

103. Guo, Y.; Li, F.; Ma, X.C.; Cheng, X.G.; Zhou, H.H.; Klaassen, C.D. CYP2D plays a major role in berberine metabolism in liver of mice and humans. *Xenobiotica* **2011**, *41*, 996-1005, doi:10.3109/00498254.2011.597456.

104. Zuo, F.; Nakamura, N.; Akao, T.; Hattori, M. Pharmacokinetics of berberine and its main metabolites in conventional and pseudo germ-free rats determined by liquid chromatography/ion trap mass spectrometry. *Drug Metabolism and Disposition* **2006**, *34*, 2064-2072, doi:10.1124/dmd.106.011361.

105. Wang, D.X.; Sakoda, A.; Suzuki, M. Effects of surface oxygen of activated carbon on alkaloid adsorption: A molecular dynamics simulation study. *Adsorption-Journal of the International Adsorption Society* **1999**, *5*, 97-108, doi:10.1023/A:1026479130851.

106. Liu, Y.T.; Hao, H.P.; Xie, H.G.; Lv, H.; Liu, C.X.; Wang, G.J. Oxidative demethylenation and subsequent glucuronidation are the major metabolic pathways of berberine in rats. *Journal of Pharmaceutical Sciences* **2009**, *98*, 4391-4401, doi:10.1002/jps.21721.

107. Ma, C.H.; Li, Z.X.; Wang, L.X.; Tang, Y.H.; Xiao, H.B.; Huang, C.G. Identification of major alkaloids in rat urine by HPLC/DAD/ESI-MS/MS method following oral administration of cortex decoction. *Helvetica Chimica Acta* **2009**, *92*, 379-398, doi:10.1002/hlca.200800315.

108. Yang, Y.H.; Kang, N.; Xia, H.J.; Li, J.; Chen, L.X.; Qiu, F. Metabolites of protoberberine alkaloids in human urine following oral administration of coptidis

rhizoma decoction. *Planta Medica* **2010**, *76*, 1859-1863, doi:10.1055/s-0030-1250053.

109. Tsai, P.L.; Tsai, T.H. Hepatobiliary excretion of berberine. *Drug Metabolism and Disposition* **2004**, *32*, 405-412, doi:10.1124/dmd.32.4.405.

110. Qiu, F.; Zhu, Z.Y.; Kang, N.; Piao, S.J.; Qin, G.Y.; Yao, X.S. Isolation and identification of urinary metabolites of berberine in rats and humans. *Drug Metabolism and Disposition* **2008**, *36*, 2159-2165, doi:10.1124/dmd.108.021659.

111. Gaillot, J.; Heusse, D.; Hougton, G.W.; Aurele, J.M.; Dreyfus, J.F. Pharmacokinetics and metabolism of zopiclone. *Pharmacology* **1983**, *27*, 76-91, doi:10.1159/000137914.

112. Becquemont, L.; Mouajjah, S.; Escaffre, O.; Beaune, P.; Funck-Brentano, C.; Jaillon, P. Cytochrome P-450 3A4 and 2C8 are involved in zopiclone metabolism. *Drug Metabolism and Disposition* **1999**, *27*, 1068-1073.

113. Armenian, P.; Vo, K.T.; Barr-Walker, J.; Lynch, K.L. Fentanyl, fentanyl analogs and novel synthetic opioids: A comprehensive review. *Neuropharmacology* **2018**, *134*, 121-132, doi:10.1016/j.neuropharm.2017.10.016.

114. Volkow, N.D. The epidemic of fentanyl misuse and overdoses: Challenges and strategies. *World Psychiatry* **2021**, *20*, 195-196, doi:10.1002/wps.20846.

115. Choińska, M.; Šestáková, I.; Hrdlička, V.; Skopalová, J.; Langmaier, J.; Majer, V.; Navrátil, T. Electroanalysis of fentanyl and its new analogs: A review. *Biosensors* **2022**, *12*, 26, doi:10.3390/bios1201002.

116. Oudejans, L.; See, D.; Dodds, C.; Corlew, M.; Magnuson, M. Decontamination options for indoor surfaces contaminated with realistic fentanyl preparations. *Journal of Environmental Management* **2021**, *297*, 113327, doi:10.1016/j.jenvman.2021.113327.

117. Qi, L.H.; Cheng, Z.X.; Zuo, G.M.; Li, S.M.; Fan, Q.P. Oxidative degradation of fentanyl in aqueous solutions of peroxides and hypochlorites. *Defence Science Journal* **2011**, *61*, 30-35, doi:10.14429/dsj.61.68.

118. Xu, L.; Ren, L.J.; Wang, Z.H.; Tian, X.T.; Qi, L.H.; Fan, Q.P.; Xiang, Y.L. Oxidative treatment of fentanyl compounds in water by sodium bromate combined with sodium sulphite. *Water Science and Technology* **2015**, *72*, 38-44, doi:10.2166/wst.2015.185.

119. Garg, A.; Solas, D.W.; Takahashi, L.H.; Cassella, J.V. Forced degradation of fentanyl: Identification and analysis of impurities and degradants. *Journal of Pharmaceutical and Biomedical Analysis* **2010**, *53*, 325-334, doi:10.1016/j.jpba.2010.04.004.

120. Kahánková, T. *Analýza syntetických opioidů a produktů jejich metabolismu s využitím elektrochemických a separačních metod*. Diplomová práce, Univerzita Palackého v Olomouci, Olomouc, 2022.

121. Skopalová, J.; Jerga, R.; Štolbová, D.; Zajacová Cechová, M.; Cankař, P.; Barták, P. Electrochemical oxidation of fentanyl and its analogues. *Proceedings of International Conference Modern Electrochemical Methods XL* **2021**, str. 108-111.

6 Přílohy – Autorčiny publikace použité v habilitační práci

Příloha 1

Electrochemical oxidation of 5-hydroxymethyl tolterodine and identification of its oxidation products using liquid chromatography and mass spectrometry.

Kučerová, P.; **Skopalová**, **J.***; Kučera, L.; Táborský, J.; Švecová, H.; Lemr, K.; Cankař, P.; Barták, P.

Electrochimica Acta **2016**, *215*, 617-625

Electrochimica Acta 215 (2016) 617–625

Contents lists available at ScienceDirect

Electrochimica Acta

journal homepage: www.elsevier.com/locate/electacta

Electrochemical oxidation of 5-hydroxymethyl tolterodine and identification of its oxidation products using liquid chromatography and mass spectrometry

Pavla Kučerová[a], Jana Skopalová[a,*], Lukáš Kučera[a], Jakub Táborský[a], Hana Švecová[a], Karel Lemr[a], Petr Cankař[b], Petr Barták[a]

[a] Regional Centre of Advanced Technologies and Materials, Department of Analytical Chemistry, Faculty of Science, Palacký University, 17. listopadu 12, 771 46 Olomouc, Czech Republic

[b] Department of Organic Chemistry, Faculty of Science, Palacký University, 17. listopadu 12, 771 46 Olomouc, Czech Republic

ARTICLE INFO

Article history:
Received 10 June 2016
Received in revised form 24 August 2016
Accepted 29 August 2016
Available online 30 August 2016

Keywords:
5-hydroxymethyl tolterodine
oxidation products
voltammetry
mass spectrometry
mechanism

ABSTRACT

The electrochemical behavior of 5-hydroxymethyl tolterodine (5-HMT), the active metabolite of antimuscarinic drugs tolterodine and fesoterodine used to treat urge incontinence and overactive bladder, was investigated using cyclic and differential pulse voltammetry at glassy carbon electrode. Electrooxidation of 5-HMT proceeds as a complex pH-dependent process. Controlled potential electrolysis of 5-HMT solutions was performed at platinum gauze electrode in aqueous-methanolic media. Electrolyzed solutions were analyzed using ultra performance liquid chromatography with electrospray ionization quadrupole time-of-flight mass spectrometry. Two main oxidation centers of the studied molecule were located: the *p*-hydroxybenzyl alcohol group and the tertiary amino group. Oxidation of the first center proceeds in several steps leading to the formation of 5-formyl tolterodine, *p*-benzoquinone derivative and several dimeric, hydroxylated and methoxylated products depending on pH of the solution and electrode potential. The second center is oxidized preferentially in alkaline media at higher potentials under the hydrolytic cleavage of diisopropylamine and formation of corresponding aldehydes. Mechanism of the electrochemical oxidation of 5-HMT has been proposed.

1. Introduction

5-Hydroxymethyl tolterodine (5-HMT, Fig. 1a) is the main active metabolite of antimuscarinic drugs tolterodine (TOL, Fig. 1b) and fesoterodine (FES, Fig. 1c), which are commercially available under the name Detrol/Detrusitol and Toviaz, respectively. Both drugs are indicated for the treatment of urinary urge incontinence (UUI) and other symptoms associated with an overactive bladder. TOL or FES metabolize to 5-HMT in human body via cytochrome P450 (CYP) 2D6 enzyme or ubiquitous nonspecific esterases, respectively. FES is rapidly and extensively metabolized to 5-HMT. Tolterodine is only partially metabolized to 5-HMT and their ratio varies among individuals due to different activity of CYP2D6 [1]. According to recent studies, FES proves superior efficacy in treatment of UUI over tolterodine. 5-HMT is very efficient muscarinic receptor antagonist and pharmacodynamic effects of fesoterodine in human body are thought to be mediated via 5-HMT [1,2]. 5-HMT is further metabolized by CYP3A4 and CYP2D6 in the liver to its inactive metabolites namely carboxy (SPM 5590), carboxy-*N*-desisopropyl (SPM 7789) and *N*-desisopropyl metabolite (SPM 7790). None of them contribute significantly to the antimuscarinic activity of the drug. After oral administration of fesoterodine, approximately 70% of the administered dose is recovered in urine as the active metabolite (5-HMT, 16%), carboxy metabolite (34%), carboxy-*N*-desisopropyl metabolite (18%), or *N*-desisopropyl metabolite (1%), and about 7% is recovered in feces [3,4].

5-HMT is mainly analyzed along with its prodrug TOL or FES. High performance liquid chromatography/mass spectrometry (HPLC/MS) is the most frequently used method for determination of 5-HMT [5–9]. Gas chromatography/mass spectrometry (GC/MS) is applicable after derivatization of 5-HMT [10]. Electroanalytical methods could be used to mimic the formation of possible oxidative metabolites [11]. Furthermore, the hyphenation of electrochemistry, chromatography and mass spectrometry is promising to simulate and investigate (bio)transformation of drugs [12] or pesticides [13]. For the purpose, electrospray

* Corresponding author. Tel.: +420 585 634 442, fax: +420 585 634 433.
E-mail address: jana.skopalova@upol.cz (J. Skopalová).

http://dx.doi.org/10.1016/j.electacta.2016.08.137
0013-4686/

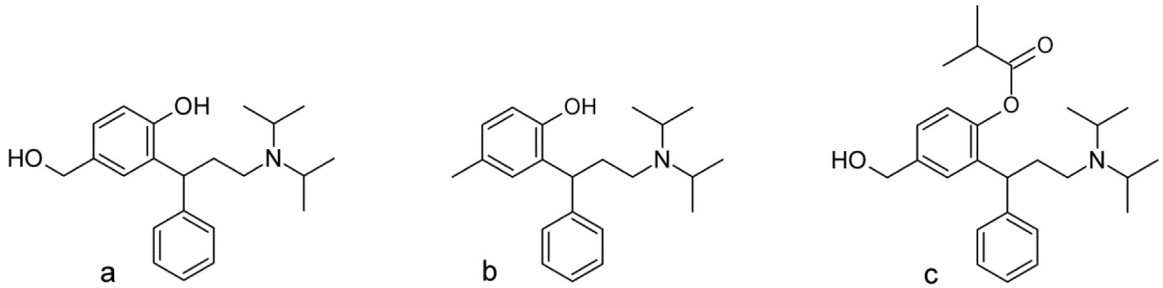

Fig. 1. Chemical structures of 5-hydroxymethyl tolterodine (a), tolterodine (b) and fesoterodine (c).

ionization is a widely used ionization technique of great compatibility with electrochemistry [14,15].

Electrochemical oxidation of tolterodine and fesoterodine have been described recently [12,16] including characterization and identification of some of their oxidation products. To the best of our knowledge [12], the electrochemical behavior of 5-HMT has not been fully described yet. The aim of the paper is to better understand the general redox reactions of the compound responsible for the main pharmaceutical activity of these antimuscarinics. For this purpose, 5-HMT was electrochemically oxidized under the conditions of controlled potential electrolysis and products were analyzed by ultra-performance liquid chromatography with electrospray ionization mass spectrometry (UPLC/ESI-MS). Several new oxidation products were discovered (in addition to previously described), reasonable oxidation mechanism was proposed and crucial reaction steps involved in the general oxidation pathway were verified using simple model compounds.

2. Experimental

2.1. Reagents

5-Hydroxymethyl tolterodine was synthesized from (*R*)-fesoterodine fumarate (99%), which was obtained from IS Chemical Technology, China. Methanol, sulfuric acid (p.a., Lach-Ner, Czech Republic), acetonitrile and *p*-xylene (HPLC gradient grade, Sigma-Aldrich, Czech Republic), ammonium acetate (p.a., >98.0%, Lach-Ner, Czech Republic) and ultrapure water (Merck Millipore, Darmstadt, Germany) were used. Britton-Robinson (BR) buffers were prepared from phosphoric acid, acetic acid and boric acid (0.04 mol dm^{-3} each, p.a., Lachema, Czech Republic), pH values were adjusted with sodium hydroxide (0.2 mol dm^{-3}, p.a., Lach-Ner, Czech Republic).

2.2. Synthesis of 5-hydroxymethyl tolterodine

Fesoterodine fumarate (200 mg, 0.38 mmol) was dissolved in a mixture of methanol (2 cm^3) and conc. aqueous ammonia (2 cm^3). The reaction mixture was stirred at room temperature for 18 hours. Then the solvents were evaporated on a rotary evaporator under reduced pressure. The residue was diluted with water (2 cm^3) and extracted with ethyl acetate (5 cm^3). Ethyl acetate was evaporated. The resulting oily crude product was dissolved in chloroform (1 cm^3), applied to a flash chromatography column with silica gel and eluted with a mixture of chloroform/methanol/conc. aqueous ammonia 10:1:0.1 to give 71.7 mg of pure 5-hydroxymethyl tolterodine as yellowish oil. The total yield was 55% and the purity of the product was higher than 98% (HPLC).

2.3. Voltammetric measurements

Voltammetric measurements were performed using an Eco-Tribo-Polarograph with Polar.Pro v. 4 software (Polaro-Sensors, Czech Republic) and an Autolab PGSTAT128N with NOVA 1.10 software (Metrohm Autolab, the Netherlands). A three-electrode system consisted of a glassy carbon working electrode (GCE, disk diameter 3.0 mm, Bioanalytical Systems, USA), a platinum wire auxiliary electrode and a saturated calomel reference electrode (SCE). The working electrode was polished using 0.05 μm alumina slurry on wet microcloth (Buehler, USA) and sonicated in distilled water for 60 s before each measurement. Cyclic voltammograms were recorded at a scan rate of 0.05 V s^{-1}, unless otherwise stated. Differential pulse voltammetry (DPV) measurements were performed at pulse amplitude of 0.05 V, pulse width of 0.1 s and a scan rate of 0.01 V s^{-1}. All experiments were performed in a low volume cell (maximum 2 cm^3) in supporting electrolytes containing BR buffer of desired pH (as indicated) and methanol (1:1, v/v). The dependencies of peak potentials and peak currents were plotted against the pH values of the mixture of BR buffer and methanol (1:1) measured with glass pH electrode calibrated using aqueous standard buffers.

2.4. Controlled potential electrolysis

An apparatus for controlled potential electrolysis consisted of an OH-404 potentiostat (Radelkis, Budapest, Hungary) with a three-electrode system: platinum gauze working electrode, reference SCE and platinum auxiliary electrode placed in a separate cathode compartment. The electrolysis was performed at various values of constant potential in aqueous BR buffer of different pH/methanol (1:1, v/v) under nitrogen atmosphere. The potential values 0.65 and 0.9 V were chosen for pH 3 and 0.3, 0.5 and 0.9 V for pH 7 and pH 9. All samples were electrolyzed in stirred solutions (magnetic stirrer MR Hei-Standard, Heidolph, Germany, PTFE-coated micro stir bar, 7 mm × 2 mm) containing 0.5 mmol dm^{-3} 5-HMT (0.17 mg cm^{-3}) in a total volume of 1.2 cm^3 until the current decreased to a residual value.

Controlled potential coulometry was performed on Autolab PGSTAT128N with a three-electrode system comprising spectral graphite rod as a working electrode (surface area 5.42 cm^2), reference SCE and Pt auxiliary electrode placed in a cathode compartment separated from the anode part by a vycor frit. Supporting electrolyte containing BR buffer solutions of pH 7.5 and methanol (1:1, v/v) was electrolyzed at potential 1 V until the current reached its residual value (typically 20 μA). Then 100 nmol of 5-HMT was added (c = 0.1 mmol dm^3) and the solution was electrolyzed at 1 V for 2 h to reach the residual current value.

2.5. UPLC/MS, GC/MS and UV–vis spectrometry analysis

An Acquity UPLC system (Waters, Milford, Manchester, UK) equipped with a binary solvent manager, sample manager, column manager and PDA detector was used. Separation was performed on a chromatographic Vertex Plus Column (50 mm × 2 mm, 1.8 μm) Blue Orchid C18 (Knauer, Berlin, Germany). Mobile phase consisted of 0.01 mol dm^{-3} ammonium acetate in water (solvent A)/ acetonitrile (solvent B), gradient elution was performed (% v/v): 0–5 min (10–80% B), 5–6 min (80% B), 6–7 min (80–10% B) and 7–10 min (10% B) with flow rate 0.4 cm^3 min^{-1}, the temperature of the autosampler and the column oven was 20 °C and 25 °C, respectively. The injection volume was 0.02 cm^3. A QqTOF Premier mass spectrometer (Waters, Milford, MA, USA) coupled to the UPLC system provided molecular formulas and fragment spectra to confirm putative structures. The tuned electrospray ionization (ESI) parameters were as follows: spray voltage 3 kV (positive mode), source temperature 100 °C, sampling cone 30 V, desolvation temperature 150 °C, cone gas flow rate 38 dm^3 h^{-1} and desolvation gas flow rate 450 dm^3 h^{-1}. Nitrogen was used as a desolvation gas and argon as a collision gas. The data were acquired using simultaneous scanning at lower collision energy (5 eV) and at higher energy applying collision energy ramp from 15 to 35 eV or from 5 to 15 eV for OP6B. Data were processed using MassLynx 4.1 software (Waters).

The Agilent 7010 Triple Quadrupole GC/MS system with Mass Hunter software (Agilent Technologies, Palo Alto, USA) was used for proof of formic acid presence in solutions of 4-hydroxybenzyl alcohol and 4-hydroxybenzaldehyde in BR buffer of pH 3 electrolyzed at the potential 1.5 V on the platinum gauze electrode. Samples were esterified and rising methyl formate was extracted into *p*-xylene before analysis. The separation was performed on two (5%-Phenyl)-methylpolysiloxane capillary columns HP–5 ms Ultra Inert in series (15 m × 0.25 mm × 0.25 μm) with constant flow 0.9 and 1.1 cm^3 min^{-1}, respectively. Nitrogen (Messer Group GmbH, Germany) was used as a collision gas with flow rate 1.5 cm^3 min^{-1} and helium (He 5.0. Siad, Italy) as a quench gas with flow rate 2.25 cm^3 min^{-1}. The GC oven temperature was initially held at 30 °C for 5 min, ramped to 250 °C at 20 °C min^{-1} and held at 250 °C for 5 min.

UV-Vis spectrometer Lambda 25 (PerkinElmer, Waltham, MA, USA) was used for measurement of UV–vis spectra of *p*-benzoquinone in 1:1 (v/v) aqueous/methanolic solution.

3. Results and Discussion

3.1. Electrochemical behavior of 5-hydroxymethyl tolterodine

The cyclic voltammogram of 5-HMT in buffered aqueous methanolic solution of pH 7.5 (1:1, v/v) recorded at scan rate 0.05 V s^{-1} (Fig. 2a) showed two anodic signals at potentials of 0.60 V (peak A) and 0.86 V (peak B). Two small reduction peaks were observed at potentials of 0.22 V (peak C) and −0.17 V (peak D) in the reverse cathodic branch. The peak C was more intensive when the potential was held for 30 s at the switching potential E_s = 0.65 V after the first anodic scan and before starting the backward cathodic scan (Fig. 2b). In the following anodic scan, a very small oxidation signal at 0.37 V (peak E) was observed. This implies that an electroactive product providing a quasi-reversible pair of peaks C and E ($E_{p,a} - E_{p,c}$ = 0.37–0.22 = 0.15 V) was formed at the potential of peak A. The perceptible drop of the height of the peaks A and B in the second cycle was most likely caused by passivation of the electrode surface by the product(s) of electrode reaction arising from the oxidation of 5-HMT in the first potential cycle.

As can be expected from the structure of 5-HMT and from the electrochemical behavior of its metabolic precursor tolterodine [12], the phenol ring is an electroactive part of the 5-HMT molecule. Cyclic voltammogram of 4-hydroxybenzyl alcohol (Fig. 2c), obtained under the same conditions, revealed an oxidation peak at the same potential as the peak A of 5-HMT. Furthermore, potentials of two reduction peaks observed in the reverse cathodic branch of the voltammogram correspond to the potentials of the peaks C and D in the 5-HMT voltammogram. Similarly to 5-HMT, the peak C increases when the polarization direction was reversed at potential of the anodic peak A (Fig. 2d). Remarkable similarities in the voltammetric behavior of 5-HMT and 4-hydroxybenzyl alcohol strongly support the hypothesis that electrochemical oxidation of 5-HMT starts at the hydroxyl group directly bond to the aromatic ring providing the peak A.

The couple of peaks C and E appertains to reduction and re-oxidation of an intermediate formed by oxidation of 5-HMT at potential of the peak A. Similar behavior was reported for the redox pair biphenoquinone–biphenol arising in the first step of oxidation of phenol to phenoxy radical [17]. Two radicals can recombine to form biphenol which is immediately oxidized to biphenoquinone since the redox potential of biphenol is lower than that of phenol. Similar *o*-biphenol and *o*-biphenoquinone structures were found in electrochemically oxidized tolterodine solutions [12]. Likewise, the formation of such dimeric structures can be expected in case of 5-HMT.

The peak D in the cathodic branch of cyclic voltammogram of 5-HMT (Fig. 2a) appeared at the same potential (−0.17 V) as a reduction peak of *p*-benzoquinone (Fig. 2e). Its intensity increased when the potential scan was reversed more anodically at the peak B potential or higher. Supposing the similarity between 5-HMT and phenol behavior [17], the phenoxy radical formed in the first oxidation step could be further oxidized to a phenoxy cation. The cation can be easily attacked by water forming catechol or hydroquinone (after the cleavage of the hydroxymethyl substituent in the *para* position) which is further oxidized to a quinone. Such *p*-benzoquinone structures were reported as products of anodic oxidation of various *para* substituted phenols [18]. Thus, formation of similar quinone structure(s) during anodic oxidation of 5-HMT in aqueous methanolic media can be expected.

Voltammograms of 5-HMT and fesoterodine acquired under the same experimental conditions at pH 9.5 (Fig. 3) revealed the similarity between potential of the 5-HMT oxidation peak B and potential of the fesoterodine oxidation peak. Unlike 5-HMT, fesoterodine did not provide any cathodic peaks in the reverse branch of voltammograms due to the absence of a free phenolic group (oxidation of which leads to the formation of electroactive dimeric products and quinone structures). As we have recently shown [16], fesoterodine oxidation proceeds on diisopropylamine group under the cleavage of an isopropylamino group during oxidative deamination. Alkaline conditions are more favorable for this reaction. Therefore, similar reactions can be expected for 5-HMT at the potential of peak B.

The scan rate strongly influenced a course of 5-HMT cyclic voltammograms (Fig. 4). Two oxidation peaks were observed in methanol/BR buffer solution pH 7.5 (1/1, v/v) at scan rates about 0.005 V s^{-1} (Fig. 4a). Another oxidation peak (A′) was formed at scan rate 0.03 V s^{-1} (Fig. 4b). Scan rates higher than 0.15 V s^{-1} caused an overlap of signals A′ and B (Fig. 4c). These observations proved a complex redox behavior including at least three successive electrode reactions in which electroactive species with particularly close redox potentials are formed. Bifurcation of peak A at faster scan rates indicates the presence of chemical reaction following the first electron transfer step. Speed of the homogeneous reaction controls the formation of an electroactive intermediate which is subsequently oxidized at the electrode surface. Potential shift of the half peak A by 0.026 (±0.001) V per log unit in the scan range 0.01–0.5 V s^{-1} supports the assumption.

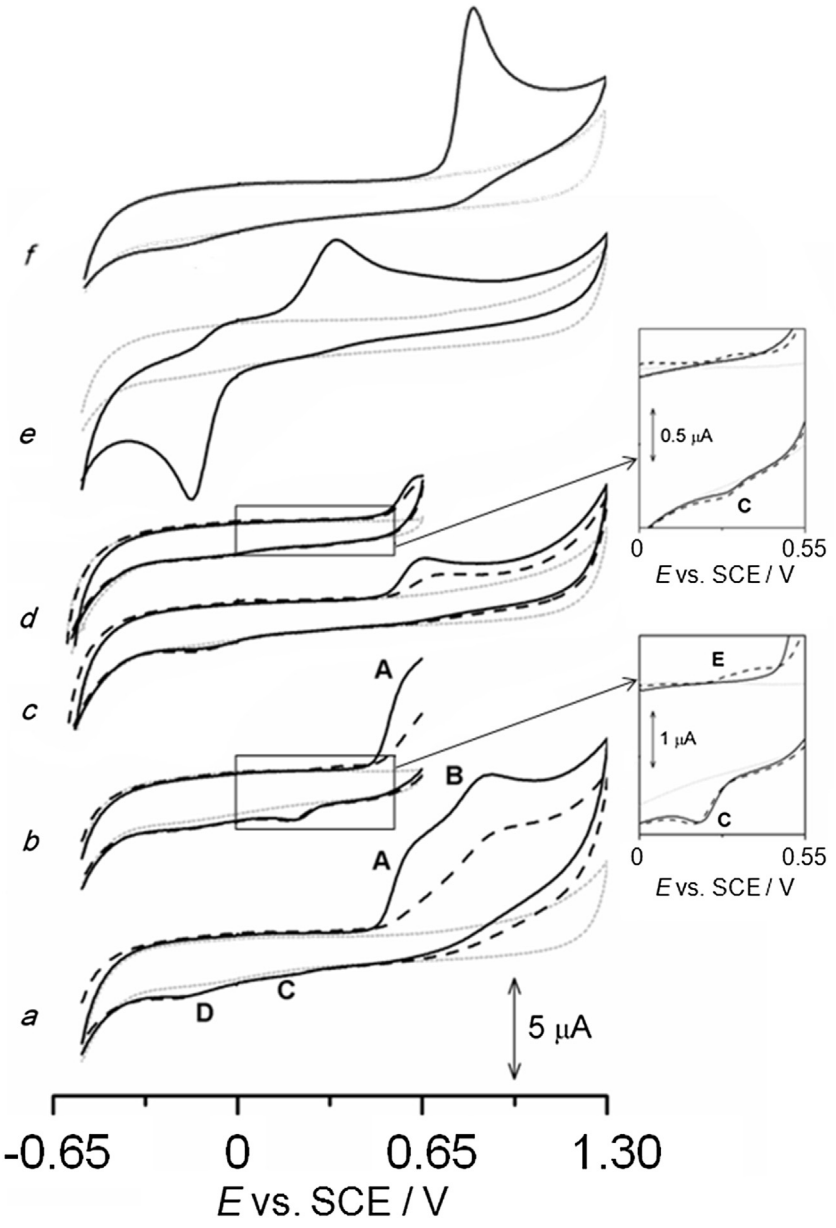

Fig. 2. Cyclic voltammograms of 5-HMT recorded with the switching potential E_s = 1.3 V (a) and E_s = 0.65 V after the accumulation 30 s at 0.65 V (b), 4-hydroxybenzyl alcohol with E_s = 1.3 V (c) and E_s = 0.65 V (d), *p*-benzoquinone with E_s = 1.3 V (e) and 4-hydroxybenzaldehyde with E_s = 1.3 V (f). Concentration of all substances: 0.5 mmol dm^{-3}, supporting electrolyte: CH_3OH/BR buffer pH 7.5 (1:1, v/v, grey line), 1st cycle (solid black line), 2nd cycle (dashed black line), scan rate 0.05 V s^{-1}, starting potential was −0.6 V for all voltammograms.

The value is between 0.03 V and 0.02 V for a tenfold change in scan rate which is typical for one-electron transfer reactions followed by first order and second order chemical reaction (dimerization), respectively [19].

Controlled potential coulometry (CPC) on spectral graphite rod electrode was used for determination of number of electrons involved in the electrode process. Total charge 56.4 mC passed through the electrolytic cell with 100 nmol of 5-HMT in BR buffer pH 7.5 and methanol (1:1) corresponding to 5.84 electrons exchanged per one molecule of the drug. Almost the same number 5.81 electrons was found using convolutive procedure [16] applied on linear sweep voltammogram recorded at 5 mV s^{-1} in solution of the same composition as in the CPC experiment (Supplementary Information file, Fig. S1). Overall, the electrochemical oxidation of 5-HMT under stated conditions is nearly 6-electron process.

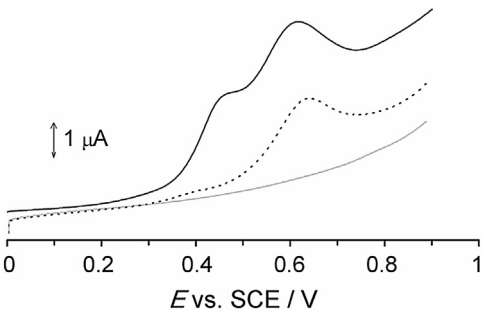

Fig. 3. Linear sweep voltammograms of 0.2 mmol dm^{-3} 5-hydroxymethyl tolterodine (black solid line) and 0.1 mmol dm^{-3} fesoterodine (dotted line) in supporting electrolyte consisting of BR buffer pH 9.5 and methanol (1:1, v/v, gray solid line), scan rate 0.1 V s^{-1}.

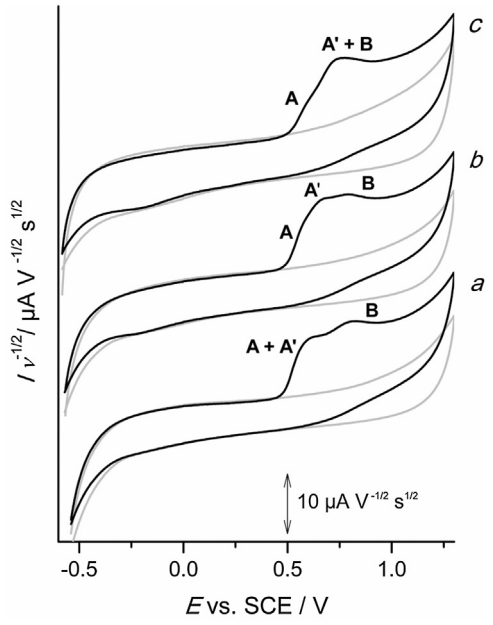

Fig. 4. Normalized cyclic voltammograms of 0.1 mmol dm^{-3} 5-HMT (black line) at scan rate 0.005 V s^{-1} (a), 0.03 V s^{-1} (b) and 0.15 V s^{-1} (c). Supporting electrolyte (grey line) CH_3OH/BR buffer pH 7.5 (1:1, v/v).

Non-integer number of transferred electrons is in compliance with higher number of electrode reactions proceeding simultaneously at the electrode (and probably involving the different reaction centers of the 5-HMT molecule) as it was observed by cyclic voltammetry at different scan rates (Fig. 4).

The 5-HMT oxidation depends on pH (see DPV curves in Supplementary information file, Fig. S2). Signal of the peak A was observed in the whole pH range reaching the maxima at pH > 9.5 (Fig. 5a). The peak B was observable in the range of pH 4–12 with the highest current intensity at pH 8.5–9.5. The potential of both oxidation peaks shifted to lower values with increasing pH (Fig. 5b). The peak A showed the shift by −62 mV/pH suggesting participation of the same number of electrons and protons in the first oxidation step. Similarly, the potential of peak B was shifted by

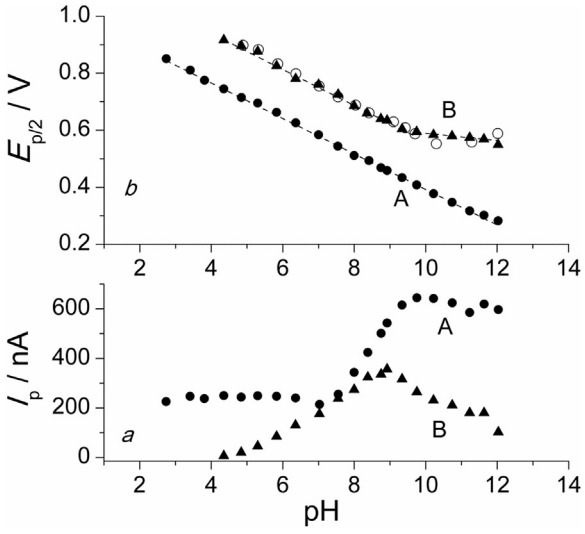

Fig. 5. Variation of DPV peak currents (a) and half-peak potentials (b) of 5-HMT peaks A and B with pH. Concentration of 5-HMT: 0.1 mmol dm^{-3}, supporting BR buffer/methanol (1:1, v/v), scan rate 0.01 V s^{-1}. Open circles stand for the dependence of DPV peak potentials vs. pH for fesoterodine under the same conditions.

−63 mV/pH up to pH 9.5 indicating the transfer of the same number of protons and electrons as well. In alkaline solutions of pH 9.5–12 the shift was less steep with the slope of −17 mV/pH corresponding to decrease of number of released protons. The change in the slope around pH 9.5 is most likely related to the change in protolytic form of the electroactive specie(s) at the electrode surface. Variation of peak B potential with pH closely copies the course of E_p – pH dependence for fesoterodine recorded under the same conditions (Fig. 5b, open circles). It supports the supposition that the oxidation process providing peak B is similar to those of fesoterodine.

Adsorption of 5-HMT as well as products of its electrode reactions on the GCE electrode surface was observed. When the clean electrode was immersed into 0.5 mmol dm^{-3} solution of 5-HMT for five minutes, then it was properly rinsed by deionized water and transferred into pure electrolyte, a small but perceptible voltammetric peak of the adsorbed 5-HMT was recorded. Adsorption of products of 5-HMT oxidation was evident from the distinct decrease of the anodic current signals in successive cyclic voltammograms (see Supplementary information file, Fig. S3) which was caused by fouling of the electrode surface with products of electrode reactions. The drop of oxidation current was more pronounced in neutral and especially in alkaline media (pH 7 and 9, respectively). This pH-dependent voltammetric behavior is in accordance with that of other phenolic compounds and can be explained by easier oxidability of phenolate anion [20] under formation of strongly adsorbed dimeric/polymeric products. However, the passivation of the electrode was not so pronounced in comparison with simple phenols (e.g. 4-chlorophenol [21]) forming compact adhesive polymeric films.

3.2. Controlled potential electrolysis and UPLC/MS analysis of 5-hydroxymethyl tolterodine oxidation products

For more detailed characterization of oxidation products, a series of experiments were performed with controlled potential electrolysis of 5-HMT on a large surface Pt electrode in methanol/aqueous BR buffer solutions of pH 3, 7 and 9. The controlled potential values suitable for exhaustive electrolysis were selected according to courses of 5-HMT cyclic voltammograms recorded at each pH (0.5 V for pH 7 and 9 and 0.9 V for all three pH). Electrolyzed solutions of 5-HMT were directly analyzed using UPLC/ESI-MS. The chromatograms and mass spectra of electrolyzed solutions were compared to those of control samples treated at potentials of 0.65 V for pH 3 and 0.3 V for pH 7 and 9, which were expected to be too low to cause electrochemical transformation of 5-HMT. The control samples as well as the untreated standard solution of 5-HMT rendered a peak with retention time (t_R) of 1.95 min and an ion $[M+H]^+$ at m/z 342 (Fig. 6a) providing fragment ions at m/z 300 (loss of propene), the most intensive ion at m/z 223 (loss of diisopropylamine and H_2O) and at m/z 195 (loss of *N*,*N*-diisopropylaminoethane and H_2O or diisopropylamine, ethene and H_2O). The fragmentation spectrum of 5-HMT corresponds to the spectrum reported in the literature [7].

3.2.1. Product of 5-HMT electrolysis with m/z *340*

An oxidation product OP1 (t_R = 2.27 min, $[M+H]^+$ at m/z 340, Table 1) was detected in samples of 5-HMT electrolyzed mostly at the potential of peak A under all three pH conditions. The yield of this product decreased in the order of pH 3 > pH 7 > pH 9. The precursor ion (m/z 340, Fig. 6b) provided a most abundant fragment at m/z 239 (loss of diisopropylamine). Neutral losses indicating presence of 5-hydroxymethyl group (loss of water, formaldehyde or methanol) were absent in the spectrum. Instead, a low intense signal at m/z 312 corresponding to loss of CO was observed. Based on the fragmentation pattern, accurate mass and

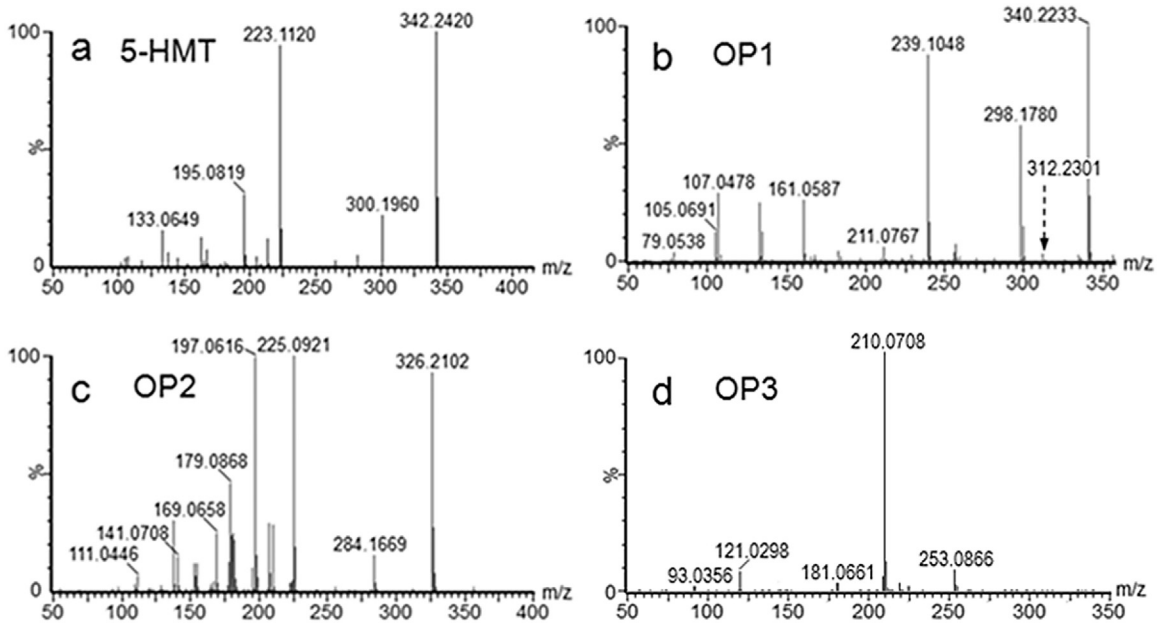

Fig. 6. MS spectra of 5-HMT standard (a) and its oxidation products: OP1 (b), OP2 (**c**), OP3 (d) acquired after electrolysis at 0.9 V (in pH 3 for OP1 and in pH 7 for OP2 and OP3). Spectra were acquired at higher energy using collision energy ramp from 15 to 35 eV with precursor ion selection (a), without precursor ion selection (b–d) in positive (a–c) or negative (d) ionization mode. Uncorrected raw *m/z* data.

Table 1
UPLC/MS analysis of 5-hydroxymethyl tolterodine and its oxidation products; *m/z* data were corrected using a reference lock mass (leucine enkephalin).

Compound	t_R (min)	*m/z*	Molecular formula	dtm (mDa)	pH	Oxidation potential
5-HMT	1.95	$[M+H]^+$ 342.2427	$C_{22}H_{32}NO_2$	−0.6		
OP1	2.27	$[M+H]^+$ 340.2292	$C_{22}H_{30}NO_2$	1.5	3, 7, 9	L, H
OP2	2.39	$[M+H]^+$ 326.2127	$C_{21}H_{28}NO_2$	0.7	3, 7	L, H
OP3	2.90	$[M-H]^-$ 253.0872	$C_{16}H_{13}O_3$	0.7	7, 9	H
OP4	2.27	$[M-H]^-$ 255.1049	$C_{16}H_{15}O_3$	2.8	7, 9	H
OP5	0.56	$[M+H]^+$ 102.1321	$C_6H_{16}N$	3.8	7, 9	H
OP6A	1.81	$[M+H]^+$ 356.2198	$C_{22}H_{30}NO_3$	−2.8	3, 7	L, H
OP6B	2.16	$[M+H]^+$ 356.2253	$C_{22}H_{30}NO_3$	1.9	3, 7	L, H
OP6C	2.31	$[M+H]^+$ 356.2242	$C_{22}H_{30}NO_3$	1.6	3, 7, 9	L, H
OP7A	2.12	$[M+H]^+$ 372.2565	$C_{23}H_{34}NO_3$	2.6	3, 7, 9	L, H
OP7B	2.58	$[M+H]^+$ 372.2552	$C_{23}H_{34}NO_3$	1.3	3, 7, 9	L, H
OP8 (dimer)	2.78	$[M+H]^+$ 665.4313	$C_{43}H_{57}N_2O_4$	−0.5	3, 7	L, H
OP9A (dimer)	2.52	$[M+H]^+$ 681.4615	$C_{44}H_{61}N_2O_4$	−1.6	7, 9	L, H
OP9B (dimer)	2.91	$[M+H]^+$ 681.4611	$C_{44}H_{61}N_2O_4$	−2.0	3, 7, 9	L
OP9C (dimer)	3.17	$[M+H]^+$ 681.4634	$C_{44}H_{61}N_2O_4$	0.3	7, 9	L, H
OP10 (dimer)	3.09	$[M+H]^+$ 679.4459	$C_{44}H_{59}N_2O_4$	−1.6	3, 7	L, H
OP11A (dimer)	2.58	$[M+H]^+$ 695.4505	$C_{44}H_{59}N_2O_5$	8.1	3	L, H
OP11B (dimer)	2.71	$[M+H]^+$ 695.4423	$C_{44}H_{59}N_2O_5$	−0.1	3, 7	L, H
OP11C (dimer)	3.34	$[M+H]^+$ 695.4429	$C_{44}H_{59}N_2O_5$	0.5	3, 7	L, H

t_R—retention time, dtm—relative difference between theoretical and experimental ion mass, L—lower potential (i.e. 0.65 V at pH 3 and 0.5 V at pH 7 and 9), H—higher potential (i.e. 0.9 V at pH 3, 7 and 9), respective products were most abundant at the underlined values of pH and oxidation potentials.

difference $\Delta m/z = 2.0187$ (two hydrogen atoms) from the value of 5-HMT protonated molecule, OP1 was identified as a product of oxidative dehydrogenation of hydroxymethyl group of 5-HMT (Scheme 1). The same substance, 5-formyl tolterodine, was found as a secondary oxidation product of tolterodine and a primary oxidation product of the own 5-HMT [12].

3.2.2. *Product of 5-HMT electrolysis with* m/z *326*

Electrolysis of 5-HMT in acidic and neutral media rendered product OP2 ($t_R = 2.39$ min, $[M+H]^+$ at *m/z* 326, Table 1) that was preferably formed at higher potentials of electrolysis corresponding to the voltammetric peak B. Fragment ions at *m/z* 197 and 169 (two successive losses of CO from an ion at *m/z* 225) observed in fragmentation spectrum of OP2 (Fig. 6c) could be eliminated from *p*-benzoquinone structure (Scheme 1). This hypothesis is supported by UV–vis spectrum of OP2 (maxima at 250, 295 and 330 nm) simultaneously recorded with MS spectra by PDA detector that well corresponded to UV–vis spectrum of *p*-benzoquinone standard recorded in 1:1 (v/v) aqueous/methanolic solution (see Supplementary information file, Fig. S4). Moreover, proposed structure of OP2 corresponds to above mentioned product with benzoquinone moiety which was formed at the potential of peak B in voltammetric experiments.

3.2.3. *Products of 5-HMT electrolysis with* m/z *253 and* m/z *255*

A product OP3, $[M-H]^-$ at *m/z* 253 was detected in negative ionization mode. Fragmentation spectrum (Fig. 6d) showed ions at *m/z* 210 (loss of acetaldehyde radical), *m/z* 181 (consecutive loss of

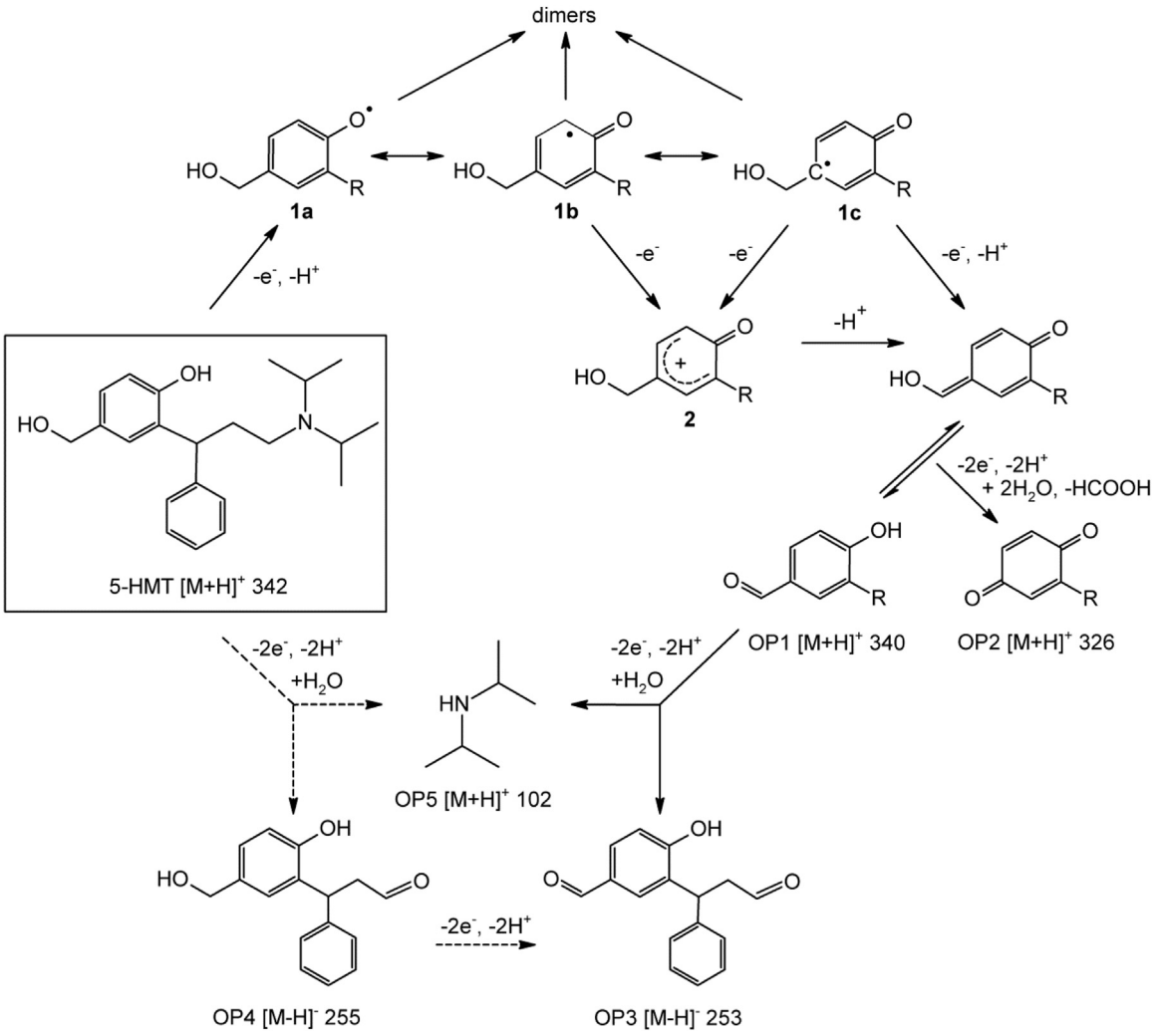

Scheme 1. Proposed mechanism of electrochemical oxidation of 5-hydroxymethyl tolterodine. Dashed arrows denote the preferential pathway valid for alkaline media and higher oxidation potentials.

formyl radical) and *m/z* 121 (p-hydroxybenzaldehyde anion). Fragmentation pattern and accurate mass (Table 1) enabled to propose the structure of the product OP3 as 4-hydroxy-3-(3-oxo-1-phenyl-propyl)-benzaldehyde. It can rise from electrochemical oxidation of tertiary amino group of OP1 and subsequent hydrolysis and elimination of diisopropylamine (Scheme 1). A signal at *m/z* 102 (t_R = 0.56 min) detected in positive ionization mode, which appertains to diisopropylamine (product OP5), supports the hypothesis. Oxidation of amino group proceeds also at the 5-HMT molecule providing a product OP4 with $[M - H]^-$ at *m/z* 255 (Scheme 1), especially in alkaline solutions of pH 9 at the potential 0.9 V. It suggests that the tertiary amino group can be oxidized independently on the phenolic moiety under specific conditions: alkaline media and sufficiently high potentials. The formation of secondary amine and corresponding aldehyde is in accordance with oxidation mechanism of tertiary amines described in literature [22,23]. Mass spectra of the products OP4 and OP5 are in Supplementary information file, Fig. S4.

3.2.4. Other products of 5-HMT electrolysis with m/z *356 and* m/z *372*

In addition to the above described main oxidation products, many other products of electrolysis were found indicating high reactivity of the 5-HMT molecule. All the products are formed by reaction of reactive intermediates generated electrochemically at higher potential (E = 0.9 V) with the used solvents – water and methanol. Mass spectra and proposed structures are available in Supplementary information file (Fig. S5, Table S1).

Three isomeric oxidation products (OP6A-C) with $[M + H]^+$ at *m/z* 356 were detected primarily in 5-HMT solutions electrolyzed at higher potential. Retention times as well as fragmentation patterns of all three products were different. In all cases accurate mass corresponds to a gain of one oxygen atom and loss of two hydrogen atoms per molecule of 5-HMT (Table 1). The most polar isomer (OP6A, t_R = 1.81 min) was mainly formed in acidic media (pH 3, E = 0.9 V). Fragmentation pattern of OP6A revealed the elimination of CO (ion at *m/z* 328) similarly to OP1 fragmentation, suggesting the presence of aldehyde group. Moreover, three neutral losses containing oxygen (combination of CO and H_2O) indicate the presence of an aldehyde group and two hydroxyl groups on the benzene ring. The most intensive fragment ion at *m/z* 209 is produced by loss of CO, H_2O and diisopropylamine. It is known that elimination of H_2O is easier for two hydroxyl groups in *o*-position on benzene ring, e.g. fragmentation of pyrocatechol provides intensive product ion after cleavage of H_2O even if different ionization techniques are applied (electron ionization [24] and atmospheric pressure chemical ionization [25]). Therefore, the product OP6A was most likely formed by anodic hydroxylation in *ortho* position of the phenol ring.

The highest amount of the second isomer with *m/z* 356 (OP6B, t_R = 2.16 min) was found in 5-HMT neutral solution electrolyzed at

E = 0.9 V. Fragmentation spectrum of OP6B was obtained using collision energy ramp from 5 to 15 eV, because the precursor ion was completely fragmented at higher collision energy values. The most intensive fragment at m/z 227 corresponds to the loss of CO and diisopropylamine, ion at m/z 296 loss of CO and methanol. Unlike OP6A from which methanol was not eliminated, the loss of methanol suggests that the 5-hydroxymethyl group remained unchanged in OP6B. Product ions at m/z 153 and at m/z 139 could correspond to 5-hydroxymethyl-3-methyl-[1,2]benzoquinone and 4-hydroxymethyl-[1,2]benzoquinone, respectively. Therefore, structure of OP6B most likely contains an *o*-quinone group arrangement.

Unlike other two isomers, the least polar isomer OP6C (m/z 356, t_R = 2.31 min) was formed preferably in alkaline media (pH 9, E = 0.9 V). Its fragmentation showed the loss of methanol (as in the case of OP6B), loss of H_2O and diisopropylamine ($\Delta m/z$ 119) (as it occurred for 5-HMT standard but not for OP6B). Other OP6C fragment ions at m/z 123 and at m/z 105 corresponds to 4-hydroxybenzaldehyde and 4-methylenecyclohexa-2,5-dienone, respectively. According to these facts, the oxidation of 5-HMT is expected on the unsubstituted benzene ring.

Two oxidation products OP7A and OP7B with $[M+H]^+$ at m/z 372 (Table 1) were found in 5-HMT solutions electrolyzed at potential of peak B. Their highest response was observed in neutral media (pH 7, E = 0.9 V). MS/MS spectra of both products differ, however some fragmentation pathways (losses of water, formaldehyde, diisopropylamine and benzene) were the same. Similarly to 5-HMT and OP6C, loss of diisopropylamine and water ($\Delta m/z$ 119) were seen in the spectrum of OP7A. Presumably, product OP7A can be formed by methoxylation of the phenol ring in the *ortho* position to –OH group. By contrast, elimination of methoxy radical from OP7B precursor ion suggests cyclohexadienone moiety of OP7B which could be formed by methoxylation of 5-HMT at the *para* position to –OH group.

Described fragmentation pathway for 5-HMT and other compounds represent probable but not necessary all alternative fragmentations. Detailed study of the fragmentation is out of scope of this paper.

3.2.5. Dimeric oxidation products

Electrolysis of 5-HMT solutions provided large number of structurally different dimers. Analysis of the MS spectra revealed that the dimeric products can arise from the coupling of reactive intermediates formed by electrode reaction of 5-HMT or its monomeric oxidation products. The most abundant of them are summarized in Table 1 (OP8–OP11, for respective MS spectra see Supplementary information file, Fig. S5).

In solutions electrolyzed at lower potentials three isomeric dimers OP9A-C ($[M+H]^+$ at m/z 681) with different fragmentation patterns were detected. They were most likely formed by coupling of two 5-HMT oxidized units. The concentration of OP9A and OP9B increased with increasing pH whereas the OP9C content was the highest in neutral solution. A dimer OP10 ($[M+H]^+$ at m/z 679) differing from OP9 products by $\Delta m/z$ = 2 was observed in acidic and neutral solutions electrolyzed at lower potential (E = 0.65 V). It could be formed most likely by dehydrogenation of an OP9 isomer.

Electrolysis at higher potential (E = 0.9 V) yielded dimeric products OP8 and OP11. The dimer OP8 ($[M+H]^+$ at m/z 665) with characteristic loss of *N*-isopropyl-*N*-vinylpropan-2-amine was probably formed by coupling of 5-HMT and OP2. The highest amount of this dimer was observed in acidic solutions. Three dimeric products OP11A-C with $[M+H]^+$ at m/z 695 were detected mainly in acidic conditions. Unlike the MS/MS spectrum of OP11C, the spectra of OP11A and OP11B were identical. All three dimers could arise from the coupling of 5-HMT with OP6A, OP6B or OP6C. Besides above mentioned dimers, further dimeric structures were observed, e.g. with $[M+H]^+$ at m/z 635, 649, 651, 669, 689 and 747, mostly in acidic and neutral solutions. They were not probably formed via oxidative coupling of the above mentioned monomeric products. Identification of these dimeric structures is in progress.

3.3. Mechanism of electrochemical oxidation of 5-HMT

Based on the voltammetric data and UPLC/MS analysis of the products of controlled potential electrolysis, the mechanism of the anodic oxidation of 5-HMT can be proposed as follows (Scheme 1).

The first oxidation step involves removing of an electron and a proton from the phenol group. The formed phenoxy radical can exist in various tautomeric forms 1a, 1b and 1c. All the structures can provide dimers with C-C or C-O-C linkage (products OP9A-C). The C-C linked dimer can be subsequently oxidized to a quinone structure which was observed on the cyclic voltammograms (peaks C and E). The product with corresponding mass (OP10) was detected in acidic and neutral solutions electrolyzed at the potential of peak A. Similar reactions of the phenol moiety has been observed in the case of tolterodine [12].

Subsequent oxidation and deprotonation of the radical 1 can give rise to an aldehyde group (product OP1) from the benzyl alcohol [26]. Relation between the oxidation of phenol group and the hydroxymethyl group can be deduced from comparison of voltammograms of 4-hydroxybenzyl alcohol with those of benzyl alcohol and 3-phenoxybenzyl alcohol. Both last mentioned alcohols did not provide a distinguishable peak under the experimental conditions (1:1 methanol/buffer solution pH 7.5) in which 4-hydroxybenzyl alcohol showed a well-defined oxidation signal at the potential close to the first oxidation peak of 5-HMT (Supplementary information file, Fig. S6). Higher content of the product OP1 detected in the solutions electrolyzed at lower potential supports the hypothesis that it was formed at potential of the voltammetric peak A. Based on the described observation, possibility of direct oxidation of the hydroxymethyl group [27,28] seems to be less favorable and it could be expected to proceed at higher potentials as in the case of fesoterodine [16].

Phenol group in the oxidation product OP1 is oxidized at higher potential corresponding to the voltammetric peak B. The hypothesis resulting from the analogy with the first oxidation step was confirmed by comparison of voltammogram of 5-HMT with those of 4-hydroxybenzaldehyde serving as a simple model compound for conclusive evidence (Fig. 2f). Product OP2 with *p*-benzoquinone structure was found as a product of the successive oxidation of OP1 at higher potentials in acidic and neutral media. OP2 can be formed after nucleophilic attack of water on the phenoxonium cation arising from two-electron oxidation of OP1 followed by subsequent release of proton. However, another reaction mechanisms involving cleavage of the benzylic carbon and formation of a single-carbon specie come into consideration as well (several reactions, including among others analogies to Bayer-Villiger rearrangement [29] could be found in literature). On all accounts, distinguishable signal of formic acid, as the most oxidized single-carbon specie, was detected by GC-MS in solutions of 4-hydroxybenzyl alcohol and 4-hydroxybenzaldehyde electrolyzed in acidic media on the platinum gauze electrode. Acidic catalysis, necessary for the Bayer-Villiger rearrangement, is in accordance with acidic conditions under which the highest yield of OP2 product was formed. Therewithal, the nucleophilic attack of water and/or methanol on the phenoxonium ion (2) or on the phenoxonium ion which could arise from subsequent oxidation of OP1 led to hydroxylated and/or methoxylated products (OP6, OP7) found in higher amount after electrolysis at 0.9 V.

Simultaneously, the tertiary amino group of 5-HMT and OP1 is oxidized at higher potentials corresponding to peak B followed by hydrolytic cleavage producing the secondary amine OP5 and the

aldehydes OP4 and OP3, respectively (Scheme 1). As resulted from the UPLC/MS analysis of the electrolyzed solutions, the deamination proceeds more easily in alkaline media where the amino group is deprotonated (apparent pK_a 9.5 was estimated from the E_p – pH dependence of the peak B). This is in agreement with higher electrochemical reactivity of the tertiary amino group of fesoterodine at pH 9 [16]. It could be assumed that the product OP2 tend to oxidative deamination as well. Presence of an UV–vis absorption peak with t_R = 1.99 min and maxima at 330 nm in chromatogram of 5-HMT solutions (pH 3 and 7) electrolyzed at E = 0.9 V confirmed this assumption though the corresponding final product was detected neither in positive nor in negative ionization mode of MS analysis.

4. Conclusions

Voltammetric techniques combined with controlled potential electrolysis and UPLC/MS analysis of the oxidation products revealed two main reaction centers in the molecule of the 5-HMT: the *p*-hydroxybenzyl alcohol group and the tertiary *N*-diisopropylamino group. Electrochemical reaction on the first moiety provided 5-formyl tolterodine and a benzoquinone derivative besides several dimeric products. Oxidation of the second center accompanied by hydrolysis led to the cleavage of diisopropyl amine and formation of 4-hydroxy-3-(3-oxo-1-phenylpropyl)benzaldehyde and 3-(3,6-dioxocyclohexa-1,4-dien-1-yl)-3-phenylpropanal. Both reaction centers are susceptible also to the enzymatic oxidation by cytochrome P450 in liver [3,30,31]. Results of this study demonstrate that electrochemical oxidation is capable to disclose reactive moieties in the biologically active molecules and to provide some valuable information about intermediates formed at the metabolic transformation. The obtained knowledge can support study of oxidation mechanisms of other structurally related compounds and eventually can be used for electro-syntheses of selected oxidative metabolites occurring in the (bio)-transformation process. Last but not least, the results of this study (e.g. proposed reaction mechanism, potentials of electrochemical transformations, pH influence, adsorption phenomena) can be useful for the development of sensitive electroanalytical methods for determination of the substance.

Acknowledgements

This work was supported by the Ministry of Education, Youth and Sports of the Czech Republic (projects LO1305 and CZ.1.05/2.1.00/19.0377) and by Palacký University in Olomouc (project IGA_PrF_2016_016).

Appendix A. Supplementary data

Supplementary data associated with this article can be found, in the online version, at http://dx.doi.org/10.1016/j.electacta.2016.08.137.

References

[1] J.J. Wyndaele, Fesoterodine Individualised Treatment of Urgency Urinary Incontinence Across Patient Groups, Eur. Urol. Suppl. 10 (2011) 14.
[2] C.R. Chapple, P.E. Van Kerrebroeck, K.P. Junemann, J.T. Wang, M. Brodsky, Comparison of fesoterodine and tolterodine in patients with overactive bladder, Bju Int. 102 (2008) 1128.
[3] P. Ellsworth, S.J. Berriman, M. Brodsky, Fesoterodine: a new agent for treating overactive bladder, Am. J. Manag. Care 15 (2009) S115.
[4] B. Malhotra, M. Dickins, C. Alvey, Z. Jumadilova, X.X. Li, G. Duczynski, K. Gandelman, Effects of the moderate CYP3A4 inhibitor, fluconazole, on the pharmacokinetics of fesoterodine in healthy subjects, Br. J. Clin. Pharmacol. 72 (2011) 263.
[5] M.S. Sangoi, M. Steppe, Determination of fesoterodine in pharmaceutical formulations by using liquid chromatography-tandem mass spectrometry, Eur. J. Mass Spectrom. 16 (2010) 653.
[6] M.S. Sangoi, V. Todeschini, M. Steppe, Fesoterodine stress degradation behavior by liquid chromatography coupled to ultraviolet detection and electrospray ionization mass spectrometry, Talanta 84 (2011) 1068.
[7] M. Yadav, V. Upadhyay, V. Chauhan, G. Solanki, A. Jani, G.A. Baxi, P. Singhal, P.S. Shrivastav, LC-MS-MS Separation and Simultaneous Determination of Tolterodine and its Active Metabolite, 5-Hydroxymethyl Tolterodine in Human Plasma, Chromatographia 72 (2010) 255.
[8] J. Macek, P. Ptacek, J. Klima, Determination of tolterodine and its 5-hydroxymethyl metabolite in human plasma by hydrophilic interaction liquid chromatography-tandem mass spectrometry, J. Chromatogr. B 877 (2009) 968.
[9] R. Swart, P. Koivisto, K.E. Markides, Column switching in capillary liquid chromatography tandem mass spectrometry for the quantitation of pg/ml concentrations of the free basic drug tolterodine and its active 5-hydroxymethyl metabolite in microliter volumes of plasma, J. Chromatogr. A 828 (1998) 209.
[10] L. Palmer, L. Andersson, T. Andersson, U. Stenberg, Determination of tolterodine and the 5-hydroxymethyl metabolite in plasma, serum and urine using gas chromatography mass spectrometry, J. Pharm. Biomed. Anal. 16 (1997) 155.
[11] A. Baumann, U. Karst, Online electrochemistry/mass spectrometry in drug metabolism studies: principles and applications, Expert Opin. Drug Metab. Toxicol. 6 (2010) 715.
[12] P. Macikova, J. Skopalova, P. Cankar, B. Papouskova, R. Strakova, D. Jirovsky, V. Maier, Electrochemical Oxidation of Tolterodine, Electroanal. 25 (2013) 205.
[13] W. Lohmann, R. Dotzer, G. Gutter, S.M. Van Leeuwen, U. Karst, On-Line Electrochemistry/Liquid Chromatography/Mass Spectrometry for the Simulation of Pesticide Metabolism, J. Am. Soc. Mass Spectr. 20 (2009) 138.
[14] A. Baumann, W. Lohmann, S. Jahn, U. Karst, On-Line Electrochemistry/Electrospray Ionization Mass Spectrometry (EC/ESI-MS) for the Generation and Identification of Nucleotide Oxidation Products, Electroanal. 22 (2010) 286.
[15] N.A. Mautjana, J. Estes, J.R. Eyler, A. Brajter-Toth, One-Electron Oxidation and Sensitivity of Uric Acid in On-Line Electrochemistry and in Electrospray Ionization Mass Spectrometry, Electroanal. 20 (2008) 2501.
[16] P. Kucerova, J. Skopalova, L. Kucera, J. Hrbac, K. Lemr, Electrochemical oxidation of fesoterodine and identification of its oxidation products using liquid chromatography and mass spectrometry, Electrochim. Acta 159 (2015) 131.
[17] L. Papouchado, R.W. Sandford, G. Petrie, R.N. Adams, Anodic-Oxidation Pathways of Phenolic Compounds. 2. Stepwise Electron Transfers and Coupled Hydroxylations, J. Electroanal. Chem. 65 (1975) 275.
[18] A. Nilsson, U. Palmquist, T. Pettersson, A. Ronlan, Anodic oxidation of phenolic compounds. Part 5. Anodic methoxylation of phenols. A simple synthesis of quinones, quinone acetals, and 4-methyl-α-methoxycyclohexa-2,5-dienones, J. Chem. Soc. Perk. T 1 (1978) 696.
[19] F. Marken, A. Neudeck, A.M. Bond, Cyclic Voltammetry, in: F. Scholz (Ed.), Electroanalytical Methods: Guide to Experiments and Applications, vol. 1, Springer, Berlin, 2002 Ch. II.
[20] P. Zuman, J.J.M. Holthuis, Mechanism of electrooxidation of substituted phenols in aqueous solutions: Some podophyllotoxin derivatives as models, Recueil des Travaux Chimiques des Pays-Bas 107 (1988) 403.
[21] X.Y. Duan, L.F. Tian, W. Liu, L.M. Chang, Study on electrochemical oxidation of 4-Chlorophenol on a vitreous carbon electrode using cyclic voltammetry, Electrochim. Acta 94 (2013) 192.
[22] P.J. Smith, C.K. Mann, Electrochemical Dealkylation of Aliphatic Amines, J. Org. Chem. 34 (1969) 1821.
[23] M. Masui, H. Sayo, Anodic Oxidation of Amines. 2 Electrochemical Dealkylation of Aliphatic Tertiary Amines, J. Chem. Soc. B (1971) 1593.
[24] R. Capasso, A review on the electron ionisation and fast atom bombardment mass spectrometry of polyphenols naturally occurring in olive wastes and some of their synthetic derivatives, Phytochem. Analysis 10 (1999) 299.
[25] D. Puig, D. Barcelo, I. Silgoner, M. Grasserbauer, Comparison of three different liquid chromatography-mass spectrometry interfacing techniques for the determination of priority phenolic compounds in water, J. Mass Spectrom. 31 (1996) 1297.
[26] C. Steelink, W.E. Britton, The electrochemical oxidation of lignin model compounds I. Oxidation of 3,5-dimethoxy-4-hydroxy-α-methylbenzyl alcohol, Tetrahedron Lett. 15 (1974) 2869.
[27] O.R. Brown, S. Chandra, J.A. Harrison, The anodic oxidation of benzyl alcohol to benzaldehyde, J. Electroanal. Chem. 38 (1972) 185.
[28] O.R. Brown, S. Chandra, J.A. Harrison, The anodic oxidation of anisyl alcohol, J. Electroanal. Chem. 34 (1972) 505.
[29] M. Renz, B. Meunier, 100 Years of Baeyer – Villiger Oxidations, Eur. J. Org. Chem. 1999 (1999) 737.
[30] S.H.G. Andersson, A. Lindgren, H. Postlind, Biotransformation of tolterodine, a new muscarinic receptor antagonist, in mice, rats, and dogs, Drug Metab. Dispos. 26 (1998) 528.
[31] A.K. Aberg, Tolterodine metabolites, US 20030027856 A1 (2003).

Příloha 2

Electrochemical oxidative dimerization of monobrominated phenols and pentabromophenol in methanol-aqueous media

Marková, E.; Kučerová, P.; Bednář, P.; Barták, P.; **Skopalová**, **J.***

Monatshefte für Chemie – Chemical Monthly **2016**, *147*, 75-87

Monatsh Chem (2016) 147:75–87
DOI 10.1007/s00706-015-1597-2

ORIGINAL PAPER

Electrochemical oxidative dimerization of monobrominated phenols and pentabromophenol in methanol-aqueous media

Eva Marková[1] · Pavla Kučerová[1] · Petr Bednář[1] · Petr Barták[1] · Jana Skopalová[1]

Received: 3 September 2015 / Accepted: 27 October 2015 / Published online: 19 November 2015

Abstract The electrochemical oxidation of monobrominated phenols (2-bromophenol, 3-bromophenol, 4-bromophenol) and pentabromophenol in methanol-aqueous solutions (1:1 and 9:1, v/v) was studied by cyclic voltammetry on glassy carbon electrode in static and rotating disc arrangement. First oxidation step was followed by dimerization reaction resulting in formation of electroactive species. Products of controlled potential electrolysis of bromophenols on the platinum gauze electrode were analysed by ultra-performance liquid chromatography/time of flight mass spectrometry and by gas chromatography/mass spectrometry. C–C and C–O–C linked dimers were found as the main oxidation products in monobrominated phenols solutions electrolysed under mild conditions. Pentabromophenol provided a dimer with C–O–C linkage. On-line coupling of mass spectrometry with electrochemical flow-through cell (EC/MS) containing platinum working electrode proved formation of dimers in the case of 2-bromophenol and 4-bromphenol.

Graphical abstract

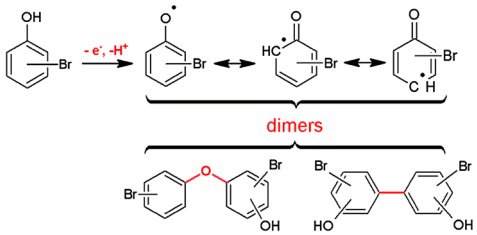

Keywords Bromophenols · Oxidations · Electrochemistry · Mass spectrometry · Voltammetry

Introduction

Brominated phenols (BPs) are chemical compounds widespread in the environment as the natural products of the marine organisms metabolism [1, 2] (e.g. marine worms, algae, etc.) and as industrial (by)products. BPs are commonly used at the production of flame retardants and as wood fungicides [1, 3, 4]. As pollutants, they were found in the air, water and sediments [1, 5–7]. Some brominated compounds were detected in the human plasma, adipose tissue, and breast milk [1, 8, 9] into which they were probably transferred via food chain, by direct contact or by inhalation [1]. The increasing production and utilization of brominated phenols increases the interest in the study of these substances, especially in connection with harmful effects on the environment and human health.

Halogenated phenols as organic contaminants of the environment can be eliminated or transformed by advanced oxidation processes, e.g. by photochemical oxidation,

Electronic supplementary material The online version of this article (doi:10.1007/s00706-015-1597-2) contains supplementary material, which is available to authorized users.

✉ Jana Skopalová
jana.skopalova@upol.cz

[1] Regional Centre of Advanced Technologies and Materials, Department of Analytical Chemistry, Faculty of Science, Palacký University, 17. listopadu 12, 771 46 Olomouc, Czech Republic

chemical oxidation with the use of various chemical agents, thermal and electrochemical oxidation. The most of these oxidation processes were described especially for the chlorophenols. In some cases, the oxidation of halogenated phenols can lead to the formation of oligomeric products. Dimers were identified as products of photochemical oxidation of chlorophenols using UV/H_2O_2 and O_3 methods in aqueous solutions [10, 11]. Photolysis of different *p*-halogenophenols in aqueous alkaline solutions leads to the formation of dihydroxybiphenyls [12]. Dimeric intermediates, especially chlorinated diphenyl ethers and biphenyls can be formed also by the Fenton-driven oxidation of 2-chlorophenol [13]. Dimers arise also from pyrolysis of brominated phenols. The C–O–C and C–C linkage of simple BPs radicals leads to dimerization and subsequent formation of ill-famed dibenzodioxins and dibenzofurans as final pyrolytic products [14–19].

Hydroxylated polybrominated diphenyl ethers (OH-PBDEs) and hydroxylated polybrominated biphenyls (OH-PBBs) were identified after chemical oxidation of BPs with MnO_2 [20] or $KMnO_4$ as strong oxidation agents [21]. OH-PBDEs are metabolites and structural analogues of polybrominated diphenyl ethers—widely used industrial flame retardants. Compounds of both groups negatively influence human health. OH-PBDEs can be formed by bromoperoxidase-catalyzed dimerization of bromophenols [22]. Most of OH-PBDEs have enhanced toxicological effects compared to polybrominated diphenyl ethers, including neurotoxicity, DNA insulting and the ability to interrupt thyroid hormone homeostasis as well as sex hormone steroidogenesis [23–26].

The electrochemical oxidation of halogenated phenols involves the generation of radicals followed by oligomeric or polymeric compounds formation [27, 28]. The course of electrochemical oxidation depends on various experimental conditions such as solvent-electrolyte system, electrode potential, phenol concentration, pH, electrode material, the number of halogen atoms and their position in an aromatic ring [28, 29]. Electrooxidation of chlorophenols (CPs) was thoroughly investigated particularly in aqueous solutions [28, 30–37]. The formation of ether-type oligomeric or polymeric products prevails in alkaline pH [30, 31, 34, 36] while carbon–carbon coupling is more common in acidic solutions [27]. The oligomeric/polymeric compounds form a film, which covers and passivates the working electrode surface [30–32, 35, 37]. Investigation of oligomeric products structures reveals that the coupling of chlorinated phenols strongly depends on the structure of the monomers. The coupling is most frequently carried via the active *ortho*- or *para*- position followed by quinol-ether mechanism (without chlorine elimination) or the nucleophilic-radical substitution with chlorine elimination from *ortho*- and/or *para*- position [36]. *Ortho*-substituted CPs are more reactive then *para*-substituted CPs [28, 35]. The electrochemical oxidation of some chlorinated phenols can lead to the formation of polychlorinated dibenzo-*p*-dioxins and dibenzofurans (PCDD/Fs) under specific conditions [38].

There are many reports devoted to the study of brominated phenols, however, direct electrochemical oxidation of these compounds is mentioned rarely [39]. The electrochemical oxidation of 2,4,6-tribromophenol (TBP) in aqueous-methanolic solutions (1:1) was described [40]. Two main oxidation products were found and identified by gas chromatography and mass spectrometry (GC/MS): 2,6-dibromo-4-(2,4,6-tribromophenoxy)phenol and 3,3′,5,5′-tetrabromo-1,1′-bi(cyclohexa-2,5-dien-1-ylidene)-4,4′-dione. Recently, TBP oxidation was studied in different short-chain primary alcohols (methanol, ethanol, propanol, and butanol) and aqueous buffer mixture (9:1). Several dimeric compounds were found. Some of them contained an alkoxy substituent derived from the used alcohol [41].

In this paper, electrochemical oxidation of three monobromophenols (2-bromophenol, 3-bromophenol, 4-bromophenol) and pentabromophenol was investigated in methanol aqueous solutions. Electrochemical behaviour of the bromophenols was studied using cyclic voltammetry on static and rotating disc glassy carbon electrode. Controlled potential electrolysis was employed for the preparation of oxidation products, gas chromatography with mass spectrometry (GC/MS) and ultra-performance liquid chromatography with photodiode array and mass spectrometry detection (UPLC/PDA/MS) for their identification. The formation of oxidation products was investigated also using on-line electrochemistry/mass spectrometry. The influence of bromine substitution on the formation of oxidation (especially dimeric) products was observed.

Results and discussion

Voltammetric behaviour of monobrominated phenols and pentabromophenol

Voltammograms of four brominated phenols (BPs) were recorded at glassy carbon electrode in the supporting electrolyte with higher content of methanol (50 or 90 %, v/v) in order to increase solubility of oxidation products and thus at least partly suppress fouling of the electrode surface. Experimental conditions, i.e. methanol content, pH of the buffer solution and material of the working electrode, were selected based on the previous studies of electrochemical oxidation of 2,4,6-tribromophenol [40, 41]. Successive cyclic voltammograms of BPs (Fig. 1a–d) show one current peak, designated Ia at the potential of about 0.8 V (for 2-BP, 4-BP, and PBP) and 0.9 V (for 3-BP) in the first anodic scan. The peak current increased

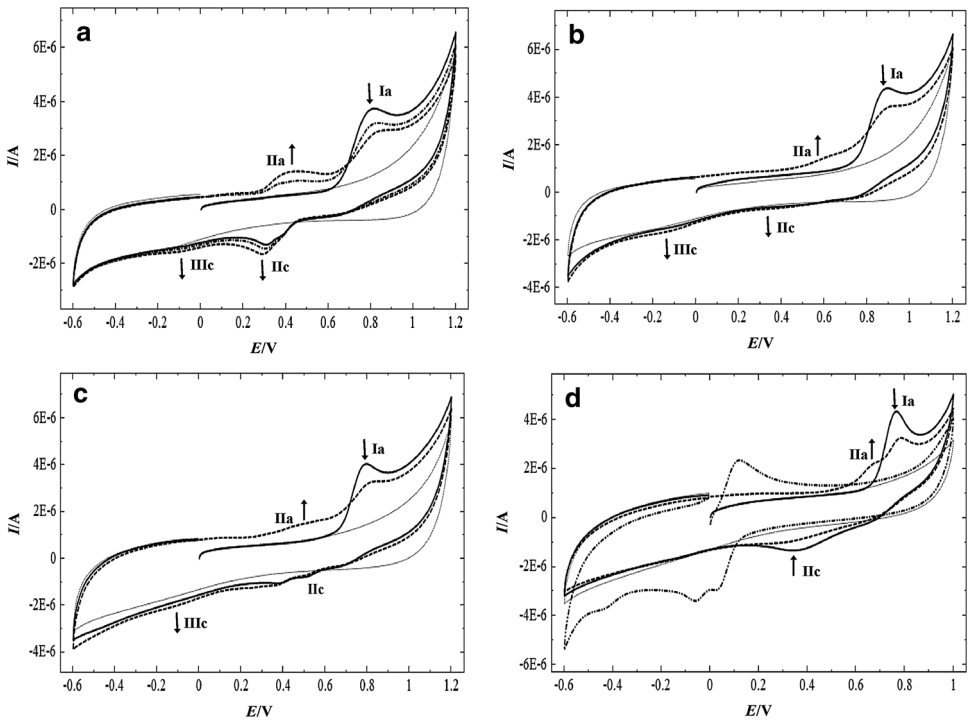

Fig. 1 Cyclic voltammograms of 2-BP (**a**), 3-BP (**b**), 4-BP (**c**), and PBP (**d**)in supporting electrolyte (*grey line*) methanol/ammonium formate buffer (pH = 6) in ratio 9:1, (v/v). Measurement was performed with glassy carbon electrode. Scan rate 0.5 V s^{-1}. In all voltammograms, first cycle (*solid line*) and fifth cycle (*dash line*) is shown, in **a** also second cycle is depicted (*dash dot line*). The curve of tetrabromoquinone (*dash dot line*) in concentration 1×10^{-4} mol dm^{-3} is shown on the picture **d**. The *arrows* indicate changes of peak heights in the successive cycles

linearly with the square root of the scan rate over the range from 5 to 500 mV s^{-1}, indicating a diffusion-controlled redox process. Significant drop in anodic peak current evident in subsequent cycles (Fig. 1, dash line) could be explained by the formation of polymeric film which passivates the working electrode surface and prevents further oxidation of bromophenol during repeated cycles [28, 30, 31].

Cathodic signal(s), marked as IIc, appeared in the reverse scan along with a new anodic current peak(s) IIa in the consecutive forward scan. The redox couple(s) of group II appeared when the scan direction was switched at the potential at which the peak Ia started to evolve or higher (Fig. 2). Therefore, this new redox couples correspond to products of anodic oxidation of respective bromophenols. The height of peaks IIa/IIc increased in consecutive cycles, while current of the peak Ia decreased. Such behaviour is typical for electropolymerization reactions [44–46] which have been reported for phenol and its derivatives [42] including chlorophenols [30, 43]. The growth of peaks of group II was more pronounced for 2-BP (Fig. 1a) whereas it was the least distinct for 3-BP (Fig. 1b). Looking in more detail, the group II evidently consists of at least two current signals in each scan direction, which are well distinguishable especially in the case of IIc/IIa peaks of 2-BP (Fig. 2) and IIc peaks of 4-BP (Fig. 1c). Observation of more current signals indicates either a successive redox reactions of one specie or redox reactions of more species. Therefore, formation of more than one electroactive oxidation

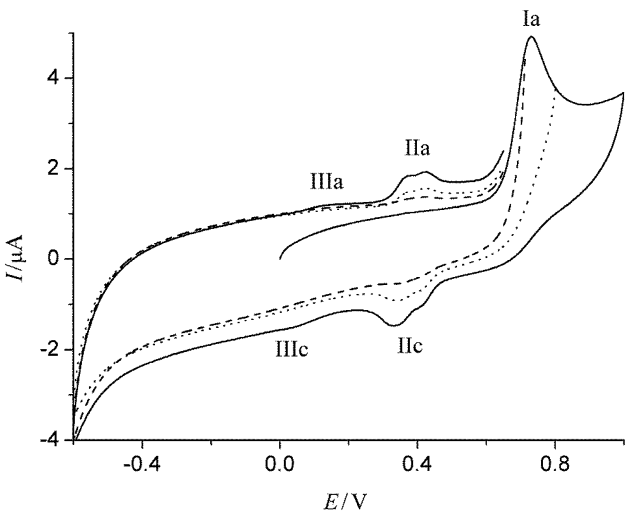

Fig. 2 Cyclic voltammograms of 2-BP (1×10^{-4} mol dm^{-3}) in methanol/ammonium formate buffer solution pH 6 (1:1, v/v) at 0.5 V s^{-1}. Switching potentials: 0.7 V (*dash*), 0.8 V (*dot*), and 1.0 V (*solid*)

product or intermediate product at the potential of anodic peak Ia of BP could be expected based on the observed group of peaks II.

When the forward potential sweep was switched about 0.2 V or more beyond the peak Ia potential, a new couple of peaks at 0.03 V (IIIc) and 0.13 V (IIIa) appeared in the consecutive cathodic and anodic scan, respectively (Fig. 2). The redox couple III most likely corresponds to

respective bromobenzoquinones as results from the comparison with the voltammogram of 2,3,5,6-tetrabromo-1,4-benzoquinone (Fig. 1d) which revealed current peaks at similar potentials. The intensity of the peaks IIIa/IIIc is very low for all four bromophenols which could be due to the fouling of the electrode surface with a film of oxidation products formed at lower potentials than the benzoquinones.

Blocking of the electrode surface by electrolysis products was clearly apparent from cyclic voltammograms recorded on rotating disc electrode (Fig. 3). In buffered solutions containing 50 % methanol, current of monobrominated phenols reached a maximum at certain potential and then continually decreased giving a more or less distorted peak shape. The decrease continued also during the reverse scan. In the successive cycles the current was nearly the same as in the supporting electrolyte (inset in Fig. 3). Similar behaviour has been reported for pentachlorophenol on graphite RDE in neutral phosphate buffer [47]. The blocking of the electrode surface was less pronounced in the 90 % methanol solutions (Fig. 3). Among monobrominated phenols, oxidation of 3-BP caused the fastest blocking of the electrode surface. By contrast, oxidation of PBP revealed only mild passivation of the electrode (Fig. 3, dash dot trace) which could be in accordance with the lowest polymerization rate reported for pentachlorophenol compared to the less chlorinated phenols [28].

The half-wave potentials of the voltammetric waves of BPs measured under the steady-state conditions was found

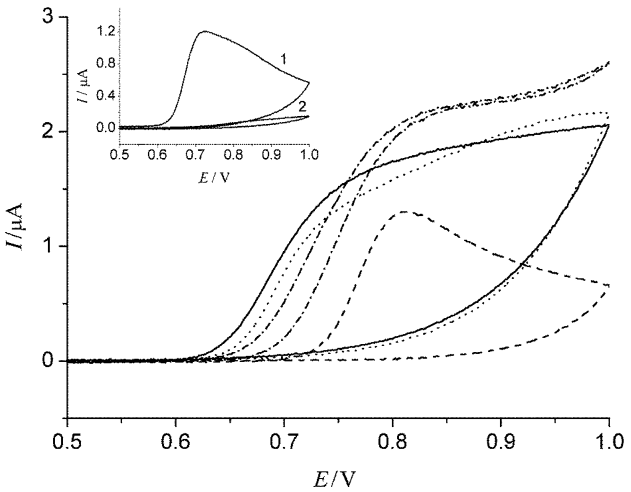

Fig. 3 Cyclic voltammograms of 1×10^{-4} mol dm^{-3} 2-BP (*solid*), 3-BP (*dash*), 4-BP (*dot*), and PBP (*dash dot*) recorded on RDE in methanol/ammonium formate buffer solution pH 6 (9:1, v/v). Angular rotation rate: 314 rad s^{-1}, scan rate: 5 mV s^{-1}. *Inset* cyclic voltammogram (two cycles, labelled *1* and *2*) of 4-BP under the same conditions but in methanol/ammonium formate buffer solution pH 6 (1:1, v/v)

to vary by about 20 mV per decade of change in rotation speed (Table 1) indicating the electrode process in which electron transfer is followed by dimerization reaction [48]. It can be expected the bromophenoxy radicals, formed in the first oxidation step, react to form the dimeric products as it was reported for chlorophenols [27, 30].

Controlled potential electrolysis and analysis of oxidation products

Electrolysis of bromophenols was performed on a platinum gauze electrode (surface area 4 cm^2) in methanol/ammonium formate buffer solution (9:1, v/v). The electrolyzed solutions of BP were diluted with mobile phase A (1:1) and directly analysed by UPLC/PDA/MS with electrospray ionization in negative mode (ESI-). Oxidation products were identified according to (a) elemental composition based on the accurate mass assignment; (b) analysis of the fragmentation spectra acquired with isolation of selected ions or without isolation using higher collision energy ramp; (c) characteristic isotopic pattern of brominated compounds. In the discussion related to the products identification, the first isotopes (i.e. monoisotopic masses) are mentioned, unless otherwise stated. Simultaneously, ethyl acetate extracts of the electrolyzed solutions were analysed by GC/MS. Blank samples containing unelectrolysed brominated phenols in the same solvent system were analysed in parallel with the electrolysed solutions and the analytical signals were compared.

The degree of BP conversion during 2 h electrolysis at $E = 1.0$ V was estimated from the area of chromatographic peaks recorded by UPLC with photodiode array (PDA) detector (Table 2). It is worth noting that the lowest and the highest conversion degree observed for 3-BP and PBP on the Pt gauze electrode, respectively, is in accordance with the strongest (3-BP) and the weakest (PBP) adsorption of the oxidation products observed with rotating disc glassy carbon electrode (Fig. 3). It suggests the adsorption of products of bromophenols oxidation is rather independent on the electrode material in this case.

Oxidation products of 2-BP

Peak of 2-bromophenol was detected by UPLC/MS in the retention time 5.22 min. Two peaks of isomeric dimer products (Fig. 4a) with $m/z = 340.88$ and with the retention times $t_R = 5.58$ min and 5.90 min were found in the solutions electrolysed at $E = 1.0$ V and $E = 1.2$ V (Table 3). Fragmentation spectrum of the first eluted dimer (Fig. 5a) showed fragment ions at $m/z = 260.9572$ (elimination of HBr, difference from the theoretical mass, dtm 8.0 ppm), $m/z = 232.9619$ (subsequent loss of CO, dtm 7.3 ppm) and a bromine anion at $m/z = 78.9279$. The loss

Table 1 Shifts of half-wave potentials of bromophenols ($c = 1 \times 10^{-4}$ mol dm^{-3}) per decade in rotation speed (varied in the range of 52–314 rad s^{-1}) measured by RDE voltammetry at the steady-state conditions in the supporting electrolyte containing methanol

Bromophenol	$dE_{1/2}/d\log\omega$/mV	Scan rate/mV s^{-1}	Methanol content/%
2-BP	18.1	5	90
	22.1	30	50
3-BP	19.6	100	50
4-BP	20.9	30	50
PBP	19.6	5	90

Table 2 The areas of BP peaks recorded by UPLC/PDA and calculated degree of BP conversion after 2 h electrolysis at $E = 1.0$ V

Compound	λ/nm	Peak area		Degree of conversion/%
		Blank	Solution oxidized	
2-BP	220	12982	8433	35
3-BP	220	14982	11220	25
4-BP	226	19685	9776	50
PBP	224	56896	13599	76

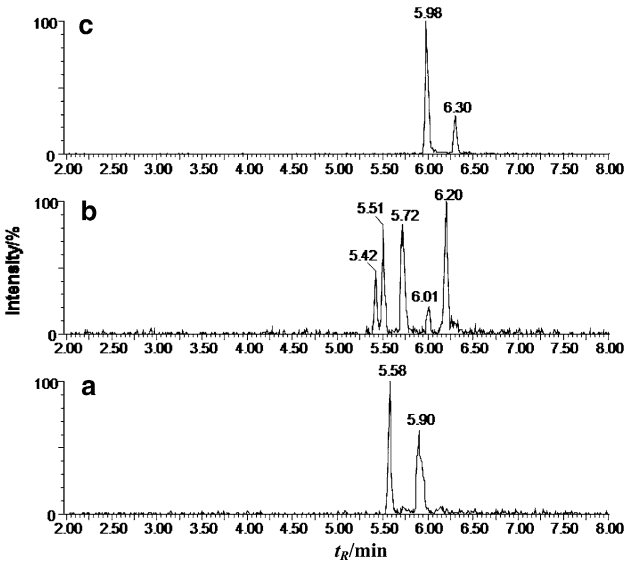

Fig. 4 Reconstructed chromatograms for the dimeric products with $m/z = 340.88$. The data were obtained by UPLC/MS analysis of 2-BP (**a**), 3-BP (**b**), and 4-BP (**c**) solutions ($c = 2 \times 10^{-4}$ mol dm^{-3}) electrolysed for 3 h at $E = 1.2$ V (**a**) and for 2 h at $E = 1.0$ V (**b**, **c**)

of HBr followed by the CO elimination could suggest that a bromine atom is located in a vicinal position to the proton donating -OH group. Such arrangement is evident in C–C coupled dimer of 2-BP (see putative structures in Fig. 5a). In the fragmentation spectrum of the second eluted dimer (Fig. 5b) only a weak signal at $m/z = 262.9545$ appeared corresponding either to the second isotopic peak of a fragment arising from the loss of HBr or to the first isotopic peak of radical-anion arising from the loss of Br. Absence of the corresponding isotopic peak is due to low signal. However, good agreement with the theoretical mass is observed (dtm 13.8 ppm, Table 3). The peak of bromine anion ($m/z = 78.9284$) confirms that also this ion is brominated. The MS data do not allow determination of position of linkage of both 2-BP units. The dimers with $m/z = 342$ were found also by GC/MS analysis in ethyl acetate extract of electrolyzed 2-BP solution providing two isomeric peaks in the retention times $t_R = 22.0$ min and 22.3 min.

In the solution electrolysed at $E = 1.2$ V for 3 h, two more dimeric products were found in low amount. The first product with $t_R = 5.46$ min and $m/z = 262.9722$ was a dimer containing only one bromine atom (Table 3). The second with $m/z = 418.7992$ and the retention time $t_R = 6.23$ min was identified as a dimer containing three bromine atoms (Table 3). Low signal of pseudomolecular and fragment ions does not allow more detailed specification of those dimers structures. Since both last mentioned dimers were found only in solution electrolysed at higher potential (1.2 V), they are most likely products of further redox transformations of the primarily generated dimeric structures.

Apart from the dimers, trimeric oxidation products were detected in all electrolyzed solutions. The most abundant one was eluted at $t_R = 6.00$ min (Table 3). However, the intensity of chromatographic peaks of the trimers was about one order of magnitude lower compared to the dimers.

Table 3 UPLC/MS analysis of bromophenols (BP) and their oxidation products

Starting compound	Oxidation product $[M–H]^-$ (m/z)	Retention time/min	Putative elemental composition	Dtm[a]/ppm
2-BP	340.8845	5.58	$C_{12}H_7O_2Br_2$	9.4
	340.8860	5.90	$C_{12}H_7O_2Br_2$	13.8
	262.9722	5.46	$C_{12}H_8O_2Br$	5.3
	418.7992	6.23	$C_{12}H_6O_2Br_3$	17.7
	510.8135	6.00	$C_{18}H_{10}O_3Br_3$	−8.8
3-BP	340.8904	5.42	$C_{12}H_7O_2Br_2$	26.7
	340.8870	5.51	$C_{12}H_7O_2Br_2$	16.7
	340.8886	5.72	$C_{12}H_7O_2Br_2$	21.4
	340.8761	6.01	$C_{12}H_7O_2Br_2$	−15.2
	340.8853	6.20	$C_{12}H_7O_2Br_2$	11.7
4-BP	340.8843	5.98	$C_{12}H_7O_2Br_2$	8.8
	340.8878	6.30	$C_{12}H_7O_2Br_2$	19.1
	262.9736	5.49	$C_{12}H_8O_2Br$	13.7
	510.8124	6.38	$C_{18}H_{10}O_3Br_3$	−11.0
	510.8260	6.54	$C_{18}H_{10}O_3Br_3$	15.7
	510.8100	6.63	$C_{18}H_{10}O_3Br_3$	−15.7
	510.8200	6.83	$C_{18}H_{10}O_3Br_3$	3.9
	446.8933	5.86	$C_{18}H_9O_4Br_2$	14.8
PBP	896.2476[b]	8.00	$C_{12}O_2$ Br_9	3.1
	420.6788	5.67	$C_6HO_2Br_4$	18.5
	434.6867	6.25	$C_7H_3O_2Br_4$	0.2
	449.6643	6.08	$C_6NO_3Br_4$	6.9

[a] Difference from the theoretical mass

[b] m/z value of the dominant isotopic ion

Oxidation products of 3-BP

Peak of 3-bromophenol was eluted in the retention time 5.33 min. At least five peaks of isomeric oxidation products with $m/z = 340.88$ (Table 3) were found on the chromatogram (Fig. 4b). In MS/MS spectrum of all isomers the bromine anion was observed. The fragment corresponding to the loss of HBr was found in MS/MS spectra of four dimers ($t_R = 5.51$, 5.72, 6.01, and 6.20 min). The fragmentation spectrum of the isomeric peak with the longest $t_R = 6.20$ min (Fig. 5c) show an intensive signal of the fragment ion at $m/z = 185.9367$ which probably corresponds to bromobenzenediol radical-anion (dtm 27.4 ppm, fragmentation indicated in the structure in Fig. 5c). This fragment is feasible for ether-type dimer with C–O–C linkage. Besides, a weak signal at $m/z = 132.8773$ confirms the stepwise degradation of aromatic ring(s). All attempts to detect trimeric oxidation product consisting of three 3-BP units were not successful and neither ion $m/z = 510.82$ (monoisotopic mass) nor ion $m/z = 512.82$ (the most abundant ion) corresponding to expected trimer(s) were detected in the electrolysed solution of 3-BP. Likewise, no dimers or trimers with eliminated bromine atom(s) were detected in solutions electrolysed under given conditions (2 h at $E = 1$ V). Oxidative coupling of 3-BP units without elimination of bromine is consistent with results reported for electrochemical polymerization of 3-chlorophenol and 3-bromophenol in acetonitrile [39].

Oxidation products of 4-BP

4-Bromophenol provides a peak in the retention time 5.27 min. By analogy to 2-BP, two isomeric peaks of dimeric products $m/z = 340.88$ in the retention times $t_R = 5.98$ min and 6.30 min were found (Fig. 4c; Table 3). Peak eluted in retention time 6.30 min shows the intensive fragment ion $m/z = 185.9318$ (Fig. 5e) corresponding to bromobenzenediol radical-anion ($C_6H_3BrO_2$, dtm −2.2 ppm). Therefore the respective oxidation product corresponds probably to dibromo diphenylether analogously to 3-BP dimer eluted at $t_R = 6.20$ min. The MS/MS spectrum of ion $m/z = 340.8843$ in retention time $t_R = 5.98$ min (Fig. 5d) provides peak at $m/z = 322.8764$ ($C_{12}H_5Br_2O$, dtm 15.8 ppm); difference $m/z = 18.0096$ corresponds to loss of H_2O. This fragment is missing in the

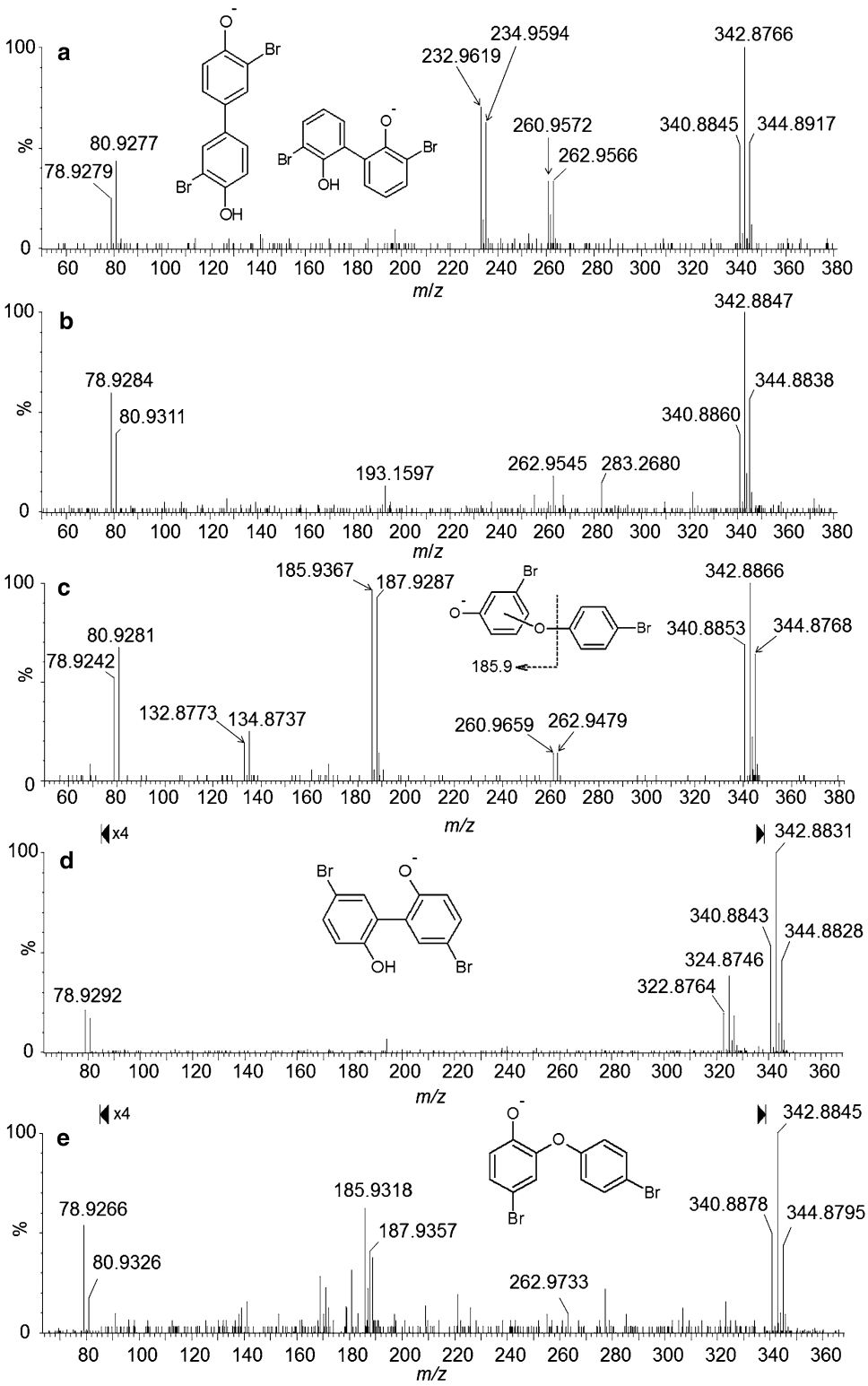

Fig. 5 Fragmentation MS spectra and putative structures of dimers formed in solution of 2-BP (**a** $t_R = 5.58$ min; **b** $t_R = 5.90$ min), 3-BP (**c** $t_R = 6.20$ min), and 4-BP (**d** $t_R = 5.98$ min; **e** $t_R = 6.30$ min) electrolysed 3 h at $E = 1.2$ V (**a**, **b**) and 2 h at $E = 1$ V. High collision energy scan (ramp CE = 10–30 eV), negative ESI mode

spectrum of the dimer eluted in 6.30 min. Easier elimination of water can be connected with a higher number of non-linked –OH groups and therefore with biphenyl (C–C linked) type of dimer. The previously mentioned dimer with proposed ether-type structure (C–O–C linkage) exhibits longer retention time due to lower polarity in comparison to the dimer with C–C bond and two polar –OH groups. This elution order is in accordance with the suggested hypothesis. The oxidation product $m/z = 342$ was also detected by GC/MS providing two isomeric peaks

in the retention times $t_R = 22.3$ min and 22.9 min. Besides, a dimer containing one bromine atom in its molecule was detected as well in $t_R = 5.49$ (Table 3), intensity of which was one order of magnitude lower compared to the dimers at $m/z = 340.88$.

Trimeric oxidation products ($m/z = 510.82$, Table 3) were detected by UPLC/MS as four chromatographically separated isomers with retention times $t_R = 6.38$, 6.54, 6.63, and 6.83 min. Combining possible C–C and C–O–C linkages four possible structures can be considered. The first eluted, most polar trimer with $t_R = 6.38$ min bears three non-linked –OH groups and two C–C linkages. This structure has the best condition for the elimination of water. This is in agreement with corresponding collision spectrum (Supplementary Material Fig. S1e), in which fragment at $m/z = 492.8022$ ($C_{18}H_8Br_3O_2$, dtm −10.6 ppm, loss of H_2O from the parent ion) is formed with relatively high yield. On the other hand the structure does not allow formation of bromobenzenediol radical-anion which is in accordance with the respective fragment ($m/z = 185.9$) missing in the spectrum. Second possibility involves structures containing two non-linked -OH groups in a trimer containing one C–C and one C–O–C linkage. This possibility corresponds with second and third eluted trimer. Second eluted trimer ($t_R = 6.54$ min, Table 3) provides intensive fragment at $m/z = 186.9386$ corresponding to bromohydroxyphenolate ($C_6H_4BrO_2$, dtm −4.8 ppm, analogous process to the formation of bromobenzenediol radical-anion). Formation of this fragment suggests the structure of trimer containing both the −OH group and C–O–C linkage on the terminal aromatic ring (the proposed structure is given in Supplementary Material Fig. S1b). Similarly, third eluted trimer ($t_R = 6.63$ min, Table 3) provides fragment at $m/z = 338.8800$ consisting of two 4-BP units ($C_{12}H_5Br_2O_2$, dtm 40.7 ppm) and fragment at $m/z = 170.9522$ (Supplementary Material Fig. S1g) corresponding to 4-BP anion (C_6H_4BrO, dtm 44.5 ppm). Those fragmentation processes occur in structures containing also one C–C and one C–O–C linkage but the terminal aromatic ring (linked to the rest of molecule via C–O–C) lacks non-linked–OH group. This suggestion is supported by the absence of bromobenzenediol radical-anion as well as bromohydroxyphenolate, i.e. fragments at $m/z = 185.9$ or 186.9. The fourth eluted trimer ($t_R = 6.83$ min, Table 3) provides bromophenol anion (C_6H_4BrO, $m/z = 170.9467$, dtm 12.3 ppm, Supplementary Material Fig. S1h) in high yield. Probability of this fragmentation process is higher in trimers containing two C–O–C linkages where cleavage of bromophenol occurs when fragmentation starts from either side of the molecule.

An ion at $m/z = 446.8933$ eluted in $t_R = 5.86$ min (Table 3) could belong to a trimer product with two bromine substituents and two oxo groups (quinone) in the structure. The last oligomeric product revealed a very low abundant ion at $m/z = 680.75$, $t_R = 6.83$ min. This product could be tentatively assigned to a tetramer of 4-BP.

Oxidation products of PBP

Pentabromophenol was eluted in retention time 6.61 min. Three oxidation products were detected in PBP solution electrolysed 2 h at $E = 1.0$ V. In low energy MS scan the spectrum averaged over peak at retention time $t_R = 8.0$ min (Table 3) provided signal of parent ion possessing isotopic cluster typical for compound substituted with 9 bromine atoms. Signal of the first isotope was not found in the spectrum (Fig. 6a). The most intensive isotope was observed at $m/z = 896.2476$. This value is in very good agreement with the theoretical value (dtm 3.1 ppm) suggesting that tetrabromo(pentabromophenoxy)phenol can be the respective oxidation product. Fragmentation spectrum of isolated ion $m/z = 896.24$ (Fig. 6b) provides intensive fragment ion at $m/z = 466.6071$ (monoisotopic mass) with the most abundant isotopic peak at $m/z = 470.5944$. This fragment corresponds to pentabromophenyl radical-anion (C_6Br_5, dtm 14.5 ppm). Second characteristic fragment is formed by cleavage of pentabromophenyl radical and bromine ($C_6Br_3O_2$, monoisotopic $m/z = 340.7581$; m/z of the most abundant isotopic peak 344.7451, dtm 12.5 ppm). Based on these data, the structure of the observed dimeric product(s) corresponds to the structure of suggested diphenyl ether(s) containing the C–O–C linkage. It was reported [47] that electrochemical oxidation of pentachlorophenol in neutral aqueous buffers provides 2,3,4,5,6-pentachloro-4-pentachlorophenoxy-2,5-cyclohexadienone as the main dimeric product. However, analogous dimer was not detected in PBP solution electrolyzed either in lower (1 V) or in higher potential (1.4 V) in 90 % methanolic solution.

Apart from the dimeric oxidation product(s), trace amount of a monomeric product eluted in $t_R = 5.67$ min (Table 3) was detected in solution electrolysed for 2 h at $E = 1.0$ V. The same peak ($t_R = 5.67$ min, $m/z = 420.6788$) was observed as the main oxidation product in solution electrolysed for 20 h at $E = 1.4$ V. Peak with the same retention time and the same mass spectrum was obtained by analysis of solution of 2,3,5,6-tetrabromo-1,4-benzoquinone standard where two peaks corresponding to reduced ($t_R = 5.67$ min, $m/z = 420.6757$, dtm 11.2 ppm) and oxidized ($t_R = 5.98$ - min, $m/z = 419.6656$, dtm 5.7 ppm) form were detected. The fact indicates that one or both forms of the redox pair tetrabromobenzoquinone/tetrabromohydroquinone could belong to the products of intensive electrochemical oxidation of PBP. In contrast to PBP, analogous tetrachloroquinone was not found after electrolysis of pentachlorophenol in buffered aqueous media probably due to

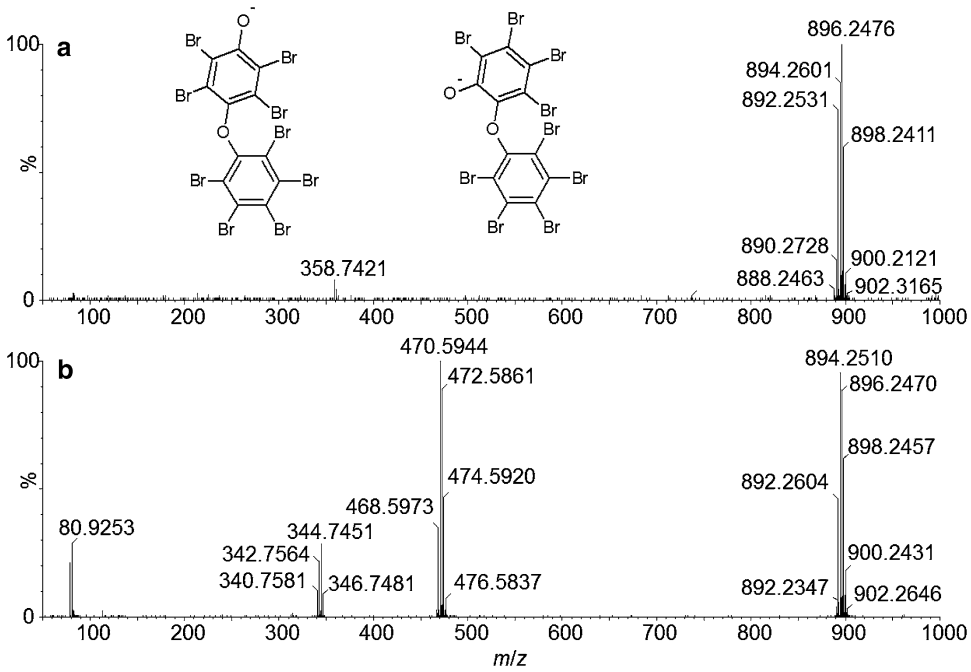

Fig. 6 MS and MS/MS spectrum of PBP dimer formed in solution of PBP ($c = 2 \times 10^{-4}$ mol dm^{-3}) electrolysed 2 h at $E = 1.0$ V. **a** MS spectrum at low collision energy 5 eV; **b** MS/MS spectrum at high collision energy (ramp 10–30 eV, quadrupole LM resolution: 2), negative ESI mode

fairly high oxidation potential of respective pentachlorophenoxy radical [47].

Under given conditions of more intensive electrolysis (20 h, $E = 1.4$ V), another monomeric oxidation product with monoisotopic ion $m/z = 434.6867$ was detected in $t_R = 6.25$ min (Table 3). Anion derived from methoxy-tetrabromophenol seems to be the most probable structure for the specie obtained in solution containing 90 % of methanol.

Finally, the minor product of PBP oxidation was detected in the retention time $t_R = 6.08$ min, $m/z = 449.6720$ (Table 3) in solution oxidized 2 h at $E = 1.0$ V. Elemental composition of this product revealed presence of nitrogen in its putative structure. This product was not obtained when the electrolysis of PBP was conducted under the same conditions but in presence of sodium ions instead of ammonium ones in the electrolyte solution. Therefore, the nitrogen containing group (a nitro group according to the exact mass and elemental composition) in the product originates from ammonium ions presented in the electrolysed media under oxidative conditions.

Results of EC/MS analysis

In addition to above mentioned off-line experiments in which the products of controlled potential electrolysis of BPs were analysed by two chromatographic techniques with MS detection, the oxidation of 2-BP, 3-BP, 4-BP, and PBP was investigated by on-line coupling of amperometric flow-through cell and mass spectrometer with electrospray ionization source (ESI/MS). The flow-through cell was equipped with platinum working electrode (surface area 0.07 cm^2) and palladium hydrogen (Pd/H_2) reference electrode.

Similar to the off-line experiments, the dimeric products of oxidation of 2-BP and 4-BP with $m/z = 340.8$ (monoisotopic mass) were observed at the potential of 1 V (vs. Pd/H_2 reference electrode). Simultaneously, the signal of trimeric product with $m/z = 510.8$ was recorded in the case of 2-BP oxidation. By contrast, no oxidation products were detected in the case of 3-BP. Electrolysis of PBP gave only one oxidation product with $m/z = 449.6$ which was found also in off-line UPLC/MS experiment in the samples of PBP oxidised at platinum gauze electrode (see above). The intensity of the signal was rather small in off-line experiments and the signal was lost in experiments conducted under more intensive conditions of electrolysis (20 h, $E = 1.4$ V) probably due to low stability of the product. On the contrary, well-resolved signal with sufficient intensity was obtained in on-line EC/MS experiments. The ability to analyse products with low stability seems to be the main advantage of on-line techniques. From this point of view, on-line coupling of electrochemical cell with mass spectrometer may be considered as to certain extent complementary technology to off-line techniques.

Dependence of the signal intensity of the oxidation products on potential applied to the working electrode revealed formation of particular products starting from certain threshold potential in agreement with oxidation potential observed in cyclic voltammograms. For oxidation of 2-BP, 4-BP, and PBP, the threshold potentials measured against Pd/H_2 reference electrode were 0.7, 0.8, and 1.0 V, respectively (Supplementary Material Fig. S2). In the

series 2-BP, 4-BP, PBP the order of threshold potentials agrees with the tendency to loss the first electron and form respective phenoxy radical.

Influence of flow rate on intensity of the dimeric product signal generated at the potential of 1.0 V was tested with 2-BP. The flow rate was varied from 9 to 3 $mm^3\ min^{-1}$ and back and the intensity of the most abundant ion at $m/z = 342.8$ (monoisotopic mass $m/z = 340.8$) of the dimeric product was recorded (Supplementary Material Fig. S3). The evident drop of signal intensity with decreasing flow rate without restoration at the increasing flow speed is most likely due to passivation of the electrode surface by oxidation products. It was observed that the signal intensity decreased due to passivation more than two orders of magnitude within about 25 min keeping the electrode at the potential 1.0 V (Supplementary Material Fig. S3). Presumably, passivation plays more important role in on-line experiments with flow-through cell containing small area platinum electrode (0.07 cm^2) in comparison to electrolytic experiments with large surface platinum electrode (4 cm^2). Nevertheless, on-line coupling of electrochemical cell with mass spectrometer represents promising technique for investigation of electrochemical processes and identification of products of electrochemical reactions due to possibility of direct and fast analysis of even unstable and reactive intermediates and products of electrochemical reactions.

Based on the results of voltammetric experiments as well as off-line and on-line combination of controlled potential electrolysis with mass spectrometric analysis of reaction products, the first step of the electrochemical oxidation of monobrominated phenols and PBP and subsequent dimerization reactions can be summarized in the Schemes 1 and 2, respectively. Under the used experimental conditions, both C–C and C–O–C linked dimers are most likely formed by electrolysis of monobrominated phenols. Dimerization is not generally accompanied by elimination of bromine but cleavage of C–Br bond can occur as a side-reaction at long term intensive electrolysis. Pentabromophenol forms solely ether type dimer(s) with bromine elimination. C–C coupling of two pentabromophenoxy units is most likely prevented by a steric hindrance.

Conclusions

Voltammetric experiments on glassy carbon electrode proved the pronounced electrochemical activity of all monobrominated phenols as well as pentabromophenol in methanol-aqueous media. Dimerization reactions provably follow the transfer of electron in the first step of the electrochemical oxidation resulting in electroactive products or intermediates. Oxidation products obtained by control potential electrolysis on gauze Pt electrode were analysed by UPLC/PDA/MS and GC/MS methods. Under given conditions, dimers were found to be the main oxidation products.

Unlike 3-BP and PBP, 2-BP and 4-BP provided trimeric products in low content. The main oxidation products of 2-BP, 4-BP, and PBP were found also in on-line coupling of electrochemical amperometric cell containing platinum working electrode with mass spectrometer. Although the adsorption of the products and passivation of relatively small electrode surface may complicate formation and analysis of the reaction products, the on-line coupling EC/MS is a powerful tool enabling investigation of reaction intermediates and products even in case of their lower stability.

Experimental

2-Bromophenol (2-BP, 98 %), 3-bromophenol (3-BP, 98 %), 4-bromophenol (4-BP, ≥98 %), pentabromophenol (PBP, 96 %), 2,3,5,6-tetrabromo-1,4-benzoquinone (TBQ) were purchased from Sigma-Aldrich. Methanol (LiChrosolv for HPLC, Merck, Germany) was used as solvent for voltammetric measurements and controlled potential electrolysis. Britton-Robinson (B-R) buffer was prepared from phosphoric acid, acetic acid, boric acid (all p.a., Lachema, Czech Republic) and sodium hydroxide (p.a., Lach-Ner, Czech Republic). Ionic strength of B-R buffer was adjusted with sodium perchlorate (p.a., Sigma-Aldrich). Ammonium formate buffer was prepared from 0.1 mol dm^{-3} formic acid (89–91 %, Merck, Czech Republic) and ammonia (p.a., Lach-Ner, Czech Republic). The mobile phase for UPLC chromatographic separation was prepared from formic acid and acetonitrile (HiPerSolv CHROMANORM, gradient grade for HPLC, VWR, Czech-Republic). Ultrapure water (Merck Millipore, Darmstadt, Germany) was used for preparation of electrolyte solutions. Extraction of electrolysed solutions was performed with ethyl acetate (p.a., Penta, Czech Republic).

Voltammetric measurements

Voltammetric measurements were performed on Autolab PGSTAT128 N potentiostat (Metrohm, Utrecht, The Netherlands) in three-electrode cell with glassy carbon working electrode (2.0 mm disc diameter, Metrohm) in static or rotating disc mode, reference SCE and platinum auxiliary electrode. The surface of the working electrode was polished on the microfiber fabric (Buehler, Lake Bluff, USA) with the aqueous suspension of alumina (particle size <50 nm, Sigma-Aldrich) before each measurement. Voltammetric measurements were performed in the

Scheme 1

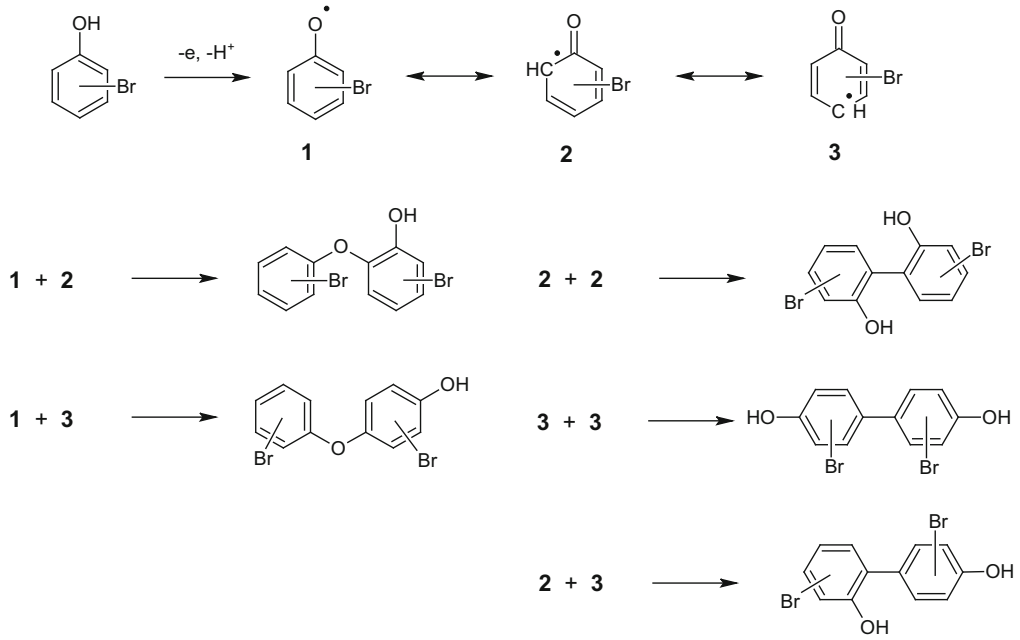

Scheme 2

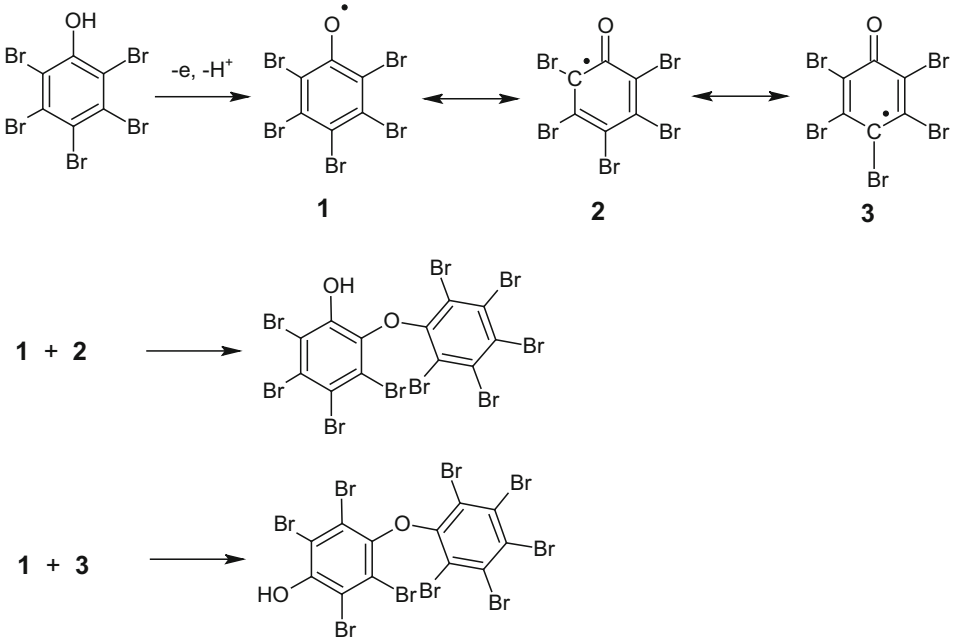

supporting electrolyte consisted of methanol and ammonium formate buffer solution pH 6.0 (9:1 or 1:1, v/v). Concentration of all brominated phenols in the solution was 1×10^{-4} mol dm^{-3}. The cyclic voltammograms were carried out at the scan rate in the range from 5 to 500 mV s^{-1}, angular rotation rate of RDE ranged from 52 to 314 rad s^{-1}.

A pH-meter inoLab720 pH with a combined glass electrode SenTix41 (all WTW, Weilheim, Germany) was used for pH adjustment of aqueous buffer solutions. The

pH meter was calibrated using aqueous calibration standards Duracal, pH 4 and pH 7 (Hamilton, Bonaduz, Switzerland).

Controlled potential electrolysis of brominated phenols

Controlled potential electrolysis was performed with a potentiostat OH-404 (Radelkis, Budapest, Hungary) in a two-compartment three-electrode cell containing platinum gauze working electrode, saturated calomel reference electrode (SCE) and platinum auxiliary electrode in the cathode compartment separated by a glass frit. The electrolysis of brominated phenols (2-BP, 3-BP, 4-BP, and PBP) solutions ($c = 2 \times 10^{-4}$ mol dm^{-3}, total volume 50 cm^3) was performed at potentials in the range of 1.0–1.4 V in stirred solution for various times as indicated (2–20 h). The supporting electrolyte consisted of ammonium formate buffer (pH 6) and methanol in the volume ratio 1:9. Unelectrolyzed solutions of brominated phenols treated and analysed according to the same protocol as described above were used as the blank samples.

UPLC/MS analysis

An Acquity UPLC system (Waters, Milford, MA, USA) equipped with binary solvent manager, sample manager, column manager and PDA detector was used. Chromatographic separation was performed on a column YMC-Triart C18 (100 × 2.0 mm i.d., 1.9 μm, 12 nm, YMC Europe, Dinslaken, Germany). The mobile phase consisted of 0.1 % aqueous formic acid (solvent A)/acetonitrile (solvent B), gradient elution (% v/v): 0–4 min (95–45 % A), 4–5 min (45–0 % A), 5–8 min (0 % A), 8.1–10 min (95 % A) was performed at flow rate 0.25 cm^3 min^{-1}. The temperature of the autosampler was held at 10 °C, a volume 10 mm^3 of sample was injected.

A Q-TOF Premier mass spectrometer (Waters, Manchester, UK) coupled to the UPLC system was used for confirmation of putative structures on the basis of determination of elemental composition. The tuned electrospray ionization (ESI) parameters were as follows: spray voltage 2.2 kV (negative mode), source temperature 110 °C, sampling cone 30 V, desolvation temperature 180 °C, cone gas flow rate 30 dm^3 h^{-1}, and desolvation gas flow rate 350 dm^3 h^{-1}. Nitrogen was used as a cone and desolvation gas, argon as a collision gas. Data were acquired using simultaneous scanning at lower collision energy (5 eV) and at higher energy applying collision energy ramp from 10 to 30 eV (either in MS or MS/MS scan). Data were processed using MassLynx 4.1 software (Waters). All experiments were done using MS^E mode recording spectra without discrimination of ions or their pre-selection (alternation of MS scans with low collision energy (CE = 5 eV) and elevated collision energy (ramp of CE = 10–30 eV or different CE value if necessary for highest possible yield of fragment ions as given in appropriate place of discussion), i.e. MS(1) and MS(2) scans). Where possible, targeted MS/MS scans were recorded in subsequent experiments.

EC/MS analysis

Electrochemical oxidation of brominated phenols with on-line mass spectrometric detection of their oxidation products was performed with potentiostat ADLC1 (Laboratorní přístroje, Prague, Czech Republic) connected to a Model 5040 Analytical cell (ESA, Chelmsford, MA, USA) containing platinum working electrode, palladium hydrogen reference electrode (Pd/H_2), and platinum auxiliary electrode. The oxidation was performed at potential range from 0 to 1.2 V. The supporting electrolyte consisted of 0.1 mol dm^{-3} ammonium formate buffer (pH 6) and methanol (1:9, v/v). The concentration of brominated phenols was 2×10^{-4} mol dm^{-3}. The samples solutions were continuously infused into the electrochemical cell by NE-1002X syringe pump (New Era Pump Systems, Farmingdale, NY, USA) with flow rate 7 mm^3 min^{-1} (unless otherwise stated). The stainless steel outlet tubing of the ESA cell was connected to the inlet of mass spectrometer via a coupler assembly (ESA). Agilent 1100 Series LC/MSD Trap (Agilent Technologies, Palo Alto, CA, USA) with electrospray ionization (ESI) interface was employed. ESI–MS conditions were as follows: negative ion mode, drying gas (N_2) flow rate 10 dm^3 min^{-1}, drying temperature 250 °C, nebulizer pressure 15 psi, capillary voltage +2500 V. Helium was used as a collision gas. Data were processed using DataAnalysis 3.3 software (Bruker Daltonik, Bremen, Germany).

GC/MS analysis

Controlled potential electrolysis of brominated phenols (2-BP, 3-BP, 4-BP, and PBP) solutions ($c = 2 \times 10^{-3}$ mol dm^{-3}, total volume 50 cm^3) was performed at potential $E = 1.0$ V in stirred solution for 60 min. The supporting electrolyte consisted of B-R buffer solution (pH 6) with 0.2 mol dm^{-3} $NaClO_4$ and methanol in the volume ratio 1:9. After electrolysis, the solutions were evaporated to dryness on a water bath and the residue was dissolved in 2 cm^3 of water and 2 cm^3 of ethyl acetate, vortexed and after phase separation 1 cm^3 of the organic phase was taken out and placed into the vial for GC/MS analysis. Two types of blank samples (unelectrolyzed brominated phenols solutions and the supporting electrolyte solution electrolyzed in the same manner as the bromophenol samples) were treated according to the same protocol as described

above and analysed in parallel with the electrolyzed bromophenol samples.

Analysis of oxidation products was carried out on gas chromatograph HP 6890 Series equipped with mass spectrometric detector Agilent 5973 N (Agilent, Palo Alto, USA). The separation was performed on a fused silica capillary column ZB-5 MS (30 m × 0.25 mm × 0.25 μm) and helium was used as carrier gas (He 5.0. Siad, Italy). The GC oven temperature was initially held at 50 °C for 2 min, ramped to 300 °C at 10 °C min^{-1} and held at 300 °C for 15 min.

Acknowledgments The authors gratefully acknowledge the financial support by the Ministry of Education, Youth and Sports of the Czech Republic (Project no. LO1305), Palacký University in Olomouc (Project IGA_PrF_2015_020) and the Czech Science Foundation (Project P206/12/1150).

References

1. Howe P, Dobson S, Malcolm HM (2005) 2,4,6-Tribromophenol and Other Simple Brominated Phenols. Concise International Chemical Assessment Document 66, World Health Organization, Geneva
2. Hyldig G (2007) In: Nollet LML (ed) Handbook of Meat, Poultry and Seafood Quality. John Wiley & Sons, p 524
3. Blanco E, Casais MC, Mejuto MC, Cela R (2005) J Chromatogr A 1068:189
4. Goodship V, Stevels A (2012) Waste electrical and electronic equipment handbook. Elsevier, p 541
5. Polo M, Llompart M, Garcia-Jares C, Gomez-Noya G, Bollain M-H, Cela R (2006) J Chromatogr A 1124:11
6. Knob R, Marák J, Staňová A, Maier V, Kaniansky D, Ševčík J (2010) J Chromatogr A 1217:3446
7. Reineke N, Biselli S, Franke S, Francke W, Heinzel N, Hühnerfuss H, Iznaguen H, Kammann U, Theobald N, Vobach M, Wosniok W (2006) Arch Environ Contam Toxicol 51:186
8. Thomsen C, Janák K, Lundanes E, Becher G (2001) J Chromatogr B 750:1
9. Smeds A, Saukko P (2003) Chemosphere 53:1123
10. Piccinini P, Pichat P, Guillard C (1998) J Photochem Photobiol A: Chem 119:137
11. Hirvonen A, Trapido M, Hentunen J, Tarhanen J (2000) Chemosphere 41:1211
12. Omura K, Matsuura T (1971) Tetrahedron 27:3101
13. Poerschmann J, Trommler U, Górecki T, Kopinke F-D (2009) Chemosphere 75:772
14. Borojovich EJC, Aizenshtat Z (2002) J Anal Appl Pyrolysis 63:129
15. Na Y, Seo J, Hong J (2003) Bull Korean Chem Soc 24:1276
16. Evans CS, Dellinger B (2003) Environ Sci Technol 37:5574
17. Yu W, Hu J, Xu F, Sun X, Gao R, Zhang Q, Wang W (2011) Environ Sci Technol 45:1917
18. Evans CS, Dellinger B (2005) Environ Sci Technol 39:7940
19. Cao H, He M, Sun Y, Han D (2011) J Phys Chem A 115:13489
20. Lin K, Yan Ch, Gan J (2014) Environ Sci Technol 48:263
21. Jiang J, Gao Y, Pang S-Y, Wang Q, Huangfu X, Liu Y, Ma J (2014) Environ Sci Technol 48:10850
22. Lin K, Gan J, Liu W (2014) Environ Sci Technol 48:11977
23. Meerts IATM, Letcher RJ, Hoving S, Marsh G, Bergman A, Lemmen JG, van der Burg B, Brouwer A (2001) Environ Health Persp 109:399
24. Dingemans MML, de Groot A, van Kleef RGDM, Bergman A, van den Berg M, Vijverbeg HPM, Westerink RHS (2008) Environ Health Persp 116:637
25. Cantón RF, Sholten DEA, Marsh G, de Jong PC, van den Berg M (2008) Toxicol Appl Pharmacol 227:68
26. Lai Y, Lu M, Gao X, Wu H, Cai Z (2011) Environ Sci Technol 45:10720
27. Ežerskis Z, Jusys Z (2002) J Appl Electrochem 32:543
28. Ureta-Zañartu MS, Bustos P, Diez MC, Mora ML, Gutiérrez C (2001) Electrochim Acta 46:2545
29. Morrow GW (2001) Anodic Oxidation of Oxygen-Containing Compounds. In: Lund H, Hammerich O (eds) Organic Electrochemistry, 4th edn. Marcel Dekker, New York, p 590
30. Ežerskis Z, Jusys Z (2001) J Appl Electrochem 31:1117
31. Ežerskis Z, Jusys Z (2001) Pure Appl Chem 73:1929
32. Codognoto L, Machado SAS, Avaca LA (2003) J Appl Electrochem 33:951
33. Rodgers JD, Jedral W, Bunce NJ (1999) Environ Sci Technol 33:1453
34. Berríos C, Arce R, Rezende MC, Ureta-Zañartu MS, Gutiérrez C (2008) Electrochim Acta 53:2768
35. Ureta-Zañartu MS, Bustos P, Berríos C, Diez MC, Mora ML, Gutiérrez C (2002) Electrochim Acta 47:2399
36. Berríos C, Marco JF, Gutiérrez C, Ureta-Zañartu MS (2009) Electrochim Acta 54:6417
37. Ureta-Zañartu MS, Mora ML, Diez MC, Berríos C, Ojeda J, Gutiérrez C (2002) J Appl Electrochem 32:1211
38. Vallejo M, San Román MF, Ortiz I (2013) Environ Sci Technol 47:12400
39. Taj S, Ahmed MF, Sankarapapavinasam S (1993) J Electroanal Chem 356:269
40. Marková E, Smyslová P, Macíková P, Skopalová J, Barták P (2012) Chem Listy 106:195
41. Marková E, Kučerová P, Skopalová J, Barták P (2015) Electroanal 27:156
42. Samet Y, Kraiem D, Abdelhedi R (2010) Prog Org Coat 69:335
43. Kawde AN, Morsy MA, Odewunmi N, Mahfouz W (2013) Electroanal 25:1547
44. Özel AD, Dikici E, Bachas LG (2013) Monatsh Chem 144:781
45. Rostami A, Omrami A, Hamedian N (2013) Monatsh Chem 144:1775
46. Wang X, Liu W, Li Ch, Chu Ch, Wang S, Yan M, Yu J, Huang J (2013) Monatsh Chem 144:1759
47. Gattrell M, MacDougall B (1999) J Electrochem Soc 146:3335
48. Compton RG, Mason D, Unwin PR (1988) J Chem Soc, Faraday Trans 1(84):473

Příloha 3

Electrochemical oxidation of 2,4,6-tribromophenol in aqueous-alcoholic media

Marková, E.; Kučerová, P.; **Skopalová**, **J.***; Barták, P.

Electroanalysis **2015**, *57*,156-165

Full Paper

Wiley Online Library

ELECTROANALYSIS

DOI: 10.1002/elan.201400412

Electrochemical Oxidation of 2,4,6-Tribromophenol in Aqueous-Alcoholic Media

Eva Marková,[a] Pavla Kučerová,[a] Jana Skopalová,*[b] and Petr Barták[a]

Abstract: Electrooxidation of 2,4,6-tribromophenol on platinum gauze electrode in 90% (v/v) alcohol (methanol, ethanol, propan-1-ol, butan-1-ol) was studied. Products were investigated by gas chromatography/mass spectrometry. Structures of several different types of monomeric as well as dimeric alkoxy derivatives have been suggested according to mass spectra of the detected products. Series of 2,6-dibromo-4-alkoxyphenols, 2,4,6-tribromo-6-alkoxycyclohexa-2,4-dien-1-ones and 2,6-dibromo-6-alkoxycyclohex-2-ene-1,4-diones were found. By analogy to identified monomeric alkoxy derivatives, a serie of dimeric 2,6-dibromo-4-(2,6-dibromo-4-alkoxyphenoxy)phenols was suggested and identified in respective chromatograms as well.

Keywords: 2,4,6-Tribromophenol · Alcohols · Electrooxidation · Gas chromatography · Mass spectrometry

1 Introduction

Phenols form a large group of electrochemically active compounds. Their electrooxidation is a remarkable process dependent on a phenol substitution and experimental conditions such as pH, solvent-electrolyte system, electrode material, concentration, current density, potential, etc. [1,2]. The oxidation in alkaline media leads to the formation of simple *ortho*- or *para*-benzoquinones, quinol-ethers or biphenyls via C–C coupling through a phenoxy radical as an intermediate product. In acidic media, nonionized phenols are oxidized via two reaction pathways through a phenoxonium ion as an intermediate product. In the first path, *ortho*-/*para*-phenoxonium ion substituent, which could be a hydroxyl group or an alkyl group with at least one ionizable hydrogen, loses a proton forming *ortho*-/*para*-benzoquinone or very reactive *ortho*-/*para*-benzoquinonemethide derivative. In the second path, phenoxonium ion reacts with a nucleophile followed by the loss of a proton and a formation of substituted dienones [1].

The oxidation of phenols through phenoxy radicals leads to the formation of polymeric products [2,3]. C–O–C bonding of the radicals which provides ether-type polymers is typical for the phenols oxidation in alkaline aqueous media while the C–C coupling prevails in acidic aqueous media to give quinone-type polymers [4,5].

The electrooxidation of phenolic compounds was investigated on various electrode materials such as Pt [2,3], Au [2,6], glassy carbon [7,8], boron-doped diamond [9,10] as well as on many metal-oxide electrodes [11,12]. Some products of phenolic compounds electrooxidation are adsorbed on working electrode surface and form polymeric films passivating the electrode surface [7,2]. The deactivation of the electrode surface is more intensive in alkaline media and also at higher concentration of phenolic compounds producing more phenoxy radicals [3].

Electrochemical oxidation of phenol and its derivatives has been performed in different solvent systems. Aqueous media were mostly employed especially in terms of electrochemical degradation of phenolic pollutants [3,7,11]. Methanol and acetonitrile were used for elucidation of electrooxidation mechanisms of variously substituted alkyl- and alkoxyphenols [13–16]. Anodic oxidation of phenol and some other phenolic compounds was investigated also in the presence of 50% methanol, ethanol and propan-1-ol [17]. The formation of remarkable well-ordered polymeric structure at the surface of Pt electrode was observed which was generated by cyclic polarization of the electrode in methanolic and ethanolic solutions of phenol. The reaction mechanism is based on the formation of a film of Pt oxide/hydroxides in presence of methanol or ethanol onto which the phenol and its electrooxidation products are deposited [17].

Concerning halogen derivatives of phenol, electrochemical behavior of chlorophenols has been studied in detail [3,4,8,18,19]. The mechanism of chlorophenols electrooxidation begins with the formation of the phenoxy radical and continues by two possible paths: one pathway yields products with quinoid structure and the other leads to the formation of insoluble polymers passivating the electrode surface [19]. The reactivity of chlorophenols depends on the number of chlorine atoms and also on their position in the aromatic ring. In general, higher chlorinated phenols are more easily oxidizable than lower chlorinated derivatives. Isomers with chlorine in *para*-position are oxidized at higher potentials than *ortho*-chloro deriva-

[a] E. Marková, P. Kučerová, P. Barták
Regional Centre of Advanced Technologies and Materials, Department of Analytical Chemistry, Faculty of Science, Palacký University
17. listopadu 12, 771 46 Olomouc, Czech Republic

[b] J. Skopalová
Department of Analytical Chemistry, Faculty of Science, Palacký University
17. listopadu 12, 771 46 Olomouc, Czech Republic
*e-mail: jana.skopalova@upol.cz

tives [19]. Many of the oligo/polymeric oxidation products fouling the electrode surface have been identified [4]. The polymerization of chlorinated phenols can proceed through the active *ortho*- and *para*-positions via quinol-ether mechanism (without chlorine elimination) or via the nucleophilic-radical substitution ($S_{RN}1$) mechanism with chlorine elimination if at least one *ortho*- and/or *para*-position is occupied by chlorine [4,18]. The electropolymerization rate of *ortho*-chlorophenols is higher than the rate of *para*-chlorophenols [18].

The aim of this study was to investigate products of electrochemical oxidation of 2,4,6-tribromophenol (TBP), which is the most widely produced brominated phenol. It is used as a fungicide and as an intermediate for the synthesis of other brominated flame retardants [20]. Knowledge of the bromophenols electrooxidation is rather rare although their similarity with chlorophenols can be expected. Electrochemical oxidation of TBP has been already studied in neutral and alkaline aqueous solutions containing 50 % methanol [21]. Bulk electrolysis of TBP on the platinum gauze electrode provided two main oxidation products: 2,6-dibromo-4-(2,4,6-tribromophenoxy)-phenol and 3,3′,5,5′-tetrabromo-1,1′-bi(cyclohexa-2,5-dien-1-ylidene)-4,4′-dione. The dimeric products occurred both dissolved in electrolyzed solutions and adsorbed on the platinum electrode [21]. In this work we present results of the study of the TBP electrooxidation in aqueous-alcohol solutions with 90 % short-chain primary alcohol: methanol, ethanol, propan-1-ol or butan-1-ol. Alcohols were used as an anticipated reaction component and its high content was expected to suppress adsorption of reaction products on the electrode surface. Oxidation products of TBP were generated by controlled potential electrolysis and identified using gas chromatography with mass spectrometry (GC/MS). The mechanism of TBP oxidation is proposed and the influence of the alcohol component in reaction mixtures is discussed.

2 Experimental

2.1 Chemicals

2,4,6-Tribromophenol (TBP, 99 %) was purchased from Sigma-Aldrich. Methanol (p.a., Penta, Czech Republic), ethanol (p.a., Sigma-Aldrich), propan-1-ol (≥99,9 % Sigma-Aldrich), butan-1-ol (p.a., Lachema, Czech Republic), were used as solvents for voltammetric measurements and controlled potential electrolysis. Britton–Robinson (B-R) buffer was prepared from phosphoric acid, acetic acid, boric acid (all p.a., Lachema, Czech Republic) and sodium hydroxide (p.a., Lach-Ner, Czech Republic). Ionic strength of B-R buffer was adjusted with sodium perchlorate (p.a., Sigma-Aldrich). Sulfuric acid (96 %, p.a.) was obtained from Penta, Czech Republic. Extraction of electrolyzed solutions was performed with ethyl acetate (p.a., Penta, Czech Republic). Deionized water (Aqual 29, Czech Republic) was used to prepare the electrolyte solutions.

2.2 Instruments and Equipment

Controlled potential electrolysis was performed on potentiostat OH-404 (Radelkis, Budapest, Hungary). Platinum gauze electrode was used as the working electrode, saturated calomel electrode (SCE) as the reference electrode and Pt plate in separate compartment served as the auxiliary electrode. Analysis of products was carried out on gas chromatograph HP 6890 Series equipped with mass spectrometric detector Agilent 5973 N (Agilent, Palo Alto, USA). The separation was performed on fused silica capillary column ZB-5 MS (30 m × 0.25 mm × 0.25 μm) and helium was used as carrier gas (He 5.0. Siad, Italy). The temperature program was set to 50 °C–2 min–10 °C/min–300 °C–15 min. A pH-meter inoLab720 pH with a combined glass electrode SenTix41 (all WTW, Weilheim, Germany) was used for pH adjustment of aqueous buffer solutions. The pH meter was calibrated using aqueous calibration standards Duracal, pH 4 and pH 7 (Hamilton, Bonaduz, Switzerland). Voltammetric measurements were performed on Eco-Tribo-Polarograph (Polaro-Sensors, Prague, Czech Republic) in three-electrode cell with glassy carbon working electrode (3.0 mm disc diameter, Bioanalytical Systems, West Lafayette, USA) or platinum working electrode (1.6 mm disc diameter, Bioanalytical Systems, West Lafayette, USA), reference SCE and platinum auxiliary electrode. The surface of the glassy carbon working electrode was polished on the microfiber fabric (Buehler, Lake Bluff, USA) with an aqueous suspension of alumina (particle size < 50 nm; Sigma-Aldrich) before each measurement. Surface of the platinum disc electrode was electrochemically activated in 0.5 mol L^{-1} H_2SO_4 in the potential range from −0.2 to 1.2 V before each measurement. Boiling points of oxidation products were generated from the software Chem3D Ultra 7.0 (CambridgeSoft, USA).

2.3 Working Procedures

2.3.1 Voltammetric Measurements

Cyclic voltammetric measurements were performed in the supporting electrolyte consisted of B-R buffer pH 6.0 and respective alcohol (90 %, v/v). Concentration of TBP in the solution was 2 mmol L^{-1}. The measurements were carried out at the scan rate of 100 mV s^{-1}.

2.3.2 Electrolysis of TBP

Controlled potential electrolysis of TBP solutions (c = 2 mmol L^{-1}, total volume 50 mL) was performed at potential E = 1.0 V in stirred solution for 60 min. The supporting electrolyte consisted of B-R buffer (pH 6) with 0.2 mol L^{-1} $NaClO_4$ and alcohol (methanol, ethanol, propan-1-ol, butan-1-ol) in volume ratio 1:9. After electrolysis, the solutions were evaporated to dryness on a water bath and the residue was dissolved in 2 mL of water and 2 mL of ethyl acetate, vortexed and after phase separation 1 mL of the organic phase was taken out and

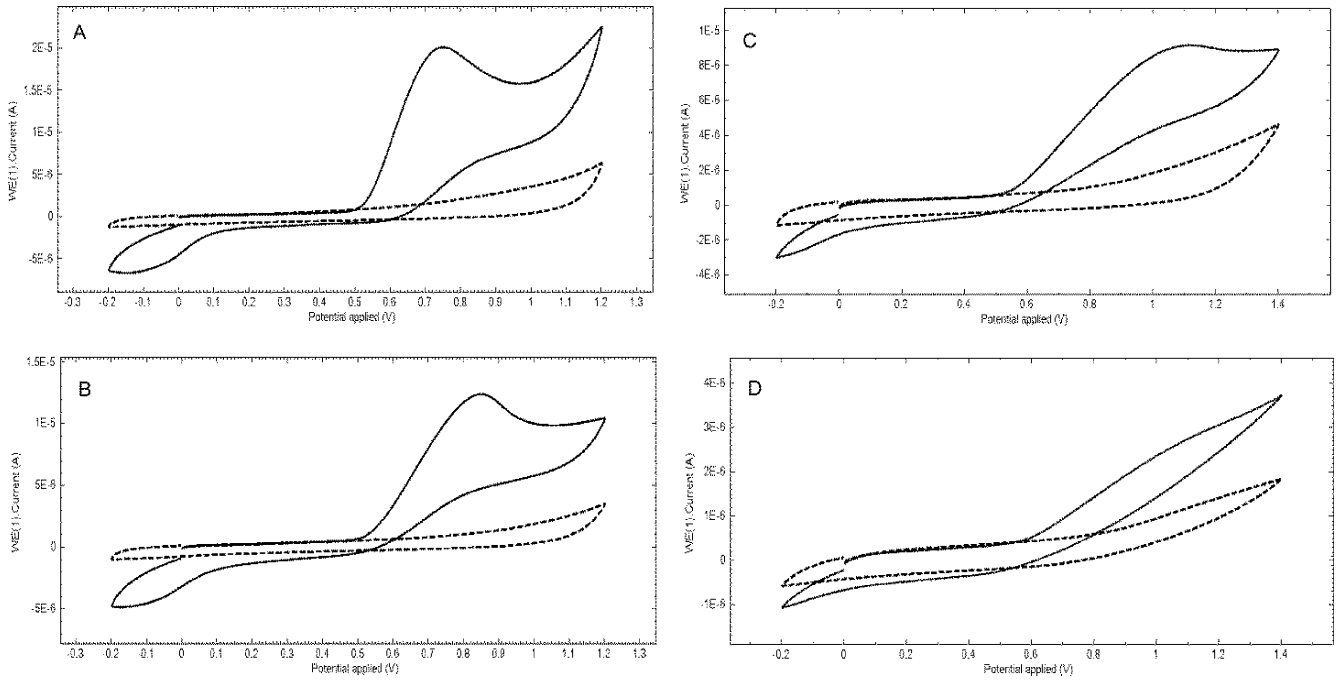

Fig. 1. Cyclic voltammograms of 2 mmol L^{-1} TBP (—) in 90 % (v/v) methanol (A), ethanol (B), propan-1-ol (C) and butan-1-ol (D) and the supporting electrolyte (---) consisting of respective alcohol/BR buffer pH 6 (9/1, v/v), scan rate 100 mV s^{-1}, measured on glassy carbon disc working electrode.

placed into the vial for GC/MS analysis. The blank samples, (i) electrolyzed supporting electrolyte without TBP and (ii) unelectrolyzed TBP in the supporting electrolyte, were treated and analyzed according to the same protocol as described above. In order to detect possible volatile oxidation products (from TBP as well as from alcohols in supporting electrolytes), small aliquots of the samples (2 mL) were diluted with 0.05 mol L^{-1} H_2SO_4 (6 mL) in

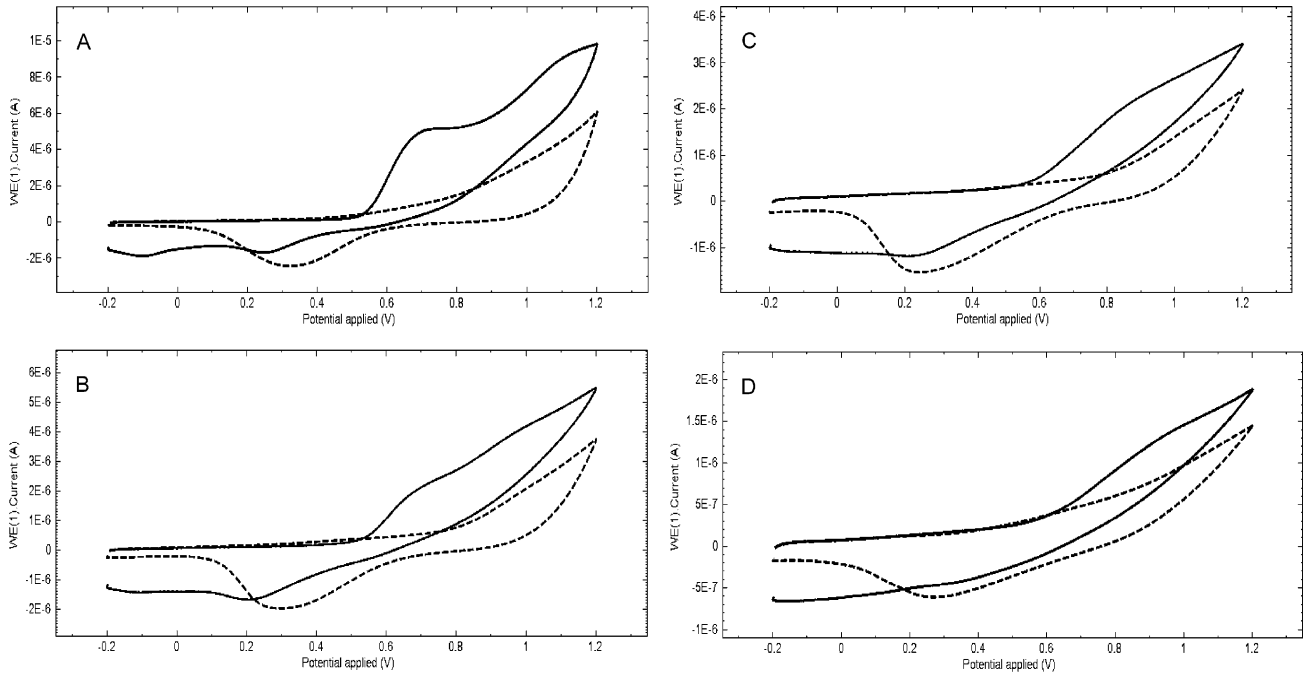

Fig. 2. Cyclic voltammograms of 2 mmol L^{-1} TBP (—) in 90 % (v/v) methanol (A), ethanol (B), propan-1-ol (C) and butan-1-ol (D) and the supporting electrolyte (---) consisting of respective alcohol/BR buffer pH 6 (9/1, v/v), scan rate 100 mV s^{-1}, measured on platinum disc working electrode.

Table 1. Characteristics and structures of TBP and its oxidation products.

	Name	Structure	Formula weight	Monoisotopic mass	Retention time (min)	Calculated boiling point (°C)
TBP	2,4,6-Tribromophenol	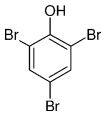	331	328	16.1	310.08
P1	2,6-Dibromobenzene-1,4-diol	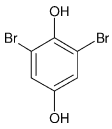	268	266	17.2	315.03
P2	2,6-Dibromocyclohexa-2,5-diene-1,4-dione	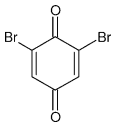	266	264	13.4	320.49
P3A	2,6-Dibromo-4-methoxyphenol	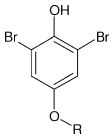	282	280	15.9	301.36
P3B	2,6-Dibromo-4-ethoxyphenol		296	294	16.7	315.52
P3C	2,6-Dibromo-4-propoxyphenol		310	308	17.7	328.77
P3D	2,6-Dibromo-4-butoxyphenol		324	322	18.9	341.11
P4A	2,4,6-Tribromo-6-methoxycyclohexa-2,4-dien-1-one	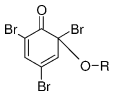	361	358	18.2	341.22
P4B	2,4,6-Tribromo-6-ethoxycyclohexa-2,4-dien-1-one		375	372	18.8	352.93
P4C	2,4,6-Tribromo-6-propoxycyclohexa-2,4-dien-1-one		389	386	19.9	364.53
P5A	2,6-Dibromo-6-methoxycyclohex-2-ene-1,4-dione	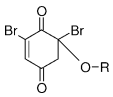	298	296	17.4	335.58
P5B	2,6-Dibromo-6-ethoxycyclohex-2-ene-1,4-dione		312	310	18.0	347.52
P5C	2,6-Dibromo-6-propoxycyclohex-2-ene-1,4-dione		326	324	19.1	359.12
P5D	2,6-Dibromo-6-butoxycyclohex-2-ene-1,4-dione		340	338	20.3	370.72
P6	3,3′,5,5′-Tetrabromo-1,1′-bi(cyclohexa-2,5-dien-1-ylidene)-4,4′-dione	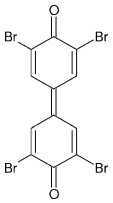	500	496	26.0	476.24
P7	2,6-Dibromo-4-(2,4,6-tribromophenoxy)phenol	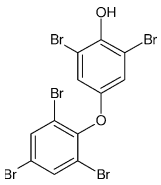	581	576	27.1	471.06
P8	2,6-Dibromo-4-(2,6-dibromo-4-hydroxyphenoxy)phenol	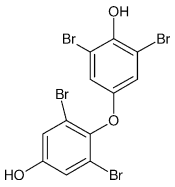	518	514	27.9	475.20
P9A	2,6-Dibromo-4-(2,6-dibromo-4-methoxyphenoxy)phenol	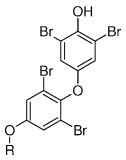	532	528	26.6	464.01
P9B	2,6-Dibromo-4-(2,6-dibromo-4-ethoxyphenoxy)phenol		546	542	26.8	475.62
P9C	2,6-Dibromo-4-(2,6-dibromo-4-propoxyphenoxy)phenol		560	556	27.4	487.22
P9D	2,6-Dibromo-4-(2,6-dibromo-4-butoxyphenoxy)phenol		574	570	28.4	498.83

12 mL vials and sampled with SPME fiber (CAR/PDMS/DVB, 2 cm, Supelco, Belefonte, USA) in the head-space for 60 min at ambient temperature under continuous stirring. Analytes were desorbed thermally (280 °C, 5 min) and separated on capillary column ZB-5 MS (30 m × 0.25 mm × 0.25 μm) with temperature program 50 °C–2 min–5 °C/min–300 °C–10 min.

For quantitative examination of electrochemical reaction, 0.5 mL of unelectrolyzed as well as electrolyzed samples of 2 mmol L^{-1} TBP were diluted with 0.05 mol L^{-1} H_2SO_4 (2 mL) and 1.5 mL ethylacetate was added. Samples were vortexed, centrifuged and 1 mL of the organic phase was taken out and placed into the vial for GC/MS analysis.

3 Results and Discussion

3.1 Voltammetric Behavior

Cyclic voltammograms of TBP in 90% methanol and 90% ethanol (Figure 1A,B) measured on glassy carbon electrode showed one well-developed anodic signal at the potential of 0.74 V and 0.85 V, respectively. Voltammetric peaks of TBP in 90% propan-1-ol and 90% butan-1-ol (Fig. 1C,D) were more flat with the maximum at the potential about 1.04 V and 1.14 V in propan-1-ol and butan-1-ol, respectively. The flat shape, lower current and the potential shift of the CV peaks suggest the longer-chain alcohols slow down the rate of the electrode reaction of TBP. Cathodic peak on the reverse branch of cyclic voltammograms corresponds to the reduction of quinoid products formed by anodic oxidation of TBP [21]. This peak is the most pronounced in the case of methanol and ethanol (Fig. 1A,B). However, the increase of cathodic current in the region between 0.1 and −0.2 V after the

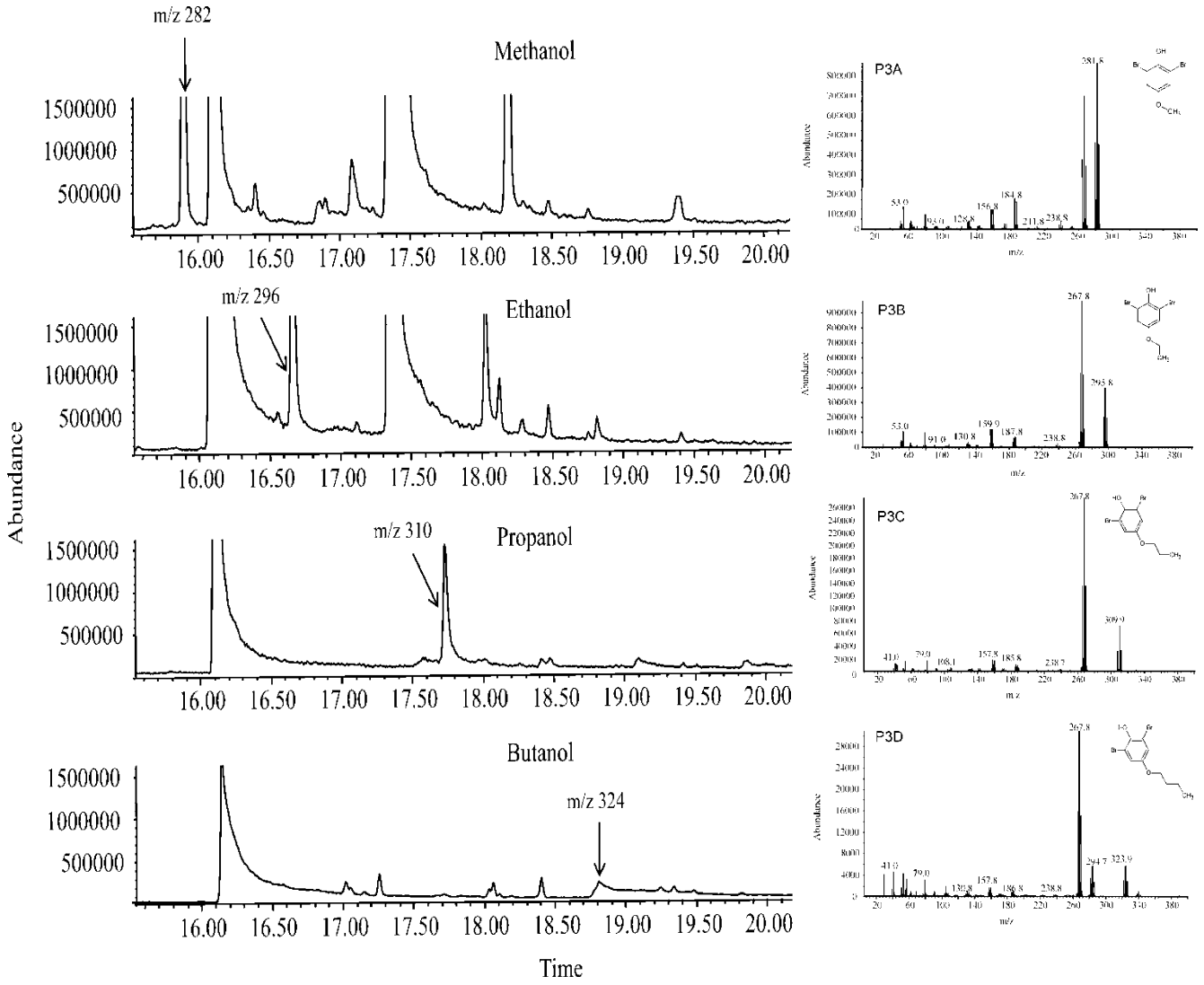

Fig. 3. Gas chromatograms and mass spectra of TBP monomeric oxidation products of P3 group.

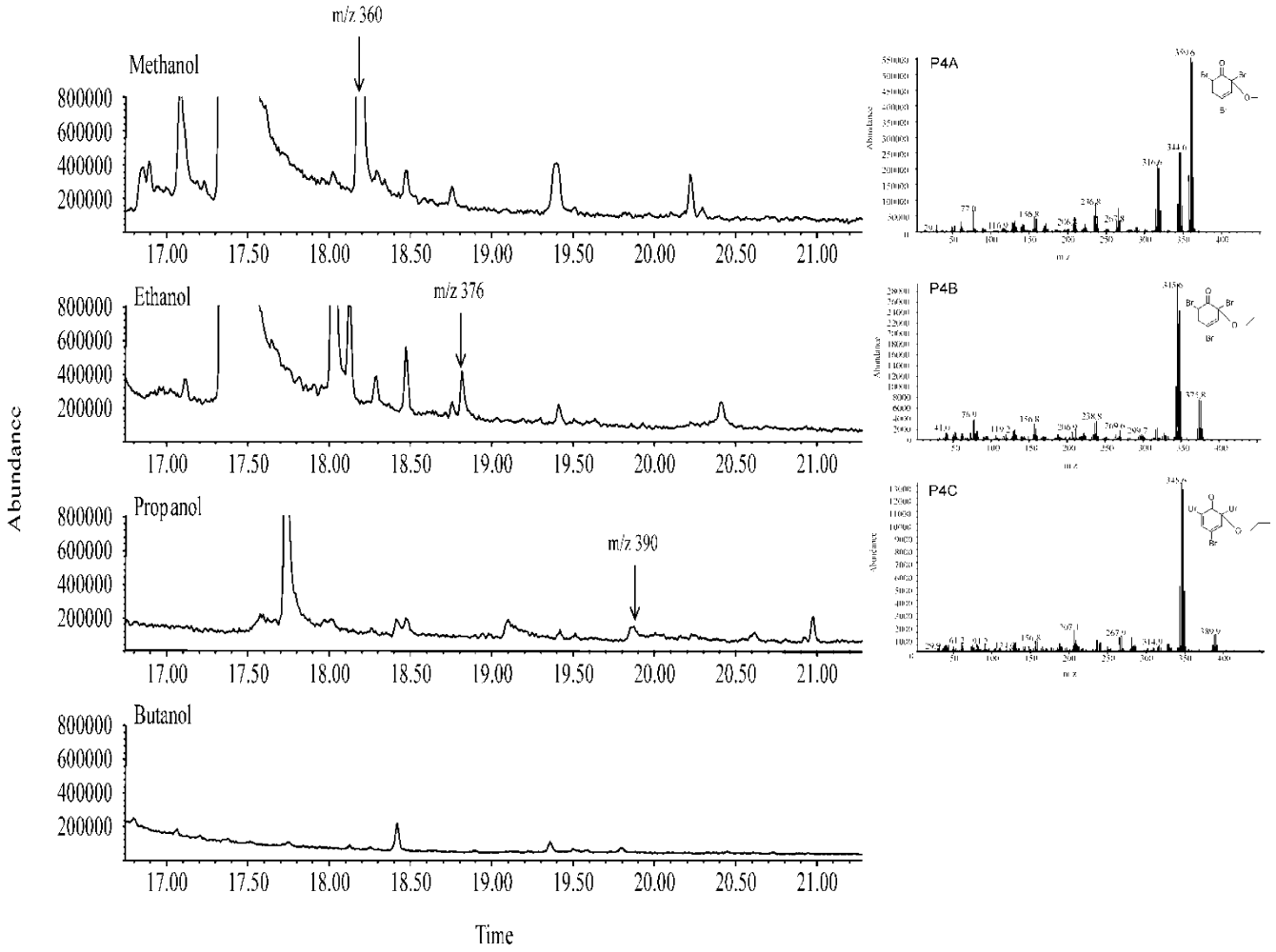

Fig. 4. Gas chromatograms and mass spectra of TBP monomeric oxidation products of P4 group.

TBP addition to the supporting electrolyte observable in the case of propan-1-ol and butan-1-ol (Figure 1C,D) suggests the quinoid products are formed also in these media. When platinum disc electrode was used for the same purpose, the course of cyclic voltammograms of TBP was quite similar at least in the anodic branch (Figure 2A–D). Potential of respective anodic peaks increased from 0.71 to 0.97 V with increasing length of carbon moiety from methanol to butan-1-ol. Since some tendency to adsorb target compounds could be expected in the case of carbon electrode, platinum was selected as a preferential electrode material for further research.

3.2 Products of Electrochemical Oxidation of TBP

According to the cyclic voltammograms, the potential of 1 V was chosen for bulk electrolysis of TBP solutions. A change of color from colorless to yellow was observed during the electrolysis. GC/MS analysis revealed two main groups of oxidation products differing strongly in retention times. The first one, with retention times ranging typically from 15.9 to 20.3 min was ascribed to monomeric oxidative products derived from the single TBP molecule. The second group with substantially longer retention times (from 26.0 to 28.4 min) and higher molecular masses was identified as a mixture of products originating during oxidative dimerization from two TBP molecules or monomeric intermediates (see Table 1 for putative structures).

In both groups several compounds were observed in all media, indicating the putative structures independent of the used alcohol (i.e. monomeric products P1, P2 and dimeric products P6, P7, P8). Other peaks were shifted in retention times according to the type of the alcohol, indicating putative structures containing certain part of the moiety derived from the particular alcohol used in the supporting electrolyte. General prefix describing the type of the structure and suffix according to the type of the alcohol are used for description of the monomeric (i.e. P3A–D, P4A–C, P5A–D) and dimeric (i.e. P9A–D) products. All found products were formed during electrolysis of TBP solutions, as it was proved by comparison with analyzed blank samples.

Product P1 with retention time (t_R) 17.2 min and *m/z* 268 (Table 1) was identified in methanol, ethanol and propan-1-ol. Analysis of the mass spectra revealed similar

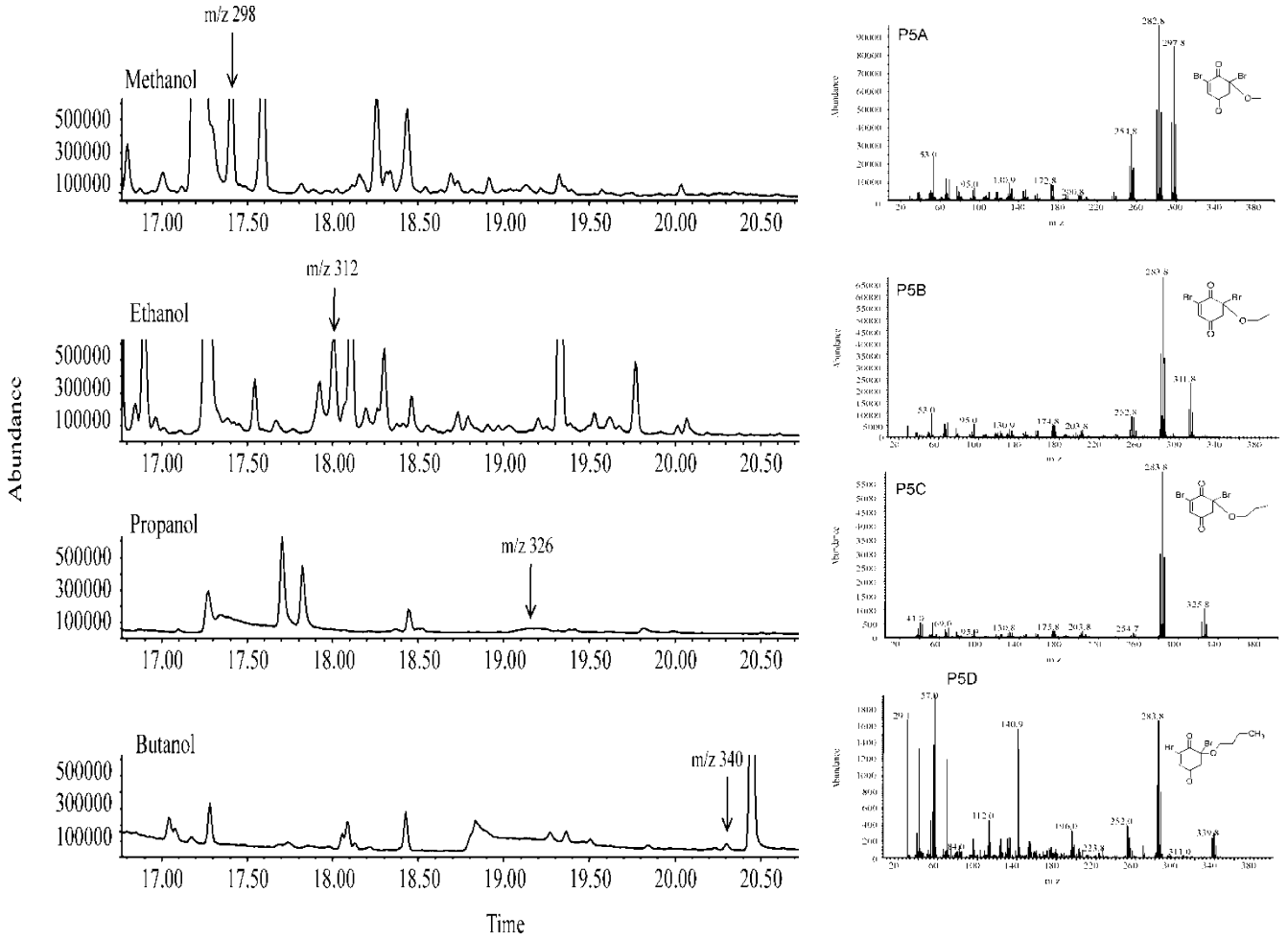

Fig. 5. Gas chromatograms and mass spectra of TBP monomeric oxidation products of P5 group.

structure of the product P1 to that of TBP with the difference that in product P1 the hydroxyl group is bonded in *para*- position instead of bromine. Product P2 (t_R 13.4 min, *m/z* 266, Table 1) forms the redox couple with P1 and could be easily derived from the TBP by hydroxylation and elimination of hydrogen bromide. This quinone was found in the all alcohol media and it is one of the products contributing to the yellowish color of the electrolyzed solution (absorption maximum at 352 nm in *n*-hexane, 362 nm in chloroform [22]).

A group of monomeric alkoxyphenols derived from the all of the alcohols under investigation (P3A-P3D) was identified according to mass spectra and increasing retention times of homologues from P3A to P3D (Table 1 and Figure 3). The alkoxy derivatives were probably formed from phenoxy radical and alcohol as a nucleophilic agent with subsequent elimination of bromine.

Monomeric products P4A–P4C (Table 1, Figure 4) may be formed directly by nucleophilic attack of alcohol to *ortho*- or *para*-position accompanied by a proton loss. Bromine is not eliminated in these reactions. The similar reaction has been described for oxidation of substituted phenols in methanol [13]. These products were identified in solution of methanol, ethanol and propan-1-ol. Retention time of respective products is extended with the length of alkoxy chain supporting homologues identification but the butoxy derivative was not found.

On the contrary, full range of homologues was identified in the case of monomeric products P5A–P5D (Table 1, Figure 5).The compounds could be formed by the hydroxylation of phenoxonium ion, elimination of the bromine and subsequent reaction with the alcohol.

Beside monomeric derivatives, dimeric products were found in all solutions as well. Two oxidation products P6 and P7 were eluted from column in retention times 26.0 min and 27.1 min with *m/z* 500 and 581, respectively (Table 1). According to MS spectra and isotopic profiles, P6 and P7 corresponded to ions with four or five atoms of bromine, respectively, and these were identified as 3,3′,5,5′-tetrabromo-1,1′-bi(cyclohexa-2,5-dien-1-ylidene)-4,4′-dione and 2,6-dibromo-4-(2,4,6-tribromophenoxy)-phenol, respectively. These products were also found in 50 % methanol [21]. The coloured product P6 (absorption maximum at about 450 nm [23]) was probably formed by recombination of two phenoxy radicals of TBP followed by elimination of bromine.

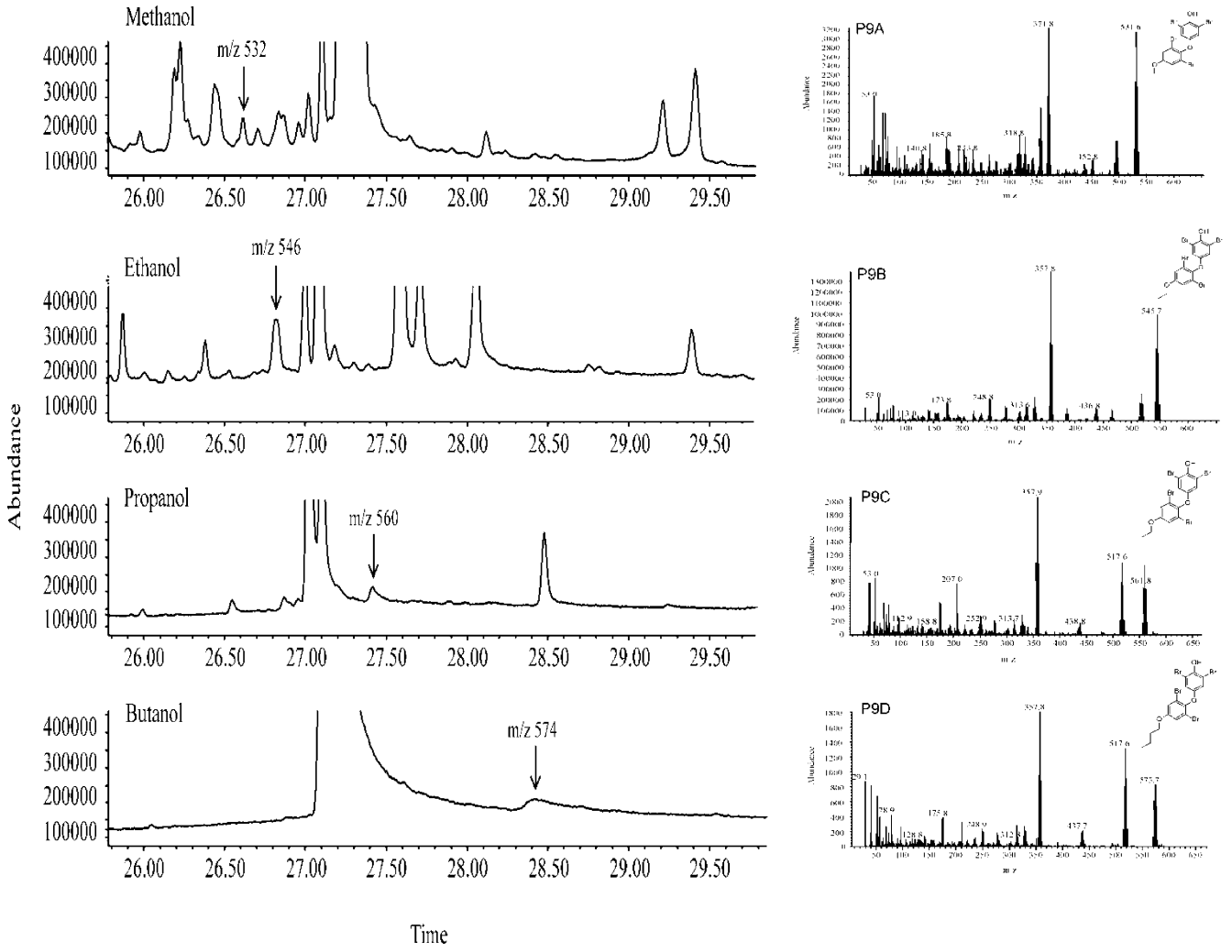

Fig. 6. Gas chromatograms and mass spectra of TBP dimeric oxidation products of P9 group.

Dimeric product P8 with t_R 27.9 and *m/z* 518 (Table 1) could be formed by reaction of phenoxy radical with the product P1 followed by the elimination of bromine. The product P8 was found in methanol, ethanol and propan-1-ol, i.e. in the same media as the product P1, which is consistent with the proposed way of its formation.

Four dimers (P9A–P9D) differing in the length of alkoxy group were found in all alcohols (Table 1). Supposed structures and mechanism of formation are similar to the product P8. With increasing number of carbon atoms in alcohol media, retention time is extended from P9A to P9D (Figure 6).

Above mentioned homologues were identified by the analysis of corresponding MS spectra and by calculated boiling point (Table 1). In mass spectra, alkoxy derivatives containing methoxy group had a typical loss of Δ *m/z* 15 (P3A, P4A, P5A and P9A). Similarly products with ethoxy-(P3B, P4B, P5B and P9B), propoxy-(P3C, P4C, P5C and P9C) and butoxy group (P3D, P5D and P9D) had a typical loss of Δ *m/z* 28, Δ *m/z* 42 and Δ *m/z* 56, respectively (Figures 3–6).

Calculated boiling points of all alkoxy derivatives increased in homologous series from C1 to C4. The values

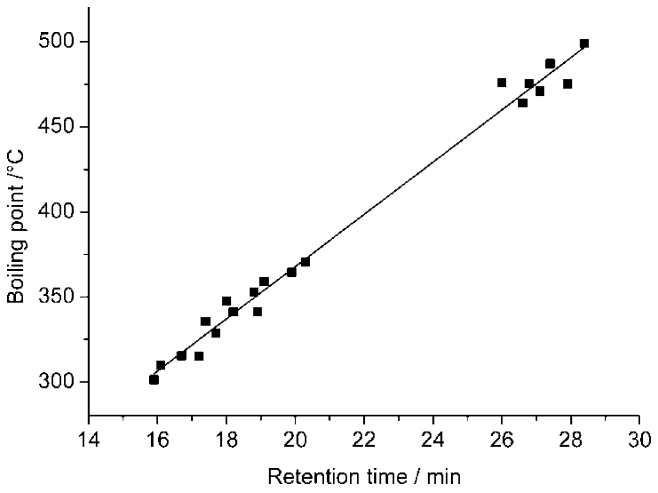

Fig. 7. Dependence of calculated boiling points on retention time for TBP and its oxidation products.

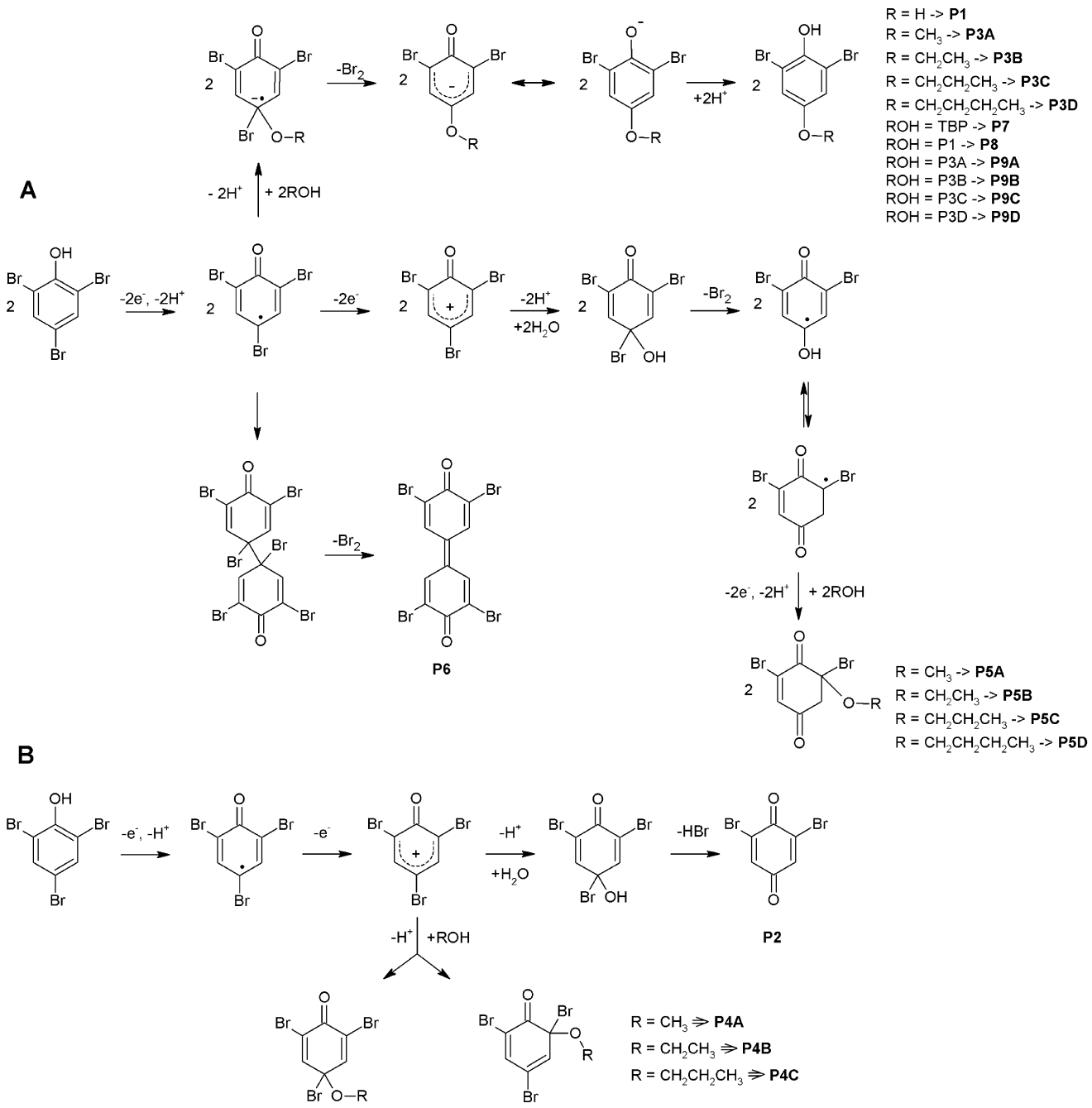

Scheme 1. Proposed mechanism of electrochemical oxidation of 2,4,6-tribromophenol.

are in relation with retention times measured on nonpolar stationary phase with linear temperature programme. Figure 7 clearly demonstrates about 100 °C higher boiling points of dimeric products in comparison with monomers.

3.3 Mechanism of TBP Electrooxidation

Two potential reaction mechanisms leading to the formation of products identified in the electrolyzed solutions of TBP are suggested in Scheme 1. In the Scheme 1A a phenoxy radical was formed in the first oxidation step. The radical could react with (i) water or alcohol from the electrolysis mixture forming P1 or P3A–P3D, respectively, (ii) another molecule of TBP forming P7, (iii) product P1 forming P8 or (iv) products P3A–P3D forming P9A–P9D. Products of group P5 could be formed from the phenoxy radical which is further oxidized to phenoxonium ion [3,9]. This ion might react with water accompanied by the elimination of bromine. Subsequent reaction with alcohol can lead to the formation of the products group P5. Recombination of two phenoxy radicals accompanied by bromine elimination gives rise to the dimeric product P6 [2,3]. The pathways suggested in the Scheme 1A are associated with the elimination of bromine molecule. Pres-

ence of bromine in electrolyzed solutions was proved by the reaction with fluorescein which provided characteristic pink color of eosin.

Scheme 1B also describes the formation of phenoxy radical from TBP, which could be further oxidized to phenoxonium ion [13]. Nucleophilic attack of water to the phenoxonium ion followed by the elimination of hydrogen bromide [1,9] results in the formation of the dibromobenzoquinone P2. Similarly, nucleophilic attack of alcohol on *ortho*- or *para*-position of the phenoxonium ion without bromine elimination gives rise to P4 group of products. This mechanism has been described as the main path for the formation of methoxylated phenols [13].

In addition to oxidation products mentioned above and included in Scheme 1, some other products corresponding to oxidation of TBP as well as alcohol used in supporting electrolyte could be formed during electrolysis. For example complete oxidation of methanol on platinum electrode can lead to CO_2 [17]. An extent of complete oxidation of alcohol decreased from methanol to propanol [17]. However, trace amounts of some other volatile compounds were detected using SPME procedure after electrolysis in solutions containing higher alcohols. For instance peaks with mass spectra similar to those of propenyl-propyl-ether isomers were detected after electrolysis of supporting electrolytes as well as TBP samples containing propanol. The investigation of other oxidation products of the alcohols as well as TBP itself is still in progress.

4 Conclusions

Twenty oxidation products (13 monomers and 7 dimers) of TBP electrolysis in 90% (v/v) alcohols were found using GC/MS. Spectral as well as retention data were used for identification of the target compounds. Five out of twenty compounds is formed without direct influence of the used alcohol and their structure does not contain any part of the alkyl moiety from the aliphatic alcohol used in supporting electrolyte. Remaining fifteen compounds contain alkoxy group derived from the used aliphatic alcohol. The alkoxy derivatives belong to the four homologous series. Expected 2,4,6-tribromo-6-butoxycyclohexa-2,4-dien-1-one has not been detected in this study.

Acknowledgements

The authors gratefully acknowledge the financial support by the Operational Program Research and Development for Innovations – European Regional Development Fund (CZ.1.05/2.1.00/03.0058), Operational Program Education for Competitiveness – European Social Fund (CZ.1.07/2.3.00/30.0041) and *Palacký University* in Olomouc (IGA_PrF_2014031). J. S. and P. B. acknowledge the support from the *Grant Agency of the Czech Republic* (P206/12/1150).

References

[1] G. W. Morrow, in *Organic Electrochemistry* (Eds: H. Lund, O. Hammerich), Marcel Dekker, New York **2001**, pp. 590–595.
[2] M. Ferreira, H. Varela, R. M. Torresi, G. Tremiliosi-Filho, *Electrochim. Acta* **2006**, *52*, 434.
[3] Z. Ežerskis, Z. Jusys, *J. Appl. Electrochem.* **2001**, *31*, 1117.
[4] Z. Ežerskis, Z. Jusys, *J. Appl. Electrochem.* **2002**, *32*, 543.
[5] P. I. Iotov, S. V. Kalcheva, *J. Electroanal. Chem.* **1998**, *442*, 19.
[6] M. S. Ureta-Zañartu, P. Bustos, M. C. Diez, M. L. Mora, C. Gutiérrez, *Electrochim. Acta* **2001**, *46*, 2545.
[7] N. B. Tahar, A. Savall, *Electrochim. Acta* **2009**, *55*, 465.
[8] C. Berríos, R. Arce, M. C. Rezende, M. S. Ureta-Zañartu, C. Gutiérrez, *Electrochim. Acta* **2008**, *53*, 2768.
[9] X. P. Zhu, S. Y. Shi, J. J. Wei, F. X. Lv, H. Z. Zhao, J. T. Kong, Q. He, J. R. Ni, *Environ. Sci. Technol.* **2007**, *41*, 6541.
[10] J. Iniesta, P. A. Michaud, M. Panizza, G. Cerisola, A. Aldaz, Ch. Comninellis, *Electrochim. Acta* **2001**, *46*, 3573.
[11] Y. J. Feng, X. Y. Li, *Water Res.* **2003**, *37*, 2399.
[12] X. Y. Li, Y. H. Cui, Y. J. Feng, Z. M. Xie, J. D. Gu, *Water Res.* **2005**, *39*, 1972.
[13] A. Nilsson, U. Palmquist, T. Pettersson, A. Ronlan, *J. Chem. Soc. Perkin Trans. 1*, **1978**, 696.
[14] A. Nilsson, A. Ronlán, *J. Chem. Soc. Perkin Trans. 1*, **1973**, 2337.
[15] A. Ronlán, *Chem. Commun.* **1971**, 1643.
[16] A. Ronlán, V. D. Parker, *J. Chem. Soc.* **1971**, 3214.
[17] S. Andreescu, D. Andreescu, O. A. Sadik, *Electrochem. Commun.* **2003**, *5*, 681.
[18] Z. Ežerskis, G. Stalnionis, Z. Jusys, *J. Appl. Electrochem.* **2002**, *32*, 49.
[19] M. S. Ureta-Zañartu, P. Bustos, C. Berríos, M. C. Diez, M. L. Mora, C. Gutiérrez, *Electochim. Acta* **2002**, *47*, 2399.
[20] P. D. Howe, S. Dobson, H. M. Malcolm, *Concise International Chemical Assessment Document 66*, World Health Organization, Geneva **2005**.
[21] E. Marková, P. Smyslová, P. Macíková, J. Skopalová, P. Barták, *Chem. Listy* **2012**, *106*, 195.
[22] E. A. Braude, *J. Chem. Soc.* **1945**, 490.
[23] O. B. Lantratova, V. A. Kuzmin, A. I. Prokofev, I. V. Khudyakov, I. E. Pokrovskaya, *Russ. Chem. Bull.* **1981**, *30*, 1459.

Received: August 8, 2014
Accepted: October 5, 2014
Published online: November 14, 2014

Příloha 4

Carbon fiber brush electrode as a novel substrate for atmospheric solids analysis probe (ASAP) mass spectrometry: Electrochemical oxidation of brominated phenols.

Skopalová, **J.***; Barták, P.; Bednář, P.; Tomková, H.; Ingr, T.; Lorencová, I.; Kučerová, P.; Papoušek, R.; Borovcová, L.; Lemr, K.

Analytica Chimica Acta **2018,** *999*, 60-68

Analytica Chimica Acta 999 (2018) 60–68

Contents lists available at ScienceDirect

Analytica Chimica Acta

journal homepage: www.elsevier.com/locate/aca

Carbon fiber brush electrode as a novel substrate for atmospheric solids analysis probe (ASAP) mass spectrometry: Electrochemical oxidation of brominated phenols

Jana Skopalová [a, *], Petr Barták [a], Petr Bednář [a], Hana Tomková [a], Tomáš Ingr [b], Iveta Lorencová [a], Pavla Kučerová [a], Roman Papoušek [a], Lucie Borovcová [a], Karel Lemr [a]

[a] Regional Centre of Advanced Technologies and Materials, Department of Analytical Chemistry, Faculty of Science, Palacký University, 17. Listopadu 12, 771 46 Olomouc, Czech Republic
[b] Department of Experimental Physics, Faculty of Science, Palacký University, 17. Listopadu 12, 771 46 Olomouc, Czech Republic

HIGHLIGHTS

- New mode of coupling of electrochemistry and mass spectrometry is presented.
- Large surface carbon fiber brush electrode was designed for atmospheric solids analysis probe.
- Electrochemically generated species were directly desorbed and ionized from electrode.
- Insoluble oligomeric and strongly adsorbed bromophenol oxidation products were identified.

GRAPHICAL ABSTRACT

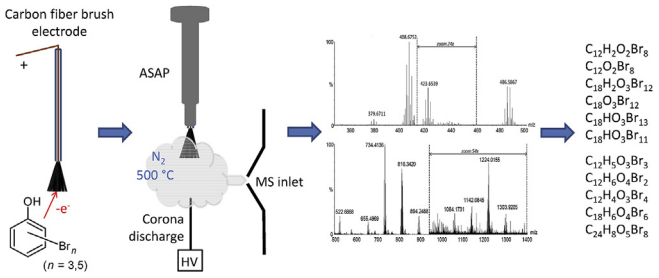

ARTICLE INFO

Article history:
Received 24 January 2017
Received in revised form
30 April 2017
Accepted 9 November 2017
Available online 14 November 2017

Keywords:
Carbon fiber brush electrode
Atmospheric solids analysis probe mass spectrometry
Ambient ionization
Bromophenols
Oxidation products
Electropolymerization

ABSTRACT

A carbon fiber brush electrode (CFBE) was newly designed and used as a substrate for both controlled potential electrolysis and atmospheric solids analysis probe (ASAP) mass spectrometry. Electropolymerized and strongly adsorbed products of electrolysis were directly desorbed and ionized from the electrode surface. Electrochemical properties of the electrode investigated by cyclic voltammetry revealed large electroactive surface area (23 ± 3 cm^2) at 1.3 cm long array of carbon fibers with diameter 6–9 μm. Some products of electrochemical oxidation of pentabromophenol and 2,4,6-tribromophenol formed a compact layer on the carbon fibers and were analyzed using ASAP. Eleven new oligomeric products were identified including quinones and biphenoquinones. These compounds were not observed previously in electrolyzed solutions by liquid or gas chromatography/mass spectrometry. The thickness around 58 nm and 45 nm of the oxidation products layers deposited on carbon fibers during electrolysis of pentabromophenol and 2,4,6-tribromophenol, respectively, was estimated from atomic force microscopy analysis and confirmed by scanning electron microscopy with energy-dispersive X-ray spectroscopy measurements.

1. Introduction

Coupling of electrochemistry with mass spectrometry belongs to important tools for investigation of electrochemical processes.

* Corresponding author.
E-mail address: jana.skopalova@upol.cz (J. Skopalová).

https://doi.org/10.1016/j.aca.2017.11.024
0003-2670/

Liquid or gas chromatography hyphenated to mass spectrometry, are used for the study of reaction mechanisms, simulation of drug metabolism, protein reactions and analysis, etc. [1–3]. They mainly provide qualitative or quantitative data concerning products in electrolyzed solutions and soluble or volatile species electrochemically extracted on the electrode surface [4–6]. Since electrochemical products may form hardly soluble layers deposited on electrode surface mass spectrometric tools analyzing such layers are required.

Carbon fiber brush electrodes (CFBEs) have found wide-spectrum applications. Advantages of CFBEs such as high specific surface, high conductivity and low cost are often exploited in electrochemical reactors for effective generation of desired reactants, e.g. hydrogen peroxide for Fenton reaction [7], production of electricity in microbial fuel cells [8–12], removal of particles and corrosive gas cleaning in electrostatic precipitators [13]. Recently they have been used as substrates for deposition of nanoparticle layers in supercapacitors [14,15].

The atmospheric solids analysis probe (ASAP) is an ambient ionization technique suitable for the direct analysis of volatile and semi-volatile compounds [16]. Solid or liquid samples are deposited on a glass capillary tube (with sealed ends) which is a routinely used substrate for sample loading. The heated nitrogen gas stream vaporizes the sample which components are ionized by corona discharge. Higher temperature of the gas can also vaporize higher oligomers for mass spectrometric analysis of polymers [17,18]. ASAP with temperature gradient ionizes low molecular species at lower gas temperature and polymers at higher temperature [19]. The ASAP has been found to be useful for the analysis of polymers with poor ionization efficiency in electrospray (ESI) [20,21] as well as those with low solubility [22].

2,4,6-Tribromophenol (TBP) and 2,3,4,5,6-pentabromophenol (PBP) are industrially important substances used as intermediates in production of brominated flame retardants or as wood preservatives [23]. The application of these chemicals is a potential source of environmental contamination [24]. Various chemical processes have been investigated and developed for the treatment of water contaminated with phenol and its derivatives. Among other technologies, electrochemical advanced oxidation processes are widely explored [25]. The main problem with their application to elimination of phenolic wastes is electrode fouling during anodic oxidation.

In general, the electrochemical oxidation of phenol and substituted phenols is a complicated process [26] starting with formation of phenoxy radicals susceptible to formation of polymeric films on electrode surface that cause its passivation and loss of electrochemical activity [27]. Variety of methods such as X-ray photoelectron spectrometry [27,28], electrochemical surface plasmon resonance [29] and Fourier transform infrared spectroscopy [28,30–32] has been used to study nature of the passivating film. Structure and topography of the film adsorbed on carbon and platinum electrodes has been imaged by scanning tunneling microscopy [30] and scanning electron microscopy [26,31], respectively. Field emission scanning electron microscopy combined with energy dispersive X-ray analysis enabled to determine an average atomic carbon/oxygen ratio in adsorbed phenol oxidation products [31]. Chemical composition of the passivating layer can be deduced from qualitative analysis of oxidation products and intermediates presented in solutions of phenols after electrolysis. Gas chromatography [31,33,34] and HPLC [31,34–36] are most often used for this purpose. Dimeric oxidation products have been detected in electrolyzed solutions of monobrominated phenols, TBP and PBP by means of chromatography with mass spectrometric detection [34,36]. Even four isomeric trimer products have been found in case of anodic oxidation of 4-bromophenol [36]. Since it can be assumed that higher oligomeric products remain firmly adsorbed on the electrode surface bromophenols were selected as model compounds to test our novel device.

In this paper for the first time a carbon fiber brush electrode as an ASAP substrate is evaluated. Its large surface allows for deposition of sufficient amount of electrochemically generated products that are directly desorbed and ionized in the ion source. The CFBE was adapted for the insertion into the atmospheric solids analysis probe and the use with a standard atmospheric pressure ionization source of a mass spectrometer. This novel analytical device represents a new coupling of electrochemistry with mass spectrometry. Its applicability was proved detecting oligomeric products of pentabromophenol and 2,4,6-tribromophenol electrochemical oxidation. Electrochemical and surface properties of the CFBE were investigated using cyclic voltammetry, atomic force microscopy and scanning electron microscopy with energy dispersive X-ray detector.

2. Experimental

2.1. Chemicals

Tribromophenol (TBP, 99%) and pentabromophenol (PBP, 96%) were purchased from Sigma-Aldrich. Methanol (LiChrosolv for HPLC, Merck, Germany), hexan (p.a., Penta, Czech Republic) and ultrapure water (18.2 MΩ cm, from Direct Q 3UV Remote Water Purification System, Merck Millipore) were used as solvents. Buffer solution was prepared from 0.1 mol L^{-1} formic acid (89–91%, Merck) and ammonia (25%, p.a., Lach-Ner, Czech Republic). $K_4Fe(CN)_6 \cdot 3H_2O$ and $K_3Fe(CN)_6$ were of analytical grade.

2.2. Design and pretreatment of carbon fiber brush electrode

Carbon fiber brush electrodes (CFBEs) were made of carbon fibers extracted from carbon cloth (KTC-03, Karbotechnik, Plzeň, Czech Republic). A bundle of carbon fibers was tied with 0.25 mm copper wire serving as electrical contact. The length of the resulting brush was cut to appropriate length (3 cm) and the brush was pulled in a piece of a glass melting point tube (outer diameter 1.9 mm, inner diameter 1.3 mm, length 8.6 cm). The inner edges of the tube were manually grinded with a diamond drill to avoid cutting off the carbon fibers. The fibers protruded 1.3 cm from one end and the copper wire from the second end of the tube (Fig. 1). No seals or glues were used to exclude all possible interferences at ASAP-MS analysis. The thickness of the carbon fiber bundle matched the inner diameter of the glass tube in order to fix the fibers and to prevent their movement in the tube.

Before the use carbon fibers protruding from the tube were ultrasonicated in hexane, methanol and distilled water for 15 min in each solvent and dried by air stream after each sonication. Electrochemical cleaning and activation of carbon fibers were performed in solution of sulfuric acid (0.1 mol L^{-1}) by potential cycling between −1.0 V and 1.5 V vs. saturated calomel reference electrode (50 cycles at scan rate 0.5 V s^{-1}) with start and stop potential at 0 V. Finally the CFBEs were washed three times in distilled water and immediately used or dried in nitrogen stream and stored in closed glass test tube. Before mass spectrometric analysis, the CFBE was inserted into the ASAP holder and carbon fibers were soaked in ultrapure water for 10 s to fully wet the surface and analyzed immediately.

2.3. Cyclic voltammetry measurement and controlled potential electrolysis

All electrochemical measurements were performed on an

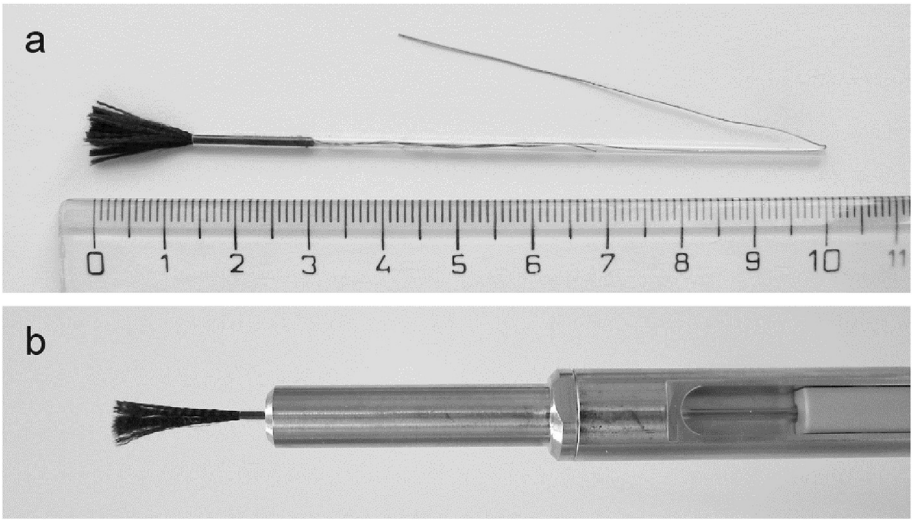

Fig. 1. Picture of (**a**) carbon fiber brush electrode (CFBE) and (**b**) CFBE inside ASAP holder.

Autolab PGSTAT128N potentiostat/galvanostat with NOVA 1.10 software (Metrohm Autolab, the Netherlands) in a three-electrode system consisted of a working CFBE, saturated calomel reference (SCE) and platinum wire auxiliary electrodes. Electroactive surface area of CFBEs was measured by means of cyclic voltammetry in solution containing mixture of 5 mmol L^{-1} $K_3Fe(CN)_6$ and 5 mmol L^{-1} $K_4Fe(CN)_6$ in 1M KCl (diffusion coefficient $D_O = 7.17 \times 10^{-6}$ cm^2 s^{-1} $D_R = 6.56 \times 10^{-6}$ cm^2 s^{-1} at 25 °C [37]) at scan rates 0.050–0.005 V s^{-1} and estimated from the slope of the dependence of peak current on square root of scan rate according to Randles-Ševčík equation: $i_p = 268468\, n^{3/2} A D^{1/2} c v^{1/2}$ for 25 °C, where n is number of electron transferred in the redox reaction, A is area of electrode surface, c and D are concentration and diffusion coefficient of electroactive substance, respectively, and v is scan rate. Cyclic voltammograms of PBP and TBP were recorded at scan rate 0.1 V s^{-1} in solutions containing ammonium formate buffer solution of pH 6 and methanol (in volume ratio 1:9 and 1:1, respectively). Concentration of TBP and PBP in solutions was 1 mmol L^{-1} unless otherwise stated. Controlled potential electrolysis of TBP and PBP was carried out at potential 1.0 V (vs. SCE) for 60 min in stirred solutions of total volume 5 mL and the same composition as for CV experiments. Concentration of PBP and TBP varied in the range 0.5–5 mmol L^{-1}. After electrolysis, the CFBEs were thoroughly rinsed with ultrapure water and products deposited on the carbon fibers were analyzed using ASAP-MS. Bulk concentration of bromophenols before and after electrolysis was measured by linear sweep voltammetry (scan rate 0.1 V s^{-1}) with glassy carbon electrode MF-2012 (3 mm disc diameter, BASi, West Lafayette, USA).

2.4. ASAP-MS measurements

For the study of oxidation products Synapt G2S high resolution tandem mass spectrometer equipped with atmospheric solids analysis probe was used (Waters, Manchester, UK). The following parameters were applied: ionization mode ASAP, negative ion mode, corona current 1.2 μA, sampling cone 30 V, source offset 40 V, source temperature 100 °C, probe temperature: studied in the range 100–500 °C, cone gas flow 100 L h^{-1}, desolvation gas flow 100 L h^{-1}. Resolution mode was set for TOF analyzer. Collision energies 4 eV (in trap collision cell) and 2 eV (in transfer cell) were applied for acquisition of MS spectra. For fragmentation experiments (MS/MS) the energy was elevated to 20–35 eV in trap collision cell and was tuned to achieve the highest possible signals of fragments. Scan range was 50–1200 Da.

2.5. AFM imaging and SEM-EDS analysis

Dimension Icon atomic force microscope (Bruker, Santa Barbara, USA) with NanoScope 9.1 software was employed for topography measurement of carbon fiber samples extracted from CFBEs before and after electrolysis of bromophenol solutions and after sample desorption in atmospheric solids analysis probe. ScanAsyst Air AFM tip with reflective Al coating on the cantilever back side (nominal resonant frequency 70 kHz and nominal force constant 0.4 N m^{-1}) was used. Images were obtained in PeakForce tapping mode at the scan rate 0.5 Hz and the resolution 512 pixel and processed in NanoScope Analysis 1.5 software.

Scanning electron microscope VEGA3 LMU with secondary electron detector of the Everhart-Thornley type (TESCAN, Brno, Czech Republic) and XFlash silicon drift detector 410-M (Bruker Nano GmbH, Berlin, Germany) were used for imaging of carbon fibers and energy-dispersive X-ray spectroscopy (EDS) elemental analysis. The detectors were employed with an accelerating voltage of 30 kV. The samples were measured in vacuum at a pressure 10^{-2} Pa.

3. Results and discussion

3.1. Cyclic voltammetry characterization of CFBEs

Electrochemical behavior of CFBEs was characterized using cyclic voltammetry in solution containing equimolar mixture of ferri/ferrocyanide in 1 mol L^{-1} KCl. Considerable improvement of charge transfer characteristics, i.e. narrower and higher peaks with shorter peak to peak distance, was evident after CFBE ultrasonication and electrochemical pretreatment (see Online Resource, Fig. S1). Measurement of electrode surface area by means of cyclic voltammetry revealed two- to fivefold increase of the area after electrochemical activation. Mean area 23 cm^2 of 1.3 cm long pretreated carbon fiber brush was found for three electrodes independently (standard deviation 3 cm^2). Enlargement and activation of the surface is favorable with respect to mass spectrometry analysis considering expectable larger amount of species electrolyzed and captured on

the electrode. Slope of the linear log I_p − log v dependence ranged between 0.47 and 0.52 proving that planar diffusion dominates mass transport to the CFBEs surface [38]. Hence from the electrochemical point of view, the CFBE behaves as a planar electrode with large surface and correspondingly high current response (tenths to units of milliamps) with overall small geometry of microfiber array.

3.2. Cyclic voltammetry and controlled potential electrolysis of bromophenols at CFBEs

All electrochemical measurements were performed in a mixture of formic acid/ammonium formate buffer solution of pH 6 and methanol (volume ratio 1:9 and 1:1 for PBP and TBP, respectively), i.e. under the same conditions as in previous study [36]. Higher content of methanol was necessary to maintain the homogeneity of the PBP solution. Cyclic voltammograms of PBP and TBP on CFBEs (Fig. 2) exhibit an anodic current signal rising steeply from the potential around 0.5 V. Intensity of this current signal gradually decreased in successive cycles (insets in Fig. 2) in consequence of passivation of the electrode surface. Higher content of water in TBP solution can cause lower solubility of oxidation products and thus their stronger adsorption at the electrode surface and faster passivation.

Current responses observed on the reverse cathodic scans as well as new anodic peaks around 0.3 V in the consecutive forward scans, clearly visible in particular in the voltamograms of TBP (Fig. 2b), correspond to intermediates or products formed during anodic oxidation of bromophenols. Such a couple of peaks, observed previously on the cyclic voltammograms of TBP and PBP measured with conventional glassy carbon electrode [34,36], is typical for electropolymerization reactions reported for phenol and its derivatives [32].

Electrolysis performed on electrochemically activated CFBEs at constant potential of 1.0 V consumed 2.0 and 1.6 electrons per molecule of PBP and TBP, respectively, as calculated from the total charge passed in electrolytic reaction and from the decrease of amount of starting compound during electrolysis, according to Faraday's law [39]. Bulk concentration of bromophenols before and after electrolysis was checked using linear sweep voltammetry with glassy carbon electrode. Only 22% and 12% of original content of PBP and TBP, respectively, were converted during 60 min electrolysis in total volume 5 ml of 1 mmol L^{-1} solution of respective

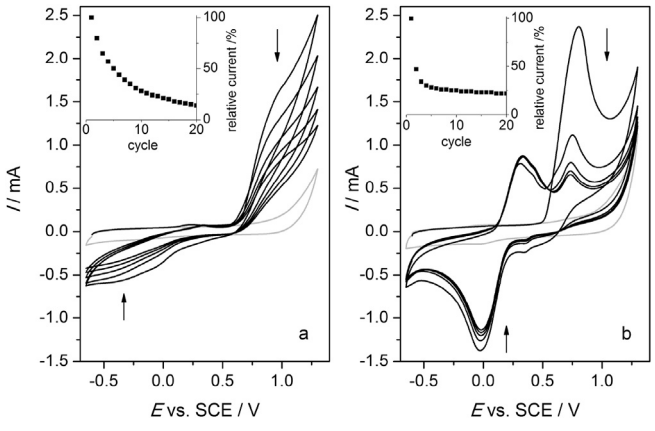

Fig. 2. Cyclic voltammograms of (**a**) PBP (c = 1 mmol L^{-1}) in supporting electrolyte (grey line) containing ammonium formate buffer of pH 6 and methanol (1:9, v/v) and (**b**) TBP (c = 1 mmol L^{-1}) in ammonium formate buffer of pH 6 and methanol (1:1, v/v) on brush carbon fiber electrode. Scan rate 100 mV s^{-1}, initial potential −0.6 V, switching potential 1.3 V. Arrows indicate changes of current in five successive cycles. Inset: relative drop of anodic current signal in consecutive 20 cycles.

bromophenol. Lower conversion efficiency in case of TBP is most likely caused by faster passivation of the electrode surface under given conditions (50% water content) as it was observed by cyclic voltammetry. Current-time curves recorded during electrolysis of bromophenols approaches residual current curve of supporting electrolyte after 60 min revealing almost complete coverage of the electrode surface with adsorbates. Extension of time would not significantly increase the conversion efficiency and consequently amount of deposited species for ASAP MS analysis.

3.3. Mass spectrometry analysis of bromophenols oxidation products deposited on CFBEs

After controlled potential electrolysis of PBP and TBP at potential 1.0 V in solution of volatile supporting electrolyte and methanol, the products deposited on the carbon fibers were analyzed by ASAP-MS. Since very poor signal was observed with dry carbon fibers, the fibers were wetted in ultrapure water. Ten seconds wetting was sufficient to improve mass spectra and was used in all experiments. The changes of response of PBP, TBP and their oxidation products with temperature were observed (Online Resource, Fig. S2). For both parent compounds and majority of studied oxidation products, the highest response was achieved at the highest applied temperature (500 °C). Experiments at a lower temperature (400 °C) provided the highest signal of three dimeric and one trimeric products of TBP oxidation (structures explained below) probably due to their lower stability at high temperatures. The signal of all studied products obtained at 500 °C was sufficient for structure elucidation. It is noteworthy that significantly lower signal of parent compounds and virtually no signal of oxidation products were observed when the oxidation potential was lowered to 0.3 V (see Online Resource, Fig. S3). It proved that the observed products were formed by electrolysis of solution (after application of sufficient potential) and not during ASAP-MS analysis.

Oxidation of PBP involves two processes - oxidation of bromophenolic skeleton and condensation of several PBP units. In the ASAP-MS spectrum of oxidized PBP (Fig. 3), signal of unoxidized PBP is apparent (m/z of the first isotope, m/z(1) 482.5902, deviation from theoretical mass, dtm 3.6 mDa; m/z of the most intense isotope, m/z(m) 486.5867, dtm 4.2 mDa). Signals of tetrabromoquinone (in the form of radical-anion $[M]^{\bullet -}$, m/z(1) 419.6625, dtm −0.7 mDa; m/z(m) 423.6539, dtm −5.2 mDa) or tetrabromohydroquinone (in the form of anion, $[M-H]^-$, m/z(1) 420.6742, dtm 7.7 mDa; m/z(m) 424.6615, dtm −5.4 mDa) represent the processes connected with a substitution of one bromine atom in PBP with oxygen or hydroxyl group, respectively. Signals with lower m/z values arise from fragmentation of PBP and its oxidation products in the mass spectrometer. Cleavage of bromine radical ($[M-Br]^{\bullet -}$, m/z(1) 404.6760, dtm −0.1 mDa; m/z(m) 408.6752, dtm 3.2 mDa) and consequent loss of carbon monoxide (m/z(1) 375.6729, dtm −0.5 mDa; m/z(m) 379.6711, dtm 1.8 mDa) from PBP are the most significant fragmentation processes.

The presence of ions with higher m/z (Fig. 3b) confirms the formation of condensation products during electrochemical oxidation. Abundant product I (see one possible isomer in Fig. 4) is formed by the substitution of one bromine in a PBP molecule by another PBP molecule (m/z(1) 888.2631, dtm 10.3 mDa; m/z(m) 894.2488, dtm 2.1 mDa). This product has been already identified by UPLC/MS in solution of electrochemically oxidized PBP [36]. Ion at m/z 816.3420 corresponds to anion of octabromo-dihydroxy-biphenyl (dtm 5.8 mDa, product II, Fig. 4) that is formed by condensation of two PBP molecules accompanied by elimination of two bromine atoms. Intensity of the adjacent isotopic ion at m/z 815.3314 is higher than its theoretical intensity in the isotopic cluster of octabromo-dihydroxy-biphenyl anion. This difference can

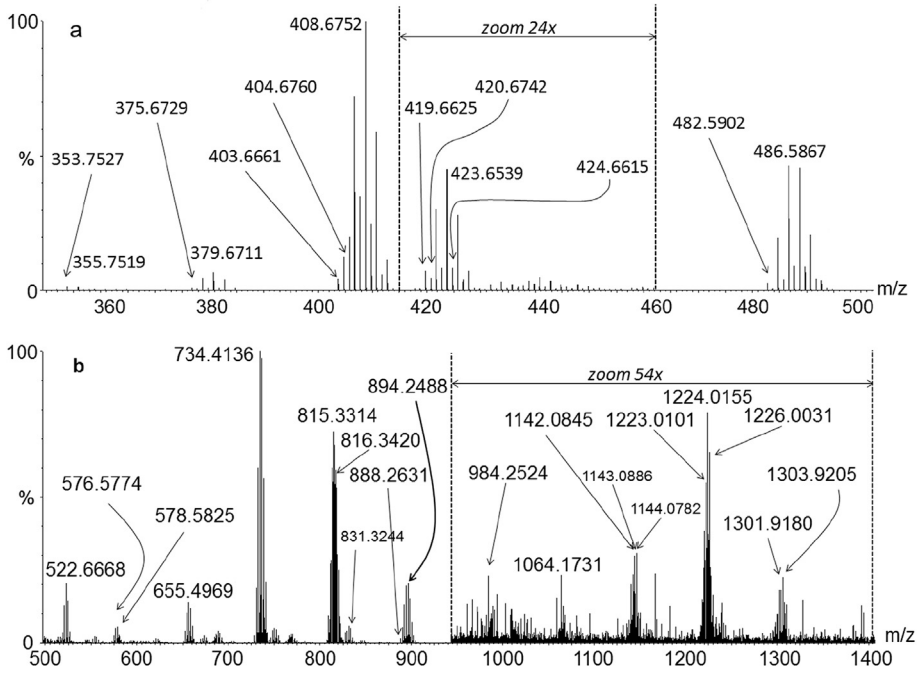

Fig. 3. ASAP mass spectrum of electrochemically oxidized PBP (negative ion mode).

be explained by the presence of a charged product III (Fig. 4) with *m*/*z*(m) one unit less, i.e. radical anion of related quinon form. Intensities of particular ions in isotopic cluster formed by a binary mixture of octabromo-dihydroxy-biphenyl anion and its quinon form were calculated considering different ratio of both forms. The ratio of anion:quinon 1:1.5 provided good agreement of theoretical and measured isotopic profile. The zoom of MS spectrum showing respective isotopic profile is given in Online Resource, Fig. S4a.

By analogy to dimers, products containing three brominated phenolic rings can also be released from carbon brush electrode under ASAP-MS conditions and are visible in mass spectra. Isotopic cluster (IC) with the most intense isotope at *m*/*z* 1224.0155 corresponds to elemental composition $C_{18}HBr_{12}O_3^-$ (dtm calculated for the most intense isotope is 15.2 mDa, first isotope is below detection limit). This molecular formula corresponds to the structure proposed in Fig. 4 (product IV). Similarly as in the case of the previously discussed dimer, isotopic profile of product IV does not correspond solely to its structure and a radical cation with *m*/*z*(m) 1223.0101 pertaining to product V (Fig. 4) explains its increased intensity. The isotopic profile fits well with the equal mixture of anion and quinon form. The zoom of MS spectrum showing the isotopic profile of those trimeric products is given in Online Resource, Fig. S4b. IC with the highest *m*/*z* values (*m*/*z*(m) 1301.9180) is related to condensation of three PBP units (for structure see product VI, Fig. 4; $C_{18}Br_{13}O_3^-$, dtm 7.1 mDa). Ions at *m*/*z* 831.3244 and 815.3314 are formed during fragmentation of product VI by cleavage of pentabromobenzene and pentabromophenol radical, respectively. Their molecular formula is $C_{12}Br_8O_3^{\bullet-}$ or $C_{12}Br_8O_2^{\bullet-}$ (dtm 1.1 and 3.1 mDa). The fragments differ in one oxygen atom and confirm the suggested ether linkage in the trimer. Ion at *m*/*z* 734.4136 can be formed by fragmentation of products I-VI which explains its high intensity in MS spectrum. Ion at *m*/*z*(m) 1142.0845 corresponds to elemental composition $C_{18}Br_{11}O_3^-$ (probably anion of the quinoid product VII, Fig. 4, dtm 8.3 mDa). Ions at *m*/*z* 1143.0886, 1064.1731, 984.2524, 815.3314, 655.4969 and 576.5774 are fragments of products I-VI. The identity of the ion at *m*/*z* 522.6668 was not revealed.

Electrochemical oxidation of tribromophenol yields even more various oxidation products. Fig. 5 shows the ASAP mass spectrum of oxidized TBP. Intact TBP provides strong signal at *m*/*z* (1) 326.7626 (*m*/*z*(m) 328.7635). Ion at *m*/*z*(m) 250.8490 is formed by fragmentation of condensed products (see below).

Several low mass oxidation products were observed. Ion at *m*/*z*(1) 263.8404 and *m*/*z*(m) 265.8380 corresponds to elemental composition $C_6H_2Br_2O_2$ (dtm(1) −1.8 mDa, dtm(m) −2.1 mDa). Its structure can be explained as dibromo-*p*-benzoquinone and/or dibromo-*o*-benzoquinone radical anions. Dibromobenzoquinones can be formed by hydroxylation and subsequent elimination of hydrogen bromide from TBP as was already described [34]. One subsequent repetition of hydroxylation and elimination of HBr in the above mentioned product provides ion at *m*/*z*(1) 200.9167 and *m*/*z*(m) 202.9155 (elemental composition $C_6H_2BrO_3$, dtm(1) −2.0 mDa, dtm(m) −1.2 mDa), i.e. anion of 6-bromo-1,2,4-benzenetriol and/or 2-bromo-4,6-dihydroxycyclohexa-2,5-dienone.

Losses of bromine radicals or hydrogen bromide seem to represent a driving force also during TBP condensation processes. Signal at *m*/*z*(1) 494.6867 and *m*/*z*(m) 498.6802 (Fig. 5a) can be explained by condensation of two oxidized TBP molecules after a loss of two bromine atoms, one from each parent molecule (-Br_2), (see product VIII, Fig. 4). The observed signal corresponds to elemental composition $C_{12}H_3Br_4O_2^{\bullet-}$. This process has already been recognized by GC-MS [34]. Substitution of one or two bromine atoms with one or two oxygens explains the abundant signals at *m*/*z*(1) 432.7688 (*m*/*z*(m) 434.7704) and *m*/*z*(1) 369.8470 (*m*/*z*(m) 371.8457). The related structures are given in Fig. 4 (product IX and X). Elemental compositions of the corresponding ions are $C_{12}H_4Br_3O_3^{\bullet-}$ and $C_{12}H_4Br_2O_4^{\bullet}$, respectively. Similarly as in the case of PBP, the deviations of measured *m*/*z* values from the theoretical masses for the first isotopes (i.e. product VIII-X, −7.8, −2.3 and −0.6 mDa, respectively) are significantly higher than for the most abundant isotopes (i.e. product VIII-X, −2.4, 1.4 and 0.1 mDa, respectively) which is related to low intensity of the first isotopes of highly brominated products. For the higher number of bromine

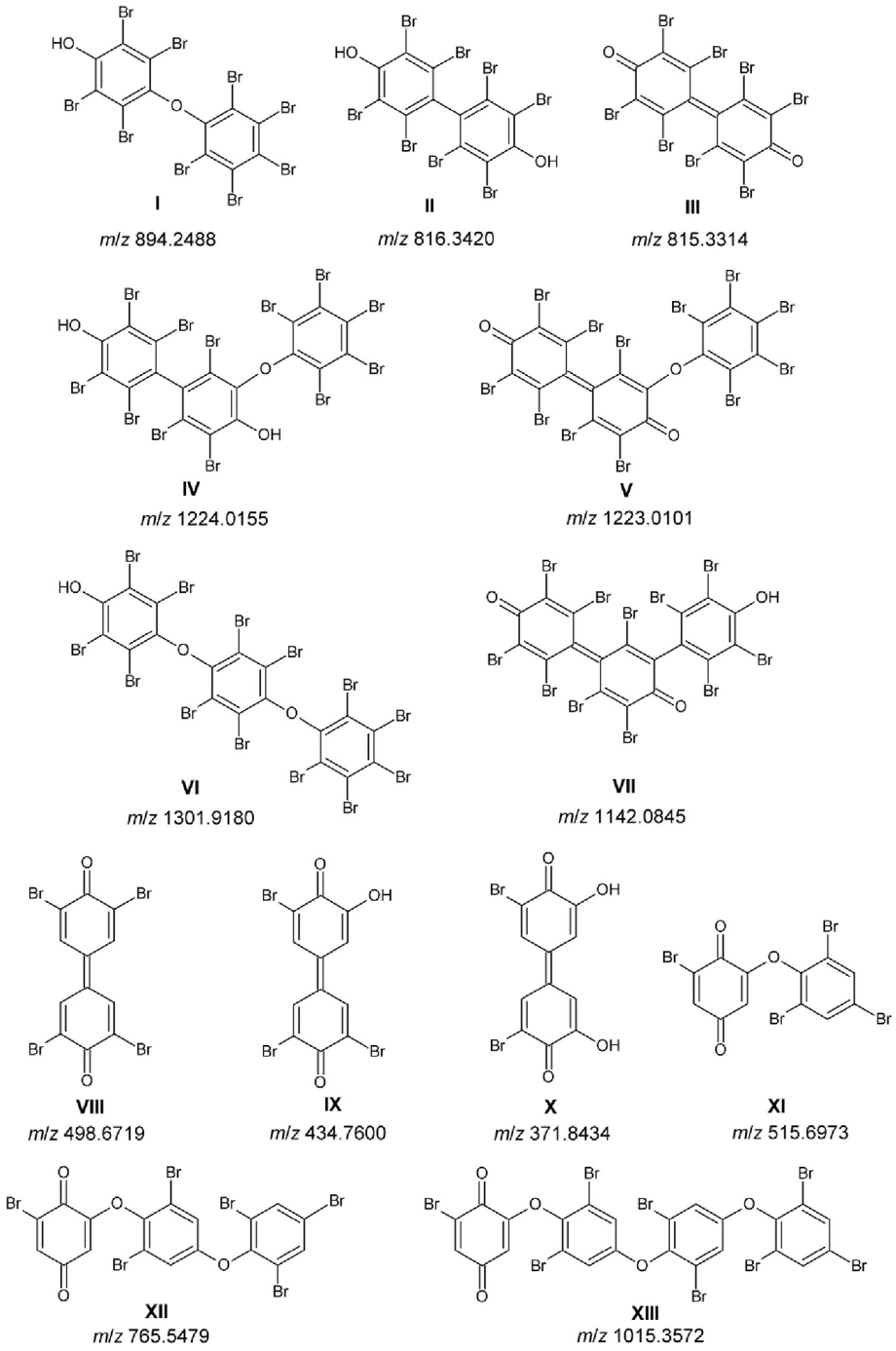

Fig. 4. Proposed structures of products (**I** – **XIII**) of electrochemically oxidized PBP and TBP with corresponding *m*/*z* of the most intense isotope.

atoms in molecule, the lower intensity of the first isotope and higher error of measured *m*/*z* value was consistently observed. Thus in the following study of higher mass oxidation products only *m*/*z*(m) is discussed.

Another dimeric oxidation product provided an abundant signal at *m*/*z*(m) 515.6793 corresponding to the molecular formula $C_{12}H_4Br_4O_3^{\bullet-}$ (product XI, dtm(m) −6.0 mDa). It could rise from coupling of a TBP molecule with a dibromobenzoquinone under a loss of hydrogen bromide. One of the possible structures of the product XI is given in Fig. 4.

Similar condensation of even three and four molecules of TBP was observed in relatively high yield as well. An abundant signal in the spectrum at *m*/*z*(m) 765.5298 (Fig. 5b) corresponds to trimeric product with molecular formula $C_{18}H_6Br_6O_4^{\bullet-}$ (product XII, Fig. 4, dtm(m) −0.7 mDa). Ion at *m*/*z*(m) 1015.3749 originated from the condensation of four TBP molecules accompanied by a loss of four bromine and two hydrogen atoms and a gain of one oxygen. This ion is present in the form of radical-anion with elemental composition $C_{24}H_8Br_8O_5^{\bullet-}$ (dtm(m) −0.8 mDa). Such tetrameric product can occur in several isomeric forms, e.g. the product XIII in Fig. 4. Collision induced dissociation of the radical-anion (MS/MS experiment) provided fragments corresponding to a loss of 1–4 bromine atoms in the form of bromine radicals and/or hydrogen bromide (the most intense fragments were found at *m*/*z*(m) 936.4550,

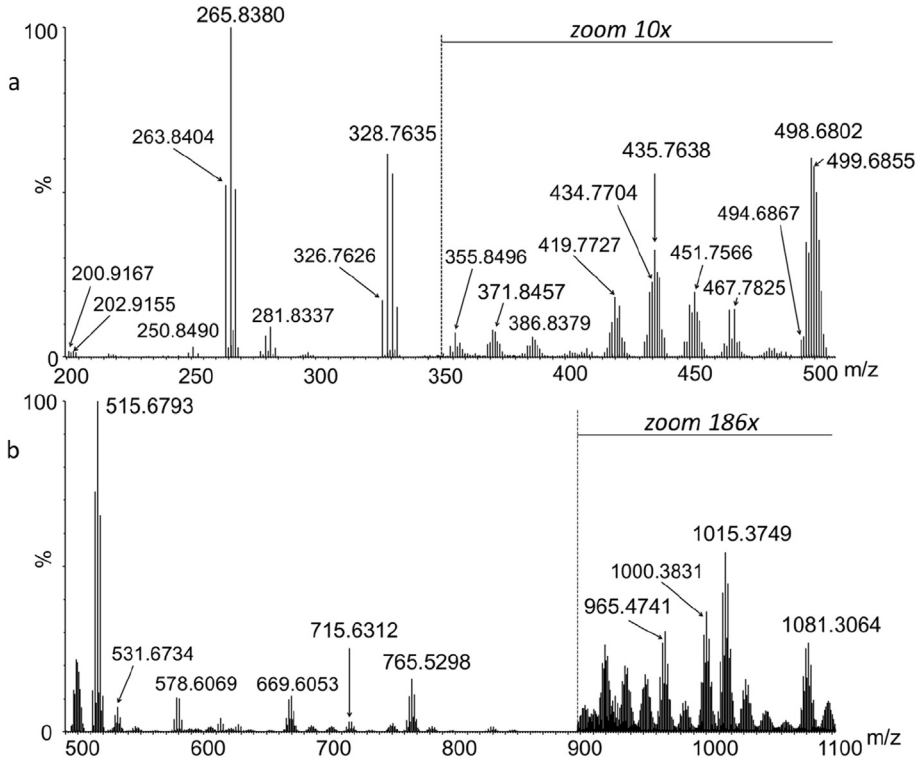

Fig. 5. ASAP mass spectrum of electrochemically oxidized TBP (negative ion mode).

854.5729, 774.6191 and 693.6839), formation of TBP anion *m*/*z*(m) 328.7623, formation of dimeric fragment, i.e. 2,6-dibromo-4-(2,4,6-tribromophenoxy)phenol (fragment at *m*/*z*(m) 578.6066) and 2-bromo-6-hydroxycyclohexa-2,5-diene-1,4-dione anion (cleavage of side quinoid ring, *m*/*z*(m) 200.9194). Those processes confirm the proposed tetrameric structure.

Another oxidation product *m*/*z* 965.4741 (Fig. 5b) was not formed by fragmentation of the above discussed ion at *m*/*z*(m) 1015 (product XIII). This was proved by absence of the ion at *m*/*z* 965.5 in MS/MS spectrum of product XIII (data not shown). The value of *m*/*z* 965.4741 corresponds to elemental composition $C_{25}H_{11}Br_7O_6^{\bullet-}$ (dtm −3.4 mDa). MS/MS spectrum of this ion contains fragments rising by the subsequent loss of two HBr molecules (*m*/*z*(m) 885.5131 and 805.5963). Beside, anion of TBP (*m*/*z*(m) 328.7513) and low abundant ion at *m*/*z*(m) 700.6050 were found. The latter mentioned fragment can arise by a cleavage of dibromo-methoxyphenyl radical which indicates the presence of methoxy group in the structure. Most likely, the signal at *m*/*z* 965.4741 corresponds to a mixture of several isomers with different position of methoxy group. The fragmentation processes confirm that this product is brominated, it is formed by a linkage of four oxidized TBP units and its structure can be derived from product XII substituting one bromine atom by a methoxy group. By analogy, the ion at *m*/*z* 715.6312 can be derived from the product XI.

Besides, the dependence of the MS response of studied compounds and their oxidation products on the starting compounds concentration was studied. The measured signal of the starting bromophenols as well as their oxidation products rose with concentration (as measured within the range 0.5–5 mmol L^{-1}) with the exception of trimer and tetramer products of TBP. In this case, maximum of the dependence was observed at concentration 2 mmol L^{-1}. Similar course was observed for the dependence of charge consumed during electrolysis on concentration of starting compound in electrolyzed solutions. The fact indicates strong passivation of the electrode surface at concentrations exceeding 2 mmol L^{-1}. From this point of view the technique may be used for semi-quantitative purposes as well, within the certain concentration range depending on the chemical nature of the target compound.

ASAP-MS technique provided complementary results to previously applied GC-MS and LC-MS [34,36]. In comparison, new products of electro-oxidation were identified, i.e. PBP dimeric (II, III) and trimeric products (IV-VII) as well as TBP dimeric (IX, X, XI), trimeric (XII) and tetrameric (XIII) products. These products were not detected in electrolyzed solution due to their low solubility in supporting electrolyte. The results of ASAP analysis confirmed electropolymerization even of highly brominated phenols observed by cyclic voltammetry. Oxidative electropolymerization of both PBP and TBP leads to coupling of oxidized monomers by C-O-C and/or C-C linkage accompanied by debromination. Similar ether type oligomeric oxidation products of related 2,4,6-trichlorophenol and pentachlorophenol have already been detected by GC-MS and reported to be formed in alkaline media at platinum electrode [33]. In addition, C-C coupling and subsequent formation of biphenoquinones by electrooxidation of PBP was observed, while all attempts to detect these compounds in electrolyzed solution in previous study were not successful [36]. The finding of new products and reaction routes is important not only from mechanistic but also from toxicological point of view because polybrominated diphenyl ether quinones were proved to form adducts with DNA [40]. CFBE and ASAP facilitated direct desorption and ionization of adsorbed and/or insoluble products from the electrode surface and contributed to the comprehensive view of the electrooxidation and electropolymerization processes.

3.4. Characterization of layers adsorbed on CFBE after electro-oxidation of bromophenols

AFM and SEM topography measurements of the carbon fibers

extracted from CFBEs before and after electrolysis of bromophenols and after thermal desorption in ASAP revealed that products of bromophenols oxidation formed a compact film on the carbon fibers. Electrochemically pretreated clean carbon fibers exhibited in AFM analysis more rough surface (root mean square roughness R_q = 11.6 nm) in comparison with the fibers after electrochemical oxidation of PBP (R_q = 6.8 nm) and TBP (R_q = 7.7 nm), see Online Resource, Fig. S5. The film of bromophenol oxidation products more or less evenly covered and smoothed the carbon fiber surface while desorption process was uneven. After ASAP ionization total desorption areas and almost intact oxidation product layers were observed on the fiber surface (Online Resource, Fig. S6).

The thickness of the film of the electrochemically deposited oxidation products was obtained from AFM profiles as a difference between the topographical height of the spots of adsorbed material remaining after thermal desorption in ASAP and clean carbon surface measured on the edge of the spots (Online Resource, Fig. S6). The average values obtained from 23 profilometry measurements were equal to 58 ± 6 nm and 45 ± 7 nm for PBP and TBP, respectively. These values were confirmed by SEM with EDS measurement where the thicknesses 48 ± 11 nm and 46 ± 8 nm were obtained for PBP and TBP, respectively. The values were computed from the carbon fiber diameter (range from 6.17 μm to 8.79 μm), measured by the secondary electron detector, and the percentage distribution of the elements of the carbon fiber determined from the EDS spectra (see Online Resource, Fig. S7). The pure spectrum of the carbon fiber with the layer of electrodeposited bromophenol oxidation products was obtained by subtracting background from the measured spectrum.

Thickness of the layer of material adsorbed on the carbon surface as measured by AFM and SEM-EDS agrees remarkably with the values obtained from the empirical calculation based on the geometrical comparison of the determined electroactive area of the electrode, estimated molar volume of TBP and PBP and analytically determined yield of the electrolysis. The yield of the electrolysis was obtained as the difference between initial and final amount of both brominated phenols (see section 3.2) and the value was equal to 1.1 μmol and 0.6 μmol for PBP and TBP, respectively. Molar volumes 169 cm^3 and 136 cm^3, respectively, were obtained for PBP and TBP by ACD/ChemSketch. The active surface area of CFBE was 23 cm^2 (see section 3.1). Resulting thickness of the layer of the oxidation products was roughly estimated from the given values as 81 nm and 35 nm for PBP and TBP, respectively. Differences between the calculated and experimental values might be caused among others by different molar volumes of particular products from those of PBP and TBP, and by different solubility of respective products rising under specific conditions. Both the chemical nature of the products and composition of electrolyzed solution (mainly methanol content which was 90 and 50% in case of PBP and TBP, respectively) might play role in this case.

4. Conclusion

A novel tool for direct mass spectrometry analysis of products electrochemically generated and adsorbed on the electrode surface was developed. After electrolysis a carbon fiber brush electrode adapted for insertion into ASAP holder was transferred to the ion source. The large electroactive surface of the CFBE facilitates effective electrochemical generation and adsorption of products. In the ion source, vaporization under higher temperatures (500 °C) enables to desorb even oligomeric substances from the electrode surface that are insoluble and therefore undetectable in electrolyzed solution. Thermal desorption and ionization in corona discharge allows to detect and subsequently to identify substances (e.g. quinones) hardly ionizable in electrospray ionization source. Obtained mass spectrometric results have been complementary to former GC/MS and LC/MS data and have provided deeper insight in electrochemical oxidation of bromophenols. The developed device is useful for the study of electrochemical reactions of species forming electropolymerized and strongly adsorbed films on the electrode surfaces, such as phenolic compounds, and represents new mode of coupling of electrochemistry with mass spectrometry allowing direct detection and analysis of compounds bound to the surface. It can be helpful for study of various electrochemical processes such as electrochemical advanced oxidation processes applying in wastewater decontamination. The described device could also be used for investigation of desorption/ionization processes in the ion source of the mass spectrometer.

Acknowledgement

The authors gratefully acknowledge the financial support by the Ministry of Education, Youth and Sport of the Czech Republic (project LO1305), the Czech Science Foundation (project P206/12/1150) and Palacký University Olomouc (projects IGA_PrF_2017_020 and IGA_PrF_2017_011).

Appendix A. Supplementary data

Supplementary data related to this article can be found at https://doi.org/10.1016/j.aca.2017.11.024.

References

[1] U. Karst, Electrochemictry/Mass Spectrometry (EC/MS) – a new tool to study drug metabolism and reaction mechanism, Angew. Chem. Int. Ed. 43 (2004) 2476–2478.
[2] S. Jahn, U. Karst, Electrochemistry coupled to (liquid chromatography/) mass spectrometry – current state and future perspectives, J. Chromatogr. A 1259 (2012) 16–49.
[3] H. Faber, M. Vogel, U. Karst, Electrochemistry/mass spectrometry as a tool in metabolism studies-A review, Anal. Chim. Acta 834 (2014) 9–21.
[4] T.J. Yang, M.R. Lee, Electrically assisted solid-phase microextraction combined with liquid chromatography mass spectrometry for determination of parathion in water, Talanta 82 (2010) 766–770.
[5] F. Guo, T. Gorecki, D. Irish, J. Pawliszyn, Solid-phase microextraction combined with electrochemistry, Anal. Commun. 33 (1996) 361–364.
[6] R.C. Sparrenberger, C.K. Cross, E.D. Conte, A solid-phase microextraction device for the analysis of electrochemical reaction products by gas chromatography/mass spectrometry, Anal. Chem. 76 (2004) 6156–6159.
[7] G.S. Xia, Y.H. Lu, H.B. Xu, Electrogeneration of hydrogen peroxide for electro-Fenton via oxygen reduction using polyacrylonitrile-based carbon fiber brush cathode, Electrochim. Acta 158 (2015) 390–396.
[8] J. Wei, P. Liang, X. Huang, Recent progress in electrodes for microbial fuel cells, Bioresour. Technol. 102 (2011) 9335–9344.
[9] A.J. Hutchinson, J.C. Tokash, B.E. Logan, Analysis of carbon fiber brush loading in anodes on startup and performance of microbial fuel cells, J. Power Sources 196 (2011) 9213–9219.
[10] H. Tursun, R. Liu, J. Li, R. Abro, X.H. Wang, Y.M. Gao, Y. Li, Carbon material optimized biocathode for improving microbial fuel cell performance, Front. Microbiol. 7 (2016), https://doi.org/10.3389/fmicb.2016.00006.
[11] R. Kakarla, B. Min, Evaluation of microbial fuel cell operation using algae as an oxygen supplier: carbon paper cathode vs. carbon brush cathode, Bioprocess Biosyst. Eng. 37 (2014) 2453–2461, https://doi.org/10.1007/s00449-014-1223-4.
[12] Y. Fenga, Q. Yanga, X. Wanga, B.E. Logan, Treatment of carbon fiber brush anodes for improving power generation in air-cathode microbial fuel cells, J. Power Sources 195 (2010) 1841–1844, https://doi.org/10.1016/j.jpowsour.2009.10.030.
[13] H.J. Kim, B. Han, Y.J. Kim, S.J. Yoa, T. Oda, Integration of a nonmetallic electrostatic precipitator and a wet scrubber for improved removal of particles and corrosive gas cleaning in semiconductor manufacturing industries, J. Air Waste Manag. Assoc. 62 (2012) 905–915, https://doi.org/10.1080/10962247.2012.686893.
[14] J. Cherusseri, K.K. Kar, Ultra-flexible fibrous supercapacitors with carbon nanotube/polypyrrole brush-like electrodes, J. Mater. Chem. A 4 (2016) 9910–9922.
[15] J. Cherusseri, K.K. Kar, Hierarchical carbon nanopetal/polypyrrole nanocomposite electrodes with brush-like architecture for supercapacitors, Phys. Chem. Chem. Phys. 18 (2016) 8587–8597.
[16] C.N. McEwen, R.G. McKay, B.S. Larsen, Analysis of solids, liquids, and biological

tissues using solids probe introduction at atmospheric pressure on commercial LC/MS instruments, Anal. Chem. 77 (2005) 7826–7831.
[17] S. Trimpin, K. Wijerathne, C.N. McEwen, Rapid methods of polymer and polymer additives identification: multi-sample solvent-free MALDI, pyrolysis at atmospheric pressure, and atmospheric solids analysis probe mass spectrometry, Anal. Chim. Acta 654 (2009) 20–25.
[18] M.J.P. Smith, N.R. Cameron, J.A. Mosely, Evaluating Atmospheric pressure Solids Analysis Probe (ASAP) mass spectrometry for the analysis of low molecular weight synthetic polymers, Analyst 137 (2012) 4524–4530.
[19] D. Lebeau, M. Ferry, Direct characterization of polyurethanes and additives by atmospheric solid analysis probe with time-of-flight mass spectrometry (ASAP-TOF-MS), Anal. Bioanal. Chem. 407 (2015) 7175–7187.
[20] C. Barrere, F. Maire, C. Afonso, P. Giusti, Atmospheric solid analysis probe-ion mobility mass spectrometry of polypropylene, Anal. Chem. 84 (2012) 9349–9354.
[21] T. Fouquet, C. Barrere-Mangote, M. Farenc, C. Afonso, P. Giusti, Atmospheric solid analysis probe mass spectrometry vs electrospray tandem mass spectrometry of polydimethylsiloxanes in positive and negative ionization modes, Rapid Commun. Mass Spectrom. 29 (2015) 982–986.
[22] E. Cossoul, M. Hubert-Roux, M. Sebban, F. Churlaud, H. Oulyadi, C. Afonso, Evaluation of atmospheric solid analysis probe ionization coupled to ion mobility mass spectrometry for characterization of poly(ether ether ketone) polymers, Anal. Chim. Acta 856 (2015) 46–53.
[23] P.D. Howe, S. Dobson, H.M. Malcolm, 2,4,6-Tribromophenol and Other Simple Brominated Phenols, World Health Organization, Geneva, 2005. http://www.who.int/ipcs/publications/cicad/cicad_66_web_version.pdf. (Accessed 15 December 2016).
[24] Å. Norström, K. Andersson, C. Rappe, Major components of some brominated aromatics used as flame retardants, Chemosphere 5 (1976) 255–261.
[25] B.P. Chaplin, Critical review of electrochemical advanced oxidation processes for water treatment applications, Environ. Sci. Process. Impacts 16 (2014) 1182–1203.
[26] S. Andreescu, D. Andreescu, O.A. Sadik, A new electrocatalytic mechanism for the oxidation of phenols at platinum electrodes, Electrochem. Commun. 5 (2003) 681–688.
[27] M. Gattrell, D.W. Kirk, A study of electrode passivation during aqueous phenol electrolysis, J. Electrochem. Soc. 140 (1993) 903–911.
[28] J.M. Skowroński, P. Krawczyk, Improved electrooxidation of phenol at exfoliated graphite electrodes, J. Solid State Electrochem 11 (2007) 223–230.
[29] C. Pirvu, C.C. Manole, Electrochemical surface plasmon resonance for in situ investigation of antifouling effect of ultra thin hybrid polypyrrole/PSS films, Electrochim. Acta 89 (2013) 63–71.
[30] M.H. Zareie, B.K. Körbahti, A. Tanyolaç, Non-passivating polymeric structures in electrochemical conversion of phenol in the presence of NaCl, J. Hazard Mater B87 (2001) 199–212.
[31] D. Fino, C.C. Jara, G. Saracco, V. Specchia, P. Spinell, Deactivation and regeneration of Pt anodes for the electro-oxidation of phenol, J. Appl. Electrochem 35 (2005) 405–411.
[32] A.N. Kawde, M.A. Morsy, N. Odewunmi, W. Mahfouz, From electrode surface fouling to sensitive electroanalytical determination of phenols, Electroanalysis 25 (2013) 1547–1555.
[33] Z. Ežerskis, Z. Jusys, Electropolymerization of chlorinated phenols on a Pt electrode in alkaline solution. Part IV: a gas chromatography mass spectrometry study, J. Appl. Electrochem 32 (2002) 543–550.
[34] E. Marková, P. Kučerová, J. Skopalová, P. Barták, Electrochemical oxidation of 2,4,6-tribromophenol in aqueous-alcoholic media, Electroanalysis 27 (2015) 156–165.
[35] J.L. Boudenne, O. Cerclier, P. Bianco, Voltammetric studies of the behavior of carbon black during phenol oxidation on Ti/Pt electrodes, J. Electrochem. Soc. 145 (1998) 2763–2768.
[36] E. Marková, P. Kučerová, P. Bednář, P. Barták, J. Skopalová, Electrochemical oxidative dimerization of monobrominated phenols and pentabromophenol in methanol-aqueous media, Monatsh. Chem. 147 (2016) 75–87.
[37] S.J. Konopka, B. McDuffie, Diffusion coefficients of ferri- and ferrocyanide ions in aqueous media, using twin-electrode thin-layer electrochemistry, Anal. Chem. 42 (1970) 1741–1746.
[38] F. Marken, A. Neudeck, A.M. Bond, Cyclic voltammetry, in: F. Scholz (Ed.), Electroanalytical Methods: Guide to Experiments and Applications, Springer-Verlag, Berlin Heidelberg, 2010, pp. 74–78.
[39] A.J. Bard, L.R. Faulkner, Electrochemical Methods: Fundamentals and Applications, John Wiley & Sons, New York, 2001, pp. 427–430.
[40] Y. Lai, M. Lu, X. Gao, H. Wu, Z. Cai, New evidence for toxicity of polybrominated diphenyl ethers: DNA adduct formation from quinone metabolites, Environ. Sci. Technol. 45 (2011) 10720–10727.

Příloha 5

Electrochemical oxidation of zopiclone

Táborský, J.; Švidrnoch, M.; Kurka, O.; Borovcová, L.; Bednář, P.; Barták, P.;
Skopalová, **J.***

Monatshefte für Chemie – Chemical Monthly **2016**, *147*, 53-60

Monatsh Chem (2016) 147:53–60
DOI 10.1007/s00706-015-1602-9

ORIGINAL PAPER

Electrochemical oxidation of zopiclone

Jakub Táborský[1] · Martin Švidrnoch[1] · Ondřej Kurka[1] · Lucie Borovcová[1] · Petr Bednář[1] · Petr Barták[1] · Jana Skopalová[1]

Received: 9 September 2015 / Accepted: 9 November 2015 / Published online: 7 December 2015

Abstract Electrochemical behaviour of zopiclone was investigated on glassy carbon electrode in static and rotation disc arrangement. Strong influence of kinetics and adsorption phenomena on the electrode processes was proved by voltammetric techniques. Controlled potential electrolysis in off-line and on-line combination with tandem mass spectrometry was employed for investigation of the products of electrochemical oxidation. *N*-Desmethyl zopiclone was identified and three other oxidation products formed by an introduction of one or two oxygen atom(s) to the molecule of zopiclone (including zopiclone *N*-oxide) were characterized. Based on mass spectrometric investigation of those products, piperazine moiety was proved as a target of electrochemical oxidation of zopiclone. Since *N*-desmethyl zopiclone and zopiclone *N*-oxide have been reported as products of enzymatic metabolism of the drug, the combination of electrochemistry with mass spectrometry may be considered as a reliable tool for simulation of some metabolic transformations.

Graphical abstract

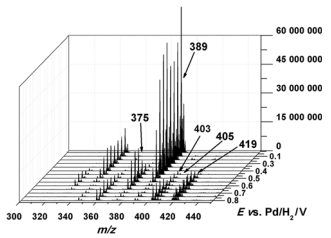

Keywords Electrochemistry · Mass spectroscopy · Voltammetry · *N*-Desmethyl zopiclone

Introduction

Zopiclone (ZOP), chemically (*RS*)-6-(5-chloropyridin-2-yl)-7-oxo-6,7-dihydro-5*H*-pyrrolo[3,4-*b*]pyrazine-5-yl 4-methylpiperazine-1-carboxylate (Fig. 1), is a hypnotic drug used for the treatment of insomnia. ZOP possesses a short duration of action with additional muscle relaxant and anticonvulsant properties. It was developed along with other so called Z-drugs, zaleplon, and zolpidem, as an alternative to the world-wide used benzodiazepines, which are controversial due to concerns about adverse psychological and physical effects, decreasing effectiveness, and physical dependence at their long-term usage.

ZOP is a chiral drug administered as a racemic mixture although the pharmacological activity is related to the (+)-(*S*)-ZOP known as eszopiclone. Both enantiomers are metabolised via cytochrome P450 enzyme system [1]. The main biotransformation products of

Electronic supplementary material The online version of this article (doi:10.1007/s00706-015-1602-9) contains supplementary material, which is available to authorized users.

✉ Jana Skopalová
jana.skopalova@upol.cz

[1] Regional Centre of Advanced Technologies and Materials, Department of Analytical Chemistry, Faculty of Science, Palacký University, 17. listopadu 12, 771 46 Olomouc, Czech Republic

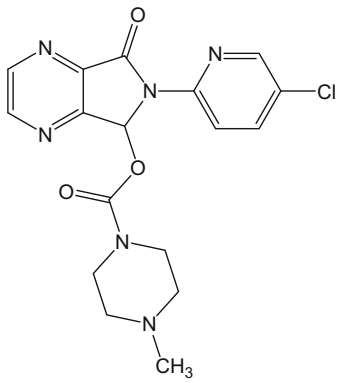

Fig. 1 Chemical structure of zopiclone

oxidative metabolism are *N*-desmethyl zopiclone and zopiclone *N*-oxide [1–4].

Chemical stability of ZOP was investigated in several studies. The drug was found to be stable under acidic conditions in aqueous-acetonitrile solutions [5]. However, rate of hydrolysis increased with pH and temperature in aqueous ethanolic media [6]. 2-Amino-5-chloropyridine was identified as the final degradation product of ZOP in alkaline solutions [7, 8].

Electrochemical behaviour of ZOP was investigated by several authors but with no attempt to identify the products of electrochemical reactions. Electrochemical reduction of ZOP was studied by Viré et al. [9] by different techniques. ZOP was reducible in two 2-electron steps in the pH range 0 to 12. The electrochemical behaviour was accompanied by strong adsorption in neutral and acidic solutions. Adsorption was employed for sensitive determination of ZOP by adsorptive stripping voltammetry [9]. Yilmaz et al. [10] have studied oxidation of ZOP at glassy carbon electrode (GCE) using adsorptive stripping voltammetry. ZOP oxidation was found to be an irreversible adsorption controlled process. Square wave voltammetry was used for determination of submicromolar concentrations of ZOP as well [10]. Number of other analytical methods has been used for ZOP determination starting from potentiometric titrimetry, prescribed by British Pharmacopeia [11] through the spectrophotometry [12] up to potentiometry with ion selective electrode [13]. However, chromatographic methods including gas [14] and liquid chromatography [15–17], often with mass selective detection, lead the dance in the field of drug analysis.

Electrochemistry coupled to mass spectrometry (EC/MS) can be used for simulation of some oxidative reactions involved in the metabolism of drugs and other xenobiotics [18]. The elucidation of oxidative metabolic reactions is a crucial point in the drug development. In general, the main route of drug elimination is oxidative biotransformation via CYP enzymes family and ZOP is not an exception as mentioned above. In vivo or in vitro experiments, commonly used for elucidation of the drug metabolism, are usually based on animal experiments which are tedious, ethically questionable, time consuming, and of limited reproducibility. Since oxidation reactions play a crucial role in the CYP-mediated biotransformation, it seems reasonable to use electrochemical oxidation as a possible instrumental tool for simulation of the oxidative degradation processes [19]. Electrochemistry coupled on-line or off-line to MS (especially to electrospray ionization mass spectrometry, ESI–MS) has been successfully used in many research areas including metabolic studies [20] as well as in peptide, protein, and DNA analysis [21] or quantification of biomolecules [22].

In this paper, electrochemical behaviour of zopiclone was studied using voltammetric methods on glassy carbon working electrode. Controlled potential electrolysis of ZOP solutions containing acetonitrile and aqueous buffer solutions of different pH followed by ESI–MS analysis of the reaction products as well as on-line coupling of EC flow-through cell with ESI–MS were used for generation and characterization of zopiclone oxidation products.

Results and discussion

Electrochemical behaviour of zopiclone

Cyclic voltammogram (Fig. 2a) of zopiclone in acetonitrile-aqueous buffer solution of pH 4.8 (1:1, v/v) recorded on glassy carbon electrode (GCE) shows one oxidation peak at potential $E_p = 1.02$ V (vs. saturated calomel reference electrode, SCE). No current response was observed in the reverse cathodic branch of voltammograms suggesting irreversibility of the electrode process. Similarly, differential pulse voltammogram (Fig. 2b) revealed one anodic peak at the potential $E_p = 1.04$ V.

The effect of the pH of BR buffer solutions on the oxidation signal of zopiclone was investigated using cyclic and linear sweep voltammetry (LSV) with GCE in static and rotating disc (RDE) arrangement, respectively. The anodic signal of zopiclone occurred in the pH range 2.8–9.5 in both arrangements. The oxidation signal was not observed in the more acidic buffer solutions (pH 1.9, 2.2, and 2.5). The limiting current measured on RDE increased with rising pH values up to pH about 6 and then remained almost constant up to pH 9.5 (Fig. 3). Oxidation in more alkaline solutions was not tested due to reported fast decomposition of ZOP under such conditions [6]. In acidic solutions with pH below 6, the oxidation of ZOP is a pH-dependent process. The half-wave potential shifts to lower values with increasing pH by −59 mV per pH unit (Fig. 3). This value indicates that the same number of protons and

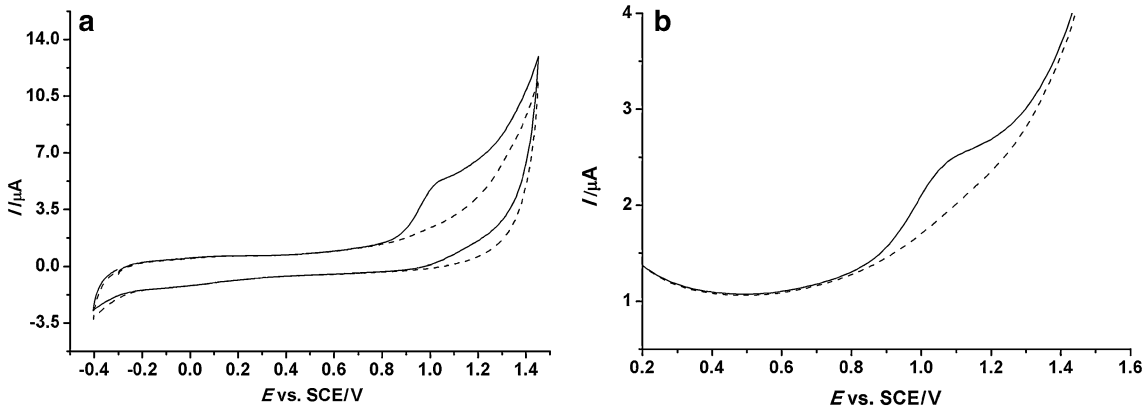

Fig. 2 Voltammograms of 5×10^{-4} mol dm^{-3} ZOP (*solid line*) in supporting electrolyte (*dashed line*) containing BR buffer solution pH 4.8 and acetonitrile (1:1, v/v) recorded by cyclic voltammetry (**a**), scan rate 50 mV s^{-1} and differential pulse voltammetry (**b**) scan rate 20 mV s^{-1}, modulation amplitude 25 mV, pulse width 500 ms

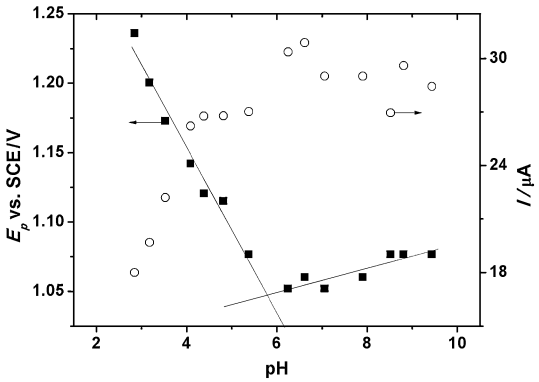

Fig. 3 Dependence of half-wave potential (*filled square*) and limiting current (*open circle*) of zopiclone ($c = 5 \times 10^{-4}$ mol dm^{-3}) on pH measured on RDE, angular rotation speed: 157 rad s^{-1}, scan rate 0.4 V s^{-1}

electrons are involved in the electrode reaction. At pH 6–9.5, the half-wave potential shift was negligible. The intersection point of two regression straight lines at pH 5.9 can be related to change in the protolytic forms of ZOP (p$K_A = 6.79$ [23]).

The effect of scan rate (v) on zopiclone oxidation was investigated by LSV on GCE in BR buffer pH 4.8 with acetonitrile (1:1, v/v). The anodic peak of ZOP increased with increasing scan rates within the range 0.01–0.9 V s^{-1}. The dependence of log I_p—log v revealed two linear segments with the slopes 0.71 (in the scan range 0.01–0.2 V s^{-1}) and 0.89 (in the range of 0.3–0.9 V s^{-1}) (see Supplementary Material, Fig. S1). The values of the slopes are higher than the theoretical value 0.5 for purely diffusion controlled process indicating the influence of adsorption on the electrochemical reaction. The dependence of the peak potential E_p on log v resulted in two straight lines. Peak potential did not change within the slow scan rates interval up to 0.2 V s^{-1}. However, a significant shift in peak potential by 41 mV per log unit was observed when scan rate exceeded 0.3 V s^{-1}. The fact indicates the influence of other processes, next to diffusion, in the rate determining step at higher scan rates. Kinetics of the electron transfer reaction, kinetics of the chemical reaction preceding the electron transfer (deprotonation seems to be the most likely in this case; see pH dependence of limiting current on Fig. 3) and adsorption on the electrode surface are the most probable reasons.

The adsorption of zopiclone on electrode surface was investigated by experiment in which electrode was immersed into the stock solution of zopiclone for 300 s, and then the electrode surface was washed with deionized water. The electrode was placed into electrolyte and CV voltammogram was recorded (see Supplementary Material, Fig. S2). A small current signal at 1 V corresponding to ZOP adsorbed on the electrode can be distinctly recognized in comparison to the blank measured with clean, mechanically polished, electrode. The signal proved the tendency of the drug to adsorb on the electrode surface. Also the sign of the nonlinearity on the calibration dependence of the peak current on the concentration of ZOP can be ascribed in large extent to the adsorption on the GCE (Supplementary Material, Fig. S3).

Dependence of limiting current on square root of rotation velocity of RDE was measured by LSV in solution of pH 4.8, pH 7.1, and pH 9.4. In neutral and alkaline solutions the limiting current increases with increasing square root of the rotation speed. The course of the dependence is typical for the mechanism influenced by both diffusion of the depolarizer and kinetics of the electron transfer (see Supplementary Material, Fig. S4). On the contrary, limiting current measured in acidic solution is almost independent on square root of rotation velocity. The course is usually observed in systems controlled by the kinetics of the electron transfer or the kinetics of the chemical reaction

preceding the electron transfer (i.e., systems where diffusion is not the rate determining step). The interpretation of the main course of the dependence fits together with conclusion resulting from the dependence of the peak potential on the scan rate during LSV mentioned above.

MS analysis of oxidation products of zopiclone

For more detailed characterization of the oxidation products two experimental arrangements were used. First arrangement consisted of an off-line controlled potential electrolysis of zopiclone on the large surface Pt electrode combined with a tandem mass spectrometric measurement of the electrolysed zopiclone solutions. Second one involved on-line coupling of electrochemical flow-through cell containing the working porous graphite electrode with mass spectrometer (EC/MS). In both types of experiment, electrolysis was performed in acetonitrile/ammonium acetate buffer solution pH 3.5, 6.8, and 9.5 (1:1, v/v).

For off-line experiment the controlled potential values suitable for exhaustive electrolysis were chosen according to courses of cyclic voltammograms of zopiclone recorded in different media. To eliminate the influence of nonelectrolytic reaction of zopiclone, the mass spectra of electrolysed solutions were compared to those of control samples. The control samples were obtained by electrolysis of zopiclone solutions at potentials where no electrochemical reaction occurs.

Figure 4a shows mass spectrum of ZOP standard in which the pseudomolecular ion $[M + H]^+$ at $m/z = 389$ is evident. MS/MS spectrum (Fig. 4b) revealed the main fragment ion at $m/z = 345$ corresponding to a loss of CO_2. This unusual scission of CO_2 from the molecule, giving evidence of rather strong association of the piperazine ring with another heterocyclic part of the ZOP structure, has already been reported [24]. Formation of fragments at $m/z = 245$ and $m/z = 263$ is described in the inset of Fig. 5b. The minor fragment at $m/z = 217$ corresponding to loss of CO from cyclopyrrolon moiety of the ion with $m/z = 245$ is also characteristic for ZOP fragmentation. Fragmentation pattern corresponds with the already published results [24]. The differences in intensities of fragments found in this work and those published in the above mentioned paper are due to different setup of collision cells. It is worth noting that ion with $m/z = 263$ has been reported as the product of zopiclone hydrolysis [8].

Figure 5a shows MS spectrum of electrolysed ZOP solution, containing the mixture of oxidation products and the rest of ZOP, which was recorded in off-line setup. Four main signals of proposed oxidation products can be observed. First oxidation product (designated as P1, $m/z = 375$) corresponds to *N*-desmethyl zopiclone (difference 14 Da from the m/z of ZOP). In MS/MS spectrum the loss of CO ($m/z = 347$) and CO_2 ($m/z = 331$), respectively, are observed (Fig. 5b). Besides, intensive signals at $m/z = 263$ and $m/z = 245$ confirm that both pyridine and the pyrrolo-pyrazine rings remain unchanged and thus, the oxidative demethylation occurs on piperazine skeleton. The fragmentation pattern of the product P1 corresponds to those reported for *N*-demethylated metabolite of zopiclone [24].

Second product (P2, $m/z = 405$) corresponds with the addition of one oxygen atom to the ZOP molecule. Presence of fragments at $m/z = 263$ and $m/z = 245$ suggests that the oxidation takes place on the piperazine ring as well (Fig. 5c). Formation of *N*-oxide related to oxidative metabolism of ZOP has been already described in literature [1]. Electrochemical formation of *N*-oxide(s) has also been reported for another drug possessing tertiary amine group [25]. Oxidation of one of nitrogen atoms in the piperazine ring is thus a reasonable possibility explaining this type of ZOP oxidation. However, oxidation of *N*-methyl group or the carbons of the piperazine skeleton accompanied by piperazine ring opening cannot be excluded in this case.

Third product (P3, Fig. 5d, $m/z = 403$) corresponds with a gain of one oxygen and loss of two hydrogen atoms. The formation of fragments at $m/z = 263$ and $m/z = 245$ suggests that pyridine and pyrrolo-pyrazine rings remain

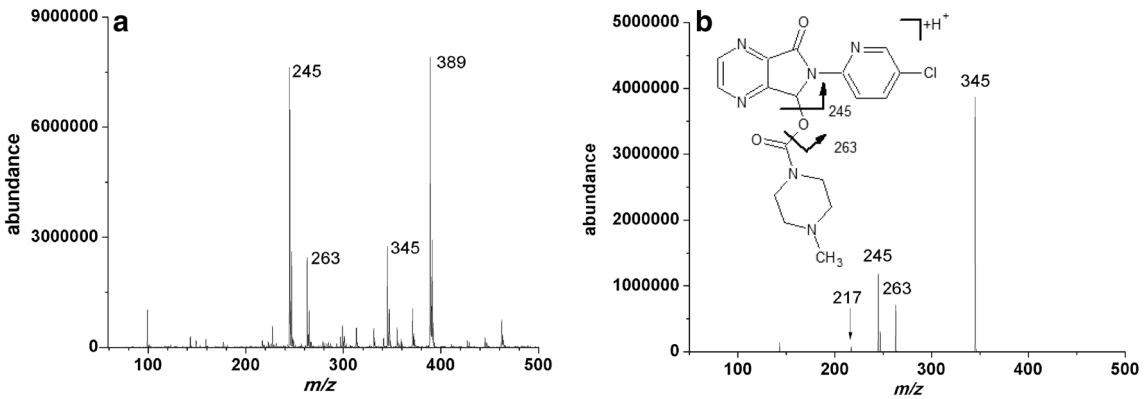

Fig. 4 MS (**a**) and MS/MS spectrum (**b**) of zopiclone (5×10^{-4} mol dm^{-3}) in water/CH_3CN (1:1, v/v)

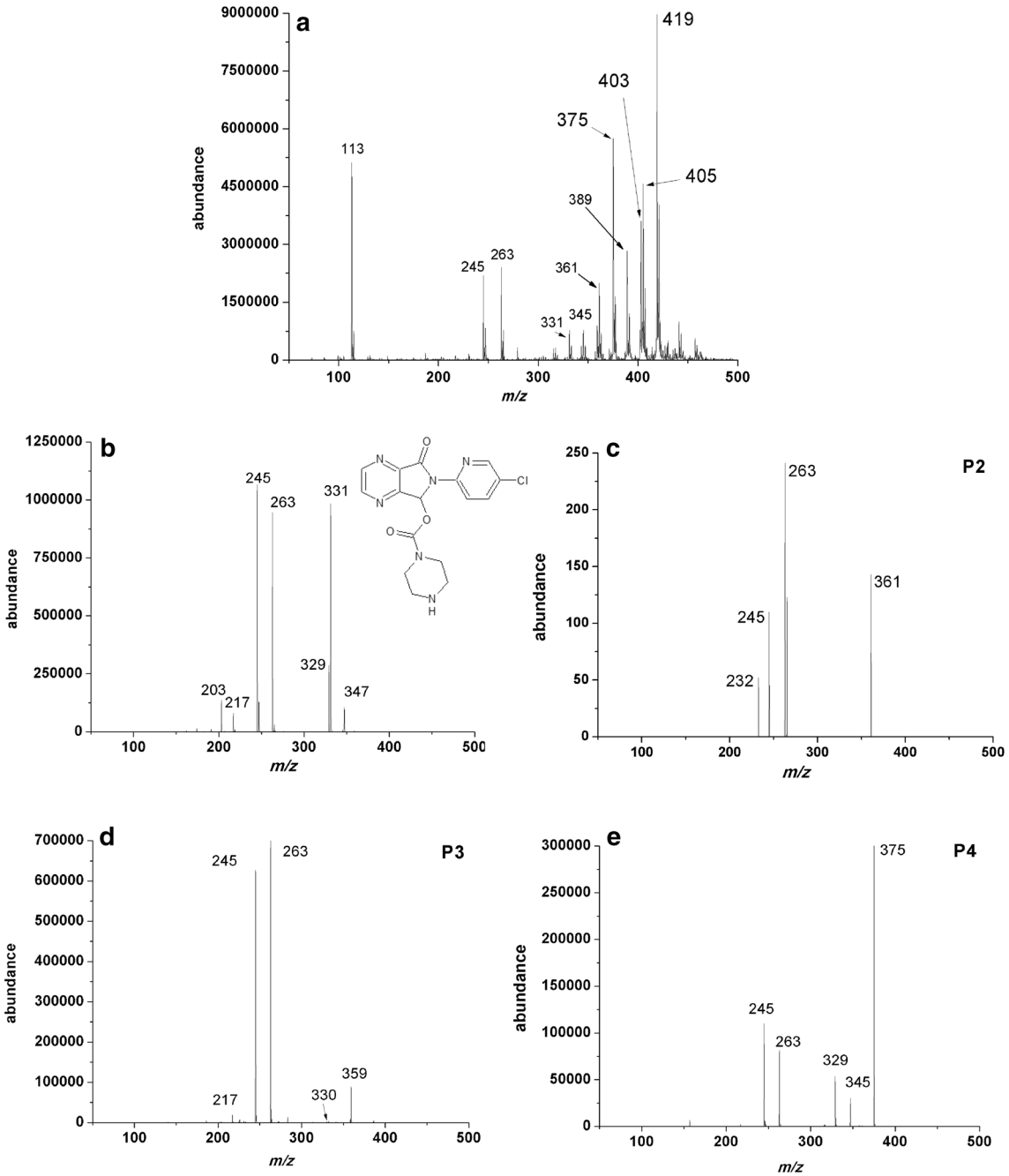

Fig. 5 MS spectrum of electrolysed ZOP (**a**), containing a mixture of oxidation products and the rest of ZOP, and MS/MS spectra of main oxidation products: P1 at $m/z = 375$ (**b**), P2 at $m/z = 405$ (**c**), P3 at $m/z = 403$ (**d**), and P4 at $m/z = 419$ (**e**) acquired in solution of zopiclone ($c = 5 \times 10^{-4}$ mol dm^{-3}) electrolysed in acetonitrile/ammonium acetate buffer solution pH 6.8 (1:1, v/v) 30 min on Pt gauze electrode at $E = 1.2$ V (vs. SCE)

intact as in the case of the previously discussed oxidation products P1 and P2. The fragment at $m/z = 359$ corresponds with loss of CO_2 typical for ZOP derivatives. Minor fragment at $m/z = 330$ corresponds probably with a cleavage of formyl radical indicating the presence of aldehyde group preferentially linked to one of the piperazine nitrogen atoms.

Fourth product (P4, $m/z = 419$) can be explained by the addition of two oxygen and loss of two hydrogen atoms. MS/MS spectrum of P4 (Fig. 5e) shows intensive signal corresponding with the loss of CO_2 typical for ZOP derivatives (dominant fragment at $m/z = 375$). As mentioned above, fragments at $m/z = 263$ and $m/z = 245$, respectively, suggest oxidative process occurring at the

piperazine ring. The introduction of two oxygen atoms into the piperazine skeleton can proceed by several ways leading to different products. One of the theoretical possibilities involves a formation of an *N*-carboxylic group. Since the loss of CO_2 from the fragment at $m/z = 375$ is missing in the MS/MS spectrum, this possibility is not likely. A formation of *N*-oxide and aldehyde group either on terminal methyl group or on piperazine carbon skeleton (accompanied by a ring opening) can be considered as another possibility. A fragment at $m/z = 345$ corresponds with a loss of formaldehyde from fragment at $m/z = 375$ suggesting the presence of aldehyde group preferentially linked to one of the nitrogen atoms from piperazine part. Fragment at $m/z = 329$ can be explained by consequent loss of oxygen atom from the fragment at $m/z = 345$. Similarly to previously discussed oxidation product P2, *N*-oxide formed on one of the piperazine nitrogen atoms is the most probable option. Thus, the oxidation product P4 presumably contains one aldehyde group and one oxygen atom linked to piperazine nitrogen atoms.

In off-line experiments the highest relative intensities (intensity of particular oxidation product divided by the sum of intensities of all signals in given spectrum) are observed in acidic conditions for all oxidation products. When compared the signals of particular oxidation products in acidic conditions, the signal of P1 reaches the highest value. This oxidation product exhibits the highest decrease of relative intensity with increasing pH as well. This fact points out different chemical property of P1 compared to the rest of detected oxidation products (e.g., p*K* value and proton-affinity in gas phase).

On-line connection of electrochemical cell directly to mass spectrometry interface was performed and compared with the results from the above discussed off-line experiments. Zopiclone solution in 1:1 (v/v) mixture of acetonitrile and ammonium acetate buffer of pH 3.5, pH 6.8, and pH 9.5 was continuously pumped through flow cell containing porous graphite electrode. Constant potential within the range from 0 to 0.8 V (vs. Pd/H_2 reference electrode) in 100 mV (0–0.4 V) and 50 mV (0.4–0.8 V) increments, respectively, was applied on the electrode and appropriate mass spectra were collected. The electrode potential of 0 V vs. Pd/H_2 reference electrode corresponded to 0.234 V vs. SCE at pH 7.0. Oxidation products were detected within 4 min after their formation in the cell at the flow rate 4 mm^3 min^{-1}. Resulting "mass voltammograms" are shown in Fig. 6. For better lucidity, the mass voltammograms are displayed in the m/z range from

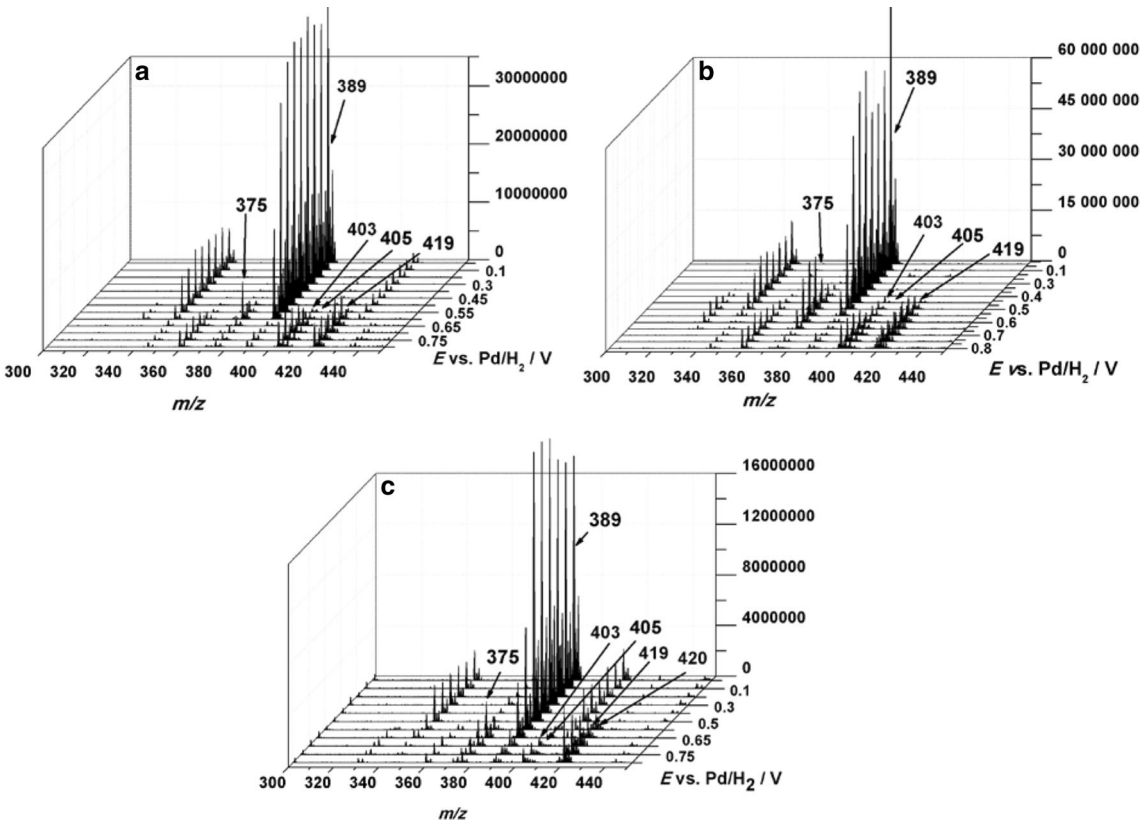

Fig. 6 Mass voltammograms of zopiclone ($c = 5 \times 10^{-4}$ mol dm^{-3}), 1:1 (v/v) acetonitrile/ammonium acetate buffer solution of pH 3.5 (**a**), pH 6.8 (**b**), and pH 9.5 (**c**) acquired in on-line EC/MS

300 to 450, in which the changes in the intensities of the signals of ZOP and its oxidation products were observed. Fragment ions with $m/z = 245$ and $m/z = 263$, common to ZOP and its oxidation products, were observed on the voltammograms at all pH and potentials (data not shown). Oxidation of zopiclone evaluated as a decrease of ZOP signal in acetate buffer solution of pH 3.5 and 6.8 starts at potential 0.5 V vs. Pd/H_2 reference electrode, in acetate buffer solution of pH 9.5 the oxidation starts at lower potential. Unlike acidic and neutral media, in alkaline solution of pH 9.5 on-line experiments reveal one more oxidation product at $m/z = 420$ (designated as P5) beside the above mentioned products P1–P4 (Fig. 6c). Even m/z value suggests the presence of odd number of nitrogen atoms. In the case of the discussed product P5 of ZOP oxidation it corresponds to incorporation of one nitrogen atom into the structure. Collision spectrum (MS^2, Supplementary Material, Fig. S5) of P5 provided three dominant fragments at $m/z = 402$, 390, and 358. The fragment at $m/z = 402$ corresponds to a loss of water suggesting the presence of one extra –OH group. Subsequent loss of CO_2, typical for ZOP derivatives, leads to the most abundant fragment at $m/z = 358$. The fragment at $m/z = 390$ can be ascribed to a loss of CH_2O, NO or CH_2-NH_2. Besides, a minor fragment at $m/z = 403$ was also observed during fragmentation of P5. Tentatively, this fragment can be explained as a loss of ammonia from parent ion. The structure of the P5 product was not revealed from the acquired MS data. Note that P5 was observed in on-line EC/MS experiments conducted in alkaline ammonium buffer. We suggest that P5 arises from a side reaction of ZOP with ammonia under oxidative conditions. When sodium ions were used as buffer constituent instead of ammonium ones, P5 product was not observed. This observation supports the proposed introduction of one nitrogen atom from ammonia to ZOP structure.

In on-line experiments the relatively sharp decrease of ZOP intensity and increase of oxidation products is observed (Supplementary Material, Fig. S6–S8). The processes occurring in acidic, neutral, and alkaline conditions reveal similar main features. The increase of P1 response starts at lower potentials compared to other oxidation products (P2–P4), intensity of signal reaches its maximum faster and at higher potentials (>0.6 V) decreases fast. The formation of the other products occurs at higher potentials and changes in intensities are less dependent on potentials compared to P1. Therefore, it can be concluded (in agreement with off-line experiments, see above) that chemical nature of P1 and process of its formation differ from those of the other oxidation products. The fact is obvious since P1 is formed by demethylation of ZOP (no extraneous substituent incomes to its molecule) while introduction of one or two oxygen atom(s) leads to formation of all remaining products (P2-P4, as well as a specific product P5 formed solely in alkaline solution in the presence of ammonia). Some oxidation products identified in electrochemical oxidation are similar to oxidation products from in vitro metabolic experiments (i.e., *N*-desmethyl zopiclone and zopiclone *N*-oxide) [1].

Conclusion

Voltammetric measurements reveal that electrochemical oxidation of zopiclone is quite complicated process influenced by kinetics and adsorption phenomena. Controlled potential electrolysis combined with mass spectrometry identification of the reaction products is a powerful tool for elucidation of electrochemical oxidation of zopiclone. Four products were found in electrolysed samples by means of off- and on-line tandem mass spectrometry. *N*-Desmethyl zopiclone was identified and three other oxidation products formed by an introduction of oxygen atom(s) to the molecule of zopiclone (including zopiclone *N*-oxide) were characterized. *N*-Desmethyl zopiclone and zopiclone *N*-oxide were formerly confirmed as in vitro metabolic products of zopiclone. The fact gives great credibility to the combination of electrochemistry with mass spectrometry for metabolic studies.

Experimental

Reagents

Zopiclone (ZOP) was obtained from Farmak (98 %, Olomouc, Czech Republic), zopiclone *N*-oxide (European Pharmacopoeia Reference Standard) was purchased from Fluka. A stock solution of 1×10^{-3} mol dm^{-3} ZOP was prepared in acetonitrile (HPLC grade, Sigma-Aldrich Czech Republic) and kept in a refrigerator. Britton-Robinson (BR) buffer solutions were prepared from phosphoric acid, acetic acid, and boric acid (0.04 mol dm^{-3} each, analytical grade, Lachema, Czech Republic). Desired pH values were adjusted with sodium hydroxide (0.2 mol dm^{-3}, analytical grade, Lach-Ner, Czech Republic). Ammonium acetate (p.a., >98.0 %, Lach-Ner, Czech Republic) was used as supporting electrolyte for MS experiments. Desired pH values were adjusted with acetic acid or ammonia (p.a., 25 % in water, Lach-Ner, Czech Republic).

Voltammetric experiments

An AutoLab PGSTAT128N electrochemical analyser (Metrohm Autolab, Utrecht, The Netherlands) with

software NOVA 1.10 was used for voltammetric experiments with three-electrode system consisting of a glassy carbon working electrode (GCE, disc diameter 3.0 mm, Bioanalytical Systems, USA) or rotating GCE (disk diameter 2.0 mm, Metrohm, The Netherlands), platinum wire auxiliary electrode, and saturated calomel reference electrode. GCE was polished using aqueous suspension of alumina powder (0.05 μm particles, Sigma-Aldrich) on a wet microcloth (Buehler, USA) and sonicated in distilled water for 30 s prior to each measurement. Cyclic voltammetry (CV) and linear sweep voltammetry (LSV) were performed at different scan rates over the range 0.02–0.8 V s^{-1} and at different pH values of the supporting buffer solution. Differential pulse voltammograms were recorded at pulse amplitude of 25 mV, pulse width 500 ms and scan rate 0.02 V s^{-1}. Hydrodynamic measurements were carried out with angular velocity ranged from 52 to 314 rad s^{-1} and scan rates 0.02 and 0.4 V s^{-1}. All experiments were performed in supporting electrolytes containing BR buffer solutions of desired pH and acetonitrile (1:1, v/v). Hydrodynamic voltammograms were processed using el-Chem Viewer software [26].

Controlled potential electrolysis

Potentiostat 100 mA (L-Chem, Horka nad Moravou, Czech Republic) with three-electrode system consisted of platinum gauze working electrode, platinum auxiliary electrode placed in a separate cathode compartment and reference SCE electrode separated from the bulk solution with a porous ceramic frit. The electrolysis was performed in mixture of acetonitrile/ammonium acetate buffer solution (1:1, v/v) of different pH values and at different potentials: pH 3.5 (0.2 V, 1.4 V), pH 6.8 (0.2 V, 1.2 V), pH 9.5 (0.2 V, 1.2 V). All samples were electrolysed in stirred solutions containing 5×10^{-4} mol dm^{-3} ZOP for 30 min.

MS and on-line EC/MS analysis

Mass spectrometer Agilent 1100 Series LC/MSD Trap (Agilent Technologies, Palo Alto, CA, USA) with electrospray ionization (ESI) was used for analysis of electrolysed solutions of ZOP. Parameters of ESI source working in the positive mode were as follows: capillary voltage 2.4 kV, source temperature 150 °C, pressure of desolvation gas 10 psi, desolvation gas flow rate 180 dm^3 h^{-1}. Nitrogen was used as desolvation gas and helium as collision gas.

On-line electrochemistry/mass spectrometry measurements were performed using ESA Conditioning cell 5021A (ESA, Chelmsford, MA, USA) connected to the potentiostat Detector ADLC 1 (Laboratorní přístroje Praha, Czech Republic). Working ZOP solution (5×10^{-4} mol dm^{-3}) in 1:1 (v/v) acetonitrile/ammonium acetate buffer solution (pH 3.5, pH 6.8, and pH 9.5) was used for on-line oxidation in the potential range from 0 to 0.8 V (vs. Pd/H_2).

Acknowledgments The authors gratefully acknowledge the financial support by the Ministry of Education, Youth and Sports of the Czech Republic (project LO1305).

References

1. Beyquemont L, Mouajjah S, Escaffre O, Beaune P, Funkc-Brentano CH, Jaillon P (1999) Drug Metab Dispos 27:1068
2. Tono MA, Jabor VAP, Bonato PS (2013) Anal Bioanal Chem 405:267
3. Jantos R, Vermeeren A, Sabljic D, Remaekers JG, Skopp G (2013) Int J Legal Med 127:69
4. Tonon MA, Bonato PS (2012) Electrophoresis 33:1606
5. Largeron M, Fleury MB (1989) J Pharm Sci 78:627
6. Fernandez C, Gimenez F, Mayrargue J, Thuillier A, Farinotti R (1995) Chirality 7:297
7. El-Shaheny RN, Alattas A, Nasr JJ, El-Enany N, Belal F (2012) J Chromatogr B 907:49
8. Mannaert E, Tytgat J, Daenens P (1997) J Anal Toxicol 21:208
9. Viré J-C, Zhang H, Quarin G, Patriarche GJ (1993) Talanta 40:313
10. Yilmaz S (2009) Colloids Surf B 71:79
11. The British Pharmacopoeia (2009) Her Majesty's Stationary Office, London **(electronic version)**
12. Paw B, Misztal G (2000) J Pharm Biomed Anal 23:819
13. Bouklouze AA, Viré J-C, Quarin GC, Kauffmann J-M (1994) Electroanalysis 6:1045
14. Van Bocxlaer L, Meyer E, Clauwaert K, Lambert W, Piette M, De Leenheer A (2006) J Anal Toxicol 1:52
15. Tonon MA, Jabor VAP, Bonato PS (2011) Anal Bioanal Chem 400:3517
16. Fernandez C, Gimenez F, Baune B, Maradeix V, Thuillier A, Farinotti R (1993) J Chromatogr A 617:271
17. Foster RT, Caillé G, Ngoc AH, Lemko CH, Kherani R, Pasutto FM (1994) J Chromatogr B 658:161
18. Lohmann W, Baumann A, Karst U (2010) LC-GC Europe 1:7
19. Jahn S, Karst U (2012) J Chromatogr A 1259:16
20. Jurva U, Wikström HV, Weidolf L, Bruins AP (2003) Rapid Commun Mass Spectrom 17:800
21. Permentier HP, Bruins AP (2004) J Am Soc Mass Spectrom 15:1707
22. Chen H, Zhang Y, Mutlib AE, Zhong M (2006) Anal Chem 78:2413
23. http://www.drugbank.com [Online]
24. Smyth WF, Joyce C, Ramachandran VN, O'Kane E, Coulter D (2004) Anal Chim Acta 506:203
25. Johansson T, Weidolf L, Jurva U (2007) Rapid Commun Mass Spectrom 21:2323
26. Hrbac J, Halouzka V, Trnkova L, Vacek J (2014) Sensors 14:13943

Příloha 6

Electrochemical oxidation of tolterodine

Macíková, P.; **Skopalová**, **J.***; Cankař, P.; Papoušková, B.; Straková, R.; Jirovský, D.; Maier, V.

Electroanalysis **2013**, *25*, 205-212

Electrochemical Oxidation of Tolterodine

Pavla Macíková,[a] *Jana Skopalová*,*[b] *Petr Cankař*,[c] *Barbora Papoušková*,[a] *Radka Straková*,[b] *David Jirovský*,[b] *Vítězslav Maier*[a]

[a] Regional Centre of Advanced Technologies and Materials, Department of Analytical Chemistry, Faculty of Science, Palacký University, 17. listopadu 1192/12, 771 46 Olomouc, Czech Republic
[b] Department of Analytical Chemistry, Faculty of Science, Palacký University, 17. listopadu 1192/12, 771 46 Olomouc, Czech Republic
[c] Department of Organic Chemistry, Faculty of Science, Palacký University, 17. listopadu 1192/12, 771 46 Olomouc, Czech Republic
*e-mail: jana.skopalova@upol.cz

Received: July 20, 2012
Accepted: August 17, 2012
Published online: October 2, 2012

Abstract
The electrochemical behavior of tolterodine, an antimuscarinic drug used to treat urge incontinence and overactive bladder, was investigated using cyclic and differential pulse voltammetry at glassy carbon electrode. Electrooxidation of tolterodine proceeds as a complex two-step pH-dependent process. Controlled potential electrolysis of tolterodine solutions was performed at platinum gauze electrode in methanolic, aqueous-methanolic and acetonitrile media. Electrolyzed solutions were analyzed using liquid chromatography with electrospray ionization quadrupole time-of-flight mass spectrometry. 5-Hydroxymethyl tolterodine, the main biologically active metabolite of tolterodine, was identified among monomeric oxidation products. Dimeric products, formed by oxidative coupling of phenoxy radicals, were found in all electrolyzed solutions. The mechanism of the electrochemical oxidation of tolterodine has been proposed.

Keywords: Tolterodine, 5-Hydroxymethyl tolterodine, Mass spectrometry, Oxidation, Voltammetry

DOI: 10.1002/elan.201200388

1 Introduction

Tolterodine (Scheme 1a) is a muscarinic receptor antagonist used for the treatment of urinary urge incontinence and other symptoms associated with an overactive bladder [1]. Two enantiomeric forms, (*R*)- and (*S*)-tolterodine, exist providing different biological effects. While the optically pure (*R*)-isomer is useful for patients with urinary incontinence that arises only from muscarinic hyperactivity, the (*S*)-isomer provides a weak sedative effect and non-cholinergic spasmolytic activity against urinary and intestinal spasms that arise from various mechanisms [2]. The most frequently used in pharmaceutical preparations form is (*R*)-*N*,*N*-diisopropyl-3-(2-hydroxy-5-methylphenyl)-3-phenylpropanamine L-hydrogen tartrate which is commercially available as Detrol or Detrusitol. Tolterodine tartrate is a white crystalline powder well soluble in water (12 mg mL^{-1}) and methanol, slightly soluble in ethanol and practically insoluble in toluene. The pK_a value is 9.87 [3].

Tolterodine is metabolized via two pathways in humans. The first is an oxidation of the 5-methyl group in the presence of cytochrome P450 2D6 to form pharmacologically active 5-hydroxymethyl tolterodine (5-HMT, Scheme 1b) which exhibits antimuscarinic activity similar to the parent drug and contributes significantly to the tolterodine therapeutic effect [3]. The other way is a dealkylation of the nitrogen by cytochrome P450 3A4 to form *N*-dealkylated tolterodine [4]. As compared with metabolisms in animals, mice and dogs show similar metabolite patterns as humans, such as 5-HMT consecutively transformed to 5-carboxylic acid metabolite of tolterodine (5-CM) and *N*-dealkylated forms of these three substances. The major metabolites in dogs and mice, 5-CM and *N*-dealkylated 5-CM, were not detected in rat urine, but other metabolites of tolterodine were found in rats formed by hydroxylation of the unsubstituted benzene ring. After oral administration in humans tolterodine is rapidly absorbed and a terminal half-life is 2–3 h. Biotransformation takes place predominantly in the liver and metabolites are excreted mostly in urine and partly in feces [5].

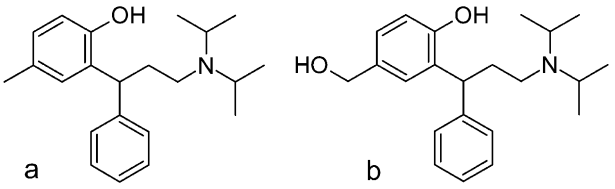

Scheme 1. Chemical structures of tolterodine (a) and 5-hydroxymethyl tolterodine (b).

Chromatographic methods, especially high performance liquid chromatography coupled to mass spectrometry (HPLC/MS) [6–9] and HPLC with UV detection [10,11] are most frequently used for the determination of tolterodine and its metabolites. Enantiospecific HPLC methods were developed for the determination of (*S*)-enantiomer impurities in (*R*)-tolterodine tartrate [12,13]. Gas chromatography/mass spectrometry (GC/MS) is applicable for determination of tolterodine and 5-HMT after derivatization [14]. A spectrophotometric method based on oxidation and complexation of tolterodine tartrate has been proposed for its analysis in pharmaceutical formulations [15].

The formation of potential oxidative metabolites could be mimicked using electroanalytical methods, which allow fast detection of sites labile towards oxidation in a molecule [16]. Electrochemical oxidation combined with chromatographic techniques and mass spectrometry can detect metabolism products of drugs [17] or pesticides [18]. An ionization technique of great compatibility with electrochemistry is electrospray ionization [19,20]. To the best of our knowledge, no electroanalytical study of tolterodine or its metabolites has been published yet.

In this paper, the electrochemical behavior of tolterodine was studied using voltammetric techniques. Controlled potential electrolysis was used to prepare tolterodine oxidation products. Detection of the products was performed by HPLC coupled to electrospray ionization quadrupole time-of-flight mass spectrometry.

2 Experimental

2.1 Reagents

Racemic tolterodine tartrate was obtained from Zentiva, Czech Republic. 5-Hydroxymethyl tolterodine was synthesized from (*R*)-fesoterodine fumarate (99%, IS Chemical Technology, China). Methanol (p.a., Lach-Ner, Czech Republic), acetonitrile (for HPLC gradient grade, Sigma-Aldrich) and doubly distilled water (Elga, U. K.) were used as solvents. Ammonium acetate (p.a., $>98.0\%$, Lach-Ner, Czech Republic) and lithium perchlorate ($\geq 98.0\%$, Fluka) served as electrolytes in methanol and acetonitrile solutions, respectively. Britton-Robinson (BR) buffers were prepared from trihydroxidooxidophosphorus phosphoric acid, acetic acid and boric acid trihydroxidoboron (0.04 mol L^{-1} each). Desired pH values were adjusted with sodium hydroxide (0.2 mol L^{-1}).

2.1.1 Synthesis of 5-Hydroxymethyl Tolterodine

Fesoterodine fumarate (102 mg, 0.19 mmol) was dissolved in ethanol (10 mL) and then aqueous ammonia 25% was added (10 mL). A reaction mixture was stirred at room temperature for 48 hours. A white precipitated solid was filtered-off, washed with water, and dried in the air, providing 55 mg (83%).

2.2 Voltammetric Measurements

Voltammetric measurements were performed on an Eco-Tribo-Polarograph with Polar.Pro v. 4 software (Polaro-Sensors, Prague, Czech Republic). A three-electrode system involved a glassy carbon working electrode (GCE, disk diameter 3.0 mm, Bioanalytical Systems, USA), a platinum wire auxiliary electrode and a saturated calomel reference electrode (SCE) for measurement in aqueous and methanolic solutions. A reference electrode consisting of a silver wire immersed in 0.1 mol L^{-1} $AgNO_3$ in CH_3CN and separated from the bulk solution with a porous ceramic frit was used for measurement in acetonitrile solutions. The working electrode was polished using 0.05 μm alumina slurry on wet microcloth (Buehler, USA) and sonicated in distilled water for 10 s before each measurement. Cyclic voltammograms were recorded at a scan rate of 100 mV s^{-1} or at different scan rates in the range from 10 to 500 mV s^{-1}. Differential pulse voltammetry (DPV) measurements were performed at a pulse amplitude of 50 mV, pulse width of 100 ms and a scan rate of 20 mV s^{-1}. All experiments were performed in a low volume cell (maximum 2 mL).

2.3 Controlled Potential Electrolysis

The apparatus for controlled potential electrolysis consisted of an OH-404 potentiostat (Radelkis, Budapest, Hungary) with a three-electrode system: platinum gauze working electrode, platinum auxiliary electrode placed in a separate cathode compartment and reference SCE (for methanolic and aqueous methanolic solutions) or reference electrode consisting of a silver wire immersed in 0.1 mol L^{-1} $AgNO_3$ in CH_3CN and separated from the bulk solution with a porous ceramic frit (for acetonitrile solutions). The electrolysis was performed in three different media at different values of constant potential: (i) in acetonitrile with 12.5 mmol L^{-1} $LiClO_4$ as the supporting electrolyte at 0.2 V, 0.7 V and 1.0 V, (ii) in methanol with 90 mmol L^{-1} CH_3COONH_4 at 0.2 V, 0.7 V and 1.0 V, (iii) in 1:1 by volume mixture of methanol and aqueous BR buffer of pH 3.0 (at 0.50 V, 0.69 V and 0.86 V), pH 7.0 (at 0.20 V, 0.43 V, 0.58 V and 0.73 V) and pH 10.0 (at 0.10 V, 0.28 V, 0.50 V and 0.61 V).

All samples were electrolyzed in stirred solutions containing 1 mmol L^{-1} (0.48 mg mL^{-1}) tolterodine tartrate in a total volume of 1.6 mL until the current decreased to a residual current value.

2.4 HPLC/MS Analysis

An Acquity UPLC system (Waters, Milford, MA, USA) equipped with binary solvent manager, sample manager, column manager and PDA detector was used. The separation was performed on a chromatographic Vertex Plus Column (50 mm × 2 mm, 1.8 μm) Blue Orchid (Knauer, Berlin, Germany). The mobile phase consisted of 0.01 mol L^{-1} ammonium acetate aqueous solution (solvent

A)/acetonitrile (solvent B), gradient elution (% v/v): 0–5 min (10–80% B), 5–6 min (80% B), 6–7 min (80–10% B) and 7–10 min (10% B). The mobile phase flow rate was 0.4 mL min^{-1}, the temperature of the autosampler was 10 °C and the column oven was set at 25 °C. The injection volume was 3 μL.

A QqTOF Premier mass spectrometer (Waters, Milford, MA, USA) coupled to the UPLC system was used for confirmation of putative structures on the basis of determination of elemental composition. Tuned electrospray ionization (ESI) parameters for the mass spectrometer were as follows: capillary voltage 3 kV (positive mode), source temperature 100 °C, sampling cone 30 V, desolvation temperature 150 °C, cone gas flow rate 38 L h^{-1} and desolvation gas flow rate 450 L h^{-1}. Nitrogen was used as a desolvation gas and argon as a collision gas. The data were acquired using simultaneous scanning at lower collision energy of 5 eV and at higher energy using collision energy ramp from 15 to 35 eV. Data were processed using MassLynx 4.1 software (Waters).

3 Results and Discussion

3.1 Electrochemical Behavior of Tolterodine

The cyclic voltammogram of tolterodine in buffered aqueous methanolic solution of pH 7.4 (Figure 1) shows two anodic peaks at potentials of 480 mV (peak A) and 680 mV (peak B). No current response was observed in the reverse cathodic branch of voltammograms indicating irreversibility of the electrode process. Peak B appeared also on the voltammogram of 5-HMT (Figure 1), preceded by a current shoulder. It is therefore likely that the oxidation step manifested by peak B is common to both substances. Peak A, absent on the voltammogram of 5-HMT, indicates the formation of this substance by the tolterodine oxidation at potentials corresponding to peak A.

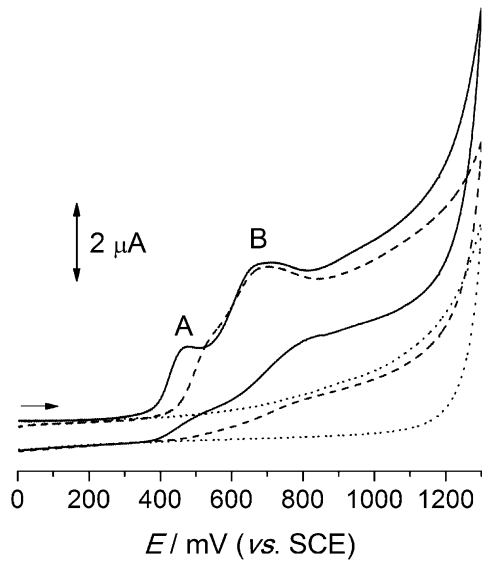

Fig. 1. Cyclic voltammograms of 0.1 mmol L^{-1} tolterodine (—), 0.1 mmol L^{-1} 5-HMT (- - - - -) and supporting electrolyte 1:1 methanol/BR buffer pH 7.4 (·····), scan rate 100 mV s^{-1}.

The effect of the scan rate on tolterodine anodic CV peaks was investigated in neutral aqueous buffered solutions of pH 7.0 without methanol and with 50% of methanol and in nonaqueous methanol/ammonium acetate solution. The height of both peaks, A and B, increases with increasing scan rate in all media. The dependences of log I_p–log v were linear with slopes of 0.62 and 0.74 for peak A and B, respectively, in aqueous solution, 0.5 and 0.75 for A and B, respectively, in aqueous/methanol mixture and 0.34 and 0.23 for A and B, respectively, in methanol/ammonium acetate. Slope values higher than 0.5, which is the theoretical value for a purely diffusion controlled process, show the influence of adsorption on the electrochemical oxidation of tolterodine, especially in aqueous solutions. A tendency of tolterodine to adsorb onto the GCE surface is suppressed in the presence of 50% methanol. Slopes less than 0.5 in methanolic medium may result from some kinetic process (e.g. dimerization) accompanying the electrode reaction.

Both CV peaks shift to positive potentials with increasing scan rate. The dependence of the peak potential E_p on log v measured in aqueous solutions can be approximated by straight lines with slopes of 15 mV and 60 mV per log unit for peak A and B, respectively. The former value conform a theoretically predicted potential shift for a two-electron reversible electrode reaction followed by an irreversible chemical reaction whereas the later one is typical for a one-electron electrode reaction when both reduced and oxidized forms are strongly adsorbed on the electrode surface [21–23].

The oxidation of tolterodine is a pH-dependent process. The number of current responses, their intensity and potentials change with acidity of the solution as can be seen in the voltammograms (Figure 2). In strongly acidic media up to pH 5.5 only a well-developed peak A and a small peak B can be observed. At pH ≥ 6.0 a third current signal C appears at more positive potentials (Figure 2, trace 2). The intensity of peaks B and C increases with increasing pH (Figure 2, trace 3) and, at pH > 9, the peaks coalesce into a large and a well-defined peak designated as B + C (Figure 2, trace 4).

The potential–pH dependence measured in 1:1 methanol/BR buffer solutions is shown in Figure 3. The potentials of all three peaks, A, B and C, shifted to less positive potentials with increasing pH. The slopes of the regression straight lines fitted to the E_p–pH data were −63 mV/pH unit for both peaks A and C. The potential shift of peak B was −65 mV/pH unit in the pH range 3.2–8.0 and −15 mV/pH unit in the pH range 8.6–12.6. The slopes close to the theoretical value of −59 mV/pH unit indicate that the first oxidation step and the next two steps up to slightly alkaline media involve the same number of electrons and protons. The intersection point of the regression straight lines likely corresponds to the dissociation constant of some tolterodine oxidation product (pK 8.5).

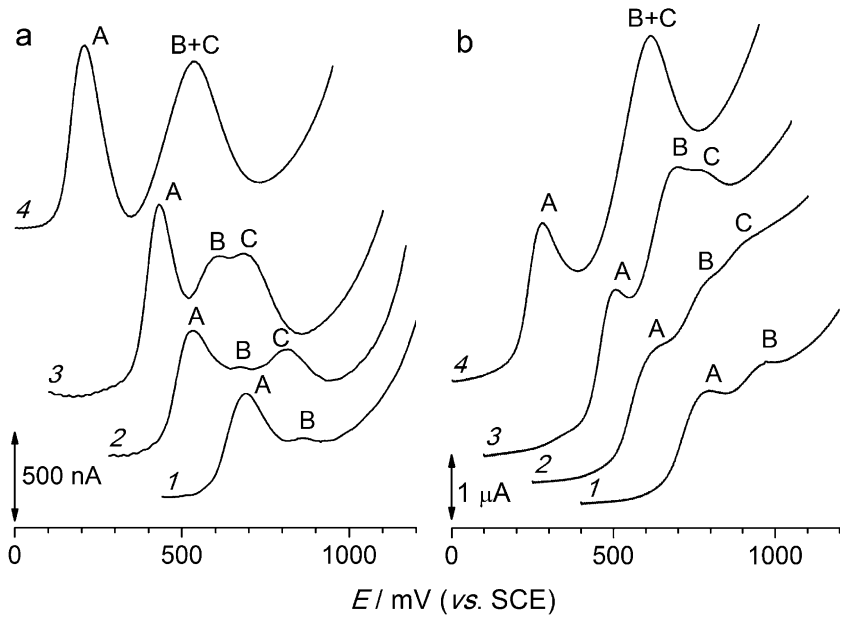

Fig. 2. DP (a) and linear sweep (b) voltammograms of 0.1 mmol L^{-1} tolterodine in methanol/aqueous BR buffer solution (1:1) of various pH: (1) pH 4.1; (2) pH 6.5; (3) pH 8.2; (4) pH 11.3. LSV scan rate 100 mV s^{-1}.

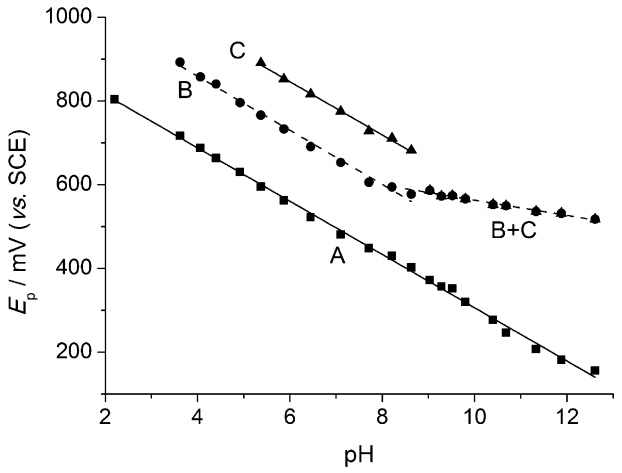

Fig. 3. Dependence of DPV peak potential of tolterodine (0.1 mmol L^{-1}) on pH for the anodic peaks A, B, C and the merged peak B + C.

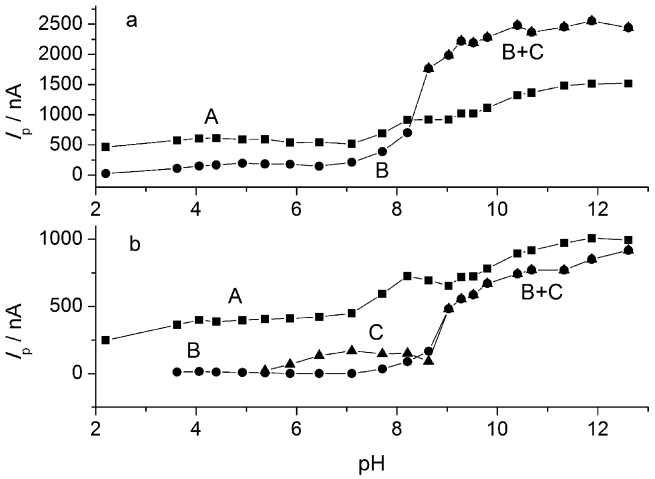

Fig. 4. Peak current–pH dependence of tolterodine anodic CV (a) and DPV (b) peaks: A (squares), B (circles) and C (triangles). Tolterodine concentration 0.1 mmol L^{-1}, CV: scan rate 100 mV s^{-1}; DPV: scan rate 20 mV s^{-1}, pulse amplitude 50 mV, pulse width 100 ms.

The current of anodic CV and DPV peaks of tolterodine remained almost unchanged with increasing pH up to neutral pH (Figure 4). An increase of the current was observed at pH > 8. It was most remarkable for the CV peaks B and C suggesting oxidation product(s) formed at the potential of peak A can be more easily oxidized in alkaline media.

3.2 Controlled Potential Electrolysis and HPLC/MS Analysis of Tolterodine Oxidation Products

For a more detailed characterization of the oxidation products, we performed a series of experiments with controlled potential electrolysis of tolterodine on the large surface Pt electrode in methanol/aqueous BR buffer solutions (pH 3.5, 7.0 and 10.0), methanol/ ammonium acetate and acetonitrile/lithium perchlorate systems. The nonaqueous medium was used in order to suppress the adsorption of oxidation products on the electrode surface. The controlled potential values suitable for exhaustive electrolysis were chosen according to courses of tolterodine cyclic voltammograms recorded in different media and pH. In aqueous methanolic media, lower potential values (0.69 V, 0.43 V and 0.28 V at pH 3, pH 7 and pH 10, respectively) corresponded to the potential of peak A, higher potentials (0.86 V, 0.58 V and 0.50 V at pH 3, pH 7

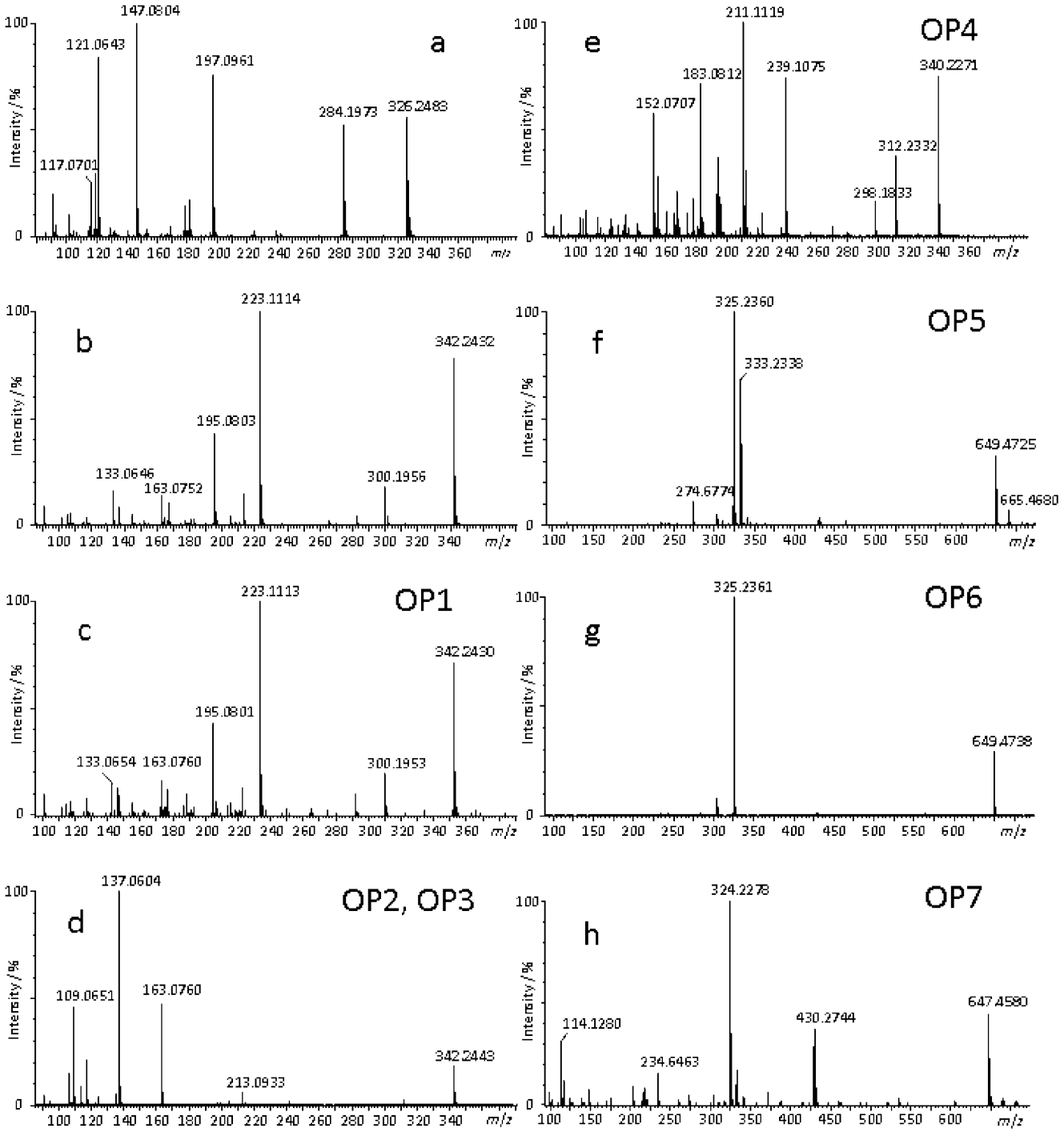

Fig. 5. MS spectra of tolterodine (a), 5-HMT (b) and products of tolterodine oxidation OP1 (c), OP2 and OP3 (d), OP4 (e), OP5 (f), OP6 (g) and OP7 (h) acquired after electrolysis (at 0.2 V for tolterodine, at 0.7 V for OP1, OP5, OP6 and OP7 and at 1.0 V for OP2, OP3 and OP4) with Pt-electrode in acetonitrile/$LiClO_4$ solutions. Spectra (f–h) were acquired at lower collision energy (5 eV), spectra (a)–(e) were acquired at higher energy using collision energy ramp from 10 to 40 eV without precursor ion selection.

and pH 10, respectively) to peak B and the highest (0.78 V and 0.61 V at pH 7 and pH 10, respectively) to peak C. Potentials of 0.7 V and 1.0 V corresponding to peaks A and B, respectively, were used in nonaqueous media. Electrolyzed solutions of tolterodine were directly analyzed using a liquid chromatography system connected to an electrospray ionization quadrupole time-of-flight mass spectrometry. In order to eliminate the influence of nonelectrolytic reaction of tolterodine, the chromatograms and mass spectra of electrolyzed solutions were compared to those of control samples. The control samples were obtained by electrolysis of tolterodine solutions

Table 1. HPLC/MS analysis of tolterodine and its oxidation products.

Compound	t_R (min)	$[M+H]^+$ (m/z)	Molecular formula	Error (ppm)
Tolterodine	2.8	326.2483	$C_{22}H_{32}NO$	−0.3
5-HMT	2.0	342.2432	$C_{22}H_{32}NO_2$	−0.3
OP1	2.0	342.2430	$C_{22}H_{32}NO_2$	−0.9
OP2	1.9	342.2443	$C_{22}H_{32}NO_2$	2.9
OP3	2.1	342.2436	$C_{22}H_{32}NO_2$	0.9
OP4	2.4	340.2271	$C_{22}H_{30}NO_2$	−1.6
OP5 (dimer)	3.6	649.4725	$C_{44}H_{61}N_2O_2$	−1.2
OP6 (dimer)	4.8	649.4738	$C_{44}H_{61}N_2O_2$	0.8
OP7 (dimer)	3.8	647.4580	$C_{44}H_{59}N_2O_2$	0.5

at potentials of 0.1 V, 0.2 V and 0.5 V for pH 10.0, pH 7.0 and pH 3.5, respectively. The potential of 0.2 V was used also for methanolic and acetonitrile media. Under these conditions no electrochemical reaction of tolterodine proceeded.

HPLC/MS analysis of tolterodine control samples as well as tolterodine standard solution resulted in a peak with retention time (t_R) of 2.8 min and a molecular ion $[M+H]^+$ at m/z 326. The fragmentation spectrum of tolterodine (Figure 5a) shows fragment ions at m/z 284 (loss of a propyl group from the amine), at m/z 197 (cleavage of *N*-ethyl-*N*,*N*-diisopropylamine group) and the most intensive ion at m/z 147 (cleavage of the *N*,*N*-diisopropylamine group together with the unsubstituted phenyl ring and a hydrogen). The fragmentation spectrum of tolterodine corresponds to the spectrum reported in the literature [7].

HPLC/MS analysis of all solutions electrolyzed at the potential of peak A revealed an oxidation product OP1 with t_R 2.0 min (Table 1). The MS spectrum of this product is identical to the spectrum of 5-HMT standard (Figure 5b,c) and corresponds to the spectrum reported in the literature [7]. The highest amount of OP1 was found in acetonitrile and buffered acidic solutions.

Other two polar products OP2 and OP3 with t_R 1.9 min and 2.1 min, respectively, were observed in the chromatograms of all solutions electrolyzed at lower potentials. Mass spectra of both products are identical (Figure 5d) and provide molecular ion at m/z 342 like the 5-HMT (Table 1). The most intensive fragment ion at m/z 137 corresponds to an ion with two oxygen and two methyl groups bonded on the benzene ring. It proves that OP2 and OP3 are regioisomers of tolterodine hydroxy derivatives with hydroxyl groups bonded to the methyl substituted aromatic ring. According to the retention data it can be estimated that the more polar OP2 product bears the hydroxyl group probably in position 4, the less polar OP3 in position 6 (Scheme 2).

Product OP4 (t_R 2.4 min) was found in solutions electrolyzed at the potential of peak B in acetonitrile and buffered acidic solutions only. The fragmentation spectrum of this product (Figure 5e) reveals a molecular ion $[M+H]^+$ at m/z 340 and a main fragment ion at m/z 211 corresponding to the cleavage of the diisopropylamine moiety and a C=O group. Therefore, OP4 is proposed to be an aldehyde that is formed by oxidation of the 5-HMT. Exact mass and calculated elemental composition confirms this supposition (Table 1).

In addition to the above mentioned products that are more polar than the parent tolterodine, there were also found less polar oxidation products in all electrolyzed solutions. Products OP5 and OP6 with t_R 3.6 min and 4.8 min, respectively, have the same molecular ion at m/z 649 (Table 1). On the mass spectra of both substances (Figure 5f, g) there is an abundant ion at m/z 325 that appertain to a doubly charged molecular ion $[M+2H]^{2+}$. It proved that both species are dimers of tolerodine. The more polar OP5 is likely formed by oxidative carbon–carbon coupling while the less polar OP6 could be a product of carbon–oxygen coupling of two phenoxy radicals that arise from one-electron oxidation of tolterodine. A compound co-eluted with OP5 (molecular ion at m/z 665 and $[M+2H]^{2+}$ at m/z 333, Figure 5f) correspond to an analogous dimer formed by the coupling of 5-HMT and tolterodine phenoxy radicals.

A dimer product OP7 (t_R 3.8 min) at m/z 647 was observed in acetonitrile electrolyzates, (Figure 5h). The absence of two hydrogens in its elemental composition (Table 1) calculated from the exact mass suggests that OP7 can be formed by electrooxidation of the OP5. Less polarity of OP7 compared to OP5 supports this supposition.

Electrolysis of tolterodine provided some side reactions with the nonaqueous solvents. By-products of tolterodine acetamidation [24] with molecular ion at m/z 383 were observed in acetonitrile/lithium perchlorate solutions. Similarly, 5-methoxymethyl tolterodine (t_R 2.5 min, $[M+H]^+$ 356 m/z) was found as a co-product obtained by electrolysis in acid aqueous methanolic solution at potential of the peak A.

3.3 Mechanism of Electrochemical Oxidation of Tolterodine

According to results obtained from voltammetry and controlled potential electrolysis combined with HPLC/MS analysis we proposed the following mechanism of electrochemical oxidation of tolterodine (Scheme 2). In the first

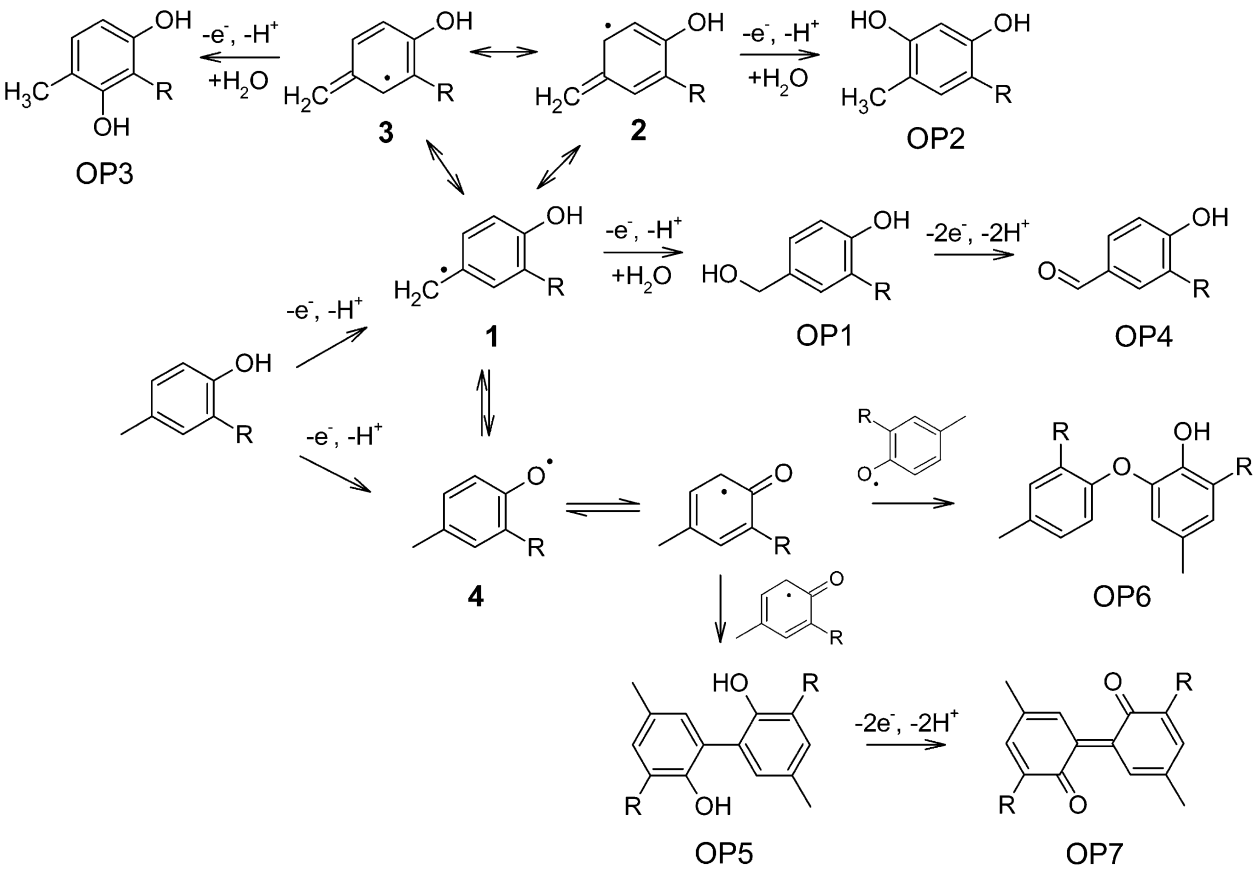

Scheme 2. Proposed mechanism of electrochemical oxidation of tolterodine.

reaction step (peak A) one-electron oxidation may lead to formation of benzyl radical (**1**) which can be further oxidized to benzylium cation [24] and hydrolyzed to produce 5-HMT (OP1). Other possible resonance forms of the benzyl radical (**2**, **3**) can also be oxidized resulting in the products OP2 and OP3. Concurrently, one-electron oxidation of tolterodine may produce the phenoxy radical (**4**) which can dimerize [25] to form the products OP5 and OP6. Deprotonation of the hydroxyl group on the aromatic ring facilitates formation of a phenoxy radical and consequently formation of dimers. It corresponds to the increase of the current of peak A in alkaline solutions (Figure 4).

In the second reaction step OP1 is oxidized to corresponding aldehyde (OP4) resulting in the peak B. This reaction is well detectable in acidic solutions. In neutral and alkaline media, deprotonation of hydroxy derivatives formed in the first step boosts formation of phenoxy radicals which can react together to form dimers. Their subsequent oxidation may result in oligomers or quinone structures (OP7). Therefore an increase of the current of peak C can be observed. Adsorption of dimers/oligomers and quinone products evidenced in the voltammetric experiments causes electrode fouling and complicates electrode reactions.

4 Conclusions

Combination of voltammetric methods and controlled potential electrolysis with HPLC/MS separation and identification of the reaction products is a very powerful tool for elucidation of a quite complex process such as electrochemical oxidation of tolterodine. Results of this study demonstrate that electrochemical reactions can partly mimic the metabolic transformation of tolterodine which proceeds in living organisms. The proposed reaction mechanism can be used to develop sensitive electroanalytical methods for determination of this drug. The experimental approaches presented in this paper could be applied to study oxidation mechanisms of other structurally related compounds and eventually to electrosyntheses of selected metabolites involved in their oxidative (bio)-transformation.

Acknowledgements

The authors gratefully acknowledge the financial support by the *Operational Program Research and Development for Innovations – European Regional Development Fund* (Project CZ.1.05/2.1.00/03.0058). The work has been also supported by the project of *Palacký University in Olo-*

mouc PRF_2012_020 and by the *Czech Science Foundation* (P206/12/1150).

References

[1] J. Wefer, M. C. Truss, U. Jonas, *World J. Urol.* **2001**, *19*, 312.
[2] G. Aberg (Bridge Pharma Inc.), US Patent 6310103, **2001**.
[3] S. Gelone, A. R. Gennaro, in *Remington: The Science and Practice of Pharmacy,* 21st ed. (Ed: D. B. Troy), Lippincott Williams and Wilkins, Philadelphia, PA **2005**, p. 1409.
[4] H. Postlind, A. Danielson, A. Lindgren, S. H. G. Andersson, *Drug Metab. Dispos.* **1998**, *26*, 289.
[5] S. H. G. Andersson, A. Lindgren, H. Postlind, *Drug Metab. Dispos.* **1998**, *26*, 528.
[6] J. Macek, P. Ptacek, J. Klima, *J. Chromatogr. B, Anal. Technol. Biomed. Life Sci.* **2009**, *877*, 968.
[7] M. Yadav, V. Upadhyay, V. Chauhan, G. Solanki, A. Jani, G. A. Baxi, P. Singhal, P. S. Shrivastav, *Chromatographia* **2010**, *72*, 255.
[8] B. B. Zhang, Z. J. Zhang, Y. Tian, F. G. Xu, *J. Chromatogr. B, Anal. Technol. Biomed. Life Sci.* **2005**, *824*, 92.
[9] R. Swart, P. Koivisto, K. E. Markides, *J. Chromatogr. A* **1998**, *828*, 209.
[10] A. Madhavi, G. S. Reddy, M. V. Suryanarayana, A. Naidu, *Chromatographia* **2008**, *68*, 399.
[11] V. Saxena, Z. Zaheer, M. Farooqui, *Indian J. Chem. Technol.* **2006**, *13*, 242.
[12] M. Puchalska, J. Zagrodzka, E. Czerniec-Michalik, M. Zezula, J. Chmiel, W. Luniewski, B Zagrodzki, *Przem. Chem.* **2012**, *91*, 358.
[13] Z. L. Xia, Z. Y. Chen, T. W. Yao, *Pharmazie* **2007**, *62*, 170.
[14] L. Palmer, L. Andersson, T. Andersson, U. Stenberg, *J. Pharm. Biomed. Anal.* **1997**, *16*, 155.
[15] D. G. Sankar, M. V. Krishna, D. V. P. Kumar, R. M. Latha, *Asian J. Chem.* **2005**, *17*, 2028.
[16] A. Baumann, U. Karst, *Expert Opin. Drug Metab. Toxicol.* **2010**, *6*, 715.
[17] A. Baumann, W. Lohmann, B. Schubert, H. Oberacher, U. Karst, *J. Chromatogr. A* **2009**, *1216*, 3192.
[18] W. Lohmann, R. Dotzer, G. Gutter, S. M. Van Leeuwen, U. Karst, *J. Am. Soc. Mass Spectrom.* **2009**, *20*, 138.
[19] A. Baumann, W. Lohmann, S. Jahn, U. Karst, *Electroanalysis* **2010**, *22*, 286.
[20] N. A. Mautjana, J. Estes, J. R. Eyler, A. Brajter-Toth, *Electroanalysis* **2008**, *20*, 2501.
[21] R. S. Nicholson, I. Shain, *Anal. Chem.* **1964**, *36*, 706.
[22] F. Marken, A. Neudeck, A. M. Bond, in *Electroanalytical Methods: Guide to Experiments and Applications* (Ed: F. Scholz), Springer, Berlin **2002**, p. 82.
[23] E. Laviron, *J. Electroanal.Chem.* **1979**, *101*, 19.
[24] O. Hammerich, J. H. P. Utley, L. Eberson, in *Organic Electrochemistry*, 4th ed. (Eds: H. Lund, O. Hammerich), Marcel Dekker, New York **2001**, p. 1008.
[25] H. J. Schäfer, in *Organic Electrochemistry*, 4th ed. (Eds.: H. Lund, O. Hammerich), Marcel Dekker, New York **2001**, p. 893.

Příloha 7

Electrochemical oxidation of fesoterodine and identification of its oxidation products using liquid chromatography and mass spectrometry

Kučerová, P.; **Skopalová**, **J.***; Kučera, L.; Hrbáč, J.; Lemr, K.

Electrochimica Acta **2015**, *159*, 131-139

Electrochimica Acta 159 (2015) 131–139

Contents lists available at ScienceDirect

Electrochimica Acta

journal homepage: www.elsevier.com/locate/electacta

Electrochemical oxidation of fesoterodine and identification of its oxidation products using liquid chromatography and mass spectrometry

Pavla Kučerová [a], Jana Skopalová [b,*], Lukáš Kučera [a], Jan Hrbáč [c], Karel Lemr [a]

[a] Regional Centre of Advanced Technologies and Materials, Department of Analytical Chemistry, Faculty of Science, Palacký University, 17. listopadu 12, 771 46 Olomouc, Czech Republic
[b] Department of Analytical Chemistry, Faculty of Science, Palacký University, 17. listopadu 12, 771 46 Olomouc, Czech Republic
[c] Department of Chemistry, Faculty of Science, Masaryk University, Kamenice 5, 625 00 Brno, Czech Republic

ARTICLE INFO

Article history:
Received 9 July 2014
Received in revised form 29 January 2015
Accepted 29 January 2015
Available online 31 January 2015

Keywords:
Fesoterodine
Oxidation
Hydrolysis
Voltammetry
Mass spectrometry

ABSTRACT

The electrochemical behavior of fesoterodine (FES), an antimuscarinic drug used for the treatment of urge incontinence and overactive bladder, was investigated using linear sweep and cyclic voltammetry at a stationary and rotating disc glassy carbon electrodes. A single two-electron anodic signal of FES was observed in neutral buffered aqueous methanolic solutions. Kinetics of alkaline hydrolysis of FES to its active metabolite 5-hydroxymethyl tolterodine was investigated by time dependent linear sweep voltammetry. Controlled potential electrolysis of FES solutions was performed at platinum gauze electrode in aqueous-methanolic media. Electrolyzed solutions were analyzed using ultra performance liquid chromatography with electrospray ionization quadrupole time-of-flight mass spectrometry. Two main products of electrochemical oxidation of fesoterodine were identified as 5-formyl fesoterodine (isobutyric acid 2-(3-diisopropylamino-1-phenyl-propyl)-4-formyl-phenyl ester) and *N*-desisopropylated fesoterodine (isobutyric acid 4-hydroxymethyl-2-(3-isopropylamino-1-phenyl-propyl)-phenyl ester). The mechanism of the electrochemical oxidation of FES has been proposed and confirmed using on-line electrochemistry/mass spectrometry with porous glassy carbon electrode.

1. Introduction

Fesoterodine fumarate (FES, **1** in Scheme 1) is a muscarinic receptor antagonist used for the treatment of urinary urge incontinence (UUI) and other symptoms associated with an overactive bladder. This drug also increases functional bladder volume [1]. Isobutyric acid 2-((*R*)-3-diisopropylammonium-1-phenylpropyl)-4-(hydroxymethyl) phenyl ester hydrogen fumarate (IUPAC) is the form of FES used in pharmaceutical preparations commercially available under the trade name Toviaz. Fesoterodine fumarate is white to off-white powder freely soluble in methanol (574 mg cm^{-3}), water (542 mg cm^{-3}), acetone (205 mg cm^{-3}), 0.9% NaCl solution (551 mg cm^{-3}), very slightly soluble in toluene (0.14 mg cm^{-3}) and practically insoluble in heptane (0.03 mg cm^{-3}). The melting point of FES is 105 °C and the pK_a value is (10.31 ± 0.01) at 23.4 °C [2].

According to recent studies, fesoterodine, a novel drug, proves superior efficacy in treatment of UUI over an older antimuscarinic drug tolterodine [3,4]. With tolterodine, FES shares the main active metabolite, 5-hydroxymethyl tolterodine (5-HMT, **2** in Scheme 1). After oral administration, FES is hydrolyzed in plasma by nonspecific esterases to 5-HMT, which is further metabolized principally via cytochromes P450 2D6 and P450 3A4 in the liver to its inactive metabolites – namely carboxy, carboxy-*N*-desisopropyl and *N*-desisopropyl metabolite [5]. All of the pharmacodynamic effects of FES in human body are thought to be mediated via 5-HMT [6].

Knowledge of drug stability is important not only for the pharmaceutical application but also for its analysis. It can prevent incorrect interpretation of the results. The stability of FES was investigated under acidic, basic, thermal, oxidative, and photolytic stress conditions. 10 % and 32 % of the drug was degraded after 6 h in 1 M HCl and 2 M HCl, respectively, 100 % after 36 h in 2 M HCl. FES was found to be highly susceptible to alkaline hydrolysis (Scheme 1) as its complete degradation occurred already after 15 min in 0.01 M NaOH (95 % after 10 min). FES was quite stable under oxidative conditions (in 2% H_2O_2).

* Corresponding author. Tel.: +420 585634442; fax: +420 585634433.
E-mail address: jana.skopalova@upol.cz (J. Skopalová).

http://dx.doi.org/10.1016/j.electacta.2015.01.190
0013-4686/

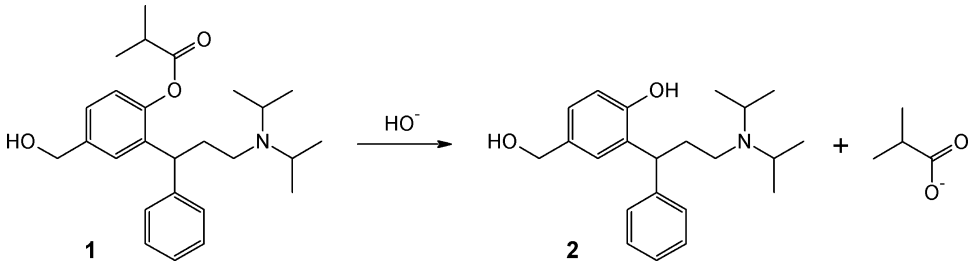

Scheme 1. Hydrolysis of fesoterodine (**1**) to 5-hydroxymethyl tolterodine (**2**).

Under thermal conditions, 17 % of FES was degraded after 36 h at 60 °C. UV-A light (365 nm) had no significant photodegradation effect on FES. On the other hand, its exposure to UV-C light (254 nm) for 6 h resulted in full degradation (for 45 min 60% degradation). The main degradation product was 5-HMT (*m/z* 342), minor products with *m/z* 356, 175, 284, 365 and 393 were also formed and identified using LC/ESI-MS [7]. Its photodegradation products appeared at *m/z* 265, 284, 293, 311, 342, 365 and 370 [8].

A limited number of publications have been focused on the determination of FES. Sangoi et al. developed methods for its determination in pharmaceutical formulations using liquid chromatography-tandem mass spectrometry with positive electrospray ionization (LC-ESI-MS/MS) [9], second-order derivative UV spectrophotometric method [10] and capillary zone electrophoresis [11]. Parekh at al. carried out the first simultaneous determination of FES and 5-HMT in human plasma samples using LC-ESI-MS/MS [12].

Combination of electrochemical methods with LC/MS identification of reaction products is increasingly used for the study of electrochemical oxidation pathways of various drugs [13–16]. LC/ESI-MS has been recently used for elucidation of electrochemical oxidation of the structurally related drug tolterodine [17]. To the best of our knowledge, no electroanalytical study of FES has been published yet. In this work, electro-oxidation of FES was studied using voltammetric techniques and coulometry. Controlled potential electrolysis was used for the preparation of FES oxidation products (OP) and ultra performance liquid chromatography with electrospray ionization mass spectrometry (UPLC/ESI-MS) for their identification.

2. Experimental

2.1. Reagents

(*R*)-fesoterodine fumarate (99%) was obtained from IS Chemical Technology, China. 5-hydroxymethyl tolterodine was synthesized from (*R*)-fesoterodine fumarate [17]. Methanol (p.a., Lach-Ner Czech Republic), acetonitrile (HPLC gradient grade, Sigma–Aldrich, Czech Republic), ammonium acetate (p.a., >98.0%, Lach-Ner Czech Republic) and ultrapure water (Merck Millipore, Darmstadt, Germany) were used. Britton-Robinson (BR) buffers were prepared from phosphoric acid, acetic acid and boric acid (0.04 mol dm^{-3} each, analytical grade, Lachema, Czech Republic), pH values were adjusted with 0.2 M NaOH (analytical grade, Lach-Ner Czech Republic). Ammonium formate buffer solutions were prepared from 0.1 mol dm^{-3} formic acid (p.a., for HPLC, 50% in water, Fluka) and ammonia (p.a, 25% in water, Lach-Ner Czech Republic). Aqueous calibration standards Duracal, pH 4, 7 and 10 (Hamilton, Bonaduz, Switzerland) were used for calibration of a pH-meter inoLab720 pH with a combined glass electrode SenTix41 (all WTW, Weilheim, Germany).

2.2. Voltammetric measurements

Voltammetric measurements were performed using Autolab PGSTAT128N with 663 VA Stand and NOVA 1.10 software (Metrohm Autolab, the Netherlands). A three-electrode system consisted of a glassy carbon working electrode (GCE, Bioanalytical Systems, USA, disk diameter 3.0 mm, surface area 0.077 cm^2) or rotating GCE (Metrohm, disc diameter 2.0 mm, surface area 0.033 cm^2), a platinum wire auxiliary electrode and a saturated calomel reference electrode (SCE). The surface area of the working electrodes was estimated by voltammetry of 5 mmol dm^{-3} potassium ferrocyanide in 0.1 mol dm^{-3} potassium chloride (diffusion coefficient 0.656×10^{-5} cm^2 s^{-1} [18]). The working electrodes were polished with 0.05 μm alumina slurry on wet microcloth (Buehler, USA) and sonicated in distilled water for 10 s before each measurement. Linear sweep (LSV) and cyclic voltammograms (CV) were recorded at a scan rate of 100 mV s^{-1} or at arbitrary scan rates ranging from 5 to 500 mV s^{-1} where appropriate. Hydrodynamic measurements were carried out with angular velocity ranged from 52 rad s^{-1} to 314 rad s^{-1} and scan rate 5 mV s^{-1}. All experiments were performed in supporting electrolytes containing BR buffer solution of desired pH and methanol (1:1, v/v). To obtain convolution voltammograms LSV data were processed using eL-Chem Viewer software [19].

2.3. Controlled potential electrolysis

An apparatus for controlled potential electrolysis consisted of an OH-404 potentiostat (Radelkis, Budapest, Hungary) with a three-electrode system: platinum gauze working electrode (a cylinder 8 mm high and 8 mm diameter, surface area 11 cm^2), platinum auxiliary electrode placed in a separate cathode compartment and reference SCE. The electrolysis was performed at various values of constant potential in supporting electrolyte containing aqueous BR buffer solutions of pH 4 or 7 and methanol (1:1, v/v) under nitrogen atmosphere. The potential values 500, 1000 and 1150 mV were chosen for pH 4 and 200, 600 and 1000 mV for pH 7. All samples were electrolyzed in stirred solutions containing 0.5 mmol dm^{-3} fesoterodine fumarate (0.26 mg cm^{-3}) in a total volume of 1.2 cm^3 until the current decreased to its residual value.

Controlled potential coulometry was performed on Autolab PGSTAT128N (Metrohm Autolab) with a three-electrode system comprising of spectral graphite rod as a working electrode (surface area 5.42 cm^2), reference SCE and Pt auxiliary electrode placed in a cathode compartment separated from the anode part by a vycor frit. Supporting electrolyte containing BR buffer solutions of pH 7 and methanol (1:1, v/v) was electrolyzed at potential 1000 mV until the current reached its residual value (typically 3 μA). Then 0.05 mg of fesoterodine fumarate was added (c = 0.1 mmol dm^{-3}) and the solution was electrolyzed at 900 mV for about 2 h to reach the residual current value.

2.4. UPLC/MS analysis

An Acquity UPLC system (Waters, Milford, MA, USA) equipped with a binary solvent manager, sample manager, column manager and PDA detector was used. Separation was performed on a chromatographic Vertex Plus Column (50 mm × 2 mm, 1.8 μm) Blue Orchid (Knauer, Berlin, Germany). Mobile phase consisted of 0.01 mol dm^{-3} ammonium acetate in water (solvent A)/acetonitrile (solvent B), gradient elution was performed (% v/v): 0–5 min (10–80% B), 5–6 min (80% B), 6–7 min (80–10% B) and 7–10 min (10% B) with flow rate 0.4 cm^3 min^{-1}, the temperature of the autosampler and the column oven was 20 °C and 25 °C, respectively. The injection volume was 0.02 cm^3.

A QqTOF Premier mass spectrometer (Waters, Manchester, UK) coupled to the UPLC system provided elemental composition to confirm putative structures. The tuned electrospray ionization (ESI) parameters were as follows: spray voltage 3 kV (positive mode), source temperature 100 °C, sampling cone 30 V, desolvation temperature 150 °C, cone gas flow rate 38 dm^3 h^{-1} and desolvation gas flow rate 450 dm^3 h^{-1}. Nitrogen was used as a cone and desolvation gas, argon as a collision gas. Data were acquired using simultaneous scanning at lower collision energy (5 eV) and at higher energy applying collision energy ramp from 15 to 35 eV. Data were processed using MassLynx 4.1 software (Waters).

2.5. EC/MS experiment

Electrochemical oxidation of FES with on-line mass spectrometric detection of its oxidation products (EC/MS) was performed as follows: Potentiostat ADLC1 (Laboratorní přístroje, Prague, Czech Republic) with Model 5021A conditioning cell (ESA, Chelmsford, MA, USA) containing porous glassy carbon working electrode, Pd counter and a Pd/H_2 reference electrode, were used for FES oxidation at potentials 0, 400, 600, 700, 800 and 900 mV. Sample solutions consisting of supporting electrolyte: 0.1 mol dm^{-3} ammonium formate buffer solution (pH 5.5, 7.0 or 9.0)/methanol (1:1, v/v) and 0.1 mmol dm^{-3} FES were continuously infused into the electrochemical cell using NE-1002X syringe pump (New Era Pump Systems, Farmingdale, NY, USA) with flow rate 8 mm^3 min^{-1}. The stainless steel outlet tubing of the ESA cell was connected to the inlet of mass spectrometer via a coupler assembly (ESA Inc.). Agilent 1100 Series LC/MSD Trap (Agilent Technologies, Palo Alto, CA, USA) with electrospray ionization (ESI) interface was employed. ESI-MS conditions were as follows: positive ion mode, drying gas (N_2) flow rate 5 dm^3 min^{-1}, drying temperature 250 °C, nebulizer pressure 12 psi, capillary voltage −3.5 kV and an end plate offset −0.5 kV. Helium was used as a collision gas. Data were processed using DataAnalysis 3.3 software (Bruker Daltonik, Bremen, Germany).

3. Results and discussion

3.1. Electrochemical behavior of fesoterodine and its stability at various pH values

The cyclic voltammogram of FES (Fig. 1) in supporting electrolyte consisted of BR buffer solution pH 7.4 and methanol (1:1, v/v) shows one anodic peak at the potential of 750 mV. No current response was observed in reverse cathodic branch of voltammogram even if the potential was switched just behind the oxidation peak (at 820 mV), which indicates irreversibility of the electrode process. The wave-shaped cathodic branch of voltammogram suggests the presence of homogenous chemical reaction following the electron transport (EC mechanism) [20].

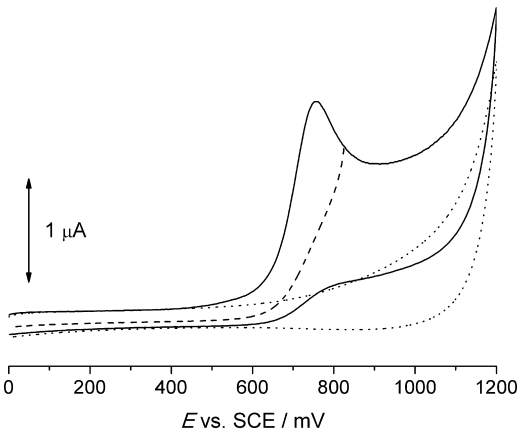

Fig. 1. Cyclic voltammogram of 0.1 mmol dm^{-3} fesoterodine (solid line) and supporting electrolyte 1:1 methanol/BR buffer pH 7.4 (dot line), scan rate 100 mV s^{-1}. The dash line represents cyclic voltammogram when the polarity was switched behind the oxidation peak (at 820 mV).

The stability of FES was investigated in neutral and alkaline solutions (pH 7, 9.5 and 12). Linear sweep voltammograms were recorded in different time intervals after mixing of FES stock solution in methanol with buffer solution. In the pH 7 the solution of FES provided a single oxidation peak at the potential of 780 mV (Fig. 2a) in all time intervals up to 25 h. A slight drop in the peak current (by 9 % in the first hour) resulted most likely from adsorption of FES on inner surface of the electrochemical cell. Adsorbability of the drug was confirmed by the following

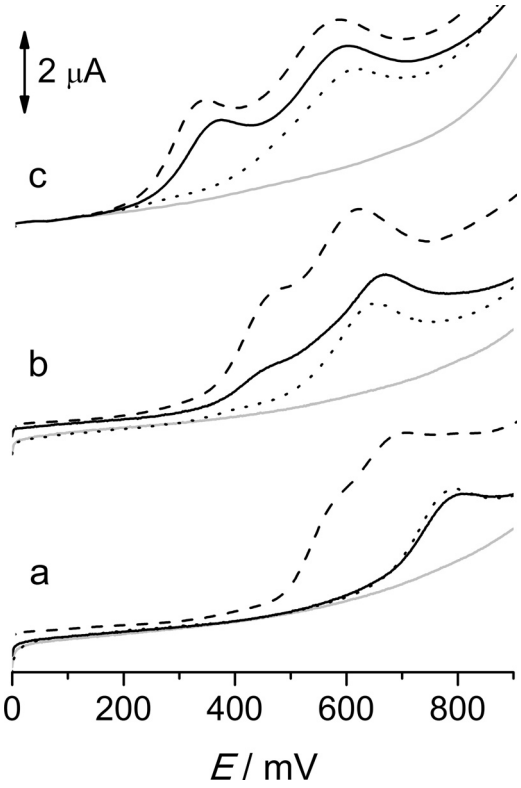

Fig. 2. Linear sweep voltammograms of 0.1 mmol dm^{-3} fesoterodine and 0.2 mmol dm^{-3} 5-hydroxymethyl tolterodine (- - -) in BR buffers pH 7 (a), 9.5 (b) and 12 (c). LSV of the supporting electrolyte methanol/BR buffer 1:1, v/v (——). FES solution was measured immediately after mixing of FES stock solution in methanol with BR buffer (0 min, ····) and after 180 min (180 min, ——), scan rate 100 mV s^{-1}.

experiment. The polished glassy carbon electrode was left in the 0.1 mmol dm^{-3} FES solution for five minutes. Then the electrode was properly washed by distilled water and transferred into pure electrolyte where the voltammetric peak of FES was recorded proving adsorption of the drug on the electrode surface.

In the solutions of pH 9.5 and pH 12 a new voltammetric peak at lower potential (450 mV and 350 mV, respectively) was recorded in addition to the FES peak at 660 mV and 580 mV, respectively (Fig. 2b and c). The new peak obtained in 180 min corresponds to the first oxidation signal of 5-hydroxymethyl tolterodine (5-HMT; 480 mV and 320 mV for pH 9.5 and 12, respectively; Fig. 2) which is the main metabolite of FES. Obviously, FES hydrolyzes to 5-HMT in alkaline solutions (Scheme 1) which is in agreement with literature [7]. The intensity of the new peak increased with time and reached the steady state values 80 nA and 1.3 μA for pH 9.5 and pH 12 (Fig. 3), respectively. In neutral solution of pH 7 (Fig. 2a), no peak of 5-HMT was observed on the voltammogram even after 25 h proving the stability of FES under these conditions.

The evolution of 5-HMT peak current in time (Fig. 3) enabled to evaluate the kinetics of alkaline hydrolysis of FES ester bond (Scheme 1). The ester hydrolysis is generally the second order reaction and its rate depends on concentration of both reactants [21]. Assuming the constant concentration of hydroxide (which is at pH 12 in hundredfold excess compared to FES concentration 0.1 mmol dm^{-3}) the second order reaction can be simplified to the pseudo first order reaction [21]. Under this assumption, the rate constant of FES hydrolysis was calculated from the equation $y = a(1 - e^{-krt}) + c$, where y is the peak current of 5-HMT in time t,a is the limit value of 5-HMT peak current, k_r is the rate constant and c is the 5-HMT peak current in time 0 s [22]. The rate constant was $(k_r \pm s) = (1.17 \pm 0.05) \times 10^{-3}$ s^{-1} at (23 ± 1) °C. Calculated half-time of FES hydrolysis (10 min) is in accordance with the literature data [7] considering that the content of 50% methanol used in our experiment can slow down the FES hydrolysis.

The influence of the scan rate on the CV response of FES was evaluated in methanol/aqueous BR buffer solution of pH 7.4 (1:1, v/v) (see Supplementary Information file). The anodic current peak of FES increased linearly with the square root of scan rate in the range 5–500 mV s^{-1}. The log i_p – log ν (i_p in nA, ν in mV s^{-1}) dependence was linear with the slope 0.49, which indicated diffusion controlled process. The FES oxidation peak shifted to more positive potential values with increasing scan rate. The E_p – log ν dependence was linear and its slope 41 mV per log unit. Assuming a totally irreversible system, for which E_p is shifted in a positive direction by 1.15$RT/\alpha F$ for tenfold increase in ν [23] the value of charge transfer coefficient $\alpha = 0.72$ (at 23 °C) was calculated. Similar value $\alpha = 0.71$ was obtained also from the equation

$$E_p - E_{p/2} = 1.857RT/\alpha F, \quad (1)$$

where $E_{p/2}$ is the potential where the current is at half the peak value [23].

The calibration dependence of FES anodic response was measured by LSV in the range from 0.01 to 1.0 mmol dm^{-3} in methanol/aqueous BR buffer solution pH 7.4 (1:1, v/v). The dependence was linear up to 0.1 mmol dm^{-3} with the slope (8.18 ± 0.05) μA dm^3 mmol^{-1}, and the intercept (0.022 ± 0.003) μA and the coefficient of determination equal to 0.9998. The linearity in the measured range confirmed diffusion controlled electrode process. Slight distortion of calibration curve observed at concentrations ranging from 0.1 to 1 mmol dm^{-3} (see Supplementary Information file) is due to adsorption of FES on the electrode surface as it was described above.

The oxidation of FES is pH-dependent (Fig. 4). No response was observed in strongly acidic media. A distinguishable oxidation peak evolved at pH ≥ 4 and its current increased up to pH 7.5. For pH > 7.5, the FES current response had not any specific trend and its height ranged possibly due to fast hydrolysis from 2.0 to 2.5 μA.

FES peak potentials shifted to lower values with increasing pH up to pH 10 (Fig. 4). The regression straight line fitted to the E_p–pH dependence had the slope values (−62 ± 3) mV pH^{-1} in the pH range 4–10. The slope close to the theoretical value −59 mV pH^{-1} indicates that the number of protons and electrons are equal. In more alkaline buffer solutions (pH > 10) peak potential was almost constant. The break point at pH 10 could correspond to the apparent dissociation constant of FES (pK = 10.31) [2].

Investigation of FES oxidation behavior using LSV with rotating disc electrode supported the results of CV study and yielded some new information. Fig. 5 shows a set of voltammograms recorded with FES solutions at different pH. As in LSV with stationary electrode, the limiting current increased with increasing pH reaching the maximum in alkaline solutions. Simultaneously, the steepness of the curves increased indicating higher reversibility of the electrochemical process. Dependence of limiting current on square root of rotation velocity (inset of Fig. 5) shows a nonlinear course typical for kinetically controlled process in acidic media whereas linear course obtained in neutral and alkaline solutions reflects diffusion character of the current. Moreover, in alkaline media a new oxidation wave revealed at more positive potentials which was not distinguishable on the LSV with stationary

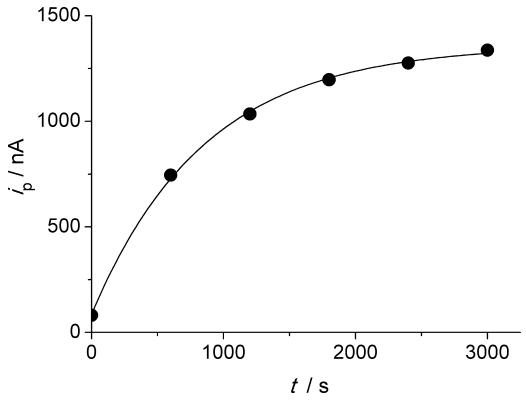

Fig. 3. Time evolution of CV peak of 5-hydroxymethyl tolterodine formed by hydrolysis of 0.1 mmol dm^{-3} FES in methanol/aqueous BR buffer solution of pH 12 (1:1, v/v), scan rate 100 mV s^{-1}.

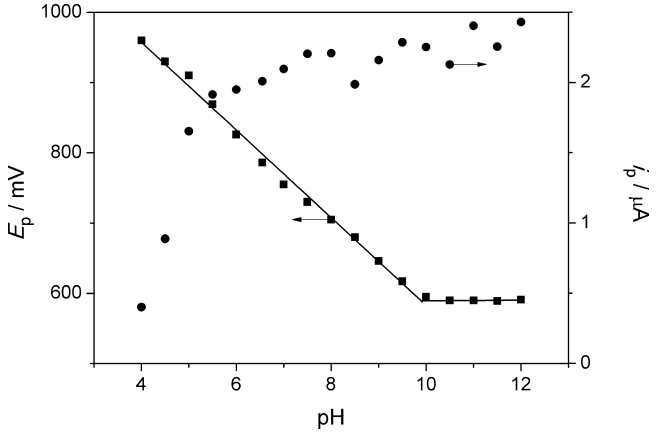

Fig. 4. Dependence of fesoterodine CV peak current (●) and potential (■) on pH. Concentration of FES: 0.1 mmol dm^{-3}, methanol/BR buffer (1:1, v/v), scan rate: 100 mV s^{-1}.

electrode. As the pH was raised, the half-wave potential of this second wave shifted toward a less positive potential by about −8 mV pH^{-1} and its limiting current increased. This current wave appertained most likely to the oxidation of some product formed on the electrode at lower potentials.

Number of electrons n involved in electrode process was determined by constant-potential coulometry. Total charge passed through the electrolytic cell with spectral graphite rod electrode and 0.1 mmol dm^{-3} FES solution in BR buffer pH 7 and methanol (1:1) of total volume 1 cm^3 was 0.0182 C. That corresponds to 1.89 electrons exchanged per FES molecule indicating two-electron oxidation.

The same number of electrons was also confirmed using convolutive procedure [24] applied on linear sweep voltammograms recorded at 10 and 50 mV s^{-1}. For convolution, the digitized voltammetric data were first transformed into dimensionless form using Eq. (2) [19]

$$\Psi(t) = \frac{I(t)}{FAc\sqrt{\frac{DF\nu}{RT}}}, \quad (2)$$

where $\Psi(t)$ is the dimensionless current, $I(t)$ is the current data in studied voltammogram (A), F is Faraday constant (C mol^{-1}), A electrode area (cm^2), c concentration (mol cm^{-3}), D diffusion coefficient (cm s^{-1}), ν scan rate (V s^{-1}), R universal gas constant (J K mol^{-1}) and T thermodynamic temperature (K). Afterwards, the dimensionless data were transformed into numerical semi-integrated form using the Eq. (3) [25]:

$$J(k\Delta t) = \frac{1}{\sqrt{\pi}}\sum_{j=1}^{j=k}\frac{\Psi(j\Delta t - \frac{1}{2}\Delta t)}{(k-j+\frac{1}{2})}, \quad (3)$$

where $\Psi(k)$ is an array which contains the dimensionless current data, k is the index of each individual reading contained in the array $\Psi(k)$, Δt is the time between readings of dimensionless current and j represents any value from 0 up to k.

The above described convolution results in a wave-like response, the height of which represents the number of electrons n. The slope of linear regression function fitted to the RDE data of $i_{lim} - \omega^{1/2}$ dependence at pH 7 were used for estimation of diffusion coefficient from the Levich Eq. (4) [26]:

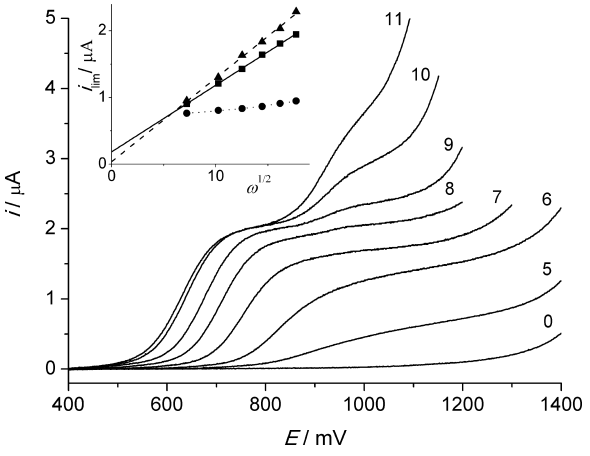

Fig. 5. Linear sweep voltamograms of 0.1 mmol dm^{-3} fesoterodine recorded with RDE in methanol/aqueous BR buffer solution (1:1, v/v) of various pH values (denoted as a number at respective curves, 0 – supporting electrolyte: methanol/BR buffer pH 4). Rotational velocity: 209 rad s^{-1}, scan rate: 5 mV s^{-1}. Inset: dependence of fesoterodine limiting current on the square root of rotational velocity at pH 5.5 (●), pH 7 (■) and pH 10, 1st wave (▲). All voltamograms were measured immediately after mixing of FES with the supporting electrolyte.

$$i_d = 0.62nFAD^{2/3}\nu^{-1/6}\omega^{1/2}c = B\omega^{1/2}, \quad (4)$$

where ν is kinematic viscosity and c bulk concentration of electroactive species. For electrode area $A = 0.033$ cm^2, kinematic viscosity $\nu = 0.01676$ cm^2 s^{-1} for water/methanol mixture (1:1, v/v) at 298.15 K [27], bulk concentration of FES 1×10^{-7} mol cm^{-3} and the slope of i_{lim}–$\omega^{1/2}$ dependence $B = (9.98 \pm 0.30) \times 10^{-8}$ A rad$^{1/2}$ s$^{-1/2}$ at pH 7, the diffusion coefficient value $D = (1.45 \pm 0.07) \times 10^{-6}$ cm2 s^{-1} was calculated. The convolution wave heights corresponding to number of electrons obtained using this diffusion coefficient were $n = 2.1$ and $n = 2.2$ for scan rates 10 mV s^{-1} and 50 mV s^{-1}, respectively (see Supplementary Information file).

3.2. Controlled potential electrolysis and UPLC/MS analysis of fesoterodine oxidation products

Series of experiments with controlled potential electrolysis of FES were performed on a large surface Pt electrode in methanol/aqueous BR buffer solutions of pH 4 and 7 to characterize oxidation products. Higher pH was not used due to considerable lability of FES in alkaline media. The potential values suitable for exhaustive electrolysis were selected according to the current peak position in cyclic voltammograms recorded at both pH values (1000 and 1150 mV for pH 4 and 600 and 1000 mV for pH 7). Electrolyzed solutions of FES were directly analyzed using UPLC/ESI-MS. In order to eliminate the influence of nonelectrolytic reaction of FES, the chromatograms and mass spectra of electrolyzed solutions were compared to control samples. They were obtained by electrolysis of FES solutions at potentials of 500 and 200 mV for pH 4 and 7, respectively. Under these conditions no electrochemical reaction of FES proceeded.

FES control samples and FES standard solution rendered a peak with retention time (t_R) of 3.0 min and an ion $[M+H]^+$ at m/z 412 (Fig. 6a) providing fragment ions at m/z 370 (loss of propene, cleavage of bonds **a** or **c**), m/z 342 (loss of propene and CO, cleavage of bonds **a** and **b**), m/z 300 (loss of two molecules of propene and loss of CO, cleavage of bonds **a, b** and **c**), m/z 282 (loss of propene, i.e. cleavage of bond **c** and iso-butyric acid (or propene, CO and H_2O), i.e. cleavage of bonds **d** (or **a**, **b** and **d**), respectively), the most intensive ion at m/z 223 (loss of diisopropylamine and iso-butyric acid, cleavage of bonds **e** and **d**), m/z 195 (loss of diisopropylamine, ethene and iso-butyric acid, cleavage of bonds **e**, **f** and **d**), m/z 167 (loss of diisopropylamine, ethene, iso-butyric acid and CO, cleavage of bonds **e**, **f, d** and **g**). The fragmentation spectrum of FES corresponds to the spectrum reported in the literature [12]. Described fragmentation pathway for FES and other compounds represent probable but not necessary all alternative fragmentations. Detail study of the fragmentation is out of scope of this paper.

Electrolysis of all FES samples revealed an oxidation product OP1 with t_R 3.3 min and molecular ion $[M+H]^+$ at m/z 410. The highest amount of OP1 was found in samples electrolyzed at higher potentials (1000 and 1150 mV for pH 7 and 4, respectively). According to molecular formula (Table 1) OP1 has two hydrogen atoms less in comparison with FES. The most intensive fragmentation peak of OP1 MS spectrum (Fig. 6b) at m/z 239 corresponds to the loss of propene, CO (or 2-methylprop-1-ene-1-one) and diisopropylamine. In comparison with FES there is no loss of H_2O, which could indicate different substitution in the position 5. By analogy to tolterodine oxidation product 5-formyl tolterodine [17], OP1 could be 5-formyl fesoterodine (Scheme 2).

The product of FES electrolysis OP2 (t_R 2.7 min, $[M+H]^+$ at m/z 370) was mostly formed in neutral media at the potential of 1000 mV (Table 2). Fragment ions of OP2 MS spectrum (Fig. 6c) are identical to fragment ions $m/z < 370$ of FES MS spectrum. It suggests N-dealkylation of FES. A compound with the same

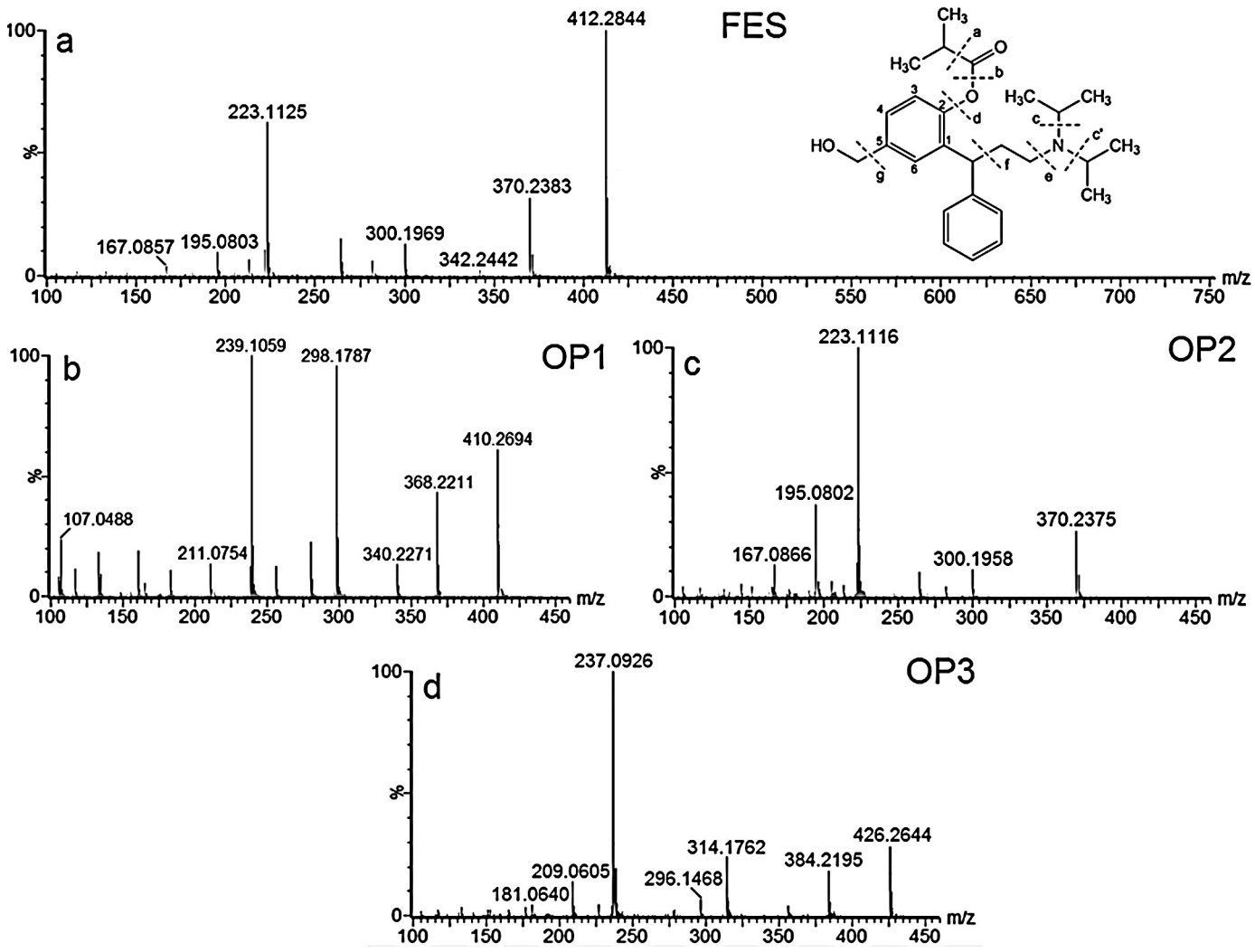

Fig. 6. MS spectra of fesoterodine standard (a) and its oxidation products OP1 (b), OP2 (c), OP3 (d) acquired after electrolysis with Pt-electrode at 1000 mV in the solution of pH 7. Spectra were obtained at higher energy using collision energy ramp from 15 to 35 eV with precursor ion selection.

molecular mass was found as a photodegradation product of FES after irradiation by UV-C light (100–280 nm) [8].

An oxidation product OP3 (t_R 2.5 min, $[M+H]^+$ at *m/z* 426) was more polar than FES and was preferably formed during FES electrolysis at higher potentials (1150 and 1000 mV in acidic and neutral media, respectively). According to its molecular formula (Table 1) OP3 has one extra oxygen atom and two hydrogen atoms less in comparison with FES. The most intensive fragment ion of its MS spectrum (Fig. 6d) at *m/z* 237 corresponds to the same bond cleavage as with the most intensive fragment ion of FES (the loss of diisopropylamine and isobutyric acid). An OP3 fragment ion at *m/z* 153 corresponds to the loss of diisopropylamine, ethene, isobutyric acid and two molecules of CO, which confirms the presence of four atoms of oxygen in the structure of OP3. The product OP3 could be

Table 1
UPLC/MS analysis of fesoterodine and its oxidation products.

Compound	t_R/min	$[M+H]^+$ (*m/z*)	Molecular formula	Error (ppm)
Fesoterodine	3.0	412.2844	$C_{26}H_{38}NO_3$	−1.9
OP1	3.3	410.2694	$C_{26}H_{36}NO_3$	−0.2
OP2	2.7	370.2375	$C_{23}H_{32}NO_3$	−1.9
OP3	2.5	426.2644	$C_{26}H_{36}NO_4$	0.0

t_R – retention time, Error – relative difference between theoretical and experimental ion mass.

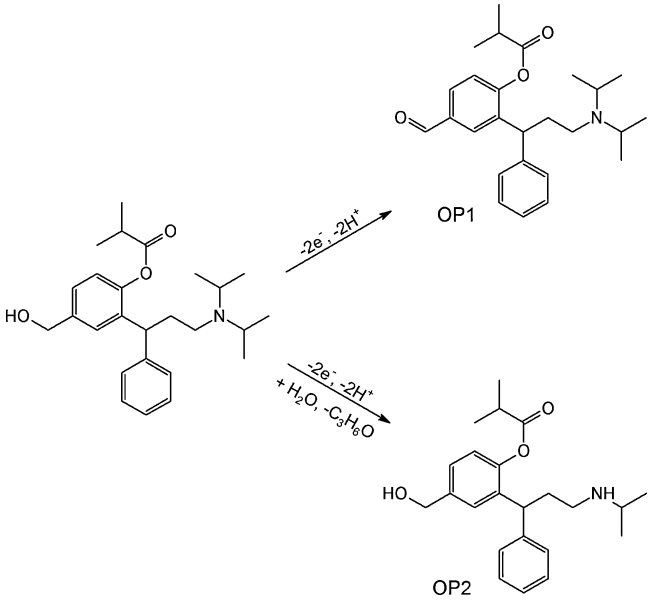

Scheme 2. Proposed mechanism of electrochemical oxidation of fesoterodine.

Table 2
Peak areas of fesoterodine, its oxidation products and 5-hydroxymethyl tolterodine in FES standard solution and FES solution electrolyzed at the potential *E* in methanolic aqueous media of pH 4 and 7 after 20 min electrolysis.

Media	E/mV	FES *m/z* 412	5-HMT *m/z* 342	OP1 *m/z* 410	OP2 *m/z* 370	OP3 *m/z* 426
FES standard	–	18175	475	0	0	0
pH 4	500	6409	344	88	3	1
pH 4	1000	5066	3	1607	51	29
pH 4	1150	1285	0	2834	52	266
pH 7	200	6547	330	273	13	1
pH 7	600[a]	6135	9	1221	87	8
pH 7	1000[b]	5119	5	4159	177	164

[a] the time of electrolysis 40 min.
[b] the time of electrolysis 48 min.

formed by hydroxylation of OP1. The hydroxyl group could be most likely substituted on the substituted benzene ring.

The main metabolic product of FES, 5-HMT, was present in most samples, even in FES standard. 5-HTM was not electrochemically formed from FES. Amount of 5-HMT was decreasing with higher potential used for electrolysis due to its oxidative conversion to several different products. MS signals of these products were of too low intensity to allow reliable identification of the respective compounds. The changes of the amount of FES, its oxidation products and 5-HMT expressed as peak areas are summarized in the Table 2.

On-line EC/MS experiment was performed to compare and consolidate the results obtained using voltammetric techniques with those of bulk electrolysis coupled with UPLC/ESI-MS identification of oxidation products. On-line EC/MS enables to detect unstable products that may not be found by long-term electrolysis off-line coupled to LC/MS system. FES solution in 1:1 (v/v) mixture of methanol and ammonium formate buffer of pH 5.5, pH 7 and pH 9 was continuously pumped through flow cell containing porous glassy carbon electrode. Constant potential in the range from 0 to 900 mV (vs. Pd/H_2 reference electrode) was applied on the electrode. The electrode potential of 0 V vs. Pd/H_2 reference electrode inbuilt into the flow-through cell corresponds to 305 mV, 234 mV and 171 mV vs. SCE at pH 5.5, pH 7.0 and pH 9.0, respectively. At the flow rate 8 $mm^3\,min^{-1}$ oxidation products were detected within 2 min after their formation in the cell. Fig. 7 shows changes of signal intensity of isolated ions of parent molecule *m/z* 412 and two most abundant products OP1 (*m/z* 410) and OP2 (*m/z* 370). It is evident that both products started to form at the same potential in acid and neutral media. In alkaline solution, formation of OP2 was preferred and started at lower potential.

Product OP3 (*m/z* 426) did not occur on MS spectra in the on-line EC/MS experiment which supports our supposition that it is a side-reaction product of long term electrolysis at higher potentials.

3.3. Mechanism of electrochemical oxidation of fesoterodine

Voltammetric experiments revealed that the oxidation of FES proceeds in one irreversible two-electron and two-proton transfer step in acidic and neutral media. The 5-formyl fesoterodine (OP1) was found to be the most abundant oxidation product of the bulk electrolysis of FES solution confirming benzyl alcohol group as the oxidizable moiety of FES (Scheme 2). The oxidation of substituted benzyl alcohols in acetonitrile provides a corresponding benzaldehyde via ECEC mechanism [28]. The oxidation mechanism involves reversible one electron transfer in which a radical cation is formed and subsequently deprotonated in a rate determining first order chemical process [29] before the release of the second electron and proton. Oxidation pathway of FES 5-hydroxymethyl group could be most likely similar. Higher pH accelerates the release of proton from the cation radical that can be observed as the increase of voltammetric current in neutral and alkaline media (Fig. 4).

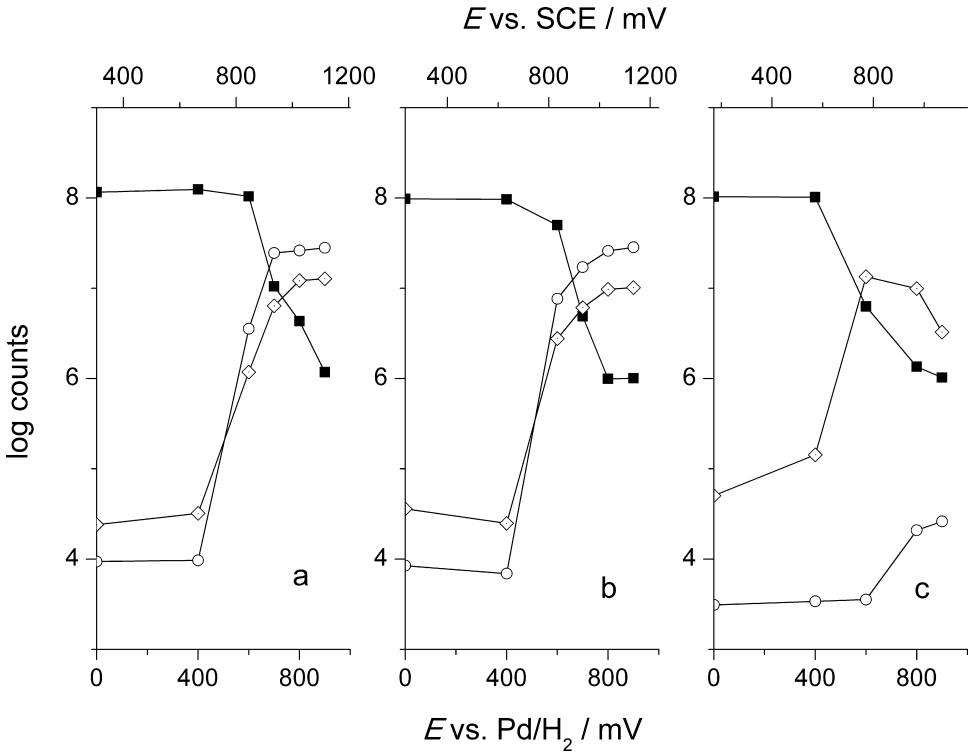

Fig. 7. Logarithm of signal intensity at different potentials of fesoterodine electrolysis in EC/MS system. Supporting electrolyte: methanol/aqueous ammonium formate buffer solution of pH 5.5 (a), pH 7.0 (b) and pH 9.0 (c) (1:1, v/v), fesoterodine concentration 0.1 mmol dm^{-3}. Isolated ions *m/z* 412 (■), *m/z* 410 (○) and *m/z* 370 (◈).

It is known that benzyl alcohol and anisyl alcohol oxidized in acetonitrile provide highly reactive radical cations that form polymers [29,30]. Unlike these alcohols no formation of polymer oxidation products of FES was observed. The 5-formyl fesoterodine may be subject to subsequent hydroxylation (product OP3, Fig. 6d) under conditions of long-term bulk electrolysis in aqueous media at sufficiently high potentials.

Anodic *N*-dealkylation was observed as another oxidation reaction of FES (product OP2, Scheme 2). The anodic oxidation of tertiary amines has been studied in non-aqueous [31], mixed acetonitrile/aqueous [32] and aqueous alkaline media [33,34]. It proceeds via ECE mechanism involving one electron transfer from the nitrogen atom and subsequent loss of a proton from vicinal alkyl leading to the formation of neutral radical. Disproportionation or subsequent oxidation of this radical and reaction with water provide *N*-dealkylated secondary amine and aldehyde as the final products. We have found that oxidative *N*-dealkylation of FES can proceed also in acidic media. Kinetically controlled voltammetric current in acidic solutions, equal number of protons and electrons involved in electrochemical process and a break point at pH = 10 corresponding to the dissociation constant of amino group of FES could indicate that the deprotonation of the ammonium ion precedes the oxidative *N*-dealkylation. Therefore, higher pH facilitates the electron transfer reaction and more OP2 product can be formed in neutral and alkaline solutions as it was detected by EC/MS method.

Overall two-electron process found by coulometric as well as voltammetric convolution analysis and simultaneous formation of both OP1 and OP2 products suggest that oxidation of FES proceeds either on benzyl alcohol or alkyl amino moiety. A product oxidized at both centers with hypothetical *m*/*z* 368 was not found either in UPLC/MS or in EC/MS spectra. Finally, a second voltammetric wave recorded by LSV with RDE in alkaline solutions likely corresponds to oxidative *N*-dealkylation of secondary amine formed in the first oxidation step [34].

4. Conclusions

Voltammetric techniques, controlled potential electrolysis combined with UPLC/ESI-MS and on-line EC/MS were used for investigation of electrochemical behavior of FES and identification of its oxidation products. In the FES molecule the hydroxymethyl group and tertiary *N*-alkyl amino group were revealed as the moieties undergoing electrochemical oxidation: dehydrogenation and *N*-dealkylation, respectively. Both reaction centers are susceptible also to the enzymatic oxidation by cytochrome P450 *in vivo* [5].

An enzymatic hydrolysis is the main metabolic transformation of FES forming active metabolite 5-HMT in living organisms. This product also arises from alkaline hydrolysis of FES and provides an anodic peak at lower potential than the parent substance. The evolution of 5-HMT peak current in time enabled to evaluate the reaction kinetics and determine the hydrolysis rate constant of FES which is a very important parameter in terms of the stability of the drug.

As resulted from this work, the combination of electrochemical techniques with (LC)/MS may serve as a powerful tool to detect reactive moieties in molecules and to elucidate mechanisms of electrochemical reactions. Generally, the approach could be usable during drugs development for screening of prospective products of oxidative metabolism as well as for electrosynthesis of respective metabolites. From analytical point of view the knowledge of principle and mechanism of reaction proceeding at the working electrode in the electrochemical cell is also useful for development of sensitive analytical methods for determination of electroactive drugs and their metabolites using various electrochemical techniques.

Acknowledgements

The authors gratefully acknowledge the financial support by the Ministry of Education, Youth and Sports of the Czech Republic (project LO1305). Pavla Kučerová acknowledges the Operational Program Education for Competitiveness – European Social Fund (project CZ.1.07/2.3.00/30.0041), Lukáš Kučera the project of Palacký University in Olomouc IGA_PrF_2014031, Jana Skopalová and Karel Lemr the Czech Science Foundation project P206/12/1150.

Appendix A. Supplementary data

Supplementary data associated with this article can be found, in the online version, at http://dx.doi.org/10.1016/j.electacta.2015.01.190.

References

[1] P. Cole, Fesoterodine, an advanced antimuscarinic for the treatment of overactive bladder: A safety update, Drug Future 29 (2004) 715.
[2] Pfizer Canada Inc., Toviaz (fesoterodine fumarate) – Product Monograph, Kirkland, Quebec, 2014.
[3] C.R. Chapple, P.E. Van Kerrebroeck, K.P. Junemann, J.T. Wang, M. Brodsky, Comparison of fesoterodine and tolterodine in patients with overactive bladder, BJU Int. 102 (2008) 1128.
[4] S. Herschorn, S. Swift, Z.H. Guan, M. Carlsson, J.D. Morrow, M. Brodsky, J. Gong, Comparison of fesoterodine and tolterodine extended release for the treatment of overactive bladder: a head-to-head placebo-controlled trial, BJU Int. 105 (2010) 58.
[5] P. Ellsworth, S.J. Berriman, M. Brodsky, Fesoterodine: a new agent for treating overactive bladder, Am. J. Manag. Care 15 (2009) S115.
[6] B. Malhotra, E. Darsey, P. Crownover, J. Fang, P. Glue, Comparison of pharmacokinetic variability of fesoterodine vs. tolterodine extended release in cytochrome P450 2D6 extensive and poor metabolizers, Br. J. Clin. Pharmacol. 72 (2011) 226.
[7] M.S. Sangoi, V. Todeschini, M. Steppe, Fesoterodine stress degradation behavior by liquid chromatography coupled to ultraviolet detection and electrospray ionization mass spectrometry, Talanta 84 (2011) 1068.
[8] M.S. Sangoi, V. Todeschini, G.K. Goelzer, M. Steppe, Photochemistry of a novel antimuscarinic drug fesoterodine and identification of its photodegradation products by LC-ESI-MS studies, J. Photochem. Photobiol. A-Chem. 256 (2013) 16.
[9] M.S. Sangoi, M. Steppe, Determination of fesoterodine in pharmaceutical formulations by using liquid chromatography-tandem mass spectrometry, Eur. J. Mass Spectrom. 16 (2010) 653.
[10] M.S. Sangoi, V. Todeschini, M. Steppe, Second-Order Derivative UV Spectrophotometric Method for the Determination of Fesoterodine and Comparison with LC, CE and LC-MS/MS in Commercial Extended-Release Tablets, Acta Chim. Slov. 59 (2012) 136.
[11] M.S. Sangoi, V. Todeschini, M. Steppe, Determination of Fesoterodine in a Pharmaceutical Preparation by a Stability-Indicating Capillary Zone Electrophoresis Method, J. AOAC Int. 96 (2013) 1308.
[12] J.M. Parekh, M. Sanyal, M. Yadav, P.S. Shrivastav, Investigation of ex vivo stability of fesoterodine in human plasma and its simultaneous determination together with its active metabolite 5-HMT by LC-ESI-MS/MS: Application to a bioequivalence study, J. Chromatogr. B 913 (2013) 1.
[13] J.G. Teixeira, A. Veiga, A.J.P. Carvalho, D.M. Teixeira, Electro-oxidation of carbamazepine metabolites: Characterization and influence in the voltammetric determination of the parent drug, Electrochim. Acta 108 (2013) 51.
[14] U. Bussy, V. Ferchaud-Roucher, I. Tea, M. Krempf, V. Silvestre, M. Boujtita, Electrochemical oxidation behavior of Acebutolol and identification of intermediate species by liquid chromatography and mass spectrometry, Electrochim. Acta 69 (2012) 351.
[15] R.G. de Lima, P.S. Bonato, R.S. da Silva, Analysis of albendazole metabolites by electrospray LC-MS/MS as a probe to elucidate electro-oxidation mechanism of albendazole, J. Pharm. Biomed. Anal. 32 (2003) 337.
[16] E. Nouri-Nigjeh, H.P. Permentier, R. Bischoff, A.P. Bruins, Electrochemical Oxidation by Square-Wave Potential Pulses in the Imitation of Oxidative Drug Metabolism, Anal. Chem. 83 (2011) 5519.
[17] P. Macikova, J. Skopalova, P. Cankar, B. Papouskova, R. Strakova, D. Jirovsky, V. Maier, Electrochemical Oxidation of Tolterodine, Electroanalysis 25 (2013) 205.
[18] S.J. Konopka, B. McDuffie, Diffusion Coefficients of Ferri- and Ferrocyanide Ions in Aqueous Media Using Twin-Electrode Thin-layer Electrochemistry, Anal. Chem. 42 (1970) 1741.

[19] J. Hrbac, V. Halouzka, L. Trnkova, J. Vacek, eL-Chem Viewer: A Freeware Package for the Analysis of Electroanalytical Data and Their Post-Acquisition Processing, Sensors 14 (2014) 13943.
[20] D. Jadreško, M. Zelić, Cyclic multipulse voltammetric techniques. Part II: *EC* mechanism, J. Electroanal. Chem. 714–715 (2014) 30.
[21] I.N. Levine, Physical Chemistry, Sixth Edition, McGraw-Hill, New York, 2009, pp. 518–523.
[22] R. Brdicka, J. Dvorak, Zaklady fysikalni chemie, Akademia, Praha, 1977, pp. 661–663.
[23] A.J. Bard, L.R. Faulkner, Electrochemical Methods: Fundamentals and Applications, Second Edition, John Wiley and Sons, New York, 2001, pp. 236.
[24] C.L. Bentley, A.M. Bond, A.F. Hollenkamp, P.J. Mahon, J. Zhang, Applications of Convolution Voltammetry in Electroanalytical Chemistry, Anal. Chem. 86 (2014) 2073.
[25] A.J. Bard, L.R. Faulkner, Electrochemical Methods: Fundamentals and Applications, Second Edition, John Wiley and Sons, New York, 2001, pp. 249.
[26] A.J. Bard, L.R. Faulkner, Electrochemical Methods: Fundamentals and Applications, Second Edition, John Wiley and Sons, New York, 2001, pp. 339.
[27] B. González, N. Calvar, E. Gómez, A. Domínguez, Density, dynamic viscosity, and derived properties of binary mixtures of methanol or ethanol with water, ethyl acetate, and methyl acetate at T = (293.15, 298.15, and 303.15)K, J. Chem. Thermodynamics 39 (2007) 1578.
[28] G.W. Morrow, Anodic Oxidation of Oxygen-Containing Compounds, in: H. Lund, O. Hammerich (Eds.), Organic Electrochemistry, Fourth Edition, Marcel Dekker, New York, 2001, pp. 611.
[29] O.R. Brown, S. Chandra, J.A. Harrison, The anodic oxidation of anisyl alcohol, J. Electroanal. Chem. 34 (1972) 505.
[30] O.R. Brown, S. Chandra, J.A. Harrison, The anodic oxidation of benzyl alcohol to benzaldehyde, J. Electroanal. Chem. 38 (1972) 185.
[31] P.J. Smith, C.K. Mann, Electrochemical Dealkylation of Aliphatic Amines, J. Org. Chem. 34 (1969) 1821.
[32] L.R. Hall, R.T. Iwamoto, R.P. Hanzlik, Electrochemical Models for Cytochrome P-450. *N*-Demethylation of Tertiary Amides by Anodic Oxidation, J. Org. Chem. 54 (1989) 2446.
[33] M. Masui, H. Sayo, Y. Tsuda, Anodic Oxidation of Amines. Part I. Cyclic Voltammetry of Aliphatic Amines at a Stationary Glassy-carbon Electrode, J. Chem. Soc. B (1968) 973.
[34] M. Masui, H. Sayo, Anodic Oxidation of Amines. Part II. Electrochemical Dealkylation of Aliphatic Tertiary Amines, J. Chem. Soc. B (1971) 1593.

Příloha 8

Electrochemical oxidation of berberine and mass spectrometric identification of its oxidation products

Skopalová, **J.;** Vacek, J.*; Papoušková, B.; Jirovský, D.; Maier, V.; Ranc, V.

Bioelectrochemistry **2012**, *87*, 15-20

Bioelectrochemistry 87 (2012) 15–20

Contents lists available at SciVerse ScienceDirect

Bioelectrochemistry

journal homepage: www.elsevier.com/locate/bioelechem

Electrochemical oxidation of berberine and mass spectrometric identification of its oxidation products

Jana Skopalová [a], Jan Vacek [b,*], Barbora Papoušková [a,c], David Jirovský [a], Vítězslav Maier [a,c], Václav Ranc [a]

[a] Department of Analytical Chemistry, Faculty of Science, Palacký University, 17. listopadu 12, 771 46 Olomouc, Czech Republic
[b] Department of Medical Chemistry and Biochemistry, Faculty of Medicine and Dentistry, Palacký University, Hněvotínská 3, 77515 Olomouc, Czech Republic
[c] Regional Centre of Advanced Technologies and Materials, Department of Analytical Chemistry, Faculty of Science, Palacký University, 17. listopadu 12, 771 46 Olomouc, Czech Republic

ARTICLE INFO

Article history:
Received 20 June 2011
Received in revised form 22 August 2011
Accepted 1 September 2011
Available online 10 September 2011

Keywords:
Berberine
Oxidation
Demethylenation
Hydroxylation
Mass spectrometry

ABSTRACT

Electrochemical oxidation of the isoquinoline alkaloid berberine in aqueous medium was studied by cyclic and differential pulse voltammetry at a glassy carbon electrode (GCE). Two anodic peaks of the quaternary form of berberine were observed at +1.2 V and +1.4 V (vs. SCE) in acidic and neutral solutions. When the anodic polarization exceeded the value of +1.1 V, the redox active film is formed on the GCE surface. The formation of adsorbed film was well-documented by quasireversible redox couple at +0.25 V which was studied in redox cycling experiments. In alkaline medium, a new anodic peak at +0.5 V appeared due to oxidation of berberine pseudobase to 8-oxoberberine. Solutions of berberine at different pH were subjected to controlled potential electrolysis on platinum gauze electrode and analyzed using liquid chromatography (HPLC) equipped with electrospray ionization/quadrupole time-of-flight mass spectrometry. The main water soluble monomeric product of berberine oxidation under physiological-near experimental conditions, OP1, was identified as demethyleneberberine cation (2,3-dihydroxy-9,10-dimethoxy-5,6-dihydroisoquinolino[3,2-a]isoquinolin-7-ium).

1. Introduction

Berberine (Fig. 1) is an isoquinoline alkaloid from the group of protoberberines. It is found in a large number of plants of *Ranunculaceae*, *Berberidaceae*, *Anonaceae*, *Manispermaceae*, *Papaveraceae*, *Fumariaceae*, *Rutaceae* and other families [1,2].

The alkaloids of the protoberberine group are the active constituents of herbal medical products widely used in traditional Chinese medicine for treatment of gastroenteritis, diarrhoea and diabetes mellitus [3]. Many other biological properties of the protoberberine alkaloids and/or their metabolites, including cytotoxic, antimicrobial, anti-inflammatory and antimalarial activity, have been reviewed recently in relation to their molecular structure [4].

It is known from the pharmacokinetic studies that oxidation plays a crucial role in the metabolism of berberine both in rats [5–8] and humans [9–11]. The major metabolic pathways are oxidative demethylenation and demethylation in metabolic phase I following by glucuronidation or sulfatation in phase II [10,11]. The reported oral bioavailability of berberine is poor and the absorbed form is easily metabolized to more polar species [8,10,11]. This suggests that the metabolites might be responsible for the pharmacological effect [8,10].

Berberine naturally occurs in the form of a quaternary iminium salt easily soluble in water. In alkaline solutions, a pseudobase is formed (p*K* 11.7 [12], Fig. 1) that can undergoes formation of the 8-oxoberberine [2,13].

Chemical synthesis and biosynthesis, methods of isolation, chemical reactivity and spectral characteristics of protoberberine alkaloids have been summarized in comprehensive reviews [2,4,14]. Electrochemical methods have been applied for the study of redox properties, adsorption and sensitive analysis of this alkaloid group. Polarographic reduction of berberine and other related substances at the dropping mercury electrode has been studied in relation to pH [15–17]. Berberine can be reduced in both acidic and neutral media in a four-electron process providing tetrahydroberberine [18,19], while two-electron reduction proceeds in alkaline media. Strong adsorption of berberine and its reduction products at the mercury electrodes limits the application of adsorptive stripping voltammetry for determination of this substance at higher concentrations [18]. A polarographic catalytic wave of berberine that is formed in the presence of H_2O_2 can be used for determination of trace amounts of berberine [20].

The electrochemical oxidation of berberine was studied using different voltammetric techniques with glassy carbon electrode (GCE) over a wide pH range [21]. Benzophenanthridine alkaloids (sanguinarine and chelerythrine) and protopine alkaloids exhibit electrooxidation and adsorption behavior similar to berberine [22–25]. Strong adsorption of sanguinarine and dihydrosanguinarine onto the surface

* Corresponding author. Tel.: +420 585 632 303; fax: +420 585 632 302.
E-mail address: jan.vacek@upol.cz (J. Vacek).

1567-5394/$ – see front matter © 2011 Elsevier B.V. All rights reserved.
doi:10.1016/j.bioelechem.2011.09.002

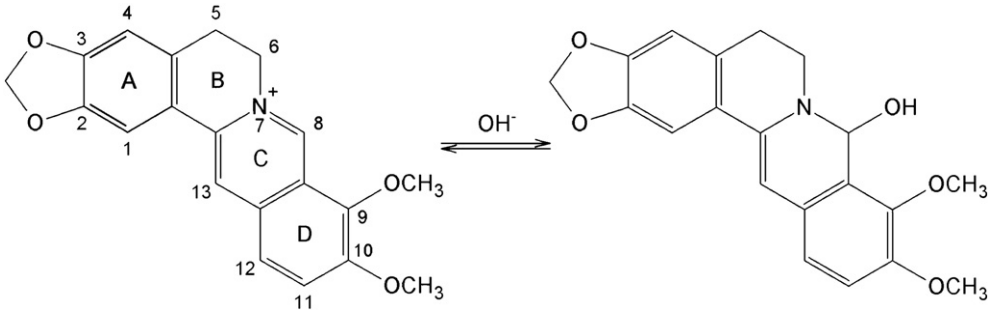

Fig. 1. Chemical structure of berberine quaternary salt (left) and berberine pseudobase (right).

of pyrolytic graphite was employed for measurements using *ex situ* (adsorptive transfer) voltammetric methods and applied to the study of the interactions of these alkaloids with DNA [24]. Formation of redox active electropolymerized films of sanguinarine and chelerythrine oxidation products on the surface of glassy carbon and gold electrodes has been observed by cyclic voltammetry and quartz crystal microbalance measurements [23].

The objective of the present study was to investigate the water soluble oxidation products of berberine. Cyclic and differential pulse voltammetry, controlled potential electrolysis and liquid chromatography with mass spectrometry were used for this purpose.

2. Material and methods

2.1. Reagents

Berberine hemisulfate salt (BHS, purity ≥ 95%, Sigma) was used without further purification. 1,3-benzodioxole, 1,2-dimethoxybenzene and catechol (all Sigma-Aldrich) were of 99.0% purity. 8-Oxoberberine was prepared according to the procedure described in ref. [26]. Stock solutions of berberine were prepared in water. 1,3-benzodioxole and 1,2-dimethoxybenzene were dissolved in supporting electrolyte using sonication immediately before measurement. All chemicals for supporting electrolyte preparation (20 mmol L^{-1} Na_2SO_4, 10 mmol L^{-1} NaOH, Britton-Robinson and 0.1 mol L^{-1} phosphate buffer) were of analytical-reagent grade. Ultrapure water from an ELGA system (average specific resistance 18.2 MΩ cm^{-1}, i.e. conductivity 0.055 μS cm^{-1}) was used for all experiments. Extraction of berberine oxidation products was performed with ethyl acetate (Lach-Ner, Czech Republic). Methanol (for HPLC, Sigma-Aldrich) was used for HPLC mobile phase preparation.

2.2. Voltammetric measurements

The cyclic and differential pulse voltammograms were measured with computer controlled Eco-Tribo Polarograph (Polaro-Sensors, Prague, Czech Republic), equipped with Polar.Pro v. 4 software. A glassy carbon electrode – GCE (disk diameter 3.0 mm, Bioanalytical Systems, USA) was used as a working electrode. A platinum wire served as an auxiliary electrode and SCE (saturated calomel electrode) was employed as a reference electrode. The working electrode was polished using 0.05 μm alumina slurry on wet micro cloth (Buehler, USA) and sonicated in distilled water for 30 s before each measurement. Oxygen was removed from solution by purging with nitrogen in case of need.

2.3. Controlled potential electrolysis

An OH-404 potentiostat (Radelkis, Budapest, Hungary) was used in a three-electrode system consisting of working platinum gauze electrode, reference SCE and counter platinum electrode placed in a separate cathode compartment. The anode compartment of the electrolytic vessel was filled with Britton-Robinson or phosphate buffer and 1 mmol L^{-1} berberine. The cathode compartment contained only buffer solution. Electrolysis was performed at constant potentials of 0.4 V and 1.4 V in acid solution (pH 3.5); at 0.4 V and 1.3 V in solution at pH 7.4; and at 0.1 V, 0.7 V and 1.15 V in alkaline solution (pH 11.0). Each sample was electrolyzed for 30 min. After this time, an aliquot (2 μL) of the electrolyzed sample was diluted with 200 μL of mobile phase (1% acetic acid in 10% methanol aqueous solution) and subjected to HPLC/MS analysis. Another aliquot (0.5 mL) was extracted with ethyl acetate (1 mL) on a shaker (1800 rpm, 30 min) and then centrifuged (7200 g, 5 min). The upper organic layer (0.9 mL) was withdrawn and evaporated under nitrogen stream. The residue was sonicated in 200 μL of mobile phase (10 min) and centrifuged (7200 g, 5 min). An aliquot of 150 μL was diluted with 150 μL of mobile phase and analyzed using HPLC/MS.

2.4. HPLC/MS analysis

An Acquity UPLC system (Waters, Milford, MA, USA) equipped with binary solvent manager, sample manager, column manager and PDA detector was used. The separation was performed on a chromatographic column (150 mm × 2.1 mm, 5 μm) Eclipse XDB-CN from Agilent (Santa Clara, USA). The mobile phase consisted of 1% acetic acid in 10% methanol aqueous solution (solvent A)/methanol (solvent B), gradient elution (% v/v): 0–9 min (10–55% B), 9–12 min (55–60% B), 12–12.1 min (60–10% B), 12.1-16 min (10% B). The mobile phase flow rate was 0.4 mL min^{-1}, the temperature of the autosampler was 10 °C and the column oven was set at 30 °C. The injection volume was 10 μL.

QqTOF Premier mass spectrometer (Waters, Milford, MA, USA) coupled to the UPLC system was used for confirmation of putative structures on the basis of determination of elemental composition. Tuned electrospray ionization (ESI) parameters for the mass spectrometer were as follows: capillary voltage 2.2 kV (positive mode), source temperature 120 °C, sampling cone 30 V, desolvation temperature 150 °C, cone gas flow rate, 38 L h^{-1} and a desolvation gas flow rate, 450 L h^{-1}. Nitrogen was used as a desolvation gas and argon as a collision gas. The data were acquired using simultaneous scanning at lower collision energy of 5 eV and at higher energy using collision energy ramp from 10 to 40 eV. Data were processed using MassLynx 4.1 software (Waters).

3. Results and Discussion

3.1. Oxidation of berberine at a glassy carbon electrode

Cyclic voltammograms of berberine in aqueous 20 mmol L^{-1} Na_2SO_4 are shown in Fig. 2. Two peaks A and B can be observed at potentials + 1.2 and + 1.4 V in the first anodic scan. The currents of both peaks changed with the scan rate depending on berberine

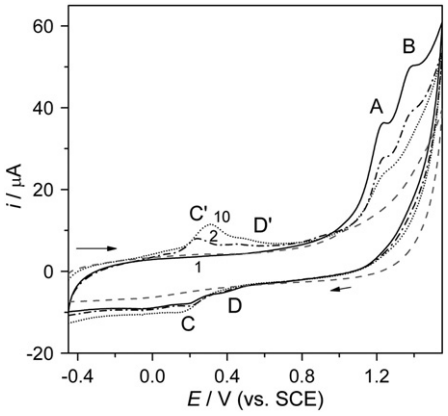

Fig. 2. Cyclic voltammograms of 200 μmol L^{-1} berberine in 20 mmol L^{-1} Na_2SO_4 on glassy carbon electrode. Initial potential −0.45 V, switching potential +1.55 V, scan rate 0.2 V s^{-1}. 1st, 2nd and 10th scans are shown (solid, dash dot and dot lines, respectively); grey dash line: supporting electrolyte. The pH value of 20 mmol L^{-1} Na_2SO_4 containing berberine was 5.6.

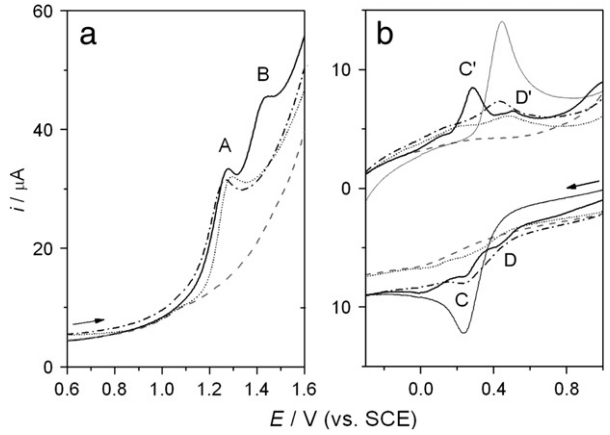

Fig. 3. Comparison of the linear sweep (a) and cyclic (b) voltammetric responses of berberine, 1,3-benzodioxole and 1,2-dimethoxybenzene (solid, dash dot and dot lines, respectively) in 20 mmol L^{-1} Na_2SO_4 as supporting electrolyte (grey dash line). For (b) switching potential +1.6 V, thin solid line denotes CV of catechol. Concentrations of all compounds were 200 μmol L^{-1}, scan rate 0.2 V s^{-1}.

concentration. The dependence of peak A current (for 10 μmol L^{-1} berberine) on scan rate, showed a linear trend and the slope of the linear plot log i_p vs. log v was 0.83 indicating considerable influence of adsorption on the anodic currents.

The cathodic currents (marked as peaks C and D in the Fig. 2) appeared at +0.25 V and +0.4 V in the reverse branch of the voltammograms. The corresponding anodic currents (peaks C' and D') were observed at +0.3 V and +0.45 V as counter-peaks to the peaks C and D in the second anodic scan. These couples of peaks behaved quasireversibly with a potential difference of 40 mV (C/C') and 50 mV (D/D') which almost did not depend on scan rate but increased with number of scans. If a scan was recorded from −0.45 to +1.0 V, no current response was observed in the reverse cathodic branch of the voltammograms. On the other hand, both cathodic peaks C and D appeared at the switching potential of +1.15 V (a half potential of peak A).

The currents of the peaks C/C' and D/D' increased in repeated cycles (Fig. 2). After a tenth scan in the potential range from −0.45 to +1.55 V, the electrode was transferred into the berberine-free supporting electrolyte and the peaks C/C' appeared on consecutive voltammograms (not shown). The peaks D/D' were negligible in the first scan and completely disappeared in following scans. The same behavior was observed when the GCE was polarized at a constant potential above +1.15 V in berberine solution and then rinsed with distilled water and transferred into berberine-free supporting electrolyte. The currents of peaks C/C' increased with increasing time and potential of electro-deposition. The film of electro-deposited oxidation products provided peaks C/C' (and also minor peaks D/D' in first scan). These observations indicate that peaks C/C' belong to the film of redox active *o*-quinoidal products formed during the oxidation of berberine (see below). The peaks D/D' may be attributed to a redox active oxidation product(s) dissolved in the solution and/or partly adsorbed on the film-modified electrode surface. The oxidation product(s) could be precursor(s) of the redox active film.

Similar formation of redox active film has been described for the oxidation of benzophenanthridine alkaloids sanguinarine and chelerythrine [23]. Formation of electrodeposited redox active film from the alkaloids on the surface of gold electrodes was confirmed by FT Raman spectroscopy and EQCM measurements [23]. The authors of this study suggested that the electropolymerization proceeds via formation of *o*-benzoquinone species.

For elucidation which part of the berberine molecule is subject to oxidation, we compared the voltammograms of berberine, 1,3-benzodioxole and 1,2-dimethoxybenzene under the same experimental conditions. Fig. 3 shows that the compounds provide anodic peaks at potentials close to the berberine peak A and C/C' quasireversible couple which can be attributed to the catechol/*o*-quinone redox system (cyclic voltammogram of catechol itself is shown in Fig. 3b). 1,3-benzodioxole, 1,2-dimethoxybenzene as well as catechol form an electro-active film on the GCE surface similar to berberine. When repeated scans were applied in solutions of 1,3-benzodioxole and/or 1,2-dimethoxybenzene and the electrode was then carefully rinsed and placed into supporting electrolyte (without tested substances), a couple of peaks C/C' corresponding to the redox active film was recorded. It is clear from these experiments that the methylenedioxy as well as methoxy group of berberine can be oxidized at potentials higher than +1.2 V (peak A) to form *o*-quinoidal products adsorbed at the electrode surface.

Voltammetric oxidation of berberine strictly depends on pH. The electrooxidation of berberine described above is typical for acidic and neutral media. The peak B was less distinct in slightly acidic and neutral media and disappeared at pH above 7.5. Simultaneously, the redox systems C/C' and D/D' behaved more irreversibly with increasing pH values. No cathodic or corresponding anodic peaks C/C' and D/D' were observed at pH>8 (Fig. 4).

A new peak E was observed in alkaline media of pH≥10.5 (Fig. 4, line 3) the height of which increased with increasing pH. The potential of the peak E shifted to less positive values (58 mV per pH unit)

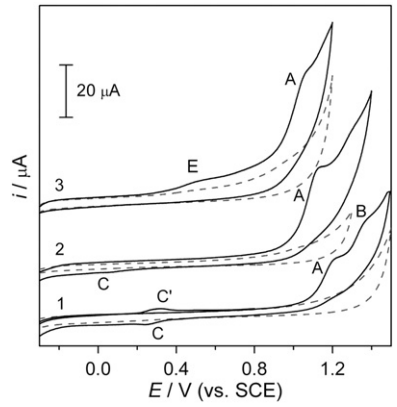

Fig. 4. Cyclic voltammograms of 200 μmol L^{-1} berberine in phosphate buffer at pH (1) 3.5, (2) 7.4 and (3) 11.0 on glassy carbon electrode, scan rate 0.2 V s^{-1}. Grey dash line denotes the supporting electrolyte. In addition to the voltammogram (1), the 2nd scan was recorded from −0.3 to +0.8 V.

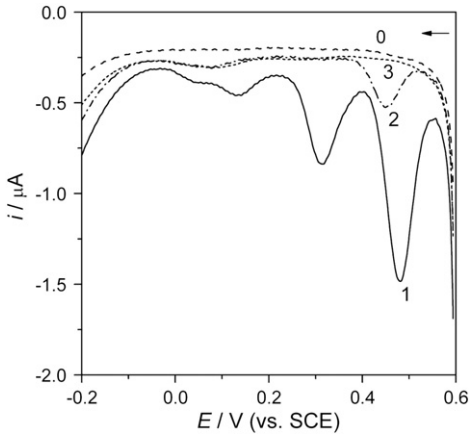

Fig. 5. Differential pulse voltammograms of berberine electrolyzed in phosphate buffers at pH 3.5 at potential of +0.4 V (0) and +1.4 V (1), pH 7.4 at +1.3 V (2) and pH 11.0 at +1.15 V (3). Samples contained 0.2 mL of electrolyzed solution in 1.8 mL of supporting electrolyte (phosphate buffer pH 3.5). DPV conditions: scan rate 20 mV s^{-1}, modulation amplitude −50 mV, pulse time 80 ms; E_{in} = +0.6 V, E_{fin} = −0.4 V.

suggesting that number of protons equals number of electrons released in the electrode reaction. Since berberine forms a pseudobase (8-hydroxy-7,8-dihydroberberine) in alkaline solutions (p*K* 11.7 [12]) it is probable that the peak E is related to oxidation of the pseudobase form. About 5.6% of berberine is present in the pseudobase form at pH 10.5 and therefore its oxidation signal can be recorded. Similar behavior has been reported recently for the alkaloid sanguinarine [24]. Oxidation of sanguinarine pseudobase was observed at pH>7 in compliance with an equilibrium constant p*K* = 8.3 [27] between quaternary cation and the pseudobase form of the alkaloid.

3.2. Constant potential electrolysis and HPLC/MS of oxidation products

In order to acquire more information about the oxidation products, we performed a series of experiments with exhaustive electrolysis of berberine with large surface Pt electrode in Britton-Robinson and 0.1 mol L^{-1} phosphate buffers at pH 3.5, 7.4, and 11.0. Differential pulse voltammograms of berberine solutions after electrolysis were recorded (Fig. 5) providing peaks that corresponded to electro-active products of berberine oxidation. It is evident that most of the reducible products were generated during the oxidation of berberine in acidic medium (Fig. 5, compare line 1 with lines 2 and 3).

Further, the electrolyzed berberine solutions were analyzed using a liquid chromatography system connected to an electrospray ionization/quadrupole time-of-flight mass spectrometry (HPLC/MS). The analysis was performed directly in electrolyzed aqueous solutions as well as in organic fractions obtained by extraction of electrolyzed solutions with ethyl acetate. In order to eliminate the influence of nonelectrolytic reaction of berberine, the chromatograms and MS spectra of electrolyzed solutions and their extracts were compared to those of control samples. The control samples were obtained by electrolysis at +0.4 V (pH 3.5 and 7.4) and +0.1 V (pH 11.0) under the same conditions where no electrode reaction(s) of berberine proceeded (Fig. 5, line 0).

HPLC/MS analysis of berberine standard solution resulted in a peak with retention time (t_R) of 5.3 min (Table 1) and a molecular ion at *m/z* 336 was observed. Main fragment ions at *m/z* 321, 320 and 292 (Fig. 6a) corresponded to previously reported data [28]. In addition, we focused on analysis of electrolyzed aqueous berberine solutions. Almost all products found were eluted in t_R shorter than that of parent compound indicating their higher polarity. The main water soluble oxidation product OP1 was observed at t_R 4.1 min (Table 1). The elemental composition of product OP1 was determined

Table 1
HPLC/MS analysis of berberine (BHS) and its oxidation products.

BHS and oxidation products	Retention time (min)	$\lambda_{max.}$ (nm)	MS peak (*m/z*)	Molecular formula	Error (ppm)
BHS	5.31	264/347	M^+ (336.1236)	$C_{20}H_{18}NO_4$	0.0
OP1	4.10	263/340	M^+ (324.1241)	$C_{19}H_{18}NO_4$	1.6
OP2	4.49	271/358	M^+ (308.0923)	$C_{18}H_{14}NO_4$	0.1
OP3	4.67	268/348	M^+ (322.1074)	$C_{19}H_{16}NO_4$	−1.7
OP4	3.45; 2.79	265/346	M^+ (352.1188; 352.1190)	$C_{20}H_{18}NO_5$	0.9; 1.4
OP5	3.04	254	M^+ (368.1133)	$C_{20}H_{18}NO_6$	−0.3
OP6	4.82	244/318	$[M+H]^+$ (384.1087)	$C_{20}H_{18}NO_7$	1.0
OP7	8.47	220/258/340	$[M+H]^+$ (352.1179)	$C_{20}H_{18}NO_5$	−1.7
OP8	7.41	225/266/308	$[M+H]^+$ (384.1082)	$C_{20}H_{18}NO_7$	−0.1

on the basis of accurate mass measurement (Fig. 6b). It can be assumed that OP1 is demethyleneberberine, present in the form of positively charged ion at *m/z* 324 (2,3-dihydroxy-9,10-dimethoxy-5,6-dihydroisoquinolino[3,2-a]isoquinolin-7-ium). The main fragment ions at *m/z* 309, 308, 306, 280 and 266 corresponded to loss of 15, 16, 18, 44 and 58 Da, respectively, and were in compliance with the fragmentation pathway of the conjugates (glucuronides and sulfates) of demethyleneberberine [6]. OP1 revealed the highest response (about 11% of the peak area of berberine in the control sample) in buffered solutions (pH 3.5) electrolyzed at the constant potential of +1.4 V.

The product OP2 (t_R 4.49 min, Table 1) with a molecular ion at *m/z* 308 is proposed to be a demethylenated and mono-demethylated berberine cation with *o*-quinone group on the ring A (Fig. 6c). In the MS spectra with higher collision energy there can be seen two major fragment ions. The first (*m/z* 293) refers to radical loss of methyl (15 Da), the second (*m/z* 264) to loss of CH_3-H-CO (44 Da) [28]. The position of methoxyl/hydroxyl groups on the ring D cannot be distinguished on a basis of the obtained MS data. Product OP2 occurred only in acidic solutions electrolyzed at +1.4 V in a yield of about 1.5% of initial berberine content. The peak at *m/z* 322 presented in the MS spectrum of OP2 corresponded to mono-demethylated berberine cation (OP3, t_R 4.67 min, Table 1) which partly co-eluted with OP2. The MS spectrum of OP3 at higher collision energy (Fig. 6d) demonstrated a fragment ion at *m/z* 307 (radical loss of methyl) apart the molecular ion (*m/z* 322). This corresponds to published MS data on berberrubine and thalifendine [8]. The signal of OP3 corresponded to 0.5% of total peak area of berberine.

The MS spectra of aqueous solutions electrolyzed at potentials above +1 V revealed minor peaks of molecular ions at *m/z* 352, 368 and 384. These ratios of *m/z* pertain to oxidation products OP4, OP5 and OP6, respectively. The highest content of products OP4 and OP5 (about 1%) was found in acidic electrolyzed solutions whereas the product OP6 was observed in highest amount (also about 1%) in alkaline media. The increments of *m/z* 16, 32 and 48 Da to the parent molecule (*m/z* 336) indicate that the products might be mono-, di- and tri-hydroxylated derivatives of berberine. Exact mass and calculated elemental composition confirm this supposition (Table 1). Both, the OP4 and OP5 are probably quaternary ammonium cations like OP1, OP2, OP3 and berberine itself because their MS spectra did not contain $[M+Na]^+$ ions. The SIM profile at *m/z* 352 showed two peaks at t_R 3.45 min and 2.79 min revealing two positional isomers of OP4. The structure of the hydroxylated products OP4, OP5 and OP6, cannot be specifically determined on the basis of their mass spectra. However, the distribution of partial charges in berberine molecule [29] permits us to estimate the probable positions of the hydroxyl groups. Assuming the EC mechanism of oxidation, the electron is most likely firstly removed from the carbon atom with the most negative partial charge. Nucleophilic substitution, which can follow in the next step, permits the hydrogen to be replaced by a hydroxyl group. The most

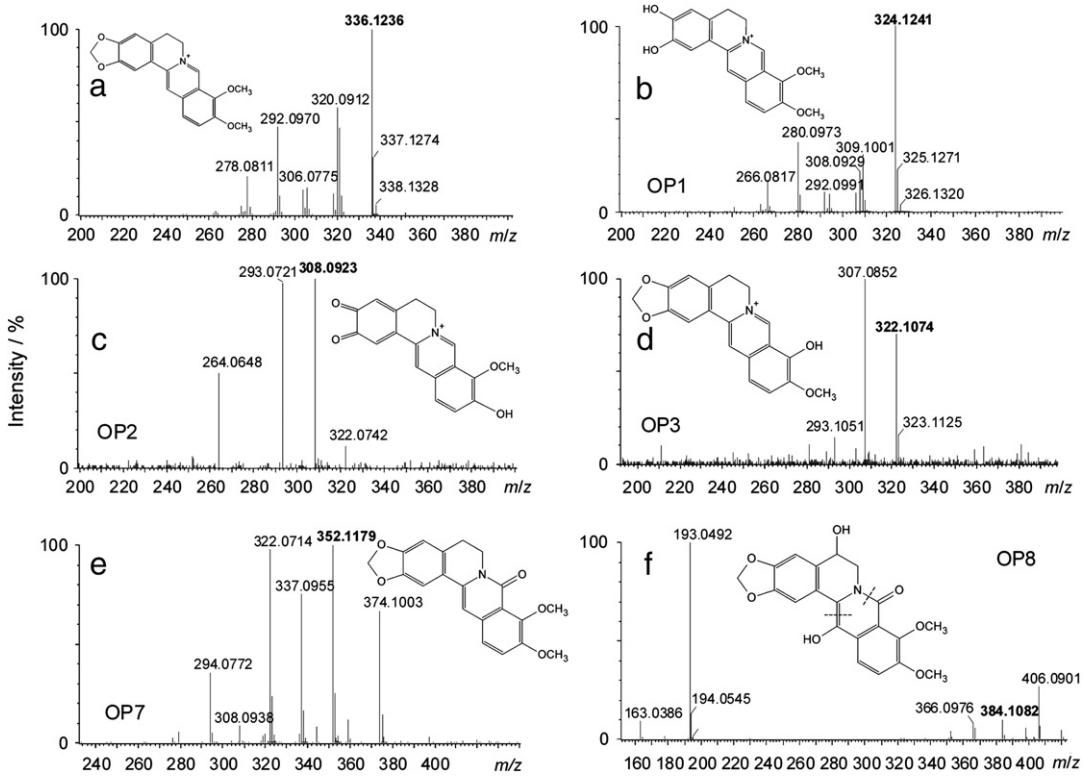

Fig. 6. MS spectra of berberine (a) and putative structures of its oxidation products OP1 (b), OP2 (c), OP3 (d), OP7 (e) and OP8 (f) acquired after electrolysis (30 min at +1.4 V for OP1, OP2 and OP3, +0.7 V for OP7 and +1.15 V for OP8) with Pt-electrode in phosphate buffer (pH 3.5 for OP1, OP2 and OP3 and pH 11.0 for OP7 and OP8). Spectra were acquired at higher energy using collision energy ramp from 10 to 40 eV without precursor ion selection.

negative partial charge was calculated at C5 [29]. Hydroxylation in this position probably leads to the product OP4. The second highest negative partial charge is located at C12 [29] indicating the next possible hydroxylation position. Unlike the mass spectra of OP4 and OP5 an intensive ion $[M+Na]^+$ at *m/z* 406 was observed in the spectrum of OP6. Moreover, the product OP6 was easily extracted into ethyl acetate. It proves that OP6 is a neutral molecule ionized in the ion source. Fragment ions at *m/z* 366, 356 and 338 in mass spectrum of OP6 refer to loss of H_2O (18 Da), CO (28 Da) and both H_2O and CO (46 Da). As the highest content of OP6 was observed in alkaline solution, it could be supposed that this oxidation product is a dihydroxy derivative of berberine pseudobase.

The product OP7 with t_R 8.47 min and molecular ion $[M+H]^+$ at *m/z* 352 (Table 1) was found only in electrolyzed alkaline solutions (pH 11). The higher retention time and good extractability into ethyl acetate shows lower polarity of product OP7 in comparison to the parent berberine molecule. The main fragment ions at *m/z* 337 and 322 (Fig. 6e) correspond to the ions formed after loss of one (15 Da) and two (30 Da) methyl radicals, respectively. The fragment ion at *m/z* 294 (a difference of 30 and 28 Da) proves the elimination of neutral fragment CO in addition to two methyl radicals. Further information was provided by accurate mass measurement and comparison of isotopic profiles. On a basis of all these data, the product OP7 can be ascribed to 8-oxoberberine. Identity of this product was confirmed by the standard prepared as described [26]. The content of OP7 in electrolyzed water solutions was, contrary to their ethyl acetate extracts, very low (around 0.3% and 0.1% for electrolysis at potentials of +0.7 V and +1.15 V, respectively), which is in accordance with low solubility of 8-oxoberberine in water.

The ethyl acetate extract of the berberine solutions electrolyzed in alkaline buffer at +0.7 and +1.15 V contained a product OP8 (t_R 7.41 min) that revealed a molecular ion at *m/z* 384 (Table 1). The elemental composition of OP8 is the same as the composition of OP6 occurring in alkaline aqueous electrolysates at t_R 4.82 min. However, it differs significantly in retention time and also in fragmentation pathway. In MS spectrum recorded with higher collision energy, a very intense fragment ion *m/z* 193 was observed (Fig. 6f). The fragmentation takes place between atoms N7-C8 and C13-C14, as it is shown in Fig. 6f. The ion at *m/z* 193 is formed from the ring D and a fragment of the ring C without nitrogen. This fragmentation process confirms the positions of hydroxyl groups on atoms C5 and C13.

4. Conclusions

The electrochemical oxidation of berberine is a complex process accompanied by formation of redox active film onto GCE surface. It proceeds primarily in acidic media on the methylenedioxy and to less extent also on the methoxy groups of berberine at potentials above +1.1 V (vs. SCE) resulting probably in *o*-diols and subsequently *o*-quinoidal species which are strongly adsorbed on the electrode surface. The main water soluble products are hydroxyl derivatives. Demethylene berberine bearing two hydroxyl groups in a vicinal position on ring A was found in electrolyzed solution in the highest yield. The identified oxidation products, especially in the conjugated form, are known to be also among main metabolites of berberine in rats and humans [5–11]. Thus, the electrochemical approaches presented here could be useful for the study of oxidation mechanisms and electrosyntheses of selected metabolites involved in oxidative biotransformation of berberine and other compounds with structural similarity.

Acknowledgement

This work was supported by the Ministry of Education, Youth and Sports of the Czech Republic (grant projects CZ.1.05/2.1.00/03.0058 of Operational Program Research and Development for Innovations - European Social Fund and MSM 6198959216) and by the Czech

Science Foundation (P503/11/P312). The authors are indebted to Dr. Alexander Oulton for language correction.

References

[1] J.S. Glasby, Encyclopedia of the alkaloids, Plenum Press, New York, 1975.
[2] M. Shamma, The isoquinoline alkaloids, chemistry and pharmacology, Academic Press, New York, 1972.
[3] T.M. Hung, J.P. Lee, B.S. Min, J.S. Choi, M.K. Na, X.F. Zhang, T.M. Ngoc, I. Lee, K.H. Bae, Magnoflorine from Coptidis Rhizoma protects high density lipoprotein during oxidant stress, Biol. Pharm. Bull. 30 (2007) 1157–1160.
[4] L. Grycova, J. Dostal, R. Marek, Quaternary protoberberine alkaloids, Phytochemistry 68 (2007) 150–175.
[5] Y.T. Liu, H.P. Hao, H.G. Xie, H. Lv, C.X. Liu, G.J. Wang, Oxidative demethylenation and subsequent glucuronidation are the major metabolic pathways of berberine in rats, J. Pharm. Sci. 98 (2009) 4391–4401.
[6] C.H. Ma, Z.X. Li, L.X. Wang, Y.H. Tang, H.B. Xiao, C.G. Huang, Identification of major alkaloids in rat urine by HPLC/DAD/ESI-MS/MS method following oral administration of Cortex Phellodendri Decoction, Helv. Chim. Acta 92 (2009) 379–398.
[7] P.L. Tsai, T.H. Tsai, Hepatobiliary excretion of berberine, Drug Metab. Dispos. 32 (2004) 405–412.
[8] F. Zuo, N. Nakamura, T. Akao, M. Hattori, Pharmacokinetics of berberine and its main metabolites in conventional and pseudo germ-free rats determined by liquid chromatography/ion trap mass spectrometry, Drug Metab. Dispos. 34 (2006) 2064–2072.
[9] J.F. Pan, C. Yu, D.Y. Zhu, H. Zhang, J.F. Zeng, S.H. Jiang, J.Y. Ren, Identification of three sulfate-conjugated metabolites of berberine chloride in healthy volunteers' urine after oral administration, Acta Pharmacol. Sin. 23 (2002) 77–82.
[10] F. Qiu, Z.Y. Zhu, N. Kang, S.J. Piao, G.Y. Qin, X.S. Yao, Isolation and identification of urinary metabolites of berberine in rats and humans, Drug Metab. Dispos. 36 (2008) 2159–2165.
[11] Y.H. Yang, N. Kang, H.J. Xia, J. Li, L.X. Chen, F. Qiu, Metabolites of protoberberine alkaloids in human urine following oral administration of Coptidis Rhizoma Decoction, Planta Med. 76 (2010) 1859–1863.
[12] W.L.F. Armarego, C.L.L. Chai, Purification of laboratory chemicals, sixth ed. Elsevier, Butterworth-Heinemann, 2009 367 pp.
[13] W.H. Perkin, LXV. A study of some derivatives of berberine closely allied to derivatives of cryptopine, J. Chem. Soc. Trans. 113 (1918) 722–765.
[14] S.P. Singh, V.I. Stenberg, S.S. Parmar, Photochemistry of alkaloids, Chem. Rev. 80 (1980) 269–282.
[15] J. Bartek, F. Santavy, Polarografie alkaloidu.19. Polarografie chelerythrinu a sanguinarinu, Chem. Listy 47 (1953) 1617–1620.
[16] E. Coufalik, F. Santavy, Polarography of alkaloids.18. Polarographic investigation of the tautomerism of cotarnine and related substances, Collect. Czech. Chem. Commun. 19 (1954) 457–464.
[17] F. Santavy, Polarography of berberine, hydrastinine and cotarnine, Coll. Czech. Chem. Commun. 14 (1949) 377–387.
[18] S. Komorsky-Lovric, Adsorption and reduction of berberine at a mercury electrode, Electroanalysis 12 (2000) 599–604.
[19] V. Simanek, F. Santavy, S. Hegerova, V. Preining, The tautomerism of quaternary salts of isoquinoline type.28. The effects of the position and nature of electron donating substituents on the spectroscopic and polarographic behavior of these substances, Coll. Czech, Chem. Commun. 37 (1972) 2746–2763.
[20] J.F. Song, Y.Y. He, W. Guo, Polarographic determination of berberine in the presence of H2O2 in medicinal plants, J. Pharm. Biomed. Anal. 28 (2002) 355–363.
[21] V.C. Diculescu, T.A. Enache, P.J. Oliveira, A.M. Oliveira-Brett, Electrochemical oxidation of berberine and of its oxidation products at a glassy carbon electrode, Electroanalysis 21 (2009) 1027–1034.
[22] V.C. Diculescu, T.A. Enache, P.J. Oliveira, A.M. Oliveira-Brett, Electrochemical oxidation of sanguinarine and of its oxidation products at a glassy carbon electrode - Relevance to intracellular effects, Electroanalysis 22 (2010) 113–120.
[23] J. Hrbac, G. Broncova, P. Matejka, T. Bystron, J. Vrba, R. Volf, J. Vicar, Electrochemistry of benzophenanthridine alkaloids. Formation and characterization of redox active films from products of sanguinarine and chelerythrine oxidation, Electroanalysis 17 (2005) 2175–2181.
[24] J. Vacek, E. Vrublova, M. Kubala, M. Janovaska, M. Fojta, E. Simkova, J. Styskala, J. Skopalova, J. Hrbac, J. Ulrichova, Oxidation of sanguinarine and its dihydro-derivative at a pyrolytic graphite electrode using *ex situ* voltammetry. Study of the interactions of the alkaloids with DNA, Electroanalysis 23 (2011) 1671–1680.
[25] E. Vrublova, J. Ulrichova, V. Simanek, M. Fojta, J. Vacek, Oxidation of protopine at a pyrolytic graphite electrode using cyclic and square-wave voltammetry, Electroanalysis 22 (2010) 2879–2883.
[26] J. Dostal, S. Man, P. Seckarova, D. Hulova, M. Necas, M. Potacek, J. Tousek, R. Dommisse, W. Van Dongen, R. Marek, Berberine and coptisine free bases, J. Mol. Struct. 687 (2004) 135–142.
[27] M. Vlckova, P. Bartak, V. Kuban, Capillary electrophoretic studies of acid-base properties of sanguinarine and chelerythrine alkaloids, J. Chromatogr. A 1040 (2004) 141–145.
[28] D.W. Wang, Z.Q. Liu, M.Q. Guo, S.Y. Liu, Structural elucidation and identification of alkaloids in Rhizoma Coptidis by electrospray ionization tandem mass spectrometry, J. Mass Spectrom. 39 (2004) 1356–1365.
[29] D.X. Wang, A. Sakoda, M. Suzuki, Effects of surface oxygen of activated carbon on alkaloid adsorption: A molecular dynamics simulation study, Adsorption 5 (1999) 97–108.

Příloha 9

Study of electrochemical oxidation of xanthohumol by ultra-performance liquid chromatography coupled to high resolution tandem mass spectrometry and ion mobility mass spectrometry

Guido, L.F.; Carvalho, D.O.; Táborský, J.; **Skopalová**, **J.**; Saldanha, H.M.E.B.; Bednář, P.*

Chromatographia **2015**, *78*, 1233-1243

Chromatographia (2015) 78:1233–1243
DOI 10.1007/s10337-015-2954-3

ORIGINAL

Study of Electrochemical Oxidation of Xanthohumol by Ultra-Performance Liquid Chromatography Coupled to High Resolution Tandem Mass Spectrometry and Ion Mobility Mass Spectrometry

Luís F. Guido[1,2] · Daniel O. Carvalho[2] · Jakub Taborsky[1] · Jana Skopalova[1] · Helena M. E. B. Saldanha[1] · Petr Bednar[1]

Received: 26 May 2015 / Revised: 18 July 2015 / Accepted: 21 July 2015 / Published online: 1 August 2015

Abstract Electrochemically assisted oxidation off-line combined with UPLC/ESI–MS and ion mobility mass spectrometry enabled us to gain insight into the oxidation mechanisms of xanthohumol. Several types of monomeric oxidation products were identified, i.e., monohydroxylated and dehydrogenated derivatives and related quinones. Besides, high contents of dimers were observed. The structures of four main oxidative condensation products of two xanthohumol molecules were proposed based on combination of retention time, exact mass measurement, fragmentation pattern, data from on-line ion mobility mass spectrometric experiments and with the support of independent electrochemical experiments. To the best of our knowledge, this is the first evidence on formation of xanthohumol dimers. The effect of the pH on the generation of oxidation products was further investigated. The monomeric and dimeric oxidation products are favored at pH of 5.5 and 4.5, respectively.

Keywords Ultra-performance liquid chromatography · Mass spectrometry · Ion mobility · Xanthohumol · Prenylchalcone · Oxidation · Dimer

Introduction

Xanthohumol (2′,4′,4-trihydroxy-6′-methoxy-3′-prenylchalcone; XN, Fig. 1) is a prenylflavonoid, categorized as a member of the chalcones family of the polyphenols, that has been found in hops (*Humulus lupulus* L.) and in the Chinese medical plant *Sophora flavescens* [1]. The female inflorescences of hops ("hop cones") are used as a raw material in beer production, contributing to beer bitterness and aroma. During wort boiling, XN is largely converted into its isomeric flavanone, isoxanthohumol (IXN), a reason why very low content of XN can be found in beer [2, 3]. In the past few years, the brewing industry has been interested in producing XN-enriched beers, mainly due to the recognized health benefits. XN possesses a large spectrum of chemopreventive mechanisms in a wide variety of cancers, such as breast [4], colon [5], colorectal [6], brain [7], ovarian [8], leukemia [9, 10] and prostate [11–13] cancer, with no effects on major organ functions after oral administration [14]. A recent study reported that XN-supplemented beer helps reducing inflammation, oxidative stress and angiogenesis, ameliorating the wound healing process [15]. The bioavailability of XN is known to be dose-dependent and approximately 33, 13, and 11 % in rats, for the low-, medium-, and high-dose groups, respectively, were reported [16].

Several studies have been conducted aimed at identifying the metabolites formed during the oxidative biotransformation of xanthohumol and related prenylflavonoids. Metabolites were identified by using liquid

Electronic supplementary material The online version of this article (doi:10.1007/s10337-015-2954-3) contains supplementary material, which is available to authorized users.

✉ Petr Bednar
petr.bednar@upol.cz

[1] Regional Centre of Advanced Technologies and Materials, Department of Analytical Chemistry, Faculty of Science, Palacky University, 17. Listopadu 12, 77146 Olomouc, Czech Republic

[2] REQUIMTE - Departamento de Química e Bioquímica, Faculdade de Ciências, Universidade do Porto, Porto, Portugal

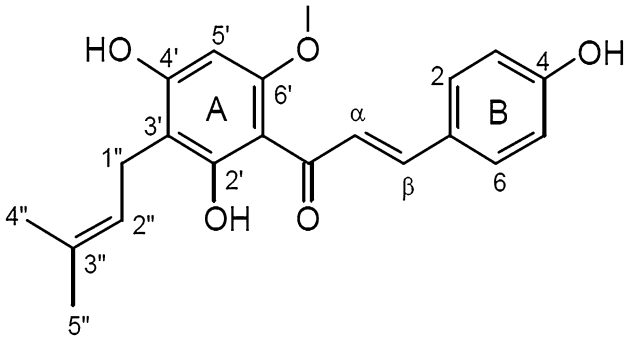

Fig. 1 Structure of xanthohumol

chromatography-tandem mass spectrometry as well as by comparison with authentic standards. Yilmazer et al. [17] were the first who studied the rat liver metabolism of xanthohumol. They determined by liquid chromatography/mass spectrometry and 1-H NMR analyses, three major polar microsomal metabolites of XN as 5″-isopropyl-5″-hydroxydihydrofurano[2″,3″:3′,4′]-2′,4-dihydroxy-6′-methoxychalcone, 5″-(2‴-hydroxyisopropyl)-dihydrofurano [2″,3″:3′,4′]-2′,4-dihydroxy-6′-methoxychalcone and a derivative of XN with an additional hydroxyl function at the B-ring. A nonpolar XN metabolite was identified as dehydrocycloxanthohumol [17]. The same research group identified C-4′ and C-4 monoglucuronides as two major in vitro XN glucuronidation products found with either rat or human liver microsomes [18]. Later, Nikolic et al. [19, 20] during in vitro studies of XN and IXN metabolism, identified hydroxylation of the prenyl moiety as the primary route of oxidative metabolism forming either *cis* or *trans* hydroxylated metabolites of IXN but only the *trans* isomer of XN. The double bond on the prenyl group of both compounds formed an epoxide which was opened by an intramolecular reaction with the neighboring hydroxyl group. Since XN can be converted into IXN through acid-catalyzed cyclization in the stomach, XN might contribute to the in vivo levels of the estrogenic 8-PN following consumption of hops extracts [20]. Colgate et al. [11] suggested that XN and its oxidation product, auroxanthohumol, may be potentially useful as a chemopreventive agent during prostate hyperplasia and prostate carcinogenesis, acting via induction of apoptosis and down-regulation of NF kappa B activation in BPH-1 cells. By using hybrid quadrupole-time-of-flight (QqTOF) analyzer, Jirasko et al. [21] identified new phase II metabolites of XN and related prenylflavonoids in in vivo studies with rats. In total, two phase I metabolites and five phase II metabolites were identified, namely through mechanisms of oxidation, demethylation, hydration and sulfatation.

Electrochemistry off-line or on-line coupled with mass spectrometry (EC–MS) and its combination with a liquid chromatographic separation of either the input material or the reaction products has appeared to be an excellent tool for investigating the redox transformations of various groups of compounds. On-line arrangement is a modern approach allowing the study of the electrochemical conversions even of short-lived species. On the other hand, off-line arrangement can be realized using a common (static) electrochemical vessel with consequent transfer of oxidized material to mass spectrometer [22]. This approach has been also useful in those applications when the effect of time of electrochemical conversion is important or must be studied. Separation step is necessary when a complex mixture of product is formed during electrolysis. Although on-line arrangement of EC–LC–MS is usable for this purpose in principle, the off-line approach is usually beneficial for more quantitative electrochemical conversion to obtain higher response of reaction products which is helpful for easier interpretation of resulting mass spectra. Insertion of separation method between electrochemical cell and mass spectrometer is necessary when isomeric products arise or the electrolytes used for electrolysis are not compatible with mass detection. Electrospray ionization (ESI) is the most common technique used in EC–(LC)–MS enabling transfer of the sample from liquid into gas phase and ionization of the analytes. Up-to-now published EC–MS modes and applications including utilization of liquid chromatography as a separation step during EC–MS experiments are thoroughly discussed in an excellent review of Jahn and Karst [23] and citations given herein.

This work aims at elucidating the oxidation mechanisms of XN. Electrochemically assisted oxidation off-line combined with UPLC/ESI–MS and ion mobility mass spectrometry (IMS–MS) enabled us to study the processes occurring during xanthohumol oxidation in details. Several types of products were identified. Formation of XN dimers during electrochemical oxidation is described for the first time. Chromatographic separation of four main isomers was achieved. The role of the pH on the generation of oxidation products of XN was described as well.

Materials and Methods

Reagents

Xanthohumol (>95 % purity) was provided by Sigma-Aldrich (St. Louis, USA). A stock standard solution (10,000 mg L^{-1}) was prepared by rigorous dissolution of 10 mg of the compound in 1 mL of absolute ethanol (HPLC grade, Sigma-Aldrich). The standard solution was stored at 4 °C and used for further dilutions. Isoxanthohumol (≥98 % purity) was purchased from Alexis Biochemicals (Lausen, Switzerland). Phloroglucinol (≥99 % purity),

p-coumaric acid (≥98 %), geraniol (98 %) and farnesol (95 %) were obtained from Sigma-Aldrich. Supporting electrolyte for cyclic voltammetry was composed of aqueous acetate buffer (50 mmol L^{-1}) and ethanol (50:50, v/v). Acetate buffer solution was prepared by mixing acetic acid and ammonium acetate (all Lachema, Neratovice, Czech Republic, p.a.). To obtain appropriate pH, necessary amount of sodium hydroxide (Lachema, p.a.) was added to buffer solutions. Formic acid, water and acetonitrile (all Sigma-Aldrich, gradient grade) were used for the preparation of mobile phases. Leucine-enkephalin (Sigma-Aldrich, HPLC grade) was used for lock mass correction (solution of 50 pg μL^{-1} in 50:50 acetonitrile:water with addition of 0.1 % formic acid, v/v/v).

Electrochemical Studies

Cyclic Voltammetry

Modular potentiostat/galvanostat Autolab PGSTAT128N (Metrohm, Switzerland) with a three-electrode system composed of a glassy carbon working electrode (GCE, disk diameter 3.0 mm, Bioanalytical Systems, USA), a platinum auxiliary and a saturated calomel reference electrode was used. GCE was polished using 0.05 μm alumina slurry on wet micro cloth (Buehler, USA) and sonicated in distilled water for 30 s prior to each experiment. Measurements were performed at three different pH (3.5, 4.5 and 5.5), different scan rates over the range 10–1000 mV s^{-1} and different potential windows. Working solutions of XN as well as other tested compounds (phloroglucinol, *p*-coumaric acid, geraniol and farnesol) at final concentration 10^{-4} mol L^{-1} were used.

Electrolysis Experiments

A potentiostat 100 mA (L-Chem, Horka nad Moravou, Czech Republic) was used in the three-electrode system that consisted of a working platinum gauze electrode, a saturated calomel electrode (SCE) and an auxiliary platinum electrode. The working and reference electrodes were placed in an anodic compartment of the electrolytic cell. A cathodic compartment containing the auxiliary electrode was separated from the anodic one by a porous ceramic frit. The working solution in the anodic compartment contained 750 μL of acetate buffer, 690 μL of pure ethanol and 60 μL of XN stock solution at 1 mmol L^{-1} final concentration. The potentials 400, 750 and 900 mV were set up for pH 3.5; 350, 700 and 900 mV for pH 4.5; 300, 650 and 850 mV for pH 5.5. Samples were electrolyzed for 30 min. 200 μL of each sample was then diluted in 80 μL of mobile phase B and 120 μL of mobile phase A (for mobile phases composition see the next section).

Ultra-Performance Liquid Chromatography/Tandem Mass Spectrometry

Waters Acquity UPLC equipped with PDA detector was used as a chromatographic system. It was coupled with electrospray ionization high-resolution tandem mass spectrometer Q-TOF Premier. Synapt G2-S high-resolution tandem mass spectrometer equipped with ion mobility cell was further used for elucidation of XN dimers structures. All the systems were provided by Waters (Milford, USA). A BEH C18 column (100 × 2.1 mm, dp 1.7 μm, Waters) was used for chromatographic separation.

Binary gradient elution with 0.1 % (v/v) formic acid (mobile phase A) and acetonitrile (mobile phase B) was used with the following profile of gradient: 0–8 min 100–10 % A, 8–9 min 10 % A and consequent re-equilibration to initial conditions: 9–9.1 min 10–100 % A, 9.1–10 min 100 % A. All separations were done at a flow rate 0.3 mL min^{-1}. Optimized parameters for Q-TOF Premier mass spectrometer were: spray voltage +2.7 kV, sampling cone 30 V, source temperature 120 °C, desolvation temperature 250 °C, cone gas flow 30 L h^{-1}, desolvation gas flow 250 L h^{-1}, collision energy 5.0 eV for precursor ion scanning [MS(1) scan] and a collision energy ramp 10.0–50.0 eV for study of fragmentation [MS(2) scan or MS/MS scan]. Nitrogen was used as a desolvation gas and argon as a collision one. Optimized parameters for Synapt G2-S mass spectrometer were as follows: capillary voltage +2.5 kV, source temperature 100 °C, sampling cone 30 V, source gas flow 0 mL min^{-1}, desolvation temperature 250 °C, cone gas flow 50 L h^{-1}, desolvation gas flow 800 L h^{-1}, trap and transfer collision energy 2 eV for precursor ion scanning [MS(1) scan] and 25 eV for study of fragmentation [MS(2) scan or MS/MS scan], respectively. Data interpretation was done on the basis of accurate mass measurements, fragmentation patterns, comparison of retention times, and ion mobility data. All experiments were done using MS^E mode data recording without discrimination of ions or their pre-selection [alternation of MS scans with low and high collision energy, i.e., MS(1) and MS(2) scans]. Whenever required, the targeted MS/MS scans were recorded in consequent experiments (precursor isolation width 1 Da).

Results

Electrochemical-Assisted Oxidation of XN

The samples for the UPLC/MS study were prepared by electrochemical oxidation. Besides, some electrochemical data appeared to support structural elucidation of XN oxidation products based on chromatographic and mass

spectrometric data. Those experiments are briefly discussed in this chapter.

The voltammetric studies were performed in the electrochemical cell containing 1 mmol L^{-1} XN in ethanol/acetate buffer solution (50:50, v/v). Three buffer solutions with pH 3.5, 4.5 and 5.5 were selected considering the acid/base equilibrium throughout the brewing process. The pH of beer is largely dependent on the fermentation stage, as yeast acts to lower the pH of wort from 5.2–5.5 to 3.8–4.5 [24]. The pH range chosen herein (between 3.5 and 5.5) includes the extreme limits of the brewing process. The given pH values were adjusted during preparation of aqueous buffer solutions prior to mixing with ethanol.

Cyclic voltammograms of XN (Fig. 2) show two anodic current waves appertaining to successive oxidation of XN. No current signals were observed in the cathodic branch of the voltammograms proving irreversibility of the electrode processes on the time scale of the experiments.

The changes of buffer solutions acidity from pH 3.5 to pH 5.5 caused a shift in XN peak potential by −57 and −55 mV/pH for the first and the second peak, respectively, indicating equal number of protons and electrons involved in the electrode reactions.

Voltammograms were recorded at different scan rates in the range 10–1000 mV s^{-1}. Logarithmic dependences of peak current on scan rate were linear with slope values 0.52 and 0.60 for the first and second peak, respectively, reflecting that the electrode processes are predominantly diffusion controlled. However, the value slightly higher than 0.5 shows partial influence of adsorption, which is more pronounced at the second oxidation step.

The number of electrons transferred in the first step of the electrochemical oxidation of XN was estimated from logarithmic analysis of the voltammetric curves recorded at a scan rate 100 mV s^{-1}. Assuming irreversible character of the electrode reaction, obtained value $\alpha z = 0.7$ (where α is a charge transfer coefficient and z is the number of transferred electrons) suggests one-electron oxidation of XN in the first step. Moreover, shift of the half potential of the first wave was 20 mV per decade change in scan rate, which is typical for dimerization reaction following one-electron transfer [25]. From all the above-mentioned results, it can be summarized that electrochemical oxidation of XN seems to proceed through a two-step irreversible process started by one-electron transfer and cleavage of one proton. Accordingly, the dimerization reaction of XN can be expected.

In order to identify products of electrochemical oxidation, bulk electrolysis of XN solution was performed in the same media as used for voltammetric study.

The electrochemical cell was operated at three selected voltages for each studied pH (400, 750 and 900 mV for pH 3.5; 350, 750 and 900 mV for pH 4.5; 300, 650 and 850 mV for pH 5.5). The potential values were selected from the course of voltammograms (Fig. 2). As no electrode reaction supposedly proceed at the lowest potential values, samples obtained under these conditions served as control. The medium and the highest potential values corresponded to the limiting currents of the first and the second oxidation wave, respectively, at which the electrode reactions proceed the most efficiently. The structures of products arising from the electrochemical conversion under the above-mentioned conditions are elucidated in the following sections (Sects. "UPLC/MS/MS Study of Xanthohumol Oxidation" and "UPLC/MS/MS Study of Oxidative Condensation Products of XN"). The effect of pH on the electrochemical-assisted oxidation of XN is discussed in the Sect. "Effect of the pH on the Generation of Oxidation Products".

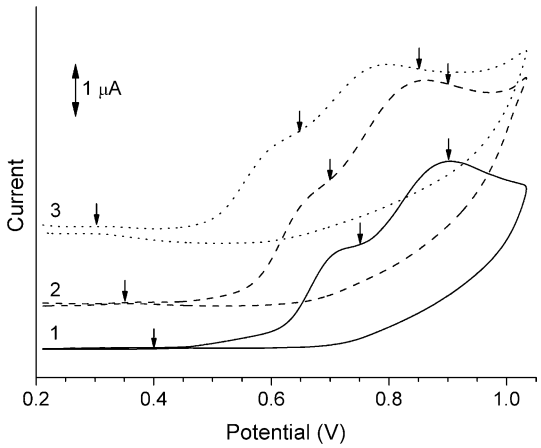

Fig. 2 Background subtracted cyclic voltammograms of xanthohumol in buffer solutions of pH 3.5 (*1*), 4.5 (*2*) and 5.5 (*3*). Scan rate 100 mV/s. *Arrows* denote potential values selected for bulk electrolysis of xanthohumol solutions

UPLC/MS/MS Study of Xanthohumol Oxidation

The electrochemically assisted oxidation of XN was studied by ultra-performance liquid chromatography/tandem mass spectrometry. Several oxidation products were found, whose concentration is greatly dependent on the working potential and selected pH, as discussed later. Several peaks can be observed in the chromatogram reconstructed for *m/z* 371.15 (Fig. 3a). The structure of the dominant peak (t_R 4.33 min, *m/z* 371.1512) corresponds to a gain of one oxygen atom compared to the XN molecule (elemental composition $C_{21}H_{23}O_6^+$, mass difference from theoretical value, dtm, corresponds to 5 ppm). The MS/MS spectrum of this ion is shown in Fig. 3b. Among characteristic fragmentation processes the cleavage of vinylphenol group can be seen (formation of fragment at *m/z* 251.0999; elemental composition $C_{13}H_{15}O_5^+$, dtm, 34 ppm), which excludes

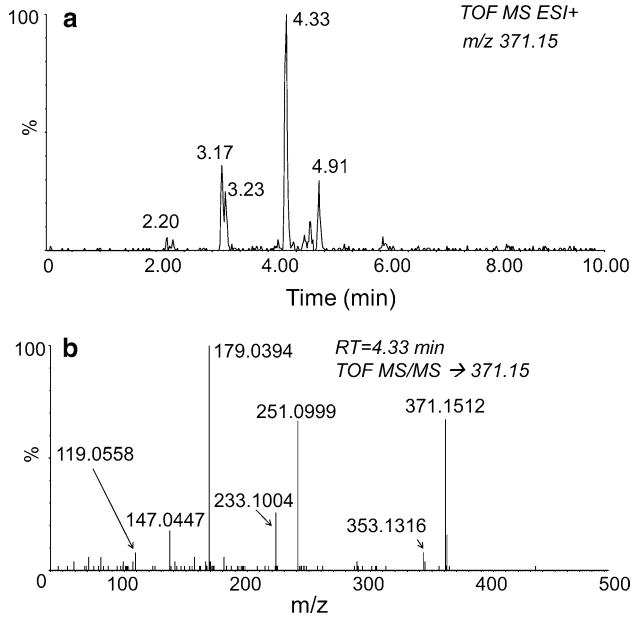

Fig. 3 Identification of hydroxylated derivatives of xanthohumol. **a** Reconstructed chromatogram at *m/z* 371.15. **b** MS/MS spectrum of the most abundant peak

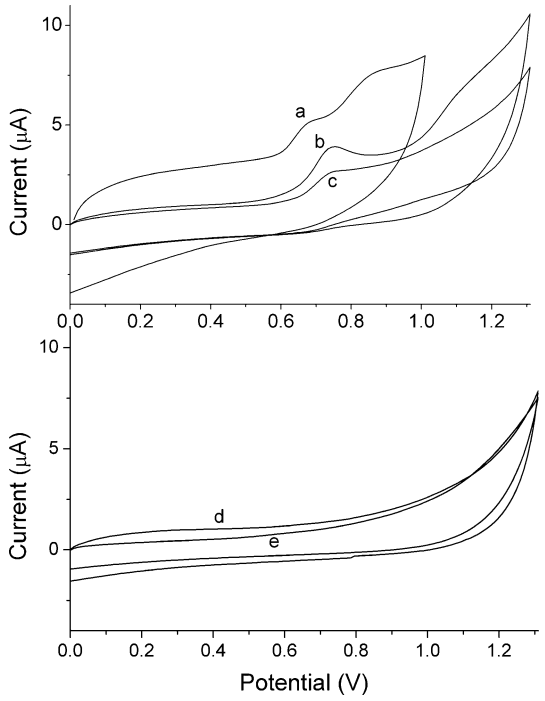

Fig. 4 Cyclic voltammograms of xanthohumol (*a*), phloroglucinol (*b*), *p*-coumaric acid (*c*), geraniol (*d*) and farnesol (*e*), pH = 3.5, scan rate 100 mV/s

hydroxylation of the B-ring. Subsequent elimination of water from the A-ring and/or from the prenyl chain would explain the ion observed at *m/z* 233.1004. This ion further cleaves the prenyl chain to form the dominant fragment at *m/z* 179.0394 (elemental composition $C_9H_7O_4^+$, dtm 28 ppm). These processes suggest that the site of oxidation is located either at A-ring or at prenyl chain but not at the side phenol group (i.e., at the B-ring, Fig. 1). (E)-(3-(4-hydroxyphenyl)allylidyne)oxonium (*m/z* 147.0447, elemental composition $C_9H_7O_2^+$, dtm 1 ppm) is the key fragment confirming that hydroxylation does not occur at the B-ring. Although *m/z* error of some of the above discussed low mass fragments is higher, which is mainly due to their low intensity in collision spectra, the selectivity of MS/MS experiment ensures proper identification in those cases. In order to localize independently the position of hydroxylation, an electrochemical oxidation of four molecules mimicking particular parts of XN molecule, i.e., *p*-coumaric acid, phloroglucinol as phenolic systems and geraniol and farnesol as a prenyl chain containing terpenoids, was performed besides XN. It is evident from the data presented in Fig. 4 that phenolic compounds are oxidized approximately at the same potential as XN in the first step, meaning that the formation of phenoxy radicals (and its resonance forms) can be expected for XN. Ortho and para positions to the oxidized phenol groups are the most reactive and thus tend

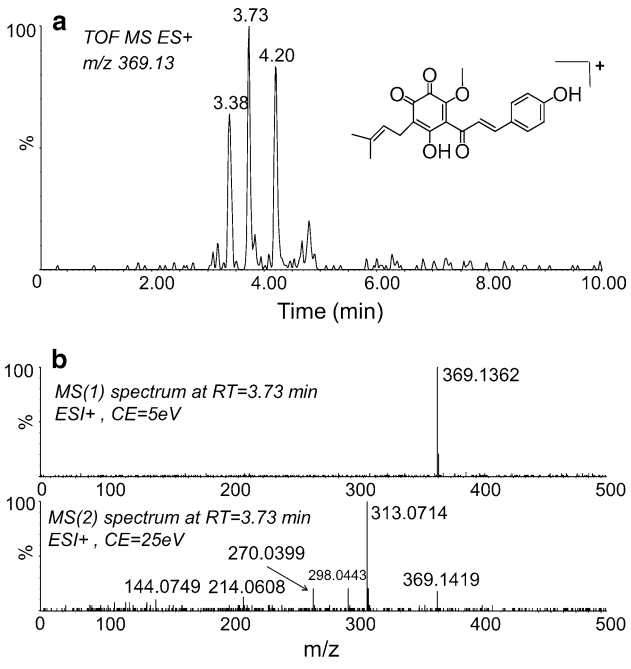

Fig. 5 Identification of quinone forms of oxidized xanthohumol. **a** Reconstructed chromatogram at *m/z* 369.13 (*insert* proposed structure of one isomer). **b** MS spectra of the most abundant peak measured at low and elevated collision energy (MS^E)

to hydroxylation (somewhat higher peak was observed for phloroglucinol compared to the *p*-coumaric acid in the voltammograms shown in Fig. 4). On the other hand, no oxidation of prenyl chains could be observed in the voltammograms of studied terpenoids. These electrochemical results point out that hydroxylation of XN occur rather at A-ring, although MS/MS experiments did not excluded hydroxylation at prenyl chain. In the previous investigation of Yilmazer et al. [17], who studied the biotransformation of XN by rat liver microsomes, the hydroxylation of A-ring was not reported. This fact corroborate the differences often found between in vitro metabolism and (electro)chemical processes involving phenolic compounds. Note, that the other chromatographically well-separated peaks observed in the reconstructed chromatogram at *m/z* 371.14, i.e., compounds eluted at t_R 3.17, 3.23 and 4.91 min (Fig. 3a) can also be tentatively ascribed to monohydroxylated XN derivatives (*m/z* 371.1523, dtm = 8 ppm; *m/z* 371.1574, dtm = 11 ppm and 371.1510, dtm = 4 ppm, respectively). However, very low yield of fragments obtained during UPLC/MS/MS experiments did not allow the determination of the position of hydroxylation.

Figure 5a shows the chromatogram reconstructed for the *m/z* 369.13. Three well-separated major peaks were observed at t_R 3.38, 3.73 and 4.20 min and *m/z* values of 369.1365, 369.1346 and 369.1335, respectively. These oxidation products resulted from the net addition of one oxygen atom to XN and loss of two hydrogen atoms, with formation of an appropriate quinone ($C_{21}H_{21}O_6^+$, dtm 7.3, 2.2 and −0.8 ppm, respectively). Fragmentation of the ion with the highest intensity (t_R 3.73 min) can be evaluated from the MS spectra with low-energy CID (Fig. 5b, upper spectrum) and high-energy CID (Fig. 5b, bottom spectrum; MS(1) and MS(2) scans in MS^E mode, chromatographic peak profiles of parent and fragment ions are identical). The fragment at *m/z* 313.0714 corresponds unambiguously to the loss of (intact) prenyl group ($C_{17}H_{13}O_6^+$, dtm 0.6 ppm). Fragments at *m/z* 298.0443 and 270.0399 arise through a cleavage of a methyl radical and a consequent loss of carbon monoxide ($C_{16}H_{10}O_6^{\cdot+}$ and $C_{15}H_{10}O_5^{\cdot+}$, dtm −11.4 and −47.8 ppm). At elevated collision energies, the prenyl group of the quinones eluting at t_R 3.38 and 4.20 min is cleaved as well (see Electronic Supplementary Material Fig. S1). Based on those data, the formation of the quinone group would occur preferentially at A- or B-ring. The lack of the base peak at *m/z* 179, which represents the common retro- Diels–Alder fragment, points to the quinone group linked at the A-ring. Its structure is given in the insert of Fig. 5a. Note that due to the low concentration of the quinone the MS/MS spectra do not provide utilizable signal of fragments.

Another set of oxidation products with nominal mass of parent ions at *m/z* 353 was observed as well. The two most intense peaks (t_R 5.55 and 6.01 min, see Electronic Supplementary Material Fig. S2a) provided exact masses of parent ions at 353.1385 and 353.1390, respectively. Formation of such products can be explained by loss of two hydrogens with respect to XN or hydroxylation and subsequent dehydration of XN. Those ions correspond with elemental composition $C_{21}H_{21}O_5^+$ (dtm −1.1 and 0.3 ppm, respectively). Fragmentation (MS/MS) of these ions gives rise to a weak signal of a common fragment at *m/z* 233.09 (see Electronic Supplementary Material Fig. S2b for the MS/MS spectrum of the most abundant peak). This fragment can be explained by the cleavage of (intact, non-dehydrogenated) 4-vinylphenol (cleavage of B-ring and α–β ethylene group). The presence of intact B-ring and the aforementioned easier electrooxidation of phenolics compared to terpenoids indicate that the oxidation based on the loss of two hydrogens proceeds particularly on the A-ring. However, an action of the prenyl group in this process is not excluded by the available mass spectrometric data. The presence of at least six chromatographically well-separated isomers exhibiting the consistent exact mass and providing the above discussed fragment can be explained by a different location of an extra double bond in the A-ring and/or prenyl chain, i.e., formation of different quinones.

UPLC/MS/MS Study of Oxidative Condensation Products of XN

In the previous section, simple oxidative processes for XN have been described. During the following electrochemical studies, a more complicated process based on mutual condensation of two molecules of XN has been observed as well. Combination of data from chromatography, exact mass measurement, detailed interpretation of collision spectra (low- and high-energy CID) as well as additional information taken from ion mobility mass spectrometry allowed an in-depth investigation of the structure of the formed dimers.

The chromatogram reconstructed at *m/z* 707.28, which corresponds to the mass of the parent ion of the formed dimers, i.e., $[2 \times XN - 2 \times H + H]^+$, is shown in Fig. 6a. The most abundant dimers, i.e., those with t_R 6.53, 7.60, 7.68 and 8.73 min, have been studied in greater detail. The exact masses of parent ions correspond with 707.2842, 707.2860, 707.2847 and 707.2852, respectively, exhibiting a very good agreement with the theoretical mass of the XN dimers (dtm corresponds with −2.0, 0.6, −1.3 and −0.6 ppm). MS/MS spectra averaged over those chromatographic peaks are shown in the Fig. 6b–e. Several similar pathways can be observed in all the spectra confirming some common features of the formed dimers, i.e., loss of isobutylene from prenyl chain ($[M+H-(CH_3)_2CCH_2]^+$, formation of fragment at *m/z* 651.2244, 651.2217, 651.2224, 651.2233, respectively; dtm 2.1, −2.0, −0.9 and 0.5 ppm,

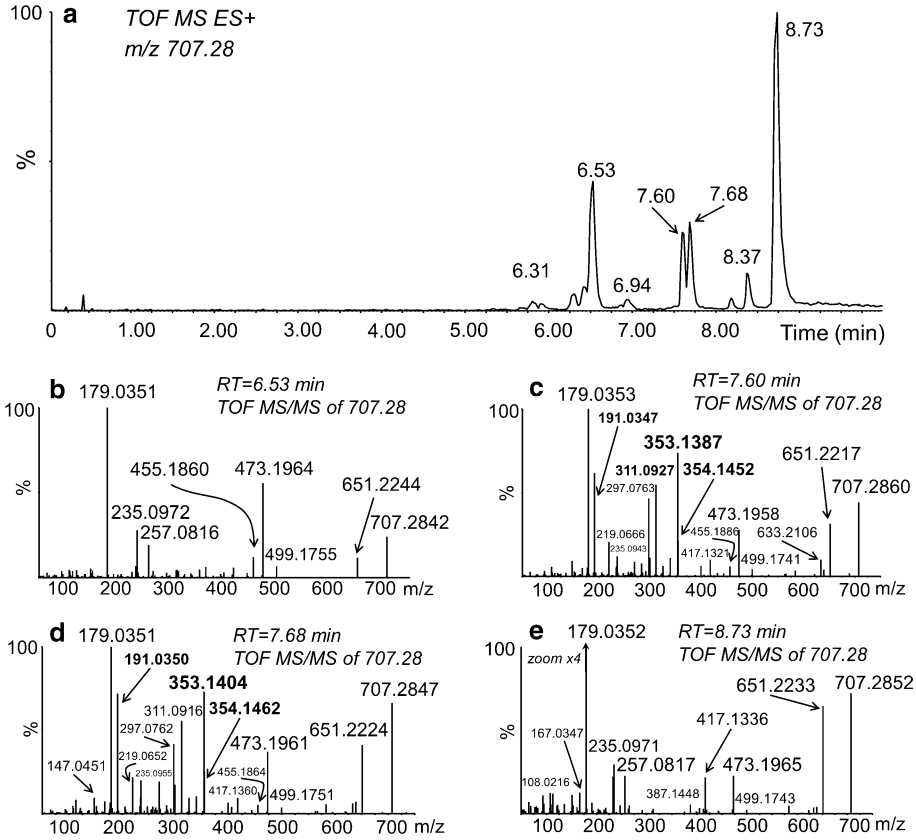

Fig. 6 Identification of the prepared dimers of xanthohumol. **a** Reconstructed chromatogram at *m/z* 707.28. **b**–**e** MS/MS spectra of the most abundant dimers

respectively), loss of prenyl chain, A-ring and carbonyl group ($[M+H-(CH_3)_2CCHCH_2C_6H(OH)_2(OCH_3)CO]^+$, formation of the fragment ion at *m/z* 473.1964, 473.1958, 473.1961, 473.1965, respectively; dtm 0.0, −1.3, −0.6 and 0.2 ppm, respectively). The dominant ion in all the collision spectra corresponds with the (3-hydroxy-5-methoxy-2H-benzo[b]oxet-4-yl)(oxo)methylium and/or (2-hydroxy-6-methoxy-3-methylene-4-oxocyclohexa-1,5-dienyl)(oxo)methylium ion (formation of the fragment ion at *m/z* 179.0351, 179.0353, 179.0351, 179.0352, respectively; dtm 3.9, 5.0, −3.9 and 4.5 ppm, respectively). The previously described behavior during collision experiments suggests that a linkage of two A-rings is not preferred and it is not included in major condensation processes. Although with low intensity, a signal corresponding to two consequent losses of prenyl chains can be found in zoom of all spectra (i.e., formation of a fragment with nominal *m/z* value 595, data not shown) supporting the hypothesis that XN units are not linked via prenyl chains.

On the other hand, the spectra c and d differ from b and e in markedly higher content of fragments with nominal mass 353 and 354. The presence of those ions can be explained by a symmetric fission of the dimers and formation of $[XN - 2 \times H]^+$ and $[XN–H]^{\cdot+}$ ions (in the c and d spectra the exact masses 353.1387, 354.1452; 353.1404 and 354.1462 are observed corresponding to dtm −0.6, 4.2; 4.2 and −1.4 ppm.). Based on chemical sense, one can suggest, that higher yield of the above-mentioned symmetric fragments would be caused by a higher tension in the bond(s) connecting both XN units present in dimer. This higher tension can be explained by a steric hindrance expectable in dimers linked by means of one A-ring (via C-5′ atom, Fig. 1). This suggestion is also in accordance with lower signal (lower stability) of the dimers eluted at t_R 7.60 and 7.68 min compared to those eluted at t_R 6.53 and 8.73 min (Fig. 6a). The occurrence of ions at *m/z* 311.0927, 311.0916 and 297.0763, 297.0762, respectively, is related to the cleavage of propylene and isobutylene from the prenyl chain. The fragmentation proceeds probably via cleavage of B-ring (mechanism of the consequent fragmentation of ion at *m/z* 353 is proposed in Electronic Supplementary Material Fig. S3a). Absence of a fragment at *m/z* 371.15 (i.e., fragment consisted of one XN unit and one additional oxygen) in the c and d spectrum would suggest that XN units in corresponding dimers are not linked via oxygen at A-ring(s) but rather via unsubstituted carbon C-5′ of XN (or a linkage via oxygen(s) represents a minor process). Based on the above data we suggest that those two peaks (t_R 7.60 and 7.68 min) belong to two isomers of XN dimers linked via C-5′ in the A-ring and C-3 or C-2 of the B-ring (C-6 and C-5 are equal with C-3; C-2). Structures of dimers linked via C-5′- C-3 and C-5′- C-2 are suggested in the

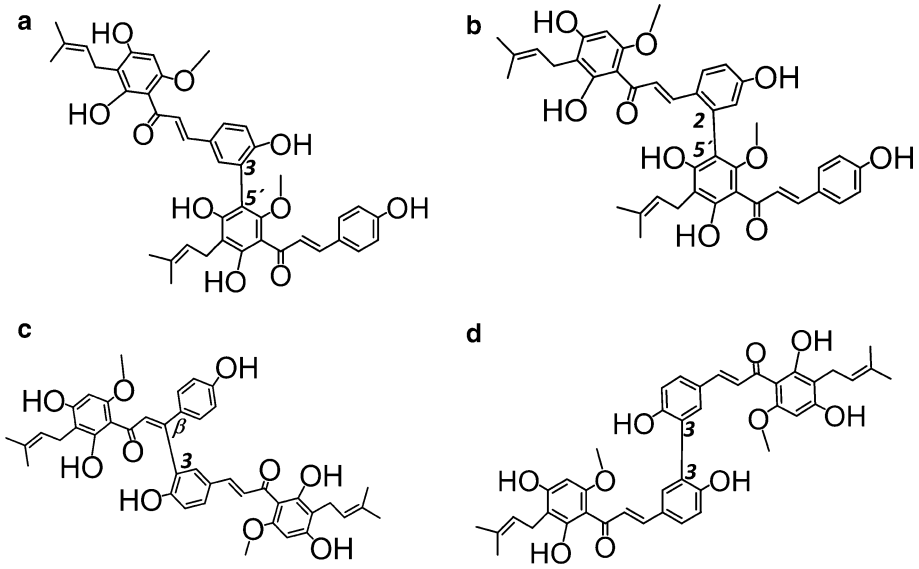

Fig. 7 Proposed structures of prepared dimers of xanthohumol (*numbers* and *Greek letter* denote particular carbons involved in linkage of two XN units in accordance with the labelling given in Fig. 1)

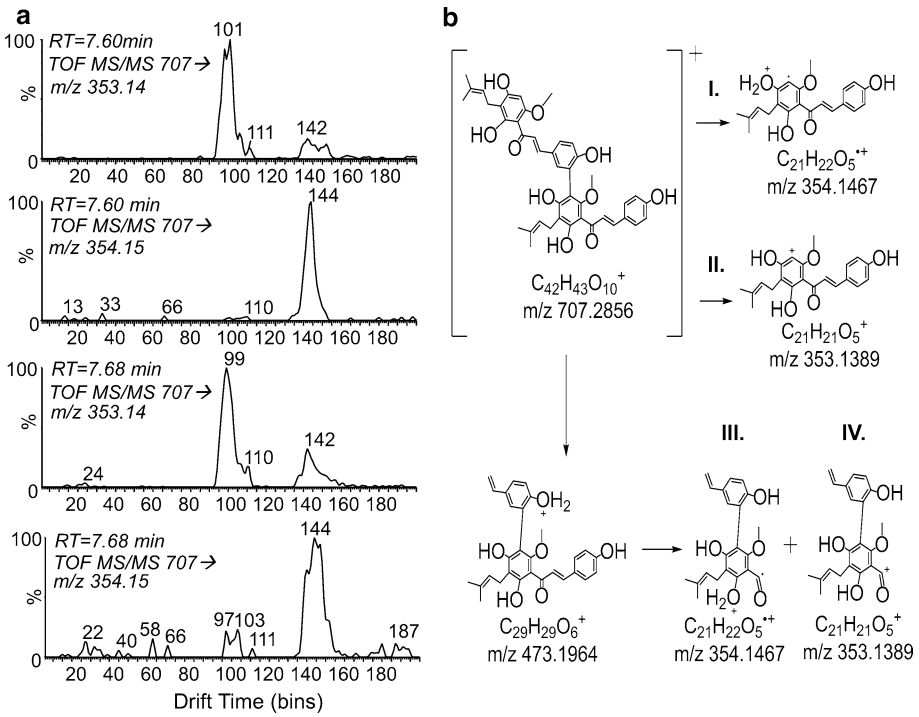

Fig. 8 Fragments at *m/z* 353.14 and 354.15 obtained after chromatographic separation and mass isolation of parent ions of dimers eluted at t_R 7.60 and 7.68 min and their fragmentation. **a** Ion mobility separation of isomeric fragments. **b** Proposed scheme of fragmentation (both kinds of fragments are separated in mobility cell)

Fig. 7 (structures a and b). Figure 8a shows the ion mobility separations of fragments at *m/z* 353.1 and 354.1 (plot of the fragment intensity versus drift time) arising from the above discussed dimers (spectra c and d in Fig. 6). This record was obtained by a complex experiment including on-line chromatographic separation of dimers, isolation of each eluted parent ion of dimers in quadrupole, subsequent fragmentation in trap cell, separation in accordance with collisional cross-section of ions in mobility cell and further partial fragmentation of separated fragments in transfer cell. Two isomeric fragments, separated according to their different cross sections (due to different shapes of fragments) are formed from both dimers. Figure 8b shows the structures of fragments proposed for C′5–C-3 linked dimer (for the C′5–C-2 linked dimer analogous structures are expected). Fragments III and IV retain the linkage between A-ring and B-ring, confirming the suggested structures of dimers a and b

Collision spectra of the first and the last major peaks (t_R 6.53 and 8.73 min, Fig. 6) differ from the previously discussed by a higher intensity of the fragment at *m/z* 235.0972 (and its ratio to parent ion). This fragment

corresponds to the elemental composition $C_{13}H_{15}O_4^+$ (dtm 0.9 ppm). Such composition unambiguously belong to acylium cation derived from 2,4-dihydroxy-6-methoxy-3-(3-methylbut-2-enyl)benzoic acid or a related resonance structure. The ion at *m/z* 257.0816 (and 257.0817) is another abundant fragment in the spectrum b and e (Fig. 6). Its mass fits well with elemental composition $C_{15}H_{13}O_4^+$ (two carbons more and two hydrogens less compared to the previously discussed fragment, dtm 0.8 ppm). Although the process is not straightforward, we suggest that the fragment is also formed by a non-symmetrical fission of the C-3–C-β or C-3–C-3 bond in XN dimer skeleton (see Electronic Supplementary Material Fig. S3b, c). Higher intensities of both fragments correspond with their possible cleavage from both sides of the dimer which could occur in dimers not linked via A-ring (suggested structures are given in Fig. 7c, d). The spectrum of the first major peak is very similar to the last one. Differences between those two spectra lie in a higher relative abundance of fragments at *m/z* 179.0352 and 417.1336 and, on the other hand, a lower intensity of signal at *m/z* 455.1860 (Fig. 6e). However, perhaps more interesting variations are hidden in minor fragments as revealed in the three cuts of both spectra set on the same intensity scale (Fig. 9). Fragments at *m/z* 613.2352 and 595.2273 occur in the spectrum of the first peak (t_R 6.53 min) but not in the last one (t_R 8.73 min). Those fragments can be readily explained by a cleavage of one phenol from dimer linked via C-β atom of one XN unit and a C-3 or C-2 atom of a B-ring of the other one. Linkage to C-3 is more probable since this carbon atom is located in ortho position to hydroxyl group (see discussion in Chapter 3.2). Structure of the fragment at *m/z* 613.2352 is displayed in Fig. 9. Consequent loss of water is apparent in the upper spectrum a. related to first eluted major dimer. Note that a fragment corresponding to the loss of two phenol units was not found in both spectra. Two additional fragments, i.e., *m/z* 375.1224 and 387.1445, exhibit significantly higher intensity in the MS/MS spectrum of the peak at t_R 8.73 min (Fig. 9). Signal at *m/z* 375.1224 can be explained by a combined loss of A-ring, two molecules of carbon monoxide and 2-methyl-2-butene (dtm −2.1 ppm). Signal at *m/z* 387.1445 may correspond to the losses of A-ring, two carbon monoxides and isobutylene (dtm 55.0 ppm).

Ion mobility separation of the fragment at *m/z* 239, obtained by the same experiment as described above (for data see Electronic Supplementary Material Fig. S4a, b), provided several isobaric fragments with different drift times that are formed from both the first and the last major dimers. Fragments at *m/z* 239.1069 and 239.1097, respectively, were found in collision spectra reconstructed for the second mobility peak (i.e., at drift time range 142–154 bins) of both dimers (see Electronic Supplementary Material Fig. S4c, d). Although occurring with relatively low intensity, those fragments correspond acceptably with the elemental composition of protonated 2-(1-(4-hydroxyphenyl)vinyl)-4-vinylphenol (or alternatively 3-(1-(4-hydroxyphenyl)vinyl)-4-vinylphenol) in the case of the first eluted dimer (dtm −1.3 ppm) and 5,5′-divinylbiphenyl-2,2′-diol (or alternatively its isomer regarding mutual linkage of rings in both 4-vinylphenol units) in the case of the fourth one (dtm −10.5 ppm, internal lock mass correction using fragment at *m/z* 473.1964 was used). The suggested structures of the above mentioned fragments (see Electronic Supplementary Material Fig. S3b, c) bear information about linkage

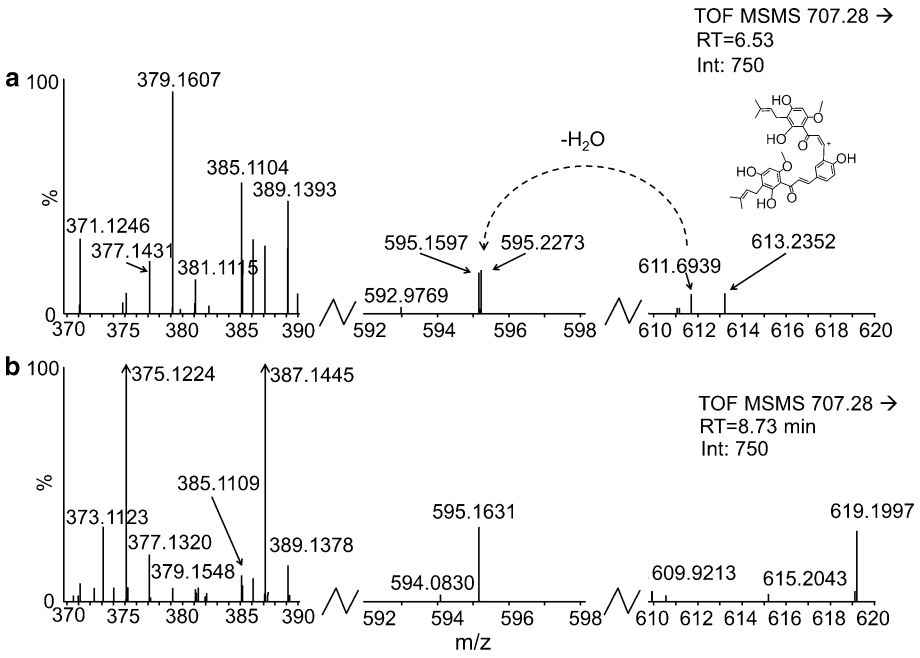

Fig. 9 Zoom of MS/MS spectra of first (**a**) and last (**b**) eluted dimer (spectra are divided in three cuts displayed for the same intensity in order to compare minor characteristic fragments), *insert* characteristic fragment rising by cleavage of phenol from the first eluted XN dimer

between XN molecules through carbon Cβ and B-ring (e.g. C-3 or C-2 position, first dimer) as well as through the B-rings (linkage of C-3 and/or C-2 atoms) of both XN units. The proposed structures of dimers linked via C-β–C-3 and C-3–C-3 are given in the Fig. 7c and d, respectively.

Effect of the pH on the Generation of Oxidation Products

The effect of the pH on the oxidation products formation in ethanolic solutions was investigated. The electrochemical-assisted oxidation assays were conducted at three different pH (3.5, 4.5 and 5.5), which comprise the pH range of the brewing process. The areas of chromatographic peaks corresponding to the found oxidation products were inspected for each pH at three selected cell potentials and the results are depicted in the Fig. 10. The obtained data demonstrate that the highest yield of XN quinones (*m/z* 369.1) is achieved at the highest studied pH (pH 5.5) and moderate potential (650 mV). In the case of monohydroxylated XN (*m/z* 371.1) the highest yield was observed in more acidic solution (pH 3.5) and highest potential (900 mV). However, the monohydroxylated oxidation product of XN is also generated at pH 5.5. Higher pH (5.5) also favors the formation of XN-2H products (*m/z* 353.1) with optimum at the highest potential (850 mV). In brief, higher pH and moderate-higher potentials are favorable for formation of those XN oxidation products. Regarding the fact that the pH is approximately 5.5 in the wort boiling step, it is plausible that one considerable fraction of XN might be lost, not only due to the isomerization into IXN, but also due to oxidation. In fact, 24 % of the XN initially present in the wort was reported to be lost without apparent reason [26].

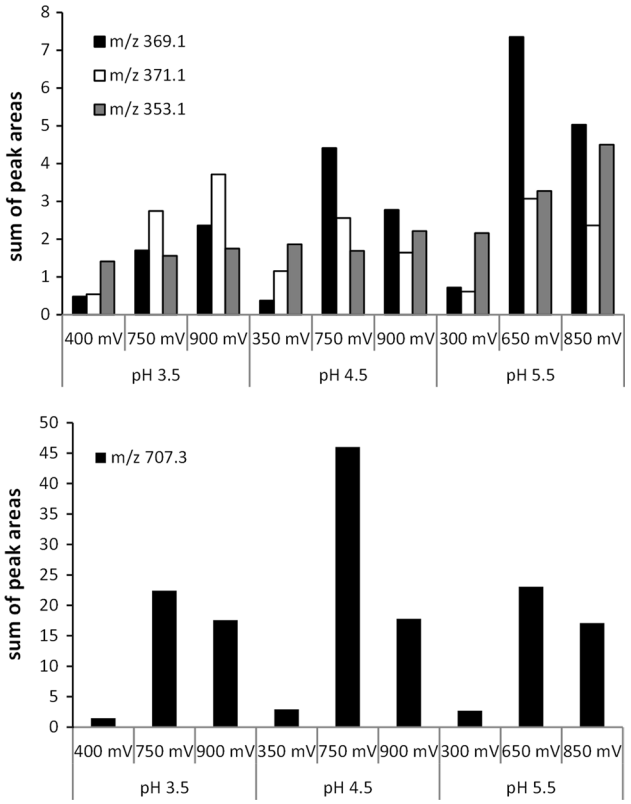

Fig. 10 Comparison of yield of the studied oxidation products (sum of peak areas of particular products in relative, reconstructed chromatograms)

Concerning the formation of XN dimers, significantly higher yield is achieved at moderate conditions (i.e., pH 4.5 and 750 mV). The fact is in accordance with the results of voltammetric experiments showing that at moderate conditions (at the potential of limiting current of the first voltammetric signal), a radical is formed in the one-electron process which is susceptible to dimer formation. Note that the sum of peak areas of dimers is roughly 6–12 times higher compared to the other oxidation products at optimal conditions for each kind of product (Fig. 10). The significance of the dimer formation during XN oxidation is thus evident. Taking into account that the pH of beer is usually between 3.8 and 4.6 [24], our results suggest that the formation of XN dimers through beer oxidation is therefore highly likely. Accordingly, the results reported herein must be regarded as a further contribution towards the elucidation of the mechanisms underlying the significant XN loss observed during the wort boiling of the brewing process.

Conclusions

Electrochemically assisted oxidation off-line combined with UPLC/ESI–MS enabled us to gain insight into the oxidation mechanisms of xanthohumol. Several types of monomeric oxidation products (i.e., monohydroxylated and dehydrogenated derivatives and related quinones) were found and chromatographic separation of major present isomers was achieved. High contents of xanthohumol dimers were observed. This is the first evidence of their formation. Structures of the formed dimers were proposed based on low- and high-energy fragmentation experiments, ion mobility mass spectrometry and comparative voltammetric experiments. The chemical structures of four main oxidative condensation products of two xanthohumol molecules are presented. They result from the linkage between C3 and C2 atoms of one unit and C3, C2, Cβ and C′5 atoms of the other. As the monomeric and dimeric oxidation products are favored at pH of wort and beer, respectively, xanthohumol oxidation processes should be taken into account by the brewing industry.

Acknowledgments This work received financial support from the European Union (FEDER funds) under the framework of QREN through Project NORTE-07-0124-FEDER-000069). LFG wishes to

thank Foundation for Science and Technology (FCT) for his Sabbatical Leave Grant (SFRH/BSAB/1272/2012). DOC wishes to acknowledge FCT for his Ph.D. studentship (SFRH/BD/79939/2011). Authors thank to the project of Ministry of Education, Youth and Sports (Project LO1305), European Social Fund OP—Education for Competitiveness (Project CZ.1.07/2.3.00/30.0041) and Grant Agency of Czech Republic (Project P206/12/1150).

Compliance with ethical standards

Conflict of interest All authors declare no conflict of interest regarding the present work.

References

1. Gerhäuser C (2005) Beer constituents as potential cancer chemopreventive agents. Eur J Cancer 41:1941–1954
2. Stevens JF, Page JE (2004) Xanthohumol and related prenylflavonoids from hops and beer: to your good health! Phytochemistry 65:1317–1330
3. Magalhães PJ, Carvalho DO, Cruz JM, Guido LF, Barros AA (2009) Fundamentals and health benefits of xanthohumol, a natural product derived from hops and beer. Nat Prod Commun 4:591–610
4. Monteiro R, Faria A, Azevedo I, Calhau C (2007) Modulation of breast cancer cell survival by aromatase inhibiting hop (*Humulus lupulus* L.) flavonoids. J Steroid Biochem Mol Biol 105:124–130
5. Pan L, Becker H, Gerhauser C (2005) Xanthohumol induces apoptosis in cultured 40-16 human colon cancer cells by activation of the death receptor- and mitochondrial pathway. Mol Nutr Food Res 49:837–843
6. Gonçalves P, Araujo JR, Pinho MJ, Martel F (2011) In vitro studies on the inhibition of colon cancer by butyrate and polyphenolic compounds. Nutr Cancer 63:282–294
7. Zajc I, Filipic M, Lah TT (2012) Xanthohumol induces different cytotoxicity and apoptotic pathways in malignant and normal astrocytes. Phytother Res 26:1709–1713
8. Drenzek JG, Seiler NL, Jaskula-Sztul R, Rausch MM, Rose SL (2011) Xanthohumol decreases Notch1 expression and cell growth by cell cycle arrest and induction of apoptosis in epithelial ovarian cancer cell lines. Gynecol Oncol 122:396–401
9. Lust S, Vanhoecke B, Janssens A, Philippe J, Bracke M, Offner F (2005) Xanthohumol kills B-chronic lymphocytic leukemia cells by an apoptotic mechanism. Mol Nutr Food Res 49:844–850
10. Harikumar KB, Kunnumakkara AB, Ahn KS, Anand P, Krishnan S, Guha S, Aggarwal BB (2009) Modification of the cysteine residues in IkappaBalpha kinase and NF-kappaB (p65) by xanthohumol leads to suppression of NF-kappaB-regulated gene products and potentiation of apoptosis in leukemia cells. Blood 113:2003–2013
11. Colgate EC, Miranda CL, Stevens JF, Bray TM, Ho E (2007) Xanthohumol, a prenylflavonoid derived from hops induces apoptosis and inhibits NF-kappaB activation in prostate epithelial cells. Cancer Lett 246:201–209
12. Deeb D, Gao X, Jiang H, Arbab AS, Dulchavsky SA, Gautam SC (2010) Growth inhibitory and apoptosis-inducing effects of xanthohumol, a prenylated chalone present in hops, in human prostate cancer cells. Anticancer Res 30:3333–3339
13. Vene R, Benelli R, Minghelli S, Astigiano S, Tosetti F, Ferrari N (2012) Xanthohumol impairs human prostate cancer cell growth and Invasion and diminishes the incidence and progression of advanced tumors in TRAMP mice. Mol Med 18:1292–1302
14. Gerhäuser C, Alt A, Heiss E, Gamal-Eldeen A, Klimo K, Knauft J, Neumann I, Scherf HR, Frank N, Bartsch H, Becker H (2002) Cancer chemopreventive activity of Xanthohumol, a natural product derived from hop. Mol Cancer Ther 1:959–969
15. Negrao R, Costa R, Duarte D, Gomes TT, Coelho P, Guimaraes JT, Guardao L, Azevedo I, Soares R (2012) Xanthohumol-supplemented beer modulates angiogenesis and inflammation in a skin wound healing model. Involvement of local adipocytes. J Cell Biochem 113:100–109
16. Legette L, Ma L, Reed RL, Miranda CL, Christensen JM, Rodriguez-Proteau R, Stevens JF (2012) Pharmacokinetics of xanthohumol and metabolites in rats after oral and intravenous administration. Mol Nutr Food Res 56:466–474
17. Yilmazer M, Stevens JF, Deinzer ML, Buhler DR (2001) In vitro biotransformation of xanthohumol, a flavonoid from hops (Humulus lupulus), by rat liver microsomes. Drug Metab Dispos 29:223–231
18. Yilmazer M, Stevens JF, Buhler DR (2001) In vitro glucuronidation of xanthohumol, a flavonoid in hop and beer, by rat and human liver microsomes. FEBS Lett 491:252–256
19. Nikolic D, Li YM, Chadwick LR, Grubjesic S, Schwab P, Metz P, van Breemen RB (2004) Metabolism of 8-prenylnaringenin, a potent phytoestrogen from hops (Humulus lupulus), by human liver microsomes. Drug Metab Dispos 32:272–279
20. Nikolic D, Li YM, Chadwick LR, Pauli GF, van Breemen RB (2005) Metabolism of xanthohumol and isoxanthohumol, prenylated flavonoids from hops (*Humulus lupulus* L.), by human liver microsomes. J Mass Spectrom 40:289–299
21. Jirasko R, Holcapek M, Vrublova E, Ulrichova J, Simanek V (2010) Identification of new phase II metabolites of xanthohumol in rat in vivo biotransformation of hop extracts using high-performance liquid chromatography electrospray ionization tandem mass spectrometry. J Chromatogr A 1217:4100–4108
22. Jirovsky D, Bednar P, Myjavcova R, Bartosova Z, Skopalova J, Tvrdonova M, Lemr K (2011) Study of electrochemical oxidation of cyanidin glycosides by online combination of electrochemistry with electrospray ionization tandem mass spectrometry. Monatsh Chem 142:1211–1217
23. Jahn S, Karst U (2012) Electrochemistry coupled to (liquid chromatography/) mass spectrometry-current state and future perspectives. J Chromatogr A 1259:16–49
24. Bamforth C (2003) Beer-tap into the art and science of brewing. Oxford University Press, Oxford
25. Marken F, Neudeck A, Bond AM (2010) Cyclic voltammetry. In: Scholz F (ed) Electroanalytical methods. Guide to experiments and applications. Springer, Berlin
26. Magalhães PJ, Dostalek P, Cruz JM, Guido LF, Barros AA (2008) The impact of a xanthohumol-enriched hop product on the behavior of xanthohumol and isoxanthohumol in pale and dark beer: a pilot scale approach. J Inst Brew 114:246–256

Příloha 10

Ion transfer voltammetric and LC/MS investigations of the oxidative degradation process of fentanyl and some of its structural analogs

Langmaier, J.; **Skopalová**, **J.***; Zajacová Cechová, M.; Kahánková, T.; Jerga, R.; Barták, P.; Samec, Z.; Navrátil, T.*

Electrochimica Acta **2023**, *441*, 141848

Electrochimica Acta 441 (2023) 141848

Contents lists available at ScienceDirect

Electrochimica Acta

journal homepage: www.journals.elsevier.com/electrochimica-acta

Ion transfer voltammetric and LC/MS investigations of the oxidative degradation process of fentanyl and some of its structural analogs

Jan Langmaier [a], Jana Skopalová [b,*], Monika Zajacová Cechová [b], Tereza Kahánková [b], Radek Jerga [b], Petr Barták [b], Zdeněk Samec [c], Tomáš Navrátil [a,*]

[a] J. Heyrovský Institute of Physical Chemistry of the Czech Academy of Sciences, Department of Electrochemistry at the Nanoscale, Dolejškova 2155/3, 182 00 Prague 8, Czech Republic

[b] Palacký University, Faculty of Science, Department of Analytical Chemistry, 17. listopadu 1192/12, 771 46 Olomouc, Czech Republic

[c] J. Heyrovský Institute of Physical Chemistry of the Czech Academy of Sciences, Department of Biophysical Chemistry, Dolejškova 2155/3, 182 00 Prague 8, Czech Republic

ARTICLE INFO

Keywords:
Fentanyl
HO• radicals
Catalytic degradation
Ion transfer voltammetry
LC/MS product identification

ABSTRACT

Ion transfer voltammetry at a polarized ionic liquid membrane and LC/MS technique were used to investigate the oxidative time-resolved degradation of the frequently (mis)used opioid fentanyl and some of its structural analogs.

The degradation is based on the reaction of opioids with hydroxyl radicals produced by the catalytic decomposition of hydrogen peroxide. Using the voltammetric technique, it was confirmed that the presence of Fe^{2+}ions and hydrogen peroxide is essential in the degradation process of fentanyl(s). An increasing concentration of ferrous ions accelerates the described reactions, while the reaction rate is much less affected by the concentration of fentanyl.

In an excess of ferrous ions, the course of the reaction can be approximated by a pseudo-first-order reaction with a half-time of 3.85 min. The generation of HO• radicals was proved to be the rate-determining step. Oxidative degradation processes of all investigated fentanyl-related drugs exhibit similar kinetics. A wide variety of fentanyl degradation products were detected and characterized using LC/MS analysis. Mono-, di- and trihydroxylated derivatives in several isomeric forms were observed most abundantly in a relatively short reaction time (5–30 min). The formation of norfentanyl has also been demonstrated.

1. Introduction

Fentanyl and a large number of its structural analogs belong to the group of novel synthetic opioids [1], which are frequently used as painkillers and anesthetics during surgery [2], and as antidepressants for symptomatic treatment of many psychiatric problems [3,4]. Apart from these undoubtedly important applications, all these drugs are often being misused by drug dealers and by patients themselves [5]. Furthermore, these substances can be misused also as chemical warfare agents (especially incapacitating agents) [6,7].

At present, fentanyl-based research substances focused mainly on their metabolic pathways, pharmacokinetics, and other pharmacological characteristics [1,8-10]. These studies have a highly interdisciplinary character with contributions from the fields of biochemistry, toxicology, and practically all areas of analytical chemistry. Many sophisticated analytical methods and approaches have been so far introduced to quantify fentanyls and their metabolic products in complicated biological matrices. Applied analytical procedures usually involve separation steps (capillary electrophoresis, high-performance liquid chromatography) coupled with mass spectrometry [9–11]. Electrochemical techniques offer rather simple and relatively inexpensive alternatives to the sensitive detection of fentanyl-related opioids [12–17]. However, the classical electrochemical approaches often include the destructive irreversible oxidation of fentanyls at high potentials [14,15] imposing thereby a limit on their use in the analysis of complicated samples of biological origin. On the other hand, electrochemistry at the interface between two immiscible electrolyte solutions (ITIES) realized at a thin layer of an ionic liquid (IL) separating two aqueous electrolyte solutions offers a non-destructive detection scheme [18–20]. Investigated ions are transferred across the polarized interface

* Corresponding authors.
E-mail addresses: jana.skopalova@upol.cz (J. Skopalová), tomas.navratil@jh-inst.cas.cz (T. Navrátil).

https://doi.org/10.1016/j.electacta.2023.141848
Received 27 October 2022; Received in revised form 29 December 2022; Accepted 3 January 2023
Available online 4 January 2023

from the aqueous phase into IL giving rise to the electric current, which is used to monitor the changes in the ion concentration in the aqueous phase. This experimental approach enables the application of various electrochemical methods, including cyclic voltammetry, square-wave, differential pulse voltammetry, and impedance spectroscopy [21,22] to obtain analytical data and kinetic or thermodynamic parameters important for the practical and theoretical considerations [23,24]. We have recently reported the study of several synthetic opioids including fentanyl and its structural analogs by ion transfer voltammetry (ITV) [25]. The method offered the possibility of the voltammetric detection of the protonated fentanyls. The analysis of the voltammetric data provided the values of the partition coefficients of the ionic and neutral fentanyl forms reflecting their analgesic potency.

Some synthetic opioids exhibit high pharmacological potency and can be therefore classified as hazardous materials. Owing to their negative impact, increasing attention has been paid to the methods of their removal from contaminated work or public places. Several studies [26–29] and a review [30] dealing with the degradation of fentanyl, and with the identification of the degradation products have been published. Acid, base, thermal, and photo-treatments, or oxidative degradation have been tested as the prospective approaches to the removal of fentanyls from the environment. On the one hand, after the exposure of fentanyl to UV light for 7 days, or after its treatment with 5 M NaOH at elevated temperature, the opioid remained almost intact [26]. On the other hand, the acid treatment of fentanyl led to the formation of some hydrolytic products, while the oxidation using 0.3% (0.088 mol dm^{-3}) H_2O_2 led to the formation of several of its N-oxide diastereomers. A study of the oxidative degradation of fentanyl in the 0.2 M aqueous solutions by peroxides and hypochlorites revealed that trichloroisocyanuric acid and a mixture of sodium percarbonate with N,N,N',N'-tetraacetylethylene diamine represent the most efficient oxidizing agents, which have completely decomposed the drug within one hour [27]. A similar approach, i.e., the oxidative treatment of fentanyl compounds dissolved in water by 1 M sodium bromate mixed with 1 M sodium sulfite at pH = 0.5, reached almost 100% degradation within 30 minutes [28]. A commercial preparation OxiClean™ containing sodium percarbonate has been developed and recommended for cleaning surfaces contaminated by fentanyl and acetylfentanyl, without disclosing any information on their possible degradation products [29]. A comprehensive review has summarized the recent progress in the area of the acid, base, thermal, photo- and oxidative degradation of fentanyls including the list of the reaction products formed [30]. Fluidized-bed Fenton technologies for industrial wastewater treatment, which rely on the oxidative power of the Fenton's reagent [31–33], have received increasing attention [34] and should be considered as alternatives to the procedures listed above.

This study aimed to examine the possibility of using Fenton's reagent [31] for efficient degradation of the novel synthetic fentanyl-based opioids in an aqueous solution. The chemical structures of the drugs examined in this study are shown in Fig. 1.

Fenton's reagent consists of a mixture of H_2O_2 in excess and Fe^{2+} ions and is frequently used to oxidize contaminants in wastewater [31] through the generation of reactive oxygen radicals [32,33]. The changes in the concentration of the fentanyl-based opioids in their protonated forms were monitored by cyclic voltammetry at a polarized ionic liquid (IL) membrane [25] and, in the case of fentanyl alone, also by LC/MS analysis. Both components of the Fenton's reagent do not represent an obstacle to the ion transfer voltammetry since H_2O_2 is a neutral molecule and the Fe^{2+} cation is sufficiently hydrophilic and cannot interfere with the transfer of the fentanyl cation inside the polarized potential window. We shall show that the presence of the Fenton's reagent containing 44 mM H_2O_2 and 0.2 mM Fe^{2+} results in complete degradation of 0.1 mM fentanyl within 300 min, while no change in the fentanyl concentration takes place when the reagent contained only H_2O_2, or Fe^{2+} alone. An analysis of the effects of the fentanyl and Fe^{2+} concentrations allowed us to propose a mechanism of fentanyl degradation and to identify its rate-determining step. We shall also present preliminary results indicating that the degradation of fentanyl-related opioids follows similar kinetics. It is noteworthy that the use of Fenton's reagent poses much less environmental threat compared to the concentrated and relatively dangerous agents used for the destruction of fentanyl in the studies referred to above. Another advantage of the present approach is the use of significantly lower concentrations of the active agents, while the degradation rates remain comparable with those reported.

2. Experimental

2.1. Chemicals

Fentanyl, furanylfentanyl, sufentanil, carfentanil and norfentanyl were obtained from Chromservis (Chromservis s.r.o., Czech Republic). Unstabilized 30% hydrogen peroxide, ammonium iron(II) sulfate hexahydrate, and LiCl were purchased as analytical grade chemicals from Lachema (Czech Republic), Sigma-Aldrich, and Fluka, respectively. Ionic liquid tridodecylmethylammonium tetrakis[3,5-bis (trifluoromethyl)phenyl]borate (IL) was prepared from the corresponding sodium and chloride salts by metathesis and purified by the procedure described elsewhere [19]. Aqueous solutions for all measurements were prepared from deionized water with a resistivity of 18.2 MΩ cm (Millipore). All electrochemical experiments were carried out at the ambient temperature of 25 ± 2 °C.

Acetonitrile (for HPLC, Sigma-Aldrich), chloroform (analytical grade, Lach-Ner, Czech Republic), and formic acid (>99%, Sigma-Aldrich) were used as received. Sodium formate used for time of flight analyzer (TOF) calibration was prepared by mixing 0.1 cm^3 of 0.1 M NaOH with 0.2 cm^3 of 10% formic acid and 20 cm^3 of mixture

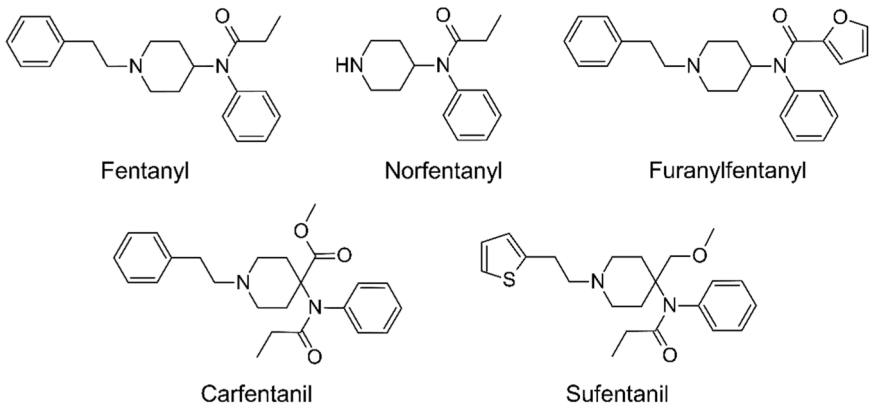

Fig. 1. Chemical structures of the studied fentanyl-based opioids.

acetonitrile/water, 80:20, (v/v).

2.2. Voltammetric measurements

An electrochemical cell with the IL membrane used in voltammetric measurements can be characterized by Scheme 1:

Ag'| AgCl|1 mM LiCl (w') | IL (o) | 1 mM LiCl, *x* mM RCl, *y* mM Fe^{2+}, *z* mM H_2O_2 (w) |AgCl|Ag (Scheme 1) where 1 mM LiCl is the supporting electrolyte (pH ≈ 7) for both aqueous phases (w', w), RCl is the chloride salt of the protonated fentanyl or fentanyl derivative in the aqueous phase (w), $x = 0 - 0.2$, Fe^{2+} and H_2O_2 represent components of Fenton's reagent, $y = 0 - 0.2$ and $z = 0$ or 44, respectively. The IL membrane phase is denoted as (o). Both reference Ag|AgCl electrodes were connected to aqueous phases (w') and (w) employing the Luggin capillaries, whose end was filled with the aqueous agar gel containing 100 mM LiCl. The supported IL membrane was prepared by impregnating a polyvinylidene fluoride microporous filter (type GVHP 1300, thickness of ≈112 μm, pore size of 0.22 μm, Millipore, USA) with IL [19]. The membrane disk (diameter of 0.9 cm) was cut out from the impregnated filter and mounted in a homemade four-electrode cell [35]. The area of the supported IL membrane exposed to the aqueous electrolyte solution was 0.07 cm^2. The cell potential *E* is described by Eq. (1):

$$E = \varphi(\mathrm{Ag}) - \varphi(\mathrm{Ag}') = \Delta_o^{w}\varphi - \Delta_o^{w'}\varphi - E_{ref} \quad (1)$$

where $\Delta_o^{w}\varphi$ and $\Delta_o^{w'}\varphi$ represent the Galvani potential differences at one or the other membrane side, and E_{ref} involves all remaining contributions to the cell potential *E*. The CHI potentiostat (Model 920C, CH Instruments, USA) controlled the cell potential and served also for the measurement of its complex impedance to estimate the solution resistance (typically 65 - 115 kΩ) for an adjustment of the ohmic potential drop automatic compensation.

Cyclic voltammograms (CVs) of the single charged ion transfers are characterized by the midpoint potential $E_m = (E_{p+} + E_{p-})/2$, where E_{p+} and E_{p-} are the positive and negative voltammetric peak potentials, respectively, and by the positive peak current I_{p+}. The transfer of a single charged ion represented here by the mono-protonated form of fentanyl (or some of its derivatives) should be controlled by linear diffusion. Consequently, the peak current I_{p+} (in A) can be described by Eq. (2) [19],

$$I_{p+} = (2.31 \times 10^5) A (D_i^{w} \nu)^{1/2} c_i^{o,w} \quad (2)$$

where D_i^{w} is the ion diffusion coefficient in the aqueous phase in $cm^2\ s^{-1}$, *A* is the interfacial area in cm^2, ν is the sweep rate in V s^{-1}, and $c_i^{o,w}$ is the bulk ion concentration in mol cm^{-3} in the aqueous phase.

Voltammetric measurements were carried out first in the absence and then in the presence of the selected protonated opioid in the right compartment of the cell with a volume of 5 cm^3 (Scheme 1). Subsequent CVs were recorded after the addition of Fe^{2+} to the right compartment (a reference CV), and then periodically at time intervals, as indicated in Figs. 2–5, after the injection of H_2O_2 into the right compartment (start of the reaction). Additions of Fe^{2+} and H_2O_2 were made in the microliter volumes from their concentrated stock solutions so that changes in the original concentration of opioids were negligible. The decreasing peak current was taken as a measure of the decreasing concentration of the opioid due to its degradation by the reaction with Fenton's reagent.

2.3. LC/ESI-MS conditions and parameters

LC/MS analysis of reaction products of fentanyl with Fenton's reagent was performed as follows. A 10 cm^3 reaction mixture containing 1 mM LiCl, 0.1 mM fentanyl, and 0.2 mM $(NH_4)_2Fe(SO_4)_2$ was prepared in a screw cap glass vial. Samples of the reaction mixture (1 cm^3) were taken at 5, 15, 30, 60, 90, 120, 180, 240 and 300 min after 44 mM H_2O_2 addition. A sample corresponding to time 0 min was taken from the mixture before the addition of H_2O_2. In each sample, the reaction was quenched by the addition of 0.2 M NaOH (alkalization to pH 11), and 1 cm^3 of chloroform was added immediately. The sample was shaken for 10 min at 1300 rpm and then 0.75 cm^3 of the chloroform phase was collected in a 2 cm^3 vial. The solvent was evaporated to dryness with a

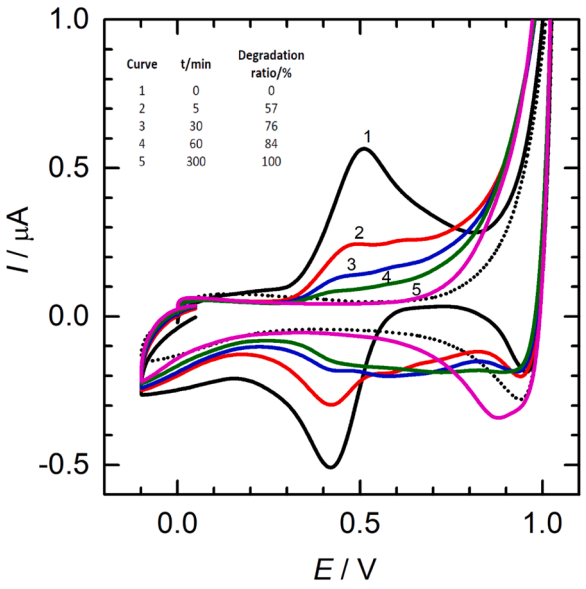

Fig. 2. CVs of the protonated fentanyl in the presence of Fenton's reagent recorded after 0 min (1), 5 min (2), 30 min (3), 60 min (4), or 300 min (5) from the start of the fentanyl degradation (injection of H_2O_2). The initial composition of the aqueous phase (w): 1 mM LiCl, 0.1 mM fentanyl in the protonated form, 0.2 mM $(NH_4)_2Fe(SO_4)_2$, and 44 mM H_2O_2. The dashed line shows the CV of the background electrolyte. The corresponding values of the degradation ratio derived from the current peak are inserted in the inset.

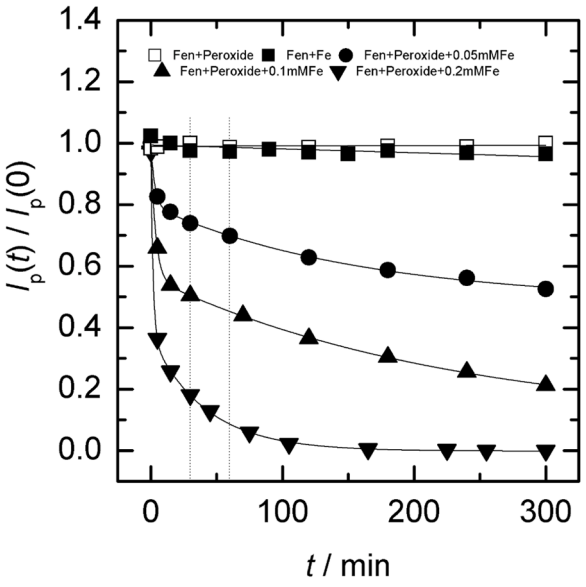

Fig. 3. The plot of the positive peak current $I_p(t)$ of the protonated fentanyl normalized to the initial current $I_p(0)$ vs. time *t*. Initial composition of the aqueous phase (w): 1 mM LiCl, 0.1 mM fentanyl in its protonated form, 44 mM H_2O_2 and 0 mM (□), 0.05 mM (●), 0.1 mM (▲) or 0.2 mM (▼) $(NH_4)_2Fe(SO_4)_2$. Curve ■ is the plot of the relative peak current vs. time *t* in the absence of H_2O_2, i.e., for the initial composition of 1 mM LiCl, 0.1 mM fentanyl in its protonated form, and 0.2 mM $(NH_4)_2Fe(SO_4)_2$. Lines show a non-linear fit to the bi-exponential decay function of time (see text), dotted vertical lines mark the values at 30 and 60 min to make them comparable with studies [27 and 28].

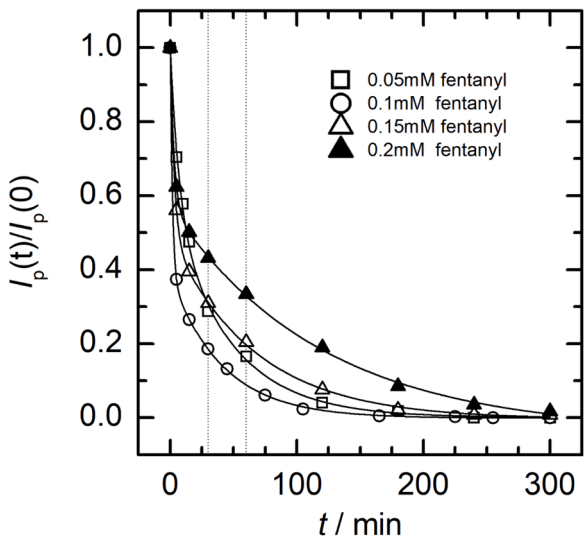

Fig. 4. The plot of the positive peak current $I_p(t)$ of the protonated fentanyl normalized to the initial current $I_p(0)$ vs. time t at various initial concentrations c^0_{Fen} of the protonated fentanyl: 0.05 mM (□), 0.1 mM (○), 0.15 mM (Δ) and 0.2 mM (▲). Initial concentrations of other components of the aqueous phase (w): 1 mM LiCl, 44 mM H_2O_2, and 0.2 mM $(NH_4)_2Fe(SO_4)_2$. Dotted vertical lines mark the values at 30 and 60 min to make them comparable with studies [27 and 28].

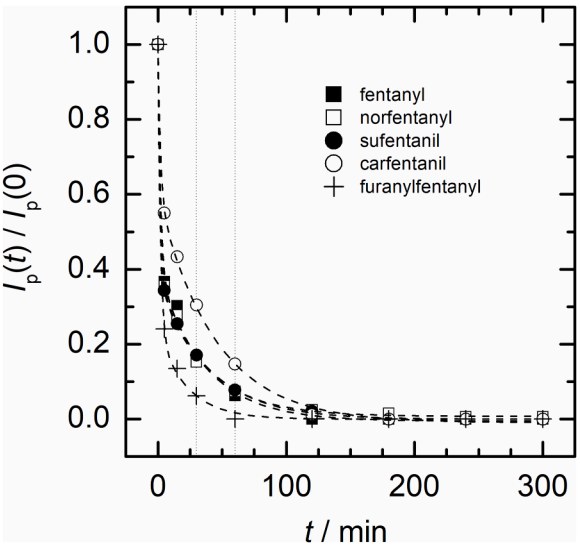

Fig. 5. The plot of the positive peak current $I_p(t)$ of the protonated fentanyl-related opioids normalized to the initial current $I_p(0)$ vs. time t for fentanyl (■), norfentanyl (□), sufentanil (●), carfentanil (○) and furanylfentanyl (+). Initial composition of the aqueous phase (w): 1 mM LiCl, 44 mM H_2O_2, 0.1 mM protonated opioid and 0.2 mM $(NH_4)_2Fe(SO_4)_2$. Dotted vertical lines mark the values at 30 and 60 min to make them comparable with studies [27 and 28].

stream of nitrogen. The residue was dissolved in 0.75 cm^3 of mobile phase (0.1% HCOOH in H_2O/0.1% HCOOH in CH_3CN, 7/3, v/v) before LC/MS analysis. Simultaneously with the reaction mixture containing fentanyl, a control without fentanyl was prepared, from which 1 cm^3 samples were taken at 0, 5, 60, and 300 min and treated in the same way.

Collected samples were filtered by membrane PTFE filter (0.45 μm pore size), transferred to HPLC vials, and injected into LC/ESI-MS instrument (Acquity UPLC system coupled to high-resolution mass spectrometer Synapt G2-S, both from Waters). LC/MS separation of fentanyl oxidation products was performed on Raptor ARC-18 LC Column (100 × 2.1 mm, 2.7 μm particle size, C18 stationary phase, from Restek). A sample volume of 5 mm^3 was injected by autosampler and the chromatographic separation was carried out using 0.1% HCOOH in H_2O as mobile phase A and 0.1% HCOOH in CH_3CN as mobile phase B with the following gradient: 0 – 2 min: 70% A, 2 min – 10 min: 70% – 0% A, 10 – 11.5 min: 0% A, 11.5 – 13 min: 0 –70% A. The flow rate set at 0.4 mm^3 min^{-1} for a run time of 13 min was used. ESI-MS conditions were set as follows: electrospray ionization was performed in positive mode; capillary voltage set at 2.0 kV, source temperature at 120 °C, desolvation temperature at 200 °C, cone gas flow at 50 dm^3 h^{-1}, desolvation gas flow at 400 dm^3 h^{-1} and nebulizer gas pressure at 6 bar were used.

MS spectra were acquired in the m/z range from 50 to 1200 Da with TOF settings in Res-mode and a scan time of 0.5 s. MS/MS experiments were performed with the transfer collision energy of 20 eV. All samples were measured in 2 repetitions.

3. Results and discussion

3.1. Voltammetric analysis

Fig. 2 shows the CVs of the protonated fentanyl measured at the beginning (full black line) and in the course of the fentanyl degradation by Fenton's reagent. The reaction proceeds fast and already the next CV measured 5 min after the start of the degradation points to a significant decrease in the fentanyl concentration. A positive current enhancement observed at potentials more positive than the peak potential can be ascribed to the ionic products of the degradation, which are more hydrophilic than the protonated fentanyl itself, e.g., norfentanyl [25]. Some of these reaction products are quite stable because even after 300 min from the start of the degradation, when the current corresponding to the protonated fentanyl decays to zero, their current signal remains apparent as a slight current enhancement at far positive potentials, cf. curve 5 in Fig. 2.

For the voltammetric measurements of the kinetics of the fentanyl degradation, the concentrations of H_2O_2, Fe^{2+} and fentanyls were chosen as a compromise concerning the degradation rate and the time scale of the voltammetric measurement, which at the applied potential sweep rate of 10 mV s^{-1} and the potential limits, enabled to repeat reliably the sweep in time intervals not shorter than 5 min. Faster reactions occurring at higher Fe^{2+} concentrations could not be therefore monitored voltammetrically, while slower reactions occurring at lower fentanyl concentrations would take too much time with a possible violation of the constant experimental conditions. Therefore, these experiments were performed with the aqueous phase (w) containing 1 mM LiCl as the background electrolyte, 0.05–0.20 mM fentanyl, 44 mM H_2O_2, and 0.05–0.20 mM $(NH_4)_2Fe(SO_4)_2$.

Fig. 3 demonstrates the effect of the concentration of Fe^{2+} in the reaction mixture on the decay of the peak current of the protonated fentanyl-related to the initial peak current with time t, which can be considered as a measure of the time profile of the degradation of the protonated fentanyl by the Fenton's reagent. These data indicate that the degradation of fentanyl (a) does not occur in the absence of Fe^{2+} (curve □), (b) it is accelerated by increasing the Fe^{2+} concentration (curves ●, ▲ and ▼), and (c) does not occur in the absence of H_2O_2 (curve ■). It is also worth noting that in the absence of Fe^{2+} even substantially higher concentrations of H_2O_2 alone do not lead to fentanyl degradation. The plots shown in Fig. 3 represent the decay of the fentanyl concentration with time and characterize the kinetics of the fentanyl degradation. A plausible description of these plots was possible by using a two-phase exponential decay function with time constant parameters t_1 and t_2:

$$x(t) = A_1 \exp\left(-\frac{t}{t_1}\right) + A_2 \exp\left(-\frac{t}{t_2}\right) \quad (3)$$

where $x(t)$ is the dimensionless concentration of fentanyl represented in Fig. 3 by the ratio of the peak currents $I_p(t)/I_p(0)$ at a time t and the

beginning of the degradation, i.e., at $t = 0$. The non-linear fit of the experimental plots to the function $x(t)$ is shown by the lines in Fig. 3. The initial rate of degradation is described by Eq. (4):

$$(-dx/dt)_0 = A_1/t_1 + A_2/t_2 \quad (4)$$

Results of the fit indicated that both the decay function and the initial rate are controlled by the first term, which makes more than 95% of the total value, and which represents a fast phase of the decay characterized by the time constant t_1 = 1.7 – 3.5 min depending on the Fe^{2+} concentration. In contrast, the second (slow) phase is characterized by the time constant t_2 = 40 – 250 min. The initial rate of fentanyl degradation $-(dx/dt)_0$ is proportional to the concentration of Fe^{2+} in Fenton's reagent with a regression line slope of 1.8 mM^{-1} min^{-1} = 30 M^{-1} s^{-1} (Appendix, Fig. S1).

The effect of the fentanyl concentration on the degradation rate can be seen in Fig. 4, which depicts the plots of the positive peak current $I_p(t)$ of the protonated fentanyl related to the initial current $I_p(0)$ vs. time t at various initial fentanyl concentrations c^0_{Fen}. In agreement with the previous study, the initial peak current $I_p(0)$ is proportional to c^0_{Fen}, cf. Fig. S2 (panel A), while the effect of c^0_{Fen} on the initial reaction rate is much less pronounced, cf. Fig. S2 (panel B).

The general mechanism of the oxidation of an organic compound R by Fenton's reagent can be described by the following reactions involving the $HO^\bullet$ radical [31,34],

$$Fe^{2+} + H_2O_2 \xrightarrow{k_1} Fe^{3+} + HO^\bullet + OH^- \quad (5)$$

$$R + HO^\bullet \xrightarrow{k_2} P_1 + P_2 + P_3 + \cdots \quad (6)$$

eventually accompanied by the following reactions involving the $HOO^\bullet$ radical,

$$Fe^{3+} + H_2O_2 \xrightarrow{k_3} Fe^{2+} + HOO^\bullet + H^+ \quad (7)$$

$$R + HOO^\bullet \xrightarrow{k_4} P_1' + P_2' + P_3' + \cdots \quad (8)$$

The nature of the P_n products of the oxidative degradation of fentanyl will be considered later. The linear effect of the Fe^{2+} concentration on the degradation of fentanyl, and the absence of an analogous effect of the fentanyl concentration suggest that the rate-determining step of the degradation could be the generation of the $HO^\bullet$ radical according to Eq. (5). On applying the steady-state approach to the first two steps described by Eq. (5) and Eq. (6), the reaction rate can be expressed by Eq. (9):

$$-\frac{dc_{Fen}}{dt} = -\frac{dc_{Fe^{2+}}}{dt} = k_1 c_{Fe^{2+}} \quad (9)$$

where the pseudo-first-order rate constant k_1 comprises the excess concentration of H_2O_2. The slope of 30 M^{-1} s^{-1} of the linear plot $-(dc_{Fen}/dt)_0$ vs. the concentration $c_{Fe^{2+}}$ (Fig. S1) then corresponds to the value of $k_1 = 3 \times 10^{-3}$ s^{-1} and the reaction half-time of 231 s or 3.85 min.

Fig. 5 displays the preliminary results of the voltammetric study of the degradation of other fentanyl-related opioids including norfentanyl, sufentanil, carfentanil, and furanylfentanyl, using the Fenton's reagent. These results indicate that the degradation of fentanyl-related opioids follows similar kinetics to fentanyl, which is characterized by the half-time of 2–8 min.

To facilitate a comparison of the rates of the degradation of the fentanyl compounds in the present and the reported [27,28] studies, the vertical dotted lines at 30 and 60 min were added to Figs. 3, 4, and 5. The $I_p(t)/I_p(0)$ values on the y-axis can actually be easily converted to percentages because the values 1 and 0 correspond to 100% and 0% of the corresponding fentanyl.

3.2. LC/MS analysis

Samples of the reaction mixture initially containing 0.1 mM fentanyl, 0.2 mM $(NH_4)_2Fe(SO_4)_2$, 1 mM LiCl, and 44 mM H_2O_2 were collected at reaction times 0, 15, 30, 60, 120, 180, 240, and 300 min, and analyzed by LC/ESI-MS after extraction into chloroform. The total ion chromatograms of the samples are shown in the Appendix, Fig. S3. Identified reaction intermediates and products are summarized in Table 1 together with their LC retention times, the values of m/z, and the differences between the observed and theoretical value of m/z for the indicated elemental composition (dtm). Apart from fentanyl, a large number of hydroxylated derivatives in various isomeric forms were identified in the reaction mixture. MS/MS analysis indicates that the hydroxylation takes place mainly on the phenethyl part of the fentanyl molecule and the piperidine ring. The terminal methyl of the ester-linked propionyl group also undergoes hydroxylation to a lesser extent. The aniline moiety of fentanyl appears to be relatively intact for hydroxylation. In addition to mono-, di- and trihydroxylated derivatives, the formation of norfentanyl (P9) has been proved by comparing the retention times and fragmentation pattern with the standard. Norfentanyl is reported to be a major metabolite of cytochrome P450-catalysed enzymatic reactions of fentanyl [1] and a product of other degradation processes [30].

The other degradation products observed (P8, P10, and P11) most likely correspond to the products reported being formed during the oxidative degradation of fentanyl in hydrogen peroxide or peracetic acid solutions [27]. After 5 h of reaction, the only product extractable into chloroform, ionizable in positive mode of electrospray, and providing an ion with an m/z value higher than 50 was observed in the reaction mixture. This product (P12) with a protonated molecule at m/z 162 was identified most probably as 1-phenylpiperidine and its concentration was about 300 times less than the starting concentration of fentanyl. The change in the concentration of fentanyl and its degradation products with time can be seen from the plots of the area under the chromatographic peaks vs. time such as those shown in Fig. 6. In the course of the degradation, the fentanyl concentration decays in the same time scale as the positive peak current $I_p(t)$ of the protonated fentanyl, cf. Fig. 4, while the concentration of the degradation products, e.g., norfentanyl, first increases from zero to a maximum, which is followed by an analogous

Table 1
List of the products or groups of the products P1-P12 of the degradation of fentanyl using Fenton's reagents, which were identified by LC/MS analysis.

Reaction products	t_R (min)	m/z $[M+H]^+$	dtm (mDa)	Elemental composition
fentanyl	1.51	337.2362	8.2	$C_{22}H_{29}N_2O$
P1 (hydroxyfentanyl)	0.87	353.2292	6.3	$C_{22}H_{29}N_2O_2$
	0.96	353.2292	6.3	$C_{22}H_{29}N_2O_2$
	1.04	353.2292	6.3	$C_{22}H_{29}N_2O_2$
	1.21	353.2292	6.3	$C_{22}H_{29}N_2O_2$
	1.9	353.2292	6.3	$C_{22}H_{29}N_2O_2$
P2 (dihydroxyfentanyl)	0.69	369.2235	5.7	$C_{22}H_{29}N_2O_3$
	0.79	369.2235	5.7	$C_{22}H_{29}N_2O_3$
	0.85	369.2235	5.7	$C_{22}H_{29}N_2O_3$
	1.14	369.2235	5.7	$C_{22}H_{29}N_2O_3$
P3 (dehydrogenated	0.78	351.2057	−1.6	$C_{22}H_{27}N_2O_2$
hydroxyfentanyl)	1.3	351.2057	−1.6	$C_{22}H_{27}N_2O_2$
P4 (dehydrogenated	0.86	367.2049	2.7	$C_{22}H_{27}N_2O_3$
dihydroxyfentanyl)	1.04	367.2049	2.7	$C_{22}H_{27}N_2O_3$
P5 (trihydroxyfentanyl)	0.65	385.2121	−0.6	$C_{22}H_{29}N_2O_4$
P6	0.61	387.2281	−0.3	$C_{22}H_{31}N_2O_4$
P7	0.65	305.1862	−0.3	$C_{17}H_{25}N_2O_3$
P8	0.62	261.2033	6.6	$C_{16}H_{25}N_2O$
P9 (norfentanyl)	0.62	233.1658	0.4	$C_{14}H_{21}N_2O$
P10 (hydroxynorfentanyl)	0.54	249.1617	1.4	$C_{14}H_{21}N_2O_2$
P11 (*N*-phenylpropanamide)	1.58	150.0936	1.7	$C_9H_{12}NO$
P12	0.63	162.1339	5.6	$C_{11}H_{16}N$

t_R – retention time, dtm – difference from the theoretical mass.

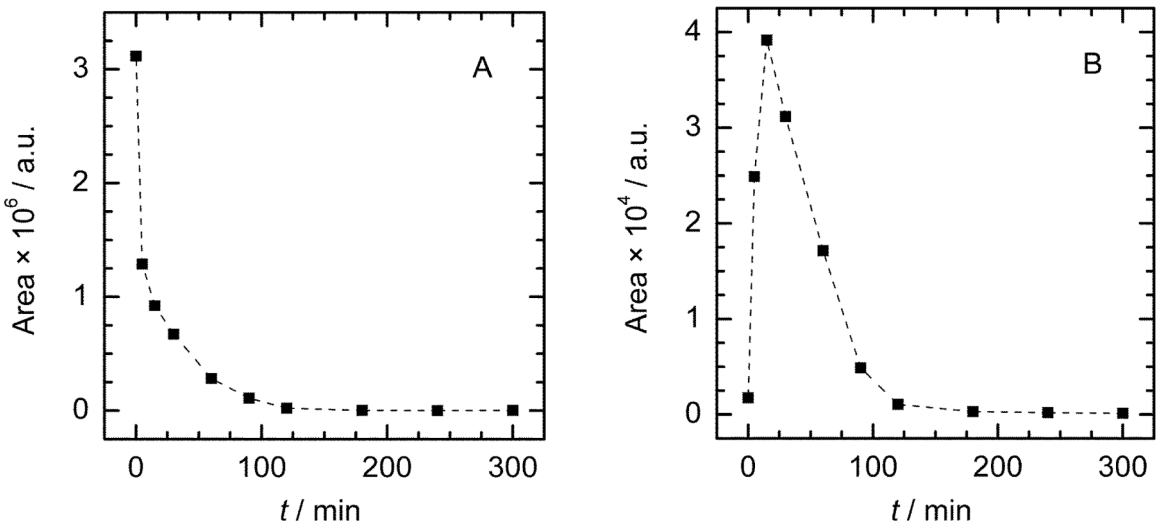

Fig. 6. Plots of the peak areas of fentanyl (A) and norfentanyl (B) taken from appropriately extracted ion chromatograms vs. time *t* of the degradation of fentanyl with Fenton's reagent.

decrease due to the subsequent product decomposition. Plots of peak areas vs. reaction time for the other degradation products can be found in the Appendix, Fig. S4.

4. Conclusion

Ion transfer voltammetry of the protonated fentanyl and the fentanyl-related opioids at a polarized ionic liquid membrane can be used to study the kinetics of their oxidative degradation using Fenton's reagent. Voltammetric data indicate that the degradation of fentanyl itself follows the pseudo-first-order rate law characterized by the reaction half-time of about 4 min. The rate-determining step of the process is the reaction of Fe^{2+} with H_2O_2 generating the $HO^{\bullet}$ radical, which is followed by the fast reaction of this radical with fentanyl and its products in the subsequent steps. The oxidative degradation of fentanyl-related opioids is apparently subject to similar kinetics. LC/MS analysis shows that the reaction of fentanyl with Fenton's reagent provides a wide range of reaction products in a relatively short reaction time (5–30 min), and supports the conclusions drawn from the voltammetric measurements in regards to the reaction time. Hydroxylated derivatives in some isomeric forms are the most abundant products in the reaction mixture. In addition to mono-, di- and trihydroxylated derivatives, the formation of norfentanyl has been proved. After 5 h of reaction, only one product with *m/z* higher than 50 was found in the reaction mixture. The results of this study show that the Fenton reaction leads to the rapid and efficient degradation of fentanyl and its structural analogs. Fenton's reagent, consisting of cheap and nontoxic components, is effective even at low concentrations of ferrous salt and H_2O_2 (less than 1 mmol dm^{-3}) and can be easily applied in solution, also by spraying. In this respect, it appears to be promising for the fast cleaning and decontamination of wastewater and surfaces (e.g., in clandestine manufacturing facilities) contaminated with hazardous fentanyl-based drugs. It can further be noted that the technique of ion transfer voltammetry coupled to LC/MS as utilized in the present study can also find application in other areas of analytical and physical chemistry to study ionic products of degradation and their kinetics (e.g., in postmortem analysis of batteries) or to follow ionic species involved in liquid electrolytes (e.g. fuel cells, electrocatalytic systems, ionic liquids, etc.).

CRediT authorship contribution statement

Jan Langmaier: Conceptualization, Methodology, Investigation, Visualization, Writing – original draft. **Jana Skopalová:** Conceptualization, Supervision, Visualization, Writing – original draft. **Monika Zajacová Cechová:** Investigation, Validation. **Tereza Kahánková:** Investigation. **Radek Jerga:** Investigation. **Petr Barták:** Investigation, Writing – review & editing. **Zdeněk Samec:** Formal analysis, Writing – original draft, Writing – review & editing. **Tomáš Navrátil:** Writing – review & editing.

Declaration of Competing Interest

The authors declare that they have no known competing financial interests or personal relationships that could have appeared to influence the work reported in this paper.

Data availability

Data will be made available on request.

Acknowledgement

This work was supported by the Czech Science Foundation (grant number 20–07350S).

Supplementary materials

Supplementary material associated with this article can be found, in the online version, at doi:10.1016/j.electacta.2023.141848.

References

[1] P. Armenian, K.T. Vo, J. Barr-Walker, K.L. Lynch, Fentanyl, fentanyl analogs and novel synthetic opioids: a comprehensive review, Neuropharmacology 134 (2018) 121–132.
[2] C. Stein, Pain inhibition by opioids-new concepts, Anaesthesist 68 (2019) 97–103.
[3] I.H. Shim, W.M. Bahk, Y.S. Wool, B.H. Yoon, Pharmacological Treatment of Major Depressive Episodes with Mixed Features: a Systematic Review, Clin. Psychopharm. Neurosci. 16 (2018) 376–382.
[4] M.A.H. Al Hattab, A.Y.M. Alahmari, M.A. Alsaaid, B.A.M. Ahmed, M.S. Abdullah, K.A. Alharbi, A.S. Almatrafi, N. Al-Abdulmohsin, W.M. Mujalli, N.M. Khawaji, Antipsychotics- classification, uses, and adverse effects, Indo Am. J. Pharm. Sci. 5 (2018) 15690–15695.
[5] W.J. Cubala, J. Springer, Quetiapine abuse and dependence in psychiatric patients: a systematic review of 25 case reports in the literature, J. Subst. Use 19 (2014) 388–393.
[6] C.A. Valdez, R.N. Leif, S. Hok, B.R. Hart, Analysis of chemical warfare agents by gas chromatography-mass spectrometry: methods for their direct detection and

derivatization approaches for the analysis of their degradation products, Rev. Anal. Chem. (2018) 37.
[7] S.L. Shafer, Carfentanil: a weapon of mass destruction, Can. J. Anaesth. 66 (2019) 351–355.
[8] S. Caccia, S. Garattini, Pharmacokinetic and pharmacodynamic significance of antidepressant drug metabolites, Pharmacol. Res. 26 (1992) 317–329.
[9] M.R. Meyer, H.H. Maurer, Current applications of high-resolution mass spectrometry in drug metabolism studies, Anal. Bioanal. Chem. 403 (2012) 1221–1231.
[10] F.T. Peters, Recent developments in urinalysis of metabolites of new psychoactive substances using LC-MS, Bioanalysis 6 (2014) 2083–2107.
[11] M.R. Meyer, H.H. Maurer, Current status of hyphenated mass spectrometry in studies of the metabolism of drugs of abuse, including doping agents, Anal. Bioanal. Chem. 402 (2012) 195–208.
[12] M. Choinska, I. Sestakova, V. Hrdlicka, J. Skopalova, J. Langmaier, V. Majer, T. Navratil, Electroanalysis of fentanyl and its new analogs: a review, Biosensors 12 (2022) 26.
[13] P. Abraham, S. Renjini, P. Vijayan, V. Nisha, K. Sreevalsan, V. Anithakumary, Review-review on the progress in electrochemical detection of morphine based on different modified electrodes, J. Electrochem. Soc. 167 (2020), 037559.
[14] C.E. Ott, H. Cunha-Silva, S.L. Kuberski, J.A. Cox, M.J. Arcos-Martínez, L.A. Arroyo-Mora, Electrochemical detection of fentanyl with screen-printed carbon electrodes using square-wave adsorptive stripping voltammetry for forensic applications, J. Electroanal. Chem. 873 (2020), 114425.
[15] N. Wester, E. Mynttinen, J. Etula, T. Lilius, E. Kalso, B.F. Mikladal, Q. Zhang, H. Jiang, S. Sainio, D. Nordlund, E.I. Kauppinen, T. Laurila, J. Koskinen, Single-walled carbon nanotube network electrodes for the detection of fentanyl citrate, ACS Appl. Nano Mater. 3 (2020) 1203–1212.
[16] M.W. Glasscott, K.J. Vannoy, P.U.A. Iresh Fernando, G.K. Kosgei, L.C. Moores, J. E. Dick, Electrochemical sensors for the detection of fentanyl and its analogs: foundations and recent advances, TrAC - Trends Anal. Chem. 132 (2020), 116037.
[17] H.M. Elbardisy, C.W. Foster, L. Cumba, L.H. Antonides, N. Gilbert, C.J. Schofield, T.S. Belal, W. Talaat, O.B. Sutcliffe, H.G. Daabees, C.E. Banks, Analytical determination of heroin, fentanyl and fentalogues using high-performance liquid chromatography with diode array and amperometric detection, Anal. Met. 11 (2019) 1053–1063.
[18] Z. Samec, J. Langmaier, T. Kakiuchi, Charge-transfer processes at the interface between hydrophobic ionic liquid and water, Pure Appl. Chem. 81 (2009) 1473–1488.
[19] J. Langmaier, Z. Samec, Voltammetry of ion transfer across a polarized room-temperature ionic liquid membrane facilitated by valinomycin: theoretical aspects and application, Anal. Chem. 81 (2009) 6382–6389.
[20] J. Langmaier, Z. Samec, Cyclic voltammetry of ion transfer across a room temperature ionic liquid membrane supported by a microporous filter, Electrochem. Commun. 9 (2007) 2633–2638.
[21] J. Langmaier, S. Zalis, Z. Samec, Lipophilicity of acetylcholine and related ions examined by ion transfer voltammetry at a polarized room-temperature ionic liquid membrane, J. Electroanal. Chem. 815 (2018) 183–188.
[22] J. Langmaier, J. Skopalová, T. Navrátil, Z. Samec, Detection of antimuscarinic agents tolterodine and fesoterodine and their metabolite 5-hydroxymethyl tolterodine by ion transfer voltammetry at a polarized room-temperature ionic liquid membrane, Electrochim. Acta 304 (2019) 54–61.
[23] J. Langmaier, S. Zalis, Z. Samec, V. Bovtun, M. Kempa, Origin of the correlation between the standard Gibbs energies of ion transfer from water to a hydrophobic ionic liquid and to a molecular solvent, Electrochim. Acta 87 (2013) 591–598.
[24] J. Langmaier, M. Pizl, Z. Samec, S. Zalis, Extreme Basicity of Biguanide Drugs in Aqueous Solutions: ion Transfer Voltammetry and DFT Calculations, J. Phys. Chem. A 120 (2016) 7344–7350.
[25] J. Langmaier, V. Maier, Z. Samec, Voltammetry of several natural and synthetic opioids at a polarized ionic liquid membrane, Chem. Electro. Chem. 8 (2021) 2519–2525.
[26] A. Garg, D.W. Solas, L.H. Takahashi, J.V. Cassella, Forced degradation of fentanyl: identification and analysis of impurities and degradants, J. Pharm. Biomed. Anal. 53 (2010) 325–334.
[27] L.H. Qi, Z.X. Cheng, G.M. Zuo, S.M. Li, Q.P. Fan, Oxidative Degradation of Fentanyl in Aqueous Solutions of Peroxides and Hypochlorites, Def. Sci. J. 61 (2011) 30–35.
[28] L. Xu, L.J. Ren, Z.H. Wang, X.T. Tian, L.H. Qi, Q.P. Fan, Y.L. Xiang, Oxidative treatment of fentanyl compounds in water by sodium bromate combined with sodium sulphite, Water Sci. Technol. 72 (2015) 38–44.
[29] N.M. Froelich, J.E. Sprague, T.J. Worst, Letter to the Editor-Elbow Grease and OxiClean for Cleaning Fentanyl- and Acetylfentanyl-contaminated Surfaces, J. Forensic Sci. 63 (2018) 336–338.
[30] M.M. Bazley, M. Logan, C. Baxter, A.A.B. Robertson, J.T. Blanchfield, Decontamination of Fentanyl and Fentanyl Analogues in Field and Laboratory Settings: a Review of Fentanyl Degradation, Aust. J. Chem. 73 (2020) 868–879.
[31] H.J.H. Fenton, Oxidation of tartaric acid in presence of iron, J. Chem. Soc.-Transac. 65 (1894) 899–911.
[32] M. Hayyan, M.A. Hashim, I.M. AlNashef, Superoxide Ion: generation and Chemical Implications, Chem. Rev. 116 (2016) 3029–3085.
[33] A. Thiam, R. Salazar, Fenton-based electrochemical degradation of metolachlor in aqueous solution by means of BDD and Pt electrodes: influencing factors and reaction pathways, Environ. Sci. Pollut. Res. 26 (2019) 2580–2591.
[34] Q.Q. Cai, B.C.Y. Lee, S.L. Ong, J.Y. Hu, Fluidized-bed Fenton technologies for recalcitrant industrial wastewater treatment-Recent advances, challenges and perspective, Water Res. 190 (2021) 116692.
[35] Z. Samec, A. Trojanek, E. Samcova, Ion and pore fluid transport properties of a Nafion® membrane separating two electrolyte solutions Part I. Kinetics of the proton and alkali metal cation transport, J. Electroanal. Chem. 389 (1995) 1–11.